

New strategies for the induction of endogenous porphyrins in eucaryotic and procaryotic cells

HEUCK, Gesine

Abstract

The present thesis presents new strategies to generate endogenous porphyrins from exogenously provided compounds for fluorescence photodetection (PD) and photodynamic therapy (PDT). One method is to administer the heme precursor 5-aminolevulinic acid (5-ALA), which leads to the accumulation of fluorescent intermediates of the heme cycle, notably protoporphyrin IX (PPIX). The hexyl ester of 5-ALA (HAL) has gained marketing authorization for the detection of bladder cancer from the European, Australian and American regulatory offices. However, its impact for other indications such as interstitial tumors is relatively small due to limited systemic bioavailability. Aiming at reducing the systemic toxicity and improving the circulation half-life of the compound, the first part of the thesis focuses on the encapsulation of HAL into polymeric nanoparticles. The second part of the thesis relates to the discovery, characterization and preliminary exploitation of a PPIX generating mechanism from heme in *E. coli*.

Reference

HEUCK, Gesine. *New strategies for the induction of endogenous porphyrins in eucaryotic and procaryotic cells*. Thèse de doctorat : Univ. Genève, 2012, no. Sc. 4415

URN : [urn:nbn:ch:unige-219862](http://nbn-resolving.org/urn:nbn:ch:unige-219862)

DOI : [10.13097/archive-ouverte/unige:21986](https://doi.org/10.13097/archive-ouverte/unige:21986)

Available at:

<http://archive-ouverte.unige.ch/unige:21986>

Disclaimer: layout of this document may differ from the published version.



UNIVERSITÉ
DE GENÈVE

New Strategies for the Induction of Endogenous Porphyrins in Eucaryotic and Procaryotic Cells

THÈSE

présentée à la Faculté des Sciences de l'Université de Genève
pour obtenir le grade de Docteur des Sciences, Mention Sciences Pharmaceutiques

par

Gesine Claudia Heuck

de

Heidelberg (Germany)

Thèse No. 4415

Genève

Atelier de reproduction Repromail

2012



**UNIVERSITÉ
DE GENÈVE**

FACULTÉ DES SCIENCES

**Doctorat ès sciences
Mention sciences pharmaceutiques**

Thèse de *Madame Gesine HEUCK*

intitulée :

**" New Strategies for the Induction of Endogenous Porphyrins in
Eucaryotic and Procaryotic Cells "**

La Faculté des sciences, sur le préavis de Messieurs N. LANGE, docteur et directeur de thèse (Section des sciences pharmaceutiques), E. ALLEMANN, professeur ordinaire (Section des sciences pharmaceutiques), Z. MALIK, professeur (The Mina and Everard Goodman Faculty of Life Sciences, Bar-Ilan University, Ramat-Gan, Israel) et L. BOLOTINE, docteur (Centre de Recherche en Automatique de Nancy, Université de Nancy, Vandoeuvre-les-Nancy, France), autorise l'impression de la présente thèse, sans exprimer d'opinion sur les propositions qui y sont énoncées.

Genève, le 23 avril 2012

Thèse - 4415 -


Le Doyen, Jean-Marc TRISCONE

N.B.- La thèse doit porter la déclaration précédente et remplir les conditions énumérées dans les "Informations relatives aux thèses de doctorat à l'Université de Genève".

A mes parents

Remerciements

Mes premiers remerciements vont au professeur Achim Göpferich, qui m'a orienté vers la Pharmacie Galénique, ainsi qu'à mon directeur de thèse, Norbert Lange. Merci, Norbert, de m'avoir défié avec ce sujet passionnant. Compte sur moi pour faire de la publicité pour l'héxyl-ALA dans le futur. Merci aussi, pour ton enthousiasme scientifique, ta confiance ainsi que ton humour, qui rend l'ambiance de ton groupe si unique et décontractée.

Ma gratitude va aussi aux professeurs Robert Gurny et Eric Allémann, qui m'ont permis de travailler dans un cadre professionnel exceptionnel, tel que le Laboratoire de Pharmacie Galénique de l'Université de Genève, et au Professeur Leonardo Scappozza de m'avoir attribué sa confiance quant aux responsabilités au sein de l'école doctorale.

Aux collaborateurs qui m'ont donné l'opportunité de mettre en valeur mon travail:

- le professeur Jean-Luc Wolfender et Karine Ndjoko-Iloset de l'Université de Genève,
- Janne Raula-Juhani et Antti Rahikkala de l'Aalto University, Helsinki, et en particulier
- la professeure Cécile Wandersman et Jeff Mellin de l'Institut Pasteur, qui m'ont autant appris sur la microbiologie, ainsi que l'esprit stratégique et l'écriture dans la recherche.

Je remercie les membres du jury, Madame Lina Bolotine, le professeur Zvi Malik et le professeur Eric Allémann d'avoir accepté de lire et d'évaluer ma thèse.

Un grand merci à Florence von Ow et Myrtha Copin (qui me rappellera toujours le bénéfice de), sans qui les tâches administratives n'auraient jamais été aussi facile à maîtriser.

Ma profonde reconnaissance va à

- Carole, Saïd et Brigitte pour faciliter le quotidien du labo que ce soit pour la vaisselle, les solvants ou la commande de produits
- Yann, Loris et Richard les maîtres pour toute question et urgence informatique
- Marco Perdigao: merci d'assurer inlassablement le bon fonctionnement du labo et d'intervenir en cas de besoin - quelle que soit le temps et l'heure (!!!). Merci aussi pour les discussions et les sorties dîner!
- Florence Delie : merci pour tes conseils concernant les questions de travaux pratiques, de nanoparticules où simplement la vie en général. Merci aussi pour ton énergie et ton initiative sportive contagieuses – les sorties pleine lune et les midis au bord du Rhône .

Je tiens à remercier mes collègues anciens et actuels du superbe groupe PDT:

- Nicolas et Sabine, qui m'ont transmis sans autres leurs savoir sur 5-ALA et ses esters
- Magali pour ses astuces CAM et nanoparticules
- Marino, David, Magdalena, Andrej, Dhananjaya et Karine pour leur soutien et aide au niveau chimique et en particulier
- Maria-Fernanda, Doris et Nawal, avec qui j'ai partagé le laboratoire pendant la plus grande partie de mon doctorat. Merci, pour votre énergie et votre humour qui ont déclenché plus d'une attaque de fou rire (surtout en fin de journée...) ainsi que votre patience et votre écoute dans les moments plus sérieux.

Mes remerciements vont aussi à Adriana, Marie-Christine, Martinus, Claudia d.T. (grazie di avere assicurato l'esercizio della lingua di Dante anche nel labo), Florence M., Amandine et Lutz (Disco-Fox rocks!) pour les nombreux conseils et coup de mains techniques.

Ma chaleureuse gratitude va à Pol-Edern, Michel, Saskia, Leo e Ale, Sarra, Gaëlle et Marieke pour les discussions et activités hors-labo (je pense Ferb, Italie, Montagne, Londres, Festivals), et en particulier Annasara (!!!) et Farnaz pour leur amitié partagée et leur soutien.

Thanks to the crazy chemists of the 1st/2nd floor (David, Javier – both fantastic representatives of bella Galicia, Jiří, Marco, Edvinas and Marius) for the fun moments at BBQs, dinners and work after-hours. You'll all make wonderful Nobel-Prize winners.

Grazie, Alberto e Giuli, Francesco e Lorenza per la vostra amicizia nei momenti felici e tristi, e le numerose iniziative culturale, sportive, turistiche, festive o non festive, assicurando che mia agenda non sia mai vuota. Vi adoro.

Alla Famiglia « Ex-Rue de Bâle » : Eli, Chiccha, Enri e Conc ! Grazie tanto di avermi accettata nella squadra italiana e di avermi insegnato questa bellissima lingua. Sono piena di ammirazione per vostra energia e disposizione per tutte le follie del mundo.

An meine „genfer Familien“ Forssmann, Cichon und Wabitsch: vielen Dank für Eure offenen Häuser, die familiäre Atmosphäre und den Beistand. Es ist schön, Euch so nah zu haben! Anne, vielen Dank für's (schon-)immer-da-sein, auch wenn geographisch manchmal fern.

An meine lieben Eltern und Geschwister, vielen Dank für Eure Verwöhnung, den Ansporn und Eure bedingungslose und unermüdliche Unterstützung, die es mir ermöglicht haben bis hierher zu kommen. Pappi und Christoph, für die anregenden Diskussionen, die mir mehr als einmal die Lust auf Versuche zurückgegeben haben, danke ich Euch.

Table of Contents

INTRODUCTION.....	1
Chapter 1. Review: Exogenously Induced Endogenous Photosensitizers.....	21
PART A: FORMULATION OF HEXAMINOLEVULINIC ACID INTO POLYMERIC NANOPARTICLES	
Chapter 2. Matrix Mediated Fluorescence Enhancement - Why Nanoparticles and PPIX Make a Friendly Couple.....	75
Annotation.....	89
Chapter 3. Nanoencapsulation of HAL into Polymeric Nanoparticles using the Aerosol Flow Reactor Method	91
PART B: PHOTODYNAMIC INACTIVATION OF <i>E. COLI</i> WITH A NEW PROTOPORPHYRIN IX GENERATING MECHANISM	
Annotation.....	115
Chapter 4. Bacteria Retrieve Iron from Heme by Keeping the Tetrapyrrol Ring Intact.....	117
Chapter 5. Counterclockwise - Photodynamic Inactivation of Bacteria with PPIX Generated from Heme.....	145
SUMMARY AND CONCLUSION.....	163
RESUME ET CONCLUSION	169
ABBREVIATIONS	173

Introduction

Although light was used for therapeutic purposes since centuries, the first cornerstone for photodynamic therapy (PDT) was set in 1900 by Oscar Raab. He reported that the chemical compound acridine orange destroys microbial organisms under irradiation with light [1]. A decade later, Friedrich Meyer-Betz demonstrated the photosensitizing effect of a porphyrin mixture in a self-experiment [2]. Today, PDT is effectively used in the treatment of inflammatory, neoplastic, microbial, viral and helminthic diseases [3], wound healing and plastic surgery. PDT is also used for cosmetic purposes such as skin rejuvenation [4] and was proposed for hair removal [5], water disinfection [6, 7] and insecticidal procedures [8].

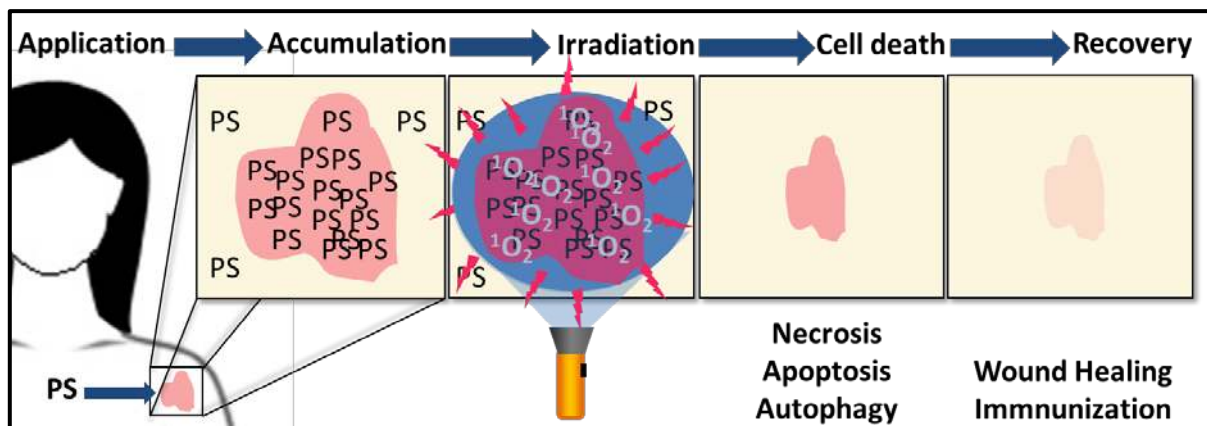


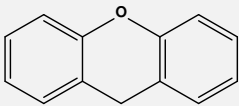
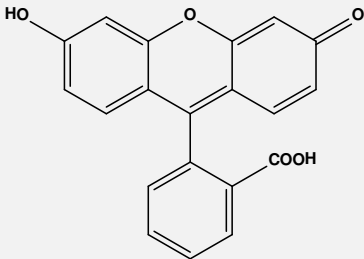
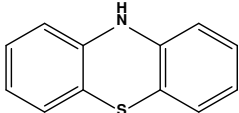
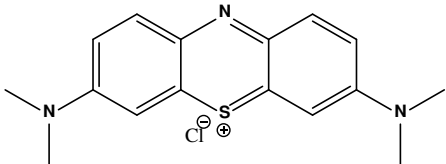
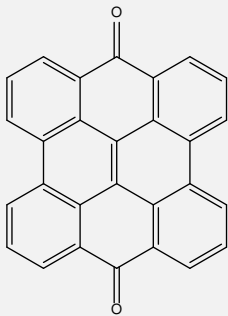
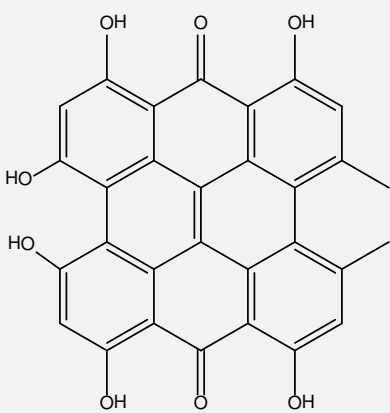
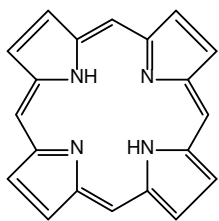
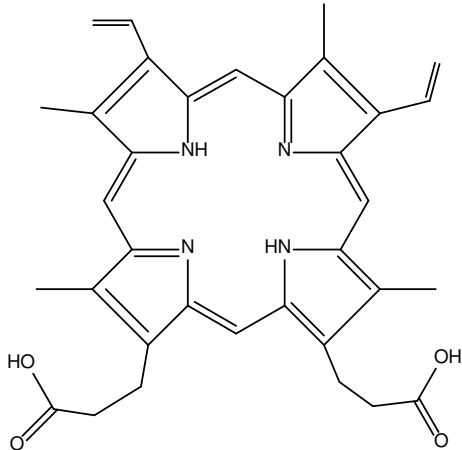
Fig. 1. Principle of PDT and PD. After application, the photosensitizer (PS) accumulates in the target tissue. Subsequent irradiation with light induces PS fluorescence and highly reactive singlet oxygen (1O_2), which induces cell death by necrosis, apoptosis or autophagy. It also triggers an inflammatory response that induces a process similar to wound healing and the creation of a tumor specific immune memory.

In distinction to phototherapy that uses only light, photodynamic therapy is based on three individually non-toxic components: a photosensitizer (PS), light and oxygen. Irradiation of the photosensitizer with light of an appropriate wavelength “activates” the photosensitizer. Subsequently, it reacts with oxygen to create highly cytotoxic reactive oxygen species (ROS) that damage the target tissue lethally (Fig.1). Policard established the link between fluorescence photodetection (PD) of malignant tissue and PDT in 1924 [9]. He observed an intrinsic fluorescence in certain tumors of humans and animals as the result of an accumulation of porphyrins. PD takes advantage of the fluorescent properties of most PSs, making it applicable as fluorescent marker for neoplastic cells [10]. The fluorescence can be detected *in situ* by optical means that are extremely sensitive, while instrumentation is simple and cost-effective. These attributes give PD a major advantage over often time-consuming conventional and/or costly modern techniques such as computerized tomography or magnetic resonance imaging.

Photosensitizers

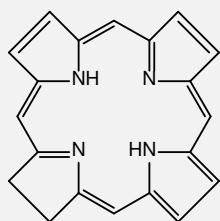
Photosensitizers may be classified according to their historical standing, the chemical structure or the mechanism of fluorescence induction. Historically, three photosensitizer generations are distinguished. The first generation specifically comprises haematoporphyrin (HP) and haematoporphyrin derivative (HpD, Photofrin[®]). Both are mixtures of porphyrin mono- and oligomers. The major drawback of these poorly defined compounds is their skin photosensitizing effect. This inconvenience was resolved by designing second generation photosensitizers such as temoporfin (m-THPC, meso-tetrahydroxyphenylchlorin, Foscan[®]) or verteporfin (BPD-A, benzophorphyrin derivative-monoacid A, Visudyne[®]) aiming at improved selectivity and defined chemical and pharmacokinetic profiles. In attempt to further increase selectivity, third generation photosensitizers are under ongoing development. They usually display an active targeting moiety for the site of interest. This may imply the conjugation of the PS with a specific substrate, e.g. a monoclonal antibody, that interacts with a tumor antigen [11-14], or the attachment of several PS to a polymer backbone susceptible to a specific enzyme at the site of interest as in the case of protease-sensitive photosensitizer prodrugs (see below) [15-17].

Tab1. Classification PS according to the chemical structure

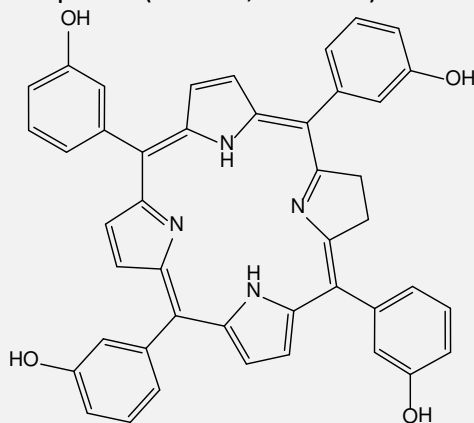
Chemical Class	Basic structure	Example
Xanthene		Fluorescein 
Phenothiazine		Methylene Blue 
Naphtodianthrone		Hypericin 
Porphyrin		Protoporphyrin IX 

Introduction

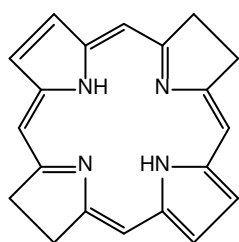
Chlorin



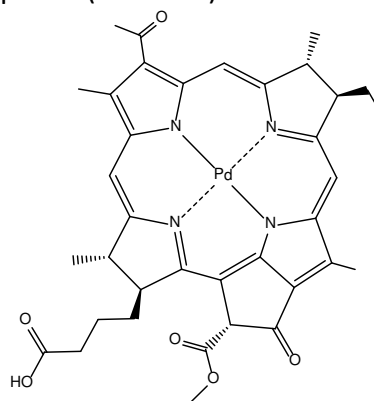
Temoporfin (mTHPC, Foscan®)



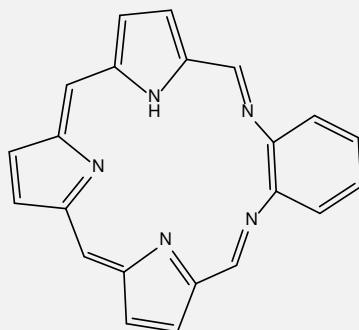
Bacteriochlorin



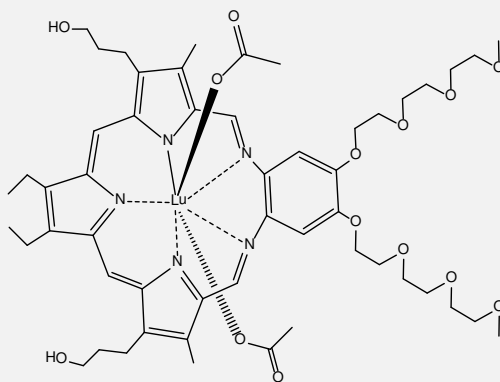
Padoporfin (Tookad®)



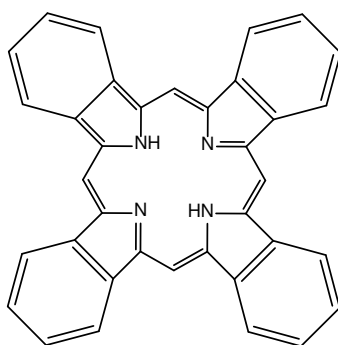
Texaphyrin



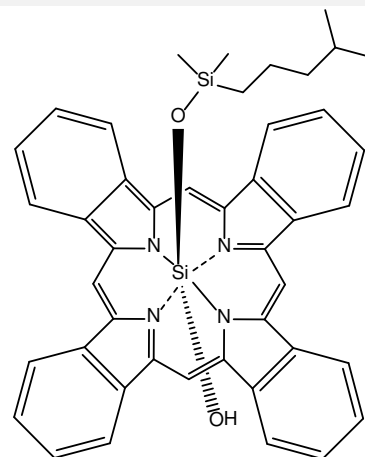
Lu(III) Texaphyrin



Phthalocyanine



Pc4



Natural and synthetic fluorescent dyes of various chemical classes can function as photosensitizers. Tab. 1 shows examples of photosensitizers classified according to their structure. The largest group is based on the scaffold of porphyrins and related structures such as chlorins, bacteriochlorins, phthalocyanines or texaphyrins. However, phenothiazines (methylene blue), xanthenes (fluorescein) and naphthodianthrone (hypericin) are also used in clinical treatment.

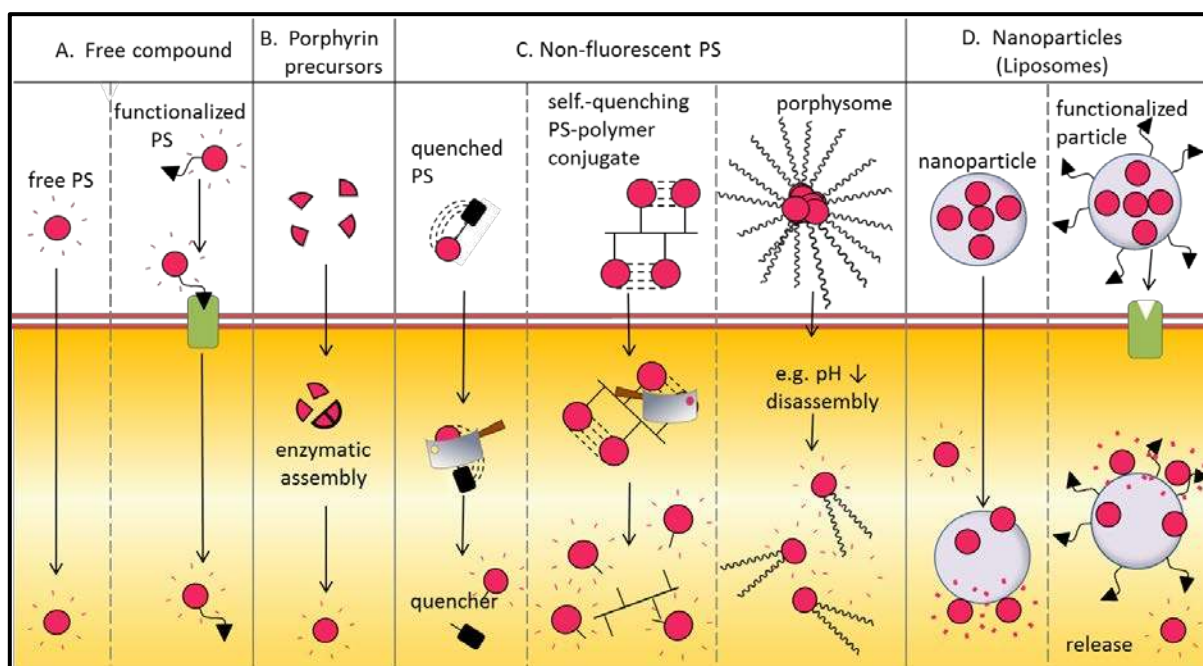


Fig. 2. Possibilities to design a PS for specific delivery and activation. PS may be administered as free compound or photo-immunoconjugate, with instant ability to fluoresce (A) or as a prodrug that is transformed by cellular enzymes into the fluorescent compound (B). PS fluorescence may also be suppressed upon administration, e.g. by attaching a chemical moiety that modifies the fluorophore or by quenching the PS. Enzymatic cleavage in the cell or disassembly of micellar structures restores PS fluorescence (C). Nanoparticles may function as carriers for PS. Adsorption of a lipophilic PS to the nanoparticle may enhance the PS fluorescence (D).

Alternatively, PS can be classified according to their mechanism function. Fig. 2 illustrates possibilities to engineer PS mediated fluorescence at the molecular level. In reality, a PS may be designed to follow multiple mechanisms. Therefore, the scheme should be considered as a theoretical approach. The simplest way is the application of a molecule with intrinsic fluorescence as in the case of the free PS or photo-immunoconjugates [18] (Fig. 2 A). A

second approach is to use a non-photosensitizer pro-drug such as the heme precursor 5-aminolevulinic acid (5-ALA) or its derivatives (Fig. 2 B). In eukaryotic cells and some proteobacteria, 5-ALA emanates as first building block of the heme biosynthesis from the enzymatic reaction of succinyl-CoA with glycine (Shemin-pathway) (Fig. 3). An alternative pathway is found in most bacteria, where 5-ALA is synthesized from glutamate (C₅-pathway) [19]. For the formation of heme, eight 5-ALA molecules are assembled enzymatically to yield the penultimate precursor of heme, protoporphyrin IX (PPIX). PPIX and earlier tetrapyrrolic heme precursors lack the ferrous iron of heme; therefore, they emit red fluorescence and act as endogenous PS. Since the heme biosynthesis is tightly regulated by a negative feedback of heme on the enzyme catalyzing 5-ALA synthesis, accumulation of these PS does not occur physiologically. However, the control mechanism can be by-passed by administering exogenous 5-ALA. 5-ALA enters the heme cycle and is enzymatically converted. A bottleneck at the level of iron incorporation into the tetrapyrrol skeleton, in combination with up-regulation of early heme biosynthetic enzymes, leads to the accumulation of the photosensitizing porphyrin intermediates, notably PPIX (Fig.3).

Chapter 1 provides a literature review of the history and *in situ* generation of endogenous PS using 5-ALA and attempts improve to this methodology. A successful concept has been implemented by the esterification of 5-ALA with short- to medium length aliphatic alcohols. The most prominent derivatives, 5-ALA methyl ester (MAL) and 5-ALA hexyl ester (HAL), show an improved local bioavailability with respect to the parent compound, while conserving strong fluorescence induction, an effect attributed to the higher lipophilicity of the esters. The hydrophilic molecule 5-ALA requires active transporters to reach the cytosol, a process susceptible to protein saturation. In contrast, MAL is believed to follow active and passive transport mechanisms, while the higher lipophilicity (logP 1.8) [20] and amphiphilic character of HAL enable it to diffuse through the cell membrane into the cytosol. This may explain why HAL induces cellular PPIX concentrations up to 50 fold above those reached with 5-ALA [21, 22].

The first part of the thesis focuses on the formulation of HAL into nanoparticles and the impact on the generation of fluorescence in two human cancer cell lines, T24 and A549, as well as a tumor model on the chorioallantoic membrane of the chicken embryo.

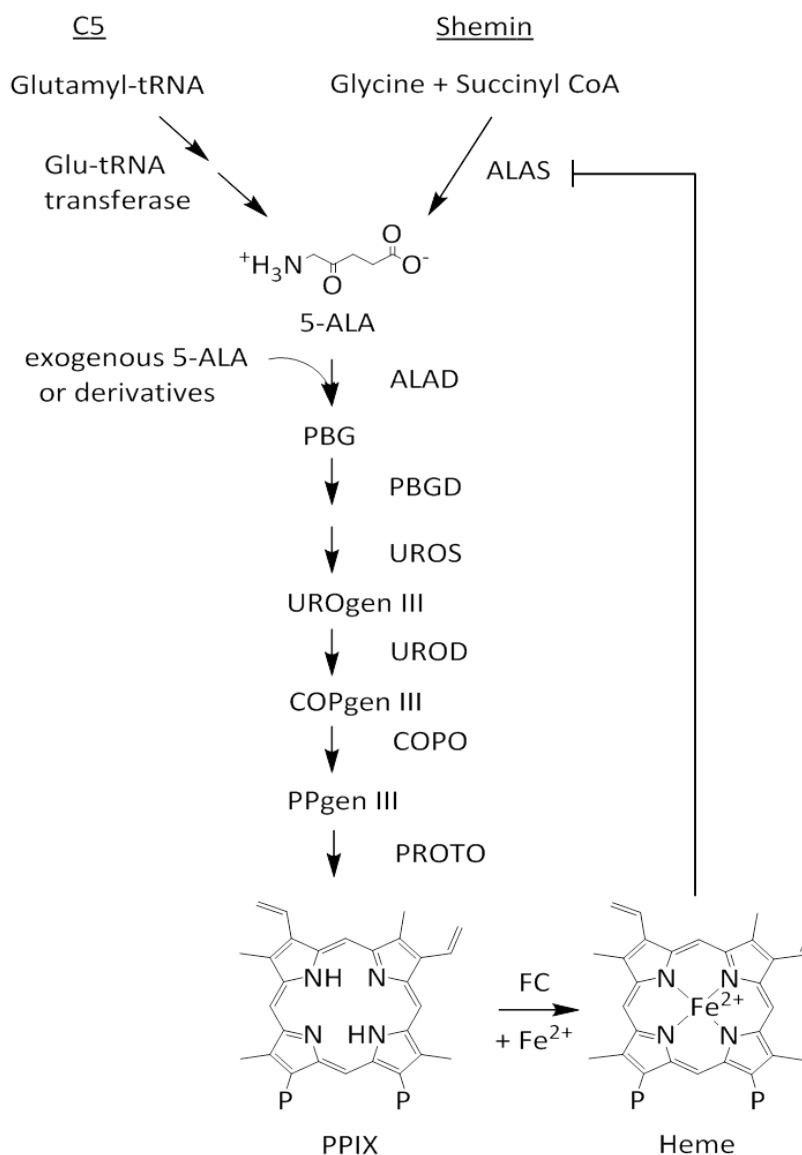


Fig. 3. Heme biosynthesis of prokaryotic (mostly C5-pathway) and eukaryotic cells (Shemin pathway). 5-ALA represents the first building block. Eight 5-ALA molecules are enzymatically assembled to PPIX. Ferrochelatase (FC) catalyzes the ferrous iron complexation by PPIX to heme. The heme cycle is regulated by a negative feedback mechanism of heme onto the synthesis of 5-ALA. The mechanism can be by-passed by applying exogenous 5-ALA and derivatives thereof. PBG: porphobilinogen, UROgenIII: uroporphyrinogen III, COPgenIII: coproporphyrinogen III, PPgenIX: protoporphyrinogen IX, ALAS: 5-ALA-synthase, ALAD: 5-ALA-dehydratase, PBGD: PBG-deaminase, UROS: UROIII synthase, UROD: UROIII decarboxylase, COPO: COPgen III oxidase, PROTO: PPgenIX oxidase

Another means for selective fluorescence generation is followed by PS prodrugs bearing the PS in a non-fluorescent/quenched form. Enzymatic cleavage at the target site “switches” the

molecule on for light emission. The PS can bear a functional group modifying the fluorophore as in the case of γ -glutamyl residue attached to hydroxymethyl rhodamine green. The fluorescence is restored upon cleavage of the γ -glutamyl residue by γ -glutamyl transpeptidases, which are overexpressed in some tumors [23].

PS molecules may also be closely assembled by attachment to a polymeric backbone or micelle forming phospholipids resulting in a self-quenching effect [15-17] [24]. Fluorescence is re-established once the target site is reached and the PS is cleaved enzymatically from the backbone. In the case of micelles disassembly into monomers, can be triggered through increased interstitial pressure or a change of pH.

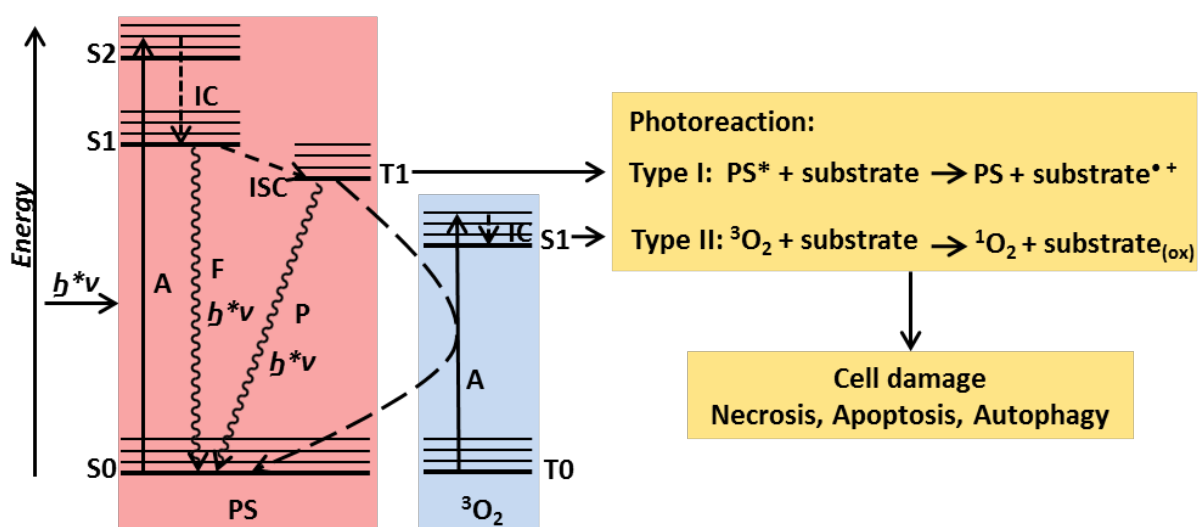


Fig. 4. Jablonski scheme of PS excitation. Absorption (A) of light energy transfers the molecule from the level of lowest energy (ground state, S0) into a higher excited state (S1, S2). The PS relaxes into the excited level of lowest energy (S1) by releasing excess energy as heat. The process is called internal conversion (IC). From the S1 level the PS can relax into the ground state by IC, light emission (fluorescence, F) or it may undergo intersystem crossing (ISC) into a triplet state (T1). Relaxation from T1 to S0 through light emission is called phosphorescence (P). Excess energy may also be transferred to a cellular substrate and trigger a Type I photoreaction or to triplet oxygen (3O_2). Energy transfer (A) to 3O_2 leads to highly reactive singlet state oxygen (1O_2) that oxidizes cellular components (Type II photoreaction). Depending on the PS and light dose, the photoreactions potentially lead to cell death.

Photosensitizers have a delocalized π -electron system capable of absorbing light of a certain wavelength. The process raises one valence electron of the chromophore from the ground state (S0) to a singlet state of higher energy (e.g. S1, S2) (Jablonski scheme, Fig. 4). Each singlet state is further divided into several vibrational and rotational energy levels. The excited state of a molecule is unstable and requires energy to be maintained. Therefore, the molecule tends to return to the ground state by releasing excess energy. Immediately after light absorption, the excited electron undergoes internal conversion, i.e. it relaxes into the excited state of lowest energy (and thus higher stability) by releasing non-radiative energy (heat). From the S1 level, the photosensitizer may reach the ground state in three different ways. The simplest one is non-radiative internal conversion. In fluorescence (F) energy is released by emission of a photon. The process marks the base for PD. Finally, the molecule can change its multiplicity from the singlet to a triplet excited state (T1). This step, referred to as intersystem crossing, involves a change of electron spin direction. From the metastable triplet state, the molecule may reach the ground state by photon emission (phosphorescence) or by transferring energy another molecule. This triggers two types of photoreaction and represents the underlying mechanism for PDT. Type I reactions describe the electron- or hydrogen transfer from a triplet state photosensitizer to another molecule in the tissue. This causes highly cytotoxic intermediates such as superoxides, hydroperoxyls, hydrogen peroxide or hydroxyl radicals (reactive oxygen species, ROS). In type II reactions, an energy transfer between the triplet PS and the ground-state triplet oxygen generates singlet oxygen. The singlet state of molecular oxygen is unstable and extremely reactive. Therefore, it forms adducts with cellular components such as lipids. The oxidative damage leads to a cascade of intra- and extra-cellular responses that trigger cell death and eventually the destruction and re-absorption of damaged tissue. PDT induced phototoxicity is regarded to occur mainly via type II reactions. The lifetime of singlet oxygen in cellular systems is considered to be 100-500 nanoseconds [25] with a diameter of action of up to 50 nm, depending on the cellular environment [26, 27]. This property of PDT is advantageous, since the damage to surrounding tissue is limited.

Ideally, a PS has no intrinsic toxicity, shows low skin photosensitization and is stable before and during application. It should absorb light distinctively to endogenous fluorophores such as collagen, ceroids and aromatic amino acids to maximize light penetration into the tissue. This can usually be avoided with photosensitizers absorbing light above 400 nm and having an emission maximum above 620 nm [10]. A long living triplet state is important to enable interaction with the surrounding tissue when the photosensitizer is used for PDT. Minimal

amounts of the agent should remain in the tissue after light treatment. For PD a high fluorescence yield and good selectivity are crucial. Depending on the irradiation time and light intensity, fluorophores lose their ability to absorb and emit light, a process called photobleaching. Even though it may be advantageous to limitation of prolonged skin photosensitization, it is important that photobleaching occur minimally during PD.

Cellular mechanism

Today, three mechanisms of cell death are discussed in association with PDT: necrosis, apoptosis and autophagy [28]. Necrosis is defined as uncontrolled, accidental cell death, where severe physical or chemical damage and acute cell injury disable the adenosine triphosphate (ATP)-production of the cell. Apoptosis is a programmed, ATP-driven cell death characterized by a series of changes in cell morphology and activation of caspases that cleave cellular substrates. Eventually the cell dissociates into membrane bound apoptotic bodies and is engulfed by neighbouring cells. Autophagy may be regarded as a recycling mechanism that helps to maintain the equilibrium between synthesis and degradation of cell components. The autophageal process is somehow ambiguous for the outcome of PDT. On one hand it exonerates the cell from cytotoxic ROS, on the other hand it may lead to cell death, depending on the extent of previous cell damage and the ability of the cell to undergo apoptosis. The main mechanism of cell death through PDT is assumed to be mitochondrially controlled apoptosis. However, it may differ according to the cell type, light dose, PS concentration and localization, as well as partial oxygen pressure [28-30].

Apart from instant cell eradication, PDT has a positive influence on the long-term tumor control by promoting auxiliary anti-tumor immune reactions [31, 32]. Hypoxic stress (due to vascular shutdown and oxygen consumption) initiates the release of inflammatory mediators. Such factors can also damage epithelial cells in tumor vasculature and promote vascular shut down. Finally, detrital cells and cell fragments stimulate the adaptive immune system. They may be phagocytosed, notably by dendritic cells that expose the tumor associated antigens to antigen recognising helper T-lymphocytes. This process initiates the development of immune memory against the tumor.

Nanoparticles for drug delivery

The therapeutic effect of a photoreactive compound in PDT can be modulated by the drug and the light dose, and the drug light interval. The development of easy-to-handle diode lasers and the use of optical fibres in combination with diffusers nowadays allow adequate delivery of light to almost any part of the body in a minimally invasive manner. All the same, it is pivotal for the PS to preferentially accumulate in the target tissue and only minimally in healthy tissue at a given time. The intrinsic tissue selectivity of a drug is dictated by its physicochemical properties, such as lipophilicity, molecular size, ionic charge and/or the presence of functional groups. Most hydrophobic PS collocate in cytosolic sites, i.e. Golgi, endoplasmic reticulum, mitochondria, lysosomes and membranes, making these structures the main targets for damage through PDT. Hydrophilic PSs lead to tumor ablation by vascular shut-down as they accumulate in the vasculature. Protein binding properties of the PS and the physiological environment of the target, for example pH and high metabolic turnover in neoplastic tissue, further broaden the selectivity criteria. For example, hydrophobic PSs bind to low density lipoproteins and may thus be transported into the cell through the membranous LDL receptor. Finally, due to physiological changes, neoplastic tissue acts as a “trap” for some therapeutic drugs [33]. Microenvironmental changes of tumor tissues are discussed in the literature review following this introduction.

It is widely accepted that the selectivity of a drug may be influenced by the vehicle in which it is formulated. During the past three decades major attention was given to the development of biodegradable polymeric nanoparticles for drug delivery [34], an idea first addressed in the 1960's by Speiser et al. [35, 36]. Today, several nanoparticulate formulations are marketed for per-oral, topical and systemic administration. They include nanocrystals, consisting of a water-insoluble drug milled to nano-sized particles (e.g. Ritalin LA[®], Novartis), drug-albumin agglomerates (Abraxane[®], Celgene), liposomes (Myocet[®], GP Pharm) and dendrimers (Vivagel, Starpharma Holdings) [37].

In recent years extensive research has been performed on the development of nanoparticles made from biodegradable polymers destined for various applications, such as the intraocular, inhalative or parenteral route.

According to the definition of the Encyclopedia of Pharmaceutical Technology, polymeric nanoparticles are “solid colloidal particles ranging in size from 10 to 1000 nm. They consist of macromolecular materials in which the active principle (drug or biologically active

material) is dissolved, entrapped, encapsulated and/or to which the principle is adsorbed or attached” [38]. These subcellular sized entities can be engineered in such way that the pharmacokinetic characteristics of the active principle may vary considerably. Thus, an active compound with adequate pharmacodynamic properties, but unsatisfying pharmacokinetic characteristics (e.g. low water solubility, insufficient cell penetration) may be rendered suitable for application by nanoencapsulation. Owing to their size, nanoparticles predominantly extravasate into tissues with fenestrated vasculature (e.g. neoplasms). This diminishes the probability of adverse effect and increases patient compliance. In the lung the small size promotes penetration of the thick mucus and diminishes the fast clearance by expectoration. The large surface area of nanoparticles allows the attachment of functional moieties to further improve tissue selectivity. Hydrophilic molecules, such as polyethylene glycol (PEG), reduce the recognition by macrophages. This increases the circulation half time of the particles in the blood or retention time in the lung. The attachment of active targeting moieties such as antibodies enhances the interaction with cellular receptors [39].

Until now the United States Food and Drug Administration (FDA) has approved four biocompatible polymers, polylactic acid (PLA), polyglycolic acid (PGA), polylactic-co-glycolic acid (PGLA), and polycaprolactone (PCL) for the use as suture material or implants [40]. The polymers are suitable for the formation of nanoparticles by various techniques. The protocol for particle preparation needs to be adapted to the drug of interest. Thus, drug loading and loading efficiency are strongly dependent on the type of the polymer, the organic solvent, the type of surfactant, if any, as well as pH- and ion-strength regulating substances in the aqueous or organic phase [41-45]. The miscibility of the organic and aqueous phase dictates the applied production method. One can distinguish three main mechanisms of nanoparticle formation in an oil-in-water system [46]. In all three processes the polymer and the drug are dissolved in the organic phase. This solution is dispersed into an aqueous phase optionally containing a surfactant such as polyvinyl alcohol or poloxamers. A drug may be encapsulated with higher efficiency, when the affinity of the drug to the polymer is higher than to the aqueous phase [43, 47].

A simple and cost effective method is the solvent displacement technique (nanoprecipitation). As described above, it implies the use of a water miscible solvent such as acetone or ethanol. The water miscibility leads to the spontaneous emulsification of the polymer containing organic solution into the aqueous phase. Subsequent interfacial turbulences, driven by

interfacial tension differences and local supersaturation of droplets containing the dissolved polymer, result in the nucleation of polymer precipitates [46, 48].

Emulsion-evaporation is used when the organic solvent (e.g. dichloromethane) is not miscible with water. It implies the emulsification of the organic phase by high mechanical impaction using a homogenizer or a sonicator probe to create nano-droplets. The emulsion is stabilized with high concentrations of surfactant during solvent evaporation. Nano-encapsulation by emulsion evaporation is generally limited to lipophilic drugs. However, hydrophilic drugs have been encapsulated by adding an emulsification step prior to formation of the oil in water emulsion. The hydrophilic drug is dissolved in an aqueous medium and emulsified in the organic phase. The water-in-oil (W/O) emulsion is subsequently dispersed into an aqueous outer phase, resulting in a water-in-oil-in-water (W/O/W) emulsion [49, 50].

When using a solvent of partial water miscibility and low volatility (e.g. benzyl alcohol) particle formation may be provoked by extracting the organic solvent into a large volume of the aqueous phase as in the emulsification-diffusion method [51]. The solvent diffusion is controlled by gradual addition of the aqueous phase. The method may be applied in a varied form, referred to as salting-out method, with water miscible solvents, e.g. acetone. The miscibility of acetone with water is initially prevented by the saturation of the aqueous phase with an electrolyte such as magnesium chloride. By adding water to the external phase the electrolyte concentration is lowered and allows the acetone to diffuse slowly from the organic phase into the aqueous medium. As a result the solvent concentration in the aqueous phase remains low. This is of interest, when a water insoluble drug is rendered soluble by the presence of the solvent [47].

Efficient encapsulation of hydrophilic and amphiphilic drugs into polymeric nanoparticles remains challenging when using the above described methods, as the compounds readily leach into the dispersing aqueous phase. Recently, new bottom-up approaches based on the spray drying technique have been developed that generate particles of down to several 100 nm [52]. The key element is the formation of solute nano-droplets from which solid nanoparticles emerge during solvent evaporation. In the aerosol flow reactor method (Fig. 5), the solution is atomized with a highly pressurized nitrogen carrier gas air jet. The droplets are then directed through a heated tubular laminar flow reactor for controlled solvent evaporation. At reactor downstream, the aerosol is strongly diluted with nitrogen gas (e.g. 25 L/min) to avoid nanoparticle deposition on the tubing wall before sampling for size measurement and/or collection for further processing (Fig. 6). Since the dispersion medium consists of an inert gas,

the drug entrapment during particle formation is maximal. Consequently, entrapment efficiency is close to 100%.

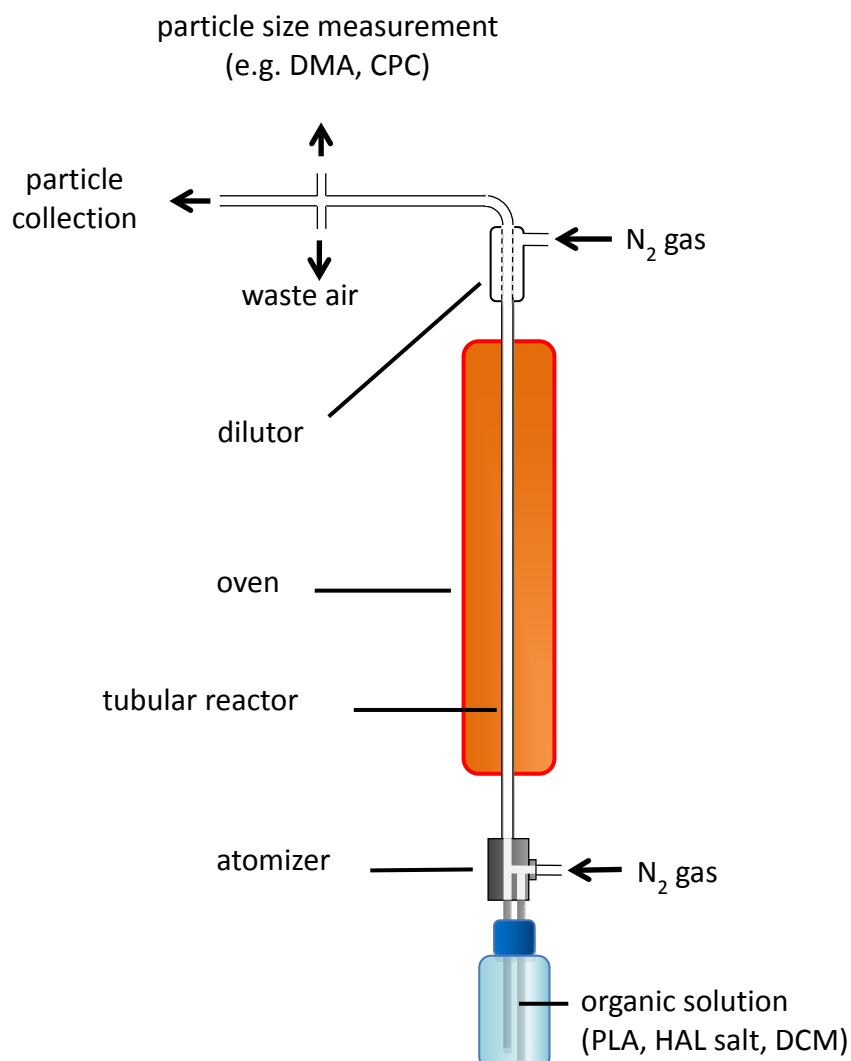


Fig. 5. Schematic set-up of the aerosol flow reactor for nanoparticle formation. The organic solution is atomized with a highly pressurized nitrogen carrier gas air jet. Subsequently, the solvent evaporates in the heated reactor tube. The evaporation generates a highly dispersed nanoparticle aerosol. The aerosol is diluted with nitrogen gas to prevent particle deposition on the tubing wall before particle collection and size measurement with a differential mobility analyzer (DMA) connected to a condensation particle counter (CPC).

Chapter 2 describes the preparation of HAL-laden nanoparticles by nanoprecipitation. The use of such a formulation on a T24 human bladder carcinoma and other cell lines induces higher porphyrin fluorescence compared to the free compound. Interestingly, the effect was found to

be due to an interaction of PPIX with the nanoparticles rather than higher porphyrin accumulation. To improve the drug loading of nanoparticles was applied the aerosol flow reactor method (chapter 3) [53].

PDT of bacteria

Although the effect of light on photosensitized microorganisms formed the starting block of PDT, interest in this application in microbiology lost attraction with Alexander Fleming's discovery of penicillin in 1928. However, bacteria have the ability to rapidly adapt to their environment. Excessive prescription of antibiotics, their misuse in animal husbandry and inappropriate treatment of patients have fostered a racing duel between the emergence of multi-resistant bacterial strains and the development of new anti-bacterial strategies, returning the interest towards antibacterial PDT, usually referred to as photodynamic inactivation (PDI) of bacteria.

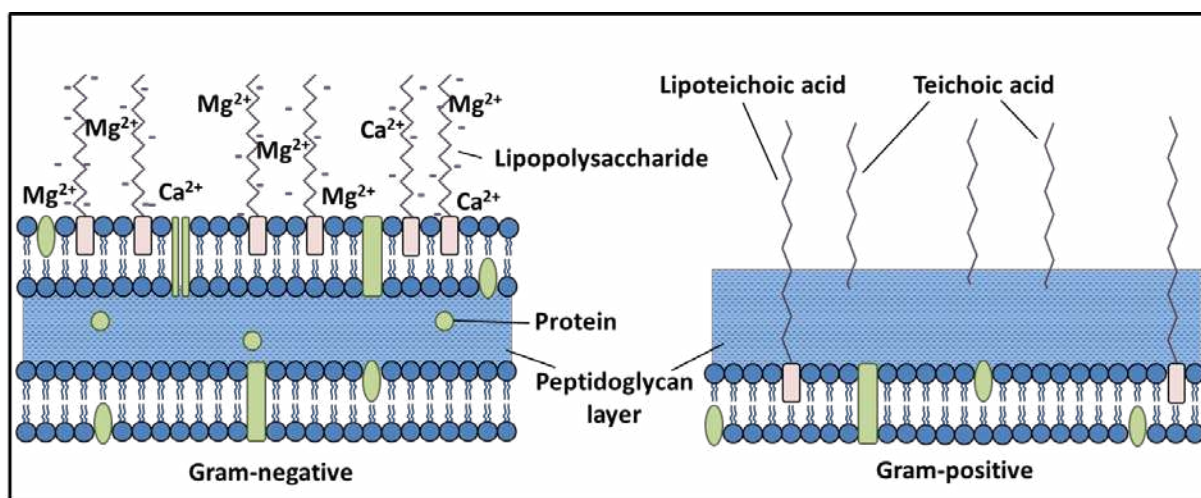


Fig. 6. Bacterial cell wall of Gram negative and Gram positive bacteria.

Similarly to eukaryotic cells bacteria accumulate porphyrins after treatment with 5-ALA and/or derivatives (Fig. 3) [54]. Chapter 4 describes a newly found enzymatic system generating PPIX by iron extraction from heme. The system was assessed with respect to bacterial photosensitization and the role of TolC, a bacterial multidrug efflux pump, for the export of PPIX was investigated. The results are presented in chapter 5.

Gram-positive and Gram-negative bacteria differ in their cell-wall architecture (Fig. 6). The cell wall of Gram-negative bacteria is made up of an inner and outer cell membrane separated by a peptidoglycane containing periplasmic space. From the outer cell membrane protrude negatively charged lipopolysaccharides stabilized by magnesium and calcium ions. The alternating lipophilic and hydrophilic layers of the Gram-negative cell wall impede the penetration of extrinsic molecules. The structure of the cell wall of Gram-positive bacteria is simpler with only one lipid bilayer followed by a peptidoglycan layer containing lipoteichoic and teichoic acids (teichos = wall, greek). It is therefore not surprising, that PDI has so far been more successful on Gram-positive bacteria [55]. A prerequisite for PS for PDI on Gram-negative bacteria is a cationic charge to allow tight interaction with the lipopolysaccharides. Destabilizing agents such as polymyxin may interfere with the structure of the lipid bilayer or complex Mg^{2+} and Ca^{2+} (EDTA), which triggers the release of lipopolysaccharides. The PS may also be conjugated to a positively charged polymer backbone (e.g. poly lysine) to improve the cell wall affinity [55, 56].

Objective of the thesis

The objective of the present work was to explore possibilities for the induction of porphyrins in eukaryotic and prokaryotic cells. The literature review following this introduction describes the concept of endogenously induced photosensitizer generation and depicts the numerous approaches devoted to improve tumor selectivity and bioavailability of the PPIX precursors.

Part A (chapter 2 and 3) focuses on the formulation of HAL into polymeric nanoparticles in order to make HAL suitable for systemic applications, e.g. by injection or inhalation.

Part B (chapters 3 and 4) describes the finding of a new PPIX generating mechanism, namely deferrochelation, in *E.coli.*, mediated by the bacterial dye decolorizing peroxidase, YfeX. Deferrochelation implies the inversion of the ultimate heme synthesis step of incorporation of iron into the PPIX skeleton [57]. Moreover, we investigated the efficacy of the mechanism for the use in antibacterial photodynamic activation (PDI) as well as the role of the multi-drug efflux pump TolC for accumulation of PPIX in *E.coli.*

Reference List

1. Raab O. Effect of fluorescent substances on Infusoria. *Z Biol* 1900; **39**: 524-46.
2. Meyer-Betz F. Wirkung des Hämatoporphyrins und anderer Derivate des Blut- und Gallenfarbstoffs. *Dtsch Arch Klin Med* 1913; **112**: 476-503.
3. Dai T, Huang YY, Hamblin MR. Photodynamic therapy for localized infections-State of the art. *Photodiagn Photodyn* 2009; **6**: 170-88.
4. Piccioni A, Fargnoli MC, Schoinas S et al. Efficacy and tolerability of 5-aminolevulinic acid 0.5% liposomal spray and intense pulsed light in wrinkle reduction of photodamaged skin. *J Dermatol Treat* 2011; **22**: 247-53.
5. Butani A, Dudelzak J, Goldberg DJ. Recent advances in laser dermatology. *J Cosmet Laser Ther* 2009; **11**: 2-10.
6. Benabbou AK, Guillard C, Pigeot-Rémy S et al. Water disinfection using photosensitizers supported on silica. *J Photochem Photobiol A* 2011; **219**: 101-8.
7. Ferro S, Guidolin L, Tognon G et al. Mechanisms involved in the photosensitized inactivation of *Acanthamoeba palestinensis* trophozoites. *J Appl Microbiol* 2009; **107**: 1615-23.
8. Sasaki K, Watanabe M, Tanaka T. Biosynthesis, biotechnological production and applications of 5-aminolevulinic acid. *Appl Microbiol Biotechnol* 2002; **58**: 23-9.
9. Policard A. Etudes sur les aspects offerts par des tumeurs experimentales examinées sous la lumière de Wood. *Compte Rendu de la Société de Biologie* 1924; **91**: 1423-8.
10. Wagnieres GA, Star WM, Wilson BC. In vivo fluorescence spectroscopy and imaging for oncological applications. *J Photochem Photobiol* 1998; **68**: 603-32.
11. Abe H, Kuroki M, Tachibana K et al. Targeted sonodynamic therapy of cancer using a photosensitizer conjugated with antibody against carcinoembryonic antigen. *Anticancer Res* 2002; **22**: 1575-80.
12. Bhatti M, Yahioğlu G, Milgrom LR et al. Targeted photodynamic therapy with multiply-loaded recombinant antibody fragments. *Int J Cancer* 2008; **122**: 1155-63.
13. Hamblin MR, Miller JL, Hasan T. Effect of charge on the interaction of site-specific photoimmunoconjugates with human ovarian cancer cells. *Cancer Res* 1996; **56**: 5205-10.
14. Vrouenraets MB, Visser GWM, Stigter M et al. Comparison of aluminum (III) phthalocyanine tetrasulfonate- and meta-tetrahydroxyphenylchlorin-monoclonal antibody conjugates for their efficacy in photodynamic therapy in vitro. *Int J Cancer* 2002; **98**: 793-8.

15. Gabriel D, Zuluaga MF, Lange N. On the cutting edge: protease-sensitive prodrugs for the delivery of photoactive compounds. *Photochem Photobiol Sci* 2011; **10**: 689-703.
16. Gabriel D, Campo MA, Gurny R, Lange N. Tailoring protease-sensitive photodynamic agents to specific disease-associated enzymes. *Bioconjugate Chem* 2007; **18**: 1070-7.
17. Campo MA, Gabriel D, Kucera P et al. Polymeric photosensitizer prodrugs for photodynamic therapy. *J Photochem Photobiol* 2007; **83**: 958-65.
18. Hamblin MR, Del GM, Rizvi I, Hasan T. Biodistribution of charged 17.1A photoimmunoconjugates in a murine model of hepatic metastasis of colorectal cancer. *Br J Cancer* 2000; **83**: 1544-51.
19. Heinemann IU, Jahn M, Jahn D. The biochemistry of heme biosynthesis. *Arch Biochem Biophys* 2008; **474**: 238-51.
20. Uehlinger P, Zellweger M, Wagnieres G et al. 5-Aminolevulinic acid and its derivatives: physical chemical properties and protoporphyrin IX formation in cultured cells. *J Photochem Photobiol B* 2000; **54**: 72-80.
21. Lange N, Jichlinski P, Zellweger M et al. Photodetection of early human bladder cancer based on the fluorescence of 5-aminolaevulinic acid hexylester-induced protoporphyrin IX: a pilot study. *Br J Cancer* 1999; **80**: 185-93.
22. Marti A, Lange N, van den Bergh H et al. Optimisation of the formation and distribution of protoporphyrin IX in the urothelium: an in vitro approach. *J Urol* 1999; **162**: 546-52.
23. Urano Y, Sakabe M, Kosaka N et al. Rapid Cancer Detection by Topically Spraying a gamma-Glutamyltranspeptidase-Activated Fluorescent Probe. *Sci Transl Med* 2011; **3**: 110ra9.
24. Lovell JF, Jin CS, Huynh E et al. Porphysome nanovesicles generated by porphyrin bilayers for use as multimodal biophotonic contrast agents. *Nat Mater* 2011; **10**: 324-32.
25. Kanofsky JR. Measurement of singlet-oxygen in vivo: progress and pitfalls. *J Photochem Photobiol* 2011; **87**: 14-7.
26. Kuimova MK, Yahioglu G, Ogilby PR. Singlet Oxygen in a Cell: Spatially Dependent Lifetimes and Quenching Rate Constants. *J Am Chem Soc* 2009; **131**: 332-40.
27. Redmond RW, Kochevar IE. Spatially resolved cellular responses to singlet oxygen. *J Photochem Photobiol* 2006; **82**: 1178-86.
28. Mroz P, Yaroslavsky A, Kharkwal GB, Hamblin MR. Cell death pathways in photodynamic therapy of cancer. *Cancers* 2011; **3**: 2516-39.
29. Chen Q, Huang Z, Chen H et al. Improvement of tumor response by manipulation of tumor oxygenation during photodynamic therapy. *J Photochem Photobiol* 2002; **76**: 197-203.

30. Fuchs J, Thiele J. The Role of Oxygen in Cutaneous Photodynamic Therapy. *Free Radical Bio Med* 1998; **24**: 835-47.
31. Garg AD, Nowis D, Golab J, Agostinis P. Photodynamic therapy: illuminating the road from cell death towards anti-tumour immunity. *Apoptosis* 2010; **15**: 1050-71.
32. Castano AP, Mroz P, Hamblin MR. Photodynamic therapy and anti-tumour immunity. *Nat Rev Cancer* 2006; **6**: 535-45.
33. Maeda H, Wu J, Sawa T et al. Tumor vascular permeability and the EPR effect in macromolecular therapeutics: a review. *J Control Release* 2000; **65**: 271-84.
34. Kreuter J. Nanoparticles - a historical perspective. *Int J Pharm* 2007; **331**: 1-10.
35. Khanna SC, Soliva M, Speiser P. Epoxy resin beads as a pharmaceutical dosage form. II. Dissolution studies of epoxy-amine beads and release of drug. *J Pharm Sci* 1969; **58**: 1385-8.
36. Khanna SC, Speiser P. Epoxy resin beads as a pharmaceutical dosage form. I. Method of preparation. *J Pharm Sci* 1969; **58**: 1114-7.
37. Bawa R. Nanoparticle-based therapeutics in humans: a survey. *Nanotechnology Law & Business* 2008; **5**: 135-55.
38. Kreuter J. Nanoparticles. In: Swarbrick JB, J.C. , ed. *Encyclopedia of Pharmaceutical Technology*. New York: Dekker, M. 1994:165-90.
39. Zeisser-Labouèbe MV, A.; Delie, F. Nanoparticles for photodynamic therapy of cancer. In: Kumar SSR, ed. *Nanomaterials for Cancer Therapy*. Weinheim Wiley-VCH 2006:40-86.
40. Administration USFaD. FDA-Inactive ingredients database. 2011 [cited; Available from: <http://www.fda.gov/Drugs/InformationOnDrugs/ucm113978.htm>]
41. Galindo-Rodriguez S, Allemann E, Doelker E, Fessi H. Versatility of three techniques for preparing ibuprofen-loaded methacrylic acid copolymer nanoparticles of controlled sizes. *J Drug Deliv Sci Technol* 2005; **15**: 347-54.
42. Konan YN, Chevallier J, Gurny R, Allemann E. Encapsulation of p-THPP into nanoparticles: Cellular uptake, subcellular localization and effect of serum on photodynamic activity. *J Photochem Photobiol* 2003; **77**: 638-44.
43. Barichello JM, Morishita M, Takayama K, Nagai T. Encapsulation of hydrophilic and lipophilic drugs in PLGA nanoparticles by the nanoprecipitation method. *Drug Dev Ind Pharm* 1999; **25**: 471-6.
44. Bilati U, Allemann E, Doelker E. Development of a nanoprecipitation method intended for the entrapment of hydrophilic drugs into nanoparticles. *Eur J Pharm Sci* 2005; **24**: 67-75.
45. Govender T, Stolnik S, Garnett MC et al. PLGA nanoparticles prepared by nanoprecipitation: drug loading and release studies of a water soluble drug. *J Control Release* 1999; **57**: 171-85.

46. Quintanar-Guerrero D, Allemann E, Fessi H, Doelker E. Preparation techniques and mechanisms of formation of biodegradable nanoparticles from preformed polymers. *Drug Dev Ind Pharm* 1998; **24**: 1113-28.
47. Layre A-M, Gref R, Richard J et al. Nanoencapsulation of a crystalline drug. *Int J Pharm* 2005; **298**: 323-7.
48. Beck-Broichsitter M, Rytting E, Lehardt T et al. Preparation of nanoparticles by solvent displacement for drug delivery: A shift in the "ouzo region" upon drug loading. *Eur J Pharm Sci* 2010; **41**: 244-53.
49. Bilati U, Allemann E, Doelker E. Poly(D,L-lactide-co-glycolide) protein-loaded nanoparticles prepared by the double emulsion method-processing and formulation issues for enhanced entrapment efficiency. *J Microencapsul* 2005; **22**: 205-14.
50. Zambaux MF, Bonneaux F, Gref R et al. Influence of experimental parameters on the characteristics of poly(lactic acid) nanoparticles prepared by a double emulsion method. *J Control Release* 1998; **50**: 31-40.
51. Quintanar-Guerrero D, Allemann E, Doelker E, Fessi H. A mechanistic study of the formation of polymer nanoparticles by the emulsification-diffusion technique. *Colloid Polym Sci* 1997; **275**: 640-7.
52. Chan H-K, Kwok PCL. Production methods for nanodrug particles using the bottom-up approach. *Adv Drug Deliv Rev* 2011; **63**: 406-16.
53. Eerikäinen H, Watanabe W, Kauppinen EI, Ahonen PP. Aerosol flow reactor method for synthesis of drug nanoparticles. *Eur J Pharm Biopharm* 2003; **55**: 357-60.
54. Fotinos N, Convert M, Piffaretti JC et al. Effects on gram-negative and gram-positive bacteria mediated by 5-aminolevulinic acid and 5-aminolevulinic acid derivatives. *Antimicrob Agents Chemother* 2008; **52**: 1366-73.
55. Durantini EN. Photodynamic inactivation of bacteria. *Curr Bioact Compd* 2006; **2**: 127-42.
56. Hamblin MR, Hasan T. Photodynamic therapy: a new antimicrobial approach to infectious disease? *Photochem Photobiol Sci* 2004; **3**: 436-50.
57. Letoffe S, Heuck G, Delepelaire P et al. Bacteria capture iron from heme by keeping tetrapyrrol skeleton intact. *Proc Natl Acad Sci USA* 2009; **106**: 11719-24.

Review

Chapter 1. Exogenously induced Endogenous Photosensitizers

Gesine Heuck and Norbert Lange

Department of Pharmaceutical Technology, School of Pharmaceutical Sciences, University of Geneva, University of Lausanne, 30, Quai Ernest Ansermet, CH – 1211 Geneva 4, Switzerland

Published in: Photosensitizers in Medicine, Environment and Security, edited by T. Nyokong, V. Ahsen, Springer Dordrecht, Heidelberg, London, New York, 391-431, 2012

ABSTRACT. The photosensitizing properties of endogenous porphyrins have been discovered about 100 years ago. Since then they have become an attractive means to detect and treat neoplastic tissue by fluorescence photodetection (PD) and photodynamic therapy (PDT), respectively. The probably most important endogenous photosensitizer is protoporphyrin IX (PPIX), the direct precursor of heme. It accumulates preferentially in neoplastic cells upon administration of 5-aminolevulinic acid (5-ALA). 5-ALA is an early precursor of heme, when applied exogenously it takes up the function of a prodrug, which is converted into PPIX by the enzymes of the heme biosynthetic pathway. Numerous approaches have been undertaken to improve the pharmacodynamics and pharmacokinetics of 5-ALA PDT with respect to tissue selectivity and biocompatibility. This chapter shall give an overview of the methods used to optimize 5-ALA PDT and PD.

Keywords: 5-aminolevulinic acid, cancer, drug delivery, fluorescence photodetection, heme, hexyl ester, photodynamic therapy, protoporphyrin IX

Introduction

Life on our planet as it exists today would probably not be possible without porphyrins. The wide distribution of these tetrapyrrol structures in fossil sediments attests their existence dating back as far as the first appearance of oxygen in the earth's atmosphere.

The benefit of porphyrins for medical purposes was discovered only in the second half of the 20th century, although their pathological manifestation was already noticed in ancient Greece by Celsus, Galen and Hippocrates. The latter described a patient having peculiar symptoms: "fears and much rambling, depression and light feverishness. Early in the morning frequent convulsion, whenever these frequent convulsions intermitted, she wandered and uttered obscenities; many pains, severe and continuous." Towards the end of the episode, her urine turned black [1]. The statement appears to be the first record of a group of diseases which much later, in the 19th century, will be known as porphyrias [2-4]. The characteristic symptoms of some of these disorders, notably the purple/red coloured stool and urine (porphurous = greek for purple) in combination with psychotic attacks led scientists and historians to retrospective diagnoses in various subjects, going as far as making porphyrias responsible for political turnovers. An example is the case of King George III, who was known for his "madness" [5]. The probability, that George III's attacks originated from porphyria is supported by the fact that two living descendants of the king suffer from variegate porphyria [6]. Symptoms of the extremely rarely occurring congenital erythropoietic porphyria, notably the pale, yellow skin, red teeth, skin aberrations, protruding teeth, avoidance of sunlight and blood thirst often accompanied by psychotic attacks and sometimes hypertrichosis (see Fig. 1), has even led scientists to explain the occurrence of werewolves and vampires [7;8]. Admittedly, the resemblance between the disease and descriptions in historical reports, together with the independent appearance of these legendary creatures in different areas on the globe give an attractive basis for such a hypothesis. Nevertheless, porphyria as possible explanation for the occurrence of legendary creatures is a step too daring.

Scherer was the first to describe the chemistry of endogenous porphyrins in 1841 [9]. He treated a dried blood sample with sulfuric acid, removed the free iron, and dissolved the water-insoluble product in ethanol. He obtained a substance of blood-red colour, which he called "iron-free hematin". Hoppe-Seyler later gave the compound the name "hematoporphyrin" [10].



Fig. 1. Photo showing a patient with congenital erythropoietic porphyria featuring severe mutilations as well as hypertrichosis.

In 1913, the German physician Meyer-Betz used hematoporphyrin in a self-experiment and injected himself 200 mg of the substance. When exposing parts of his skin to sunlight, he obtained lesions that remained for several weeks (Fig. 2). Meyer-Betz' experiment provided evidence for the close relationship between the red pigments in the urine of patients with certain forms of porphyria and their sensitivity to light [11].

In 1924 Policard observed that tumor tissue intrinsically exhibited more fluorescence than normal tissue [12]. The underlying cause, namely the preferential accumulation of porphyrins in neoplastic tissue, was identified by Auler and Banzer [13]. They also observed that injection of exogenous hematoporphyrin increased tumor fluorescence. The findings were confirmed by several studies until the mid nineteen fifties [14-16]. However, the application of hematoporphyrin for the cancer detection by fluorescence came along with a pronounced phototoxic effect. This inconvenience was due to the need of high drug doses, in order to obtain a satisfying fluorescence signal.

Schwartz et al. compared purified with raw hematoporphyrin material. To their surprise they observed stronger tumor fluorescence and higher response to x-ray radiation using the impure compound, rather than with the purified hematoporphyrin [17]. Although Schwartz did not identify the exact nature of the impurity fraction, it can be assumed that it consisted of a com-

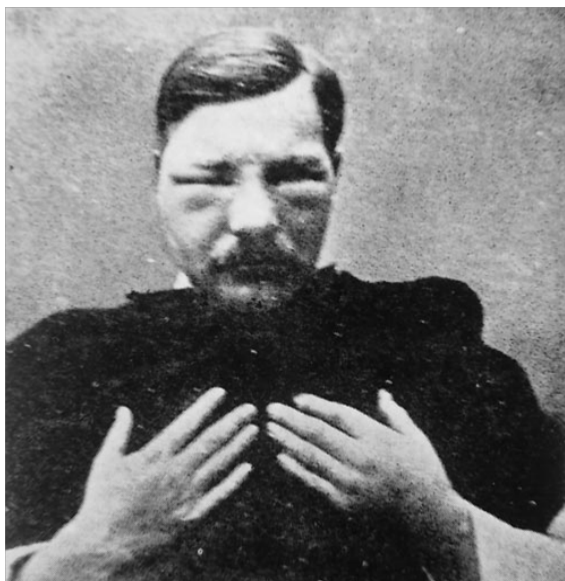


Fig. 2. Photo of Friedrich Meyer-Betz featuring lesions on face and hands after self-injection of 200 mg hematoporphyrin and exposure to sunlight.

plex mixture of porphyrin monomers and oligomers. Lipson et al. treated crude hematoporphyrin with glacial acetic acid and sulfuric acid and obtained hematoporphyrin derivative (HpD). Detection and treatment of cancer with HpD was superior to treatment with crude hematoporphyrin [18;19]. Also, lower doses of HpD could be applied [18]. In 1972 Diamond et al. observed an increase of tumor cell death *in vitro* and *in vivo* upon pre-treatment with HpD and after irradiation with cool light [20].

Three years later Dougherty et al. succeeded in the complete tumor removal in mice after application of HpD and subsequent exposure to red light [21]. Dougherty further optimized the HpD formulation by removing the monomers in the mixture, which were attributed the part for phototoxicity due to their high water solubility. The final compound, now called Porfimer sodium, obtained marketing authorization as Photofrin[®]. It is probably still the most widely used photosensitizer in medical care. Nevertheless, a major drawback remains the low selectivity of the substance, leading to skin photosensitization of subjects treated with this drug. The gravity of this adverse effect becomes even more important, when considering that cancer therapy is most often of palliative rather than curative matter. The necessity to prevent the exposure of patients to light annihilates the primary aim of palliative cancer treatment, which is the improvement of quality of life.

Realizing this problem, research focused on more selective ways of treatment in the field of photodynamic therapy (PDT) and fluorescence photodetection (PD). A breakthrough was achieved by Kennedy et al. who exogenously applied the heme precursor 5-aminolevulinic ac-

id (5-ALA) [22]. He hypothesized that PPIX, the penultimate precursor of heme with photosensitizing properties, would accumulate in the cell, if the negative feedback of heme on the biosynthesis of the early heme precursor 5-ALA is by-passed. If now the production of PPIX is faster than its transformation into heme, then PPIX will accumulate. Effectively, Kennedy found a particularly high accumulation of protoporphyrin IX (PPIX) in tumor tissue after administration of 5-ALA [22].

Tab.1. Commercialized products containing 5-ALA or derivatives

Name	Compound	Formulation	Indication	Country of licence
Levulan® Kerastick® (Dusa)	5-ALA	Alcoholic solution with application stick	Treatment of actinic keratosis	USA
Metvix® (Photocure)	5-ALA methyl ester	Cream	Treatment of precancerous and skin cancer lesions, e.g. actinic keratosis	A, AUS, B, D, DK, E, F, I, N, NZ, USA, S
Hexvix® (Photocure)	5-ALA hexyl ester	Powder for solution	Detection of bladder cancer	A, D, E, F, N, S
Gliolan® (Photonamic)	5-ALA	Powder for oral solution	Fluorescence guided resection of malignant glioma	D
Effala ® / Alacare® (Intendis)	5-ALA	Medicated plaster	Treatment of actinic keratosis	A, D, DK, E, F, FIN, IRL, I, N, PL, P, S
Cysview® (Photocure)	5-ALA hexyl ester	Powder for solution	Detection of bladder cancer	USA

The pharmacokinetics of 5-ALA together with the particular physiology of tumor cells provide the heme precursor with the attribute to accumulate preferentially in neoplastic tissue and

to be cleared within hours instead of days or weeks. This in turn reduces skin photosensitization and gives 5-ALA a major advantage over preformed photosensitizers. Today, 6 products containing 5-ALA and two of its derivatives are authorized on the market for the visualization or treatment of malignant tissue (see Table 1).

The heme biosynthetic pathway and pathological implications

Heme is essential for many processes in living organisms. Apart from its role as oxygen binding unit in red blood cells in mammals and invertebrates, it is an important metabolic cofactor in cytochrome associated enzymes. The pivotal function of heme in a living organism explains why it was found to be one of the earliest biomolecules. Palaeo-chemical investigations led to the conclusion that living organisms produced heme already four billion years ago. Its formation takes place in virtually all nucleated cells and particularly in tissues with high metabolic turnover, such as bone marrow and the liver.

The biosynthesis of heme includes eight consecutive steps, each one involving a different enzyme (see Fig. 3). Four enzymes are located in the mitochondria, while the other four enzymes operate in the cytoplasm. They are kept under strict feedback control to prevent the overproduction of intermediate products during heme biosynthesis. Genetic mutation, and/or enzyme malfunction may disturb the equilibrium, which may result in the accumulation of cytotoxic byproducts. This is why diseases involving a malfunction of the heme cycle have been grouped as porphyrias. Depending on the type of mutation and the involved enzyme, different forms of porphyria may develop.

The biochemistry of the heme biosynthesis has been reviewed in detail elsewhere [23-25]. Therefore the following intercept shall only shortly recall the respective steps to provide a better understanding of the pharmacodynamics of 5-ALA.

The basis of all biologically produced tetrapyrrols, be it in bacteria, mammals or plants, is the onset of 5-ALA and its subsequent transformation into uroporphyrinogen III (UROgenIII) [26]. While most bacteria and plants biosynthesize 5-ALA from glutamic acid in a two-step reaction, eukaryotes form 5-ALA by condensation of glycine with succinyl-CoA. The reaction takes place in mitochondria and is catalyzed by ALA-synthase (ALAS) [27]. There are two isoforms of ALAS: ALAS I, the housekeeping enzyme, is expressed throughout the body, whereas the erythropoietic ALAS II only occurs in bone marrow. Mutation of the ALAS II

encoding gene, which is located on the X-chromosome, leads to x-linked sideroblastic anaemia [23].

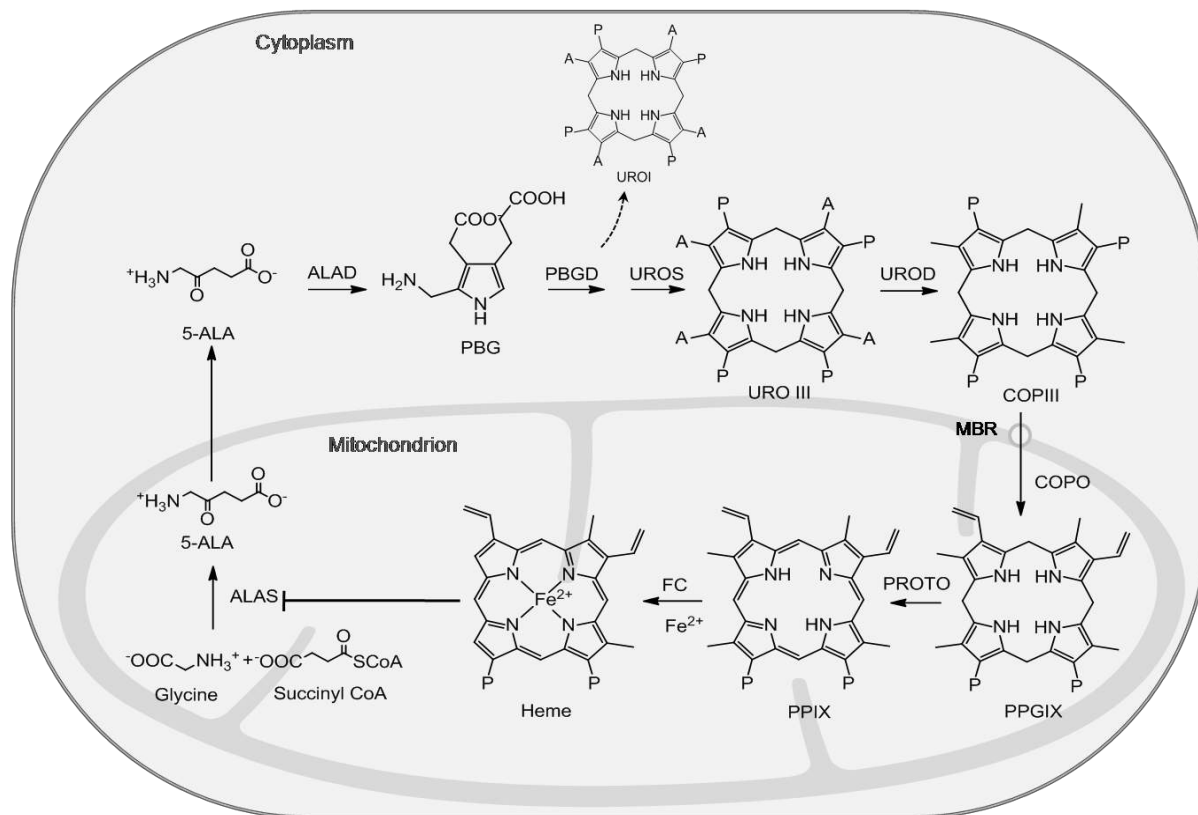


Fig. 3. The heme biosynthesis pathway. The first step, catalyzed by ALA-synthase (ALAS), consists of the mitochondrial synthesis of 5-aminolevulinic acid (5-ALA) from glycine and succinyl CoA. In the cytosol eight 5-ALA molecules are condensed in four consecutive steps to coproporphyrinogen III (COPgenIII). Each reaction is catalyzed by the corresponding enzyme. The formation uroporphyrinogen III (UROgenIII) involves the asymmetric condensation of 4 porphobilinogen molecules (PBG). Non-enzymatic, symmetric condensation leads to biologically inactive uroporphyrin I (UROI). COPgenIII is translocated into mitochondria, where its structure is transformed to protoporphyrin IX (PPIX). Subsequently, ferrochelatase (FC) mediates the complexation of Fe^{2+} by this tetrapyrrol skeleton, resulting in the formation heme. Heme regulates the synthesis of 5-ALA through a negative feedback mechanism. ALAD, ALA dehydratase; PBGD, porphobilinogen deaminase; UROS, uroporphyrinogen III synthase; UROD, uroporphyrinogen III decarboxylase; MBR, mitochondrial benzodiazepine receptor; COPO, coproporphyrin III oxidase; PPIX, protoporphyrin IX; PROTO, protoporphyrinogen IX oxidase

After its formation, 5-ALA is translocated into the cytoplasm, where it is transformed into UROgenIII. The reaction is the same in all porphyrin producing organisms and implies three steps: First, two 5-ALA molecules are asymmetrically condensed to yield the pyrrol structure of porphobilinogen (PBG). This reaction is catalyzed by ALA-dehydratase (ALAD), a zinc containing enzyme, which is synonymous to porphobilinogen-synthase (PBGS). Patients with a deficiency of ALAD accumulate 5-ALA. The similarity of 5-ALA to the neurotransmitter γ -amino butyric acid (GABA) allows it to bind to GABA-ergic receptors [28]. As a consequence the patients suffer from neuropathies, typically characterised by abdominal pain, dysfunction in the extremities and, sometimes, psychotic attacks. In lead (Pb)-poisoning the central Zn atom in ALAD is replaced by Pb resulting in an inactivation of the enzyme. The symptoms of Pb-poisoning are the same as in the disease developing from a mutation of the enzyme. Therefore ALAD-associated porphyria is also called plumboporphyria (plumbum = latin: lead).

The following two steps in the formation of UROgen III are catalyzed by two closely associated enzymes [29]: Porphobilinogen deaminase (PBGD) condenses four PBG molecules to pre-uroporphyrinogen, a the linear tetrapyrrol. This molecule may cyclize spontaneously to uroporphyrin I, which has a symmetric tetracyclic structure and is biologically inactive. The active isomer UROgen III, in contrast, necessitates the action of uroporphyrinogen III synthase (UROS). UROS catalyzes the inversion of one of the four pyrrols (the D-ring) in the porphyrin skeleton. The transformation results in the final asymmetric structure of UROgen III [30]. A deficiency of PBGD leads to acute intermittent porphyria (AIP). With 300 mutations the disorder is the most frequent form of porphyria. It may be triggered by enzyme-inducing drugs, such as barbiturates and sulphonamides, which enhance the expression of ALAS. The symptoms of AIP are of neurovisceral nature and treatment is well elaborated [31].

A defect in UROS causes congenital erythropoietic porphyria. In this rare but severe form of porphyria the accumulation of tetrapyrrols such as uroporphyrin I and its de-carboxylized form coproporphyrin I lead to discolouring of urine, hypertrichosis and skin photosensitization with subsequent mutilation [32]. Since photosensitization is caused by the reaction of tetrapyrrols to UV-radiation, the symptom is typically found in porphyrias accumulating porphyrins in the blood. Porphyrias accumulating porphyrin precursors, i.e. featuring a deficiency at the beginning of the heme cycle, are limited to neurovisceral symptoms.

After the synthesis of UROgen III the side chains of the tetrapyrrol skeleton are modified. The

first step implies the decarboxylation of UROgen III to coproporphyrinogen III (COPgenIII) through the action of uroporphyrinogen III decarboxylase (UROD). COPgenIII is translocated to the mitochondria in an ATP dependent step. It involves the mediation of the mitochondrial benzodiazepine receptor (MBR) [33;34], a small protein of 18 kD anchored in the outer mitochondrial membrane [35;36]. The MBR can be over-expressed in neoplastic tissues, such as breast [37], endometrium [38], ovary [39], liver [40], brain [41] and colon [42] cancer. It is therefore conceived to hold a key role for the tumor selectivity of 5-ALA mediated PPIX generation.

In the mitochondrial inter-membrane space, two of the four remaining carboxylate groups of the porphyrin are reduced to vinyl-residues, resulting in the water insoluble protoporphyrinogen IX. The reaction is catalyzed by coproporphyrinogen III oxidase (COPO), which is located at the outer surface of the mitochondrial membrane [43]. Protoporphyrinogen IX (PPgenIX) is then aromatized to protoporphyrin IX (PPIX) by the inner mitochondrial membrane bound protoporphyrin IX oxidase (PROTO) [44]. Mutation of PROTO causes variegate porphyria, a disease with a particularly high incidence in South Africans. The disorder spread from descendants of an immigrant in the 17th century. For this reason it is sometimes referred to as South African genetic porphyria [45].

The synthesis of heme is accomplished with the incorporation of ferrous iron into the PPIX skeleton through the enzymatic action of ferrochelatase (FC), which is also located on the inner mitochondrial membrane [46]. According to Grandchamp et al. [43], the close mitochondrial location of the enzymes for the distal steps of heme biosynthesis, COPO, PROTO and FC, removes the obstacle of translocating water-insoluble porphyrins through an aqueous environment. The acquirement of lipophilicity, in turn, seems to be necessary for the porphyrin to cross the mitochondrial membrane for the final transformation into heme. Heme acts as regulator of its own biosynthesis through a direct negative feedback on ALAS in the mitochondrial matrix [46;47].

5-ALA is an endogenous molecule. The major reason for administering an endogenous molecule as drug to a patient is to compensate a deficiency, e.g. insulin in diabetes, or to increase its physiological activity, e.g. prostaglandins as contracting agents for the uterus. Rather than compassing the replacement or increasing the physiological function of the endogenous molecule the exogenous administration of 5-ALA aims at the induction of an extrinsic effect, i.e. the controlled accumulation of the photosensitizing porphyrin, PPIX. As the direct precursor

of heme, the physiological relevance of PPIX as well as that of other porphyrins is restricted to its role as intermediate of the heme biosynthetic pathway. In a normal functioning organism PPIX concentrations are kept to a minimum. Its phototoxic effect becomes clinically relevant only in the case of intracellular accumulation as in the case of porphyrias or the targeted induction by 5-ALA.

In the context of PDT and PD, 5-ALA takes up the function of a prodrug for PPIX. Prodrugs are defined as inactive precursors of a drug, which are enzymatically or non-enzymatically transformed by the organism into the active compound. The derivation into a prodrug is generally used to obtain an increased bioavailability and/or to decrease adverse side effects. Levodopa, for example, the prodrug of dopamine, is used for the therapy of Parkinson's disease. In contrast to dopamine, Levodopa is able to cross the blood brain barrier. In the brain, it is subsequently decarboxylated to the active compound dopamine. In the case of 5-ALA, the transformation into PPIX is carried out by the enzymes of the heme cycle.

Alteration in neoplastic tissue – implications for preferential PPIX induction by 5-ALA

Enzymes of the heme biosynthetic pathway

While intracellular porphyrin concentrations are strictly controlled by heme biosynthetic enzymes in physiologically healthy tissue, this is not necessarily the case in neoplastic tissue, where levels of PPIX are sometimes elevated [2]. An explanation for the observed phenomenon is a dysfunction of tumor proteins. Effectively, tumors may over-express PPIX preceding enzymes and/or feature down-regulation of ferrochelatase.

In an early study, Kondo et al. investigated the enzyme activities of ALAD, PBGD and UROD, as well as FC in 5 normal epithelial cell lines of rat liver and 5 cell lines derived from hepatoma. The study revealed an increased activity of PBGD in all cancer lines [48]. Navone et al. compared ALAD, PBGD and UROD activity in cells derived from human breast cancer tissue to normal mammary tissue and noticed an up-regulation of PBGD and UROD. When undertaking the same investigations *in vivo* on mice, however, they did not observe any significant changes in enzyme activity [49]. Gibson et al. examined the enzymatic activity of ALAD, PBGD and FC in a tumor rat model and 4 tumor cell lines with the addition of exogenous 5-ALA. They could report an increase in PBGD activity for their *in vitro* and *in vivo* experiments [50]. Levels furthermore correlated with the mitochondrial content of the cells [51].

To study the key-role of PBGD in more detail Hilf et al. successfully transfected a mammary carcinoma cell line and a mesothelioma cell line with a PBGD encoding plasmid. Incubation with 5-ALA triggered the expression of PBGD by up to three times, but against all expectations, no increase in PPIX production was observed in PBGD transfected cells [52].

From Hilf's observations Gibson et al. concluded that PBGD was lacking its substrate PBG and that ALAD, the enzyme immediately preceding PBGD and synthesizing PBG, must account for a rate limiting step in the production of PPIX. They tested their hypothesis in three breast cancer cell lines, as well as a human mesothelioma cell line [53]. To prevent any accumulation of PBG and thus a negative feedback on the expression of ALAD, they over-expressed PBGD in all cell lines. Upon addition of excessive amounts of 5-ALA, however, ALAD levels remained unchanged. The observation supported the hypothesis that ALAD is a possible rate-limiting factor in the production of PPIX.

In agreement with other studies [54;55] Krieg et al. found that PBGD activity is dependent on the proliferation stage of cells. It was significantly higher in cancerous cell lines than in the corresponding stromal cell line. However, PBGD activity of poorly differentiated colon carcinoma cells (SW480) was higher during the plateau phase rather than during exponential growth. The opposite observation was made in moderately well differentiated HT29 cells and in normal fibroblasts (CCD18). In well differentiated CaCo2 cells PBGD activity did not seem to be affected by the growth stage [56]. It was not so for human bladder carcinoma cells when compared to urothelial cells [57]. In fact, the main responsible factor for higher PPIX accumulation in bladder carcinoma cells seemed to be a down-regulation of the "post-PPIX"-enzyme FC. Bartosova et al. found similar results using leukemic cells [58].

Hinnen et al. concluded that PPIX accumulates as a result of an imbalance between PBGD and FC expression. They introduced a so-called power index, which represents the activity ratio of PBGD to FC. The purpose of the index was to predict porphyrin concentrations in tissues after administration of 5-ALA and hence to evaluate the susceptibility of the tissue to photosensitization. Results, however, could only partially confirm this hypothesis [59]. This may be due to the fact that they were not aware of the role of ALAD.

Alteration of the iron pool

FC requires two substrates to form heme: one is PPIX; the other one is ferrous iron (Fe^{2+}). The cellular uptake of iron for the biosynthesis of heme has been extensively studied by Mor-

gan et al. [60;61]. Iron reaches the cell bound to its carrier protein, transferrin (T_f). This relatively small glycoprotein of 80kDa binds two Fe^{3+} ions with high affinity ($K_d = 10^{-23}$) at pH 7.4 [62]. The binding of ferric iron, in turn, raises the affinity to a transferrin receptor (T_fR) at the cell surface. T_fR is made up of two subunits of 94 kDa. Each subunit can bind one transferrin molecule. The T_f -iron- T_fR complex is internalized by endocytosis. In the endosome, a proton influx provokes the dissociation of iron from the receptor-protein-complex. T_f and its receptor are recycled to the cell surface, while Fe^{3+} may be transferred to sites of gene regulation in the nucleus or heme synthesis in mitochondria. Mitochondrial iron is bound to FC. It is therefore likely that FC acquires the metal directly from the mitochondrial membrane or is even involved in the iron transfer. However, further studies need to be undertaken to confirm this hypothesis.

In case of excess, iron may also be incorporated into ferritin, a storage protein composed of 24 subunits, with a molecular weight of 430-460 kDa and a capacity to store 4500 iron atoms.

The expression T_fR seems to be a characteristic feature of proliferating cells. In normal tissue, it is particularly abundant in hemoglobin synthesizing tissues and cells, such as erythroblasts and reticulocytes. During erythropoiesis the FC-mediated insertion of iron into PPIX to form heme occurs in the erythroblast stage. The need for iron explains why erythroblasts express abundant concentrations of T_fR at their cell surface. After formation of heme, T_fR is no more required. Therefore erythroblasts release T_fR into the blood plasma (soluble T_fR). The surface-bound concentration of T_fR is lower in reticulocytes, and erythrocytes virtually have no T_fR . The measurement of the soluble T_fR concentration is used as estimate for erythropoiesis.

Kearsley et al. observed in human squamous head and neck cancers that T_fR was highly expressed in the invading margin, which mainly consists of proliferating cells [63]. T_fR was not expressed inside the tumor, where cells were mostly well differentiated. In accordance with these findings, Parodi et al. reported, that T_fR expression correlated negatively with the differentiation status of erythroleukemia cells K562 after treatment with the chemical differentiation inducer cis-platin [64]. Prutki et al., however, observed the contrary in tissues obtained from colon carcinoma patients, where the T_fR expression was high in differentiated cells, but low or absent in poorly differentiated cells [65].

As shown by Page et al. [66], rat hepatocytes and some neoplastic tissues exploit additional mechanisms to internalize iron-transferrin through non-specific endocytosis. Small lung can-

cer cells on the other hand can express their own T_f and human melanoma cells express a cell membrane based T_f homologue [67].

The high metabolic turnover and the increased expression of receptors such as T_fR make it conceivable that certain neoplastic tissues feature increased iron acquisition [68]. Nevertheless, other factors may explain why the availability of Fe^{2+} for heme biosynthesis may be restricted in the same neoplastic tissue. Considering that iron binding to transferrin is pH dependent, the typically lower pH of tumor tissue may account for a pre-mature release of iron from T_f into the interstitium.

Another factor can be explained by the hosts' own protection mechanisms against neoplastic growth. During inflammation the human body reduces its total plasma iron through a self-generated iron-scavenging mechanism in addition to a reduction of iron mobilization: On one hand T_f expression from the liver is reduced. On the other hand the increased production of cytokines during inflammatory processes and tumor growth augments the expression of macrophageal ferritin in liver and spleen. One function of these macrophages is to phagocytose and digest aged erythrocytes. Iron from hemoglobin decomposition is then usually recycled, e.g. by re-introduction into the heme cycle. High ferritin levels in the macrophages, however, create a virtual iron sink and prevent the release of iron into the blood plasma.

Another macrophage-associated mechanism for the withdrawal of iron from tumor cells was proposed by Hibbs et al., who demonstrated that tumor cells released iron upon co-cultivation with activated macrophages [69]. Macrophages release unstable compounds that generate reactive nitrogen oxide (NO) intermediates. It was proposed that this may trigger the release of iron from the cells.

Finally, it is tempting to speculate that the characteristically big size of the nucleus of tumor cells and the small cytosolic volume may abet transport of iron into the nucleus for gene regulation, to the disadvantage of the iron level in mitochondria.

In conclusion, iron does not necessarily reach FC for the final step of heme biosynthesis in mitochondria despite the effort of tumor tissue to take up high concentrations of iron, thus leading to a higher accumulation of PPIX in these cells upon administration of 5-ALA.

Transporter systems for 5-ALA

Exogenous 5-ALA enhances PPIX formation in neoplastic tissue. As summarized above, a reason for this may lie in the altered kinetics of the heme biosynthesis in neoplastic cells. However, it does not explain the preferential uptake of exogenous 5-ALA by cancer cells.

Cancer cells cover their high demand for metabolites through an increased expression of nutrient transporters in tumors, such as amino acid transporters and/or their isoforms. The similarity to α -amino acids makes 5-ALA (a δ -amino acid) a candidate for competitive transport. For instance, neutral α -amino acids, and the structurally related amino acids, in particular β -alanine, taurine and GABA, inhibit the uptake of 5-ALA into WiDr tumor cells [70]. The three amino acids are substrates for the system BETA, an Na^+/Cl^- dependent transporter of broad specificity in epithelial cells of the intestine [71]. The fact that 5-ALA is translocated into the cytosol by this transporter is in accordance with the finding that cellular 5-ALA accumulation correlates with extracellular Na^+ and Cl^- concentration [70;72]. Brennan et al. showed that 5-ALA is a substrate for the neuronal GABA transporter [73], which may account for the GABA-like systemic adverse effects, such as bradycardia and decrease of blood pressure. The competitive uptake of 5-ALA instead of the neurotransmitter by GABA transporters in peripheral nerves may explain the greater sensation of pain in patients treated with 5-ALA compared to patients treated with 5-ALA esters that do not interact with the GABA transporters [70;74-76].

The competitive interaction of 5-ALA with compounds that are not substrates for the system BETA provides evidence that 5-ALA can also bind to other receptors. Döring et al., for example, showed that 5-ALA is translocated by the proton dependent intestinal PEPT1 and renal PEPT2 transporter [77]. This explains the efficient intestinal uptake and the renal reabsorption of 5-ALA from the proximal tubule. Di- and tri-peptides such as Gly-Gly and Gly-Gly-Gly, but not GABA and the other structurally related amino acids glutamate, glycine (Gly), or lysine inhibit 5-ALA uptake in both transporter systems.

5-ALA interacts with the glutamergic system in brain synaptosomes and glycine has been shown to induce renal 5-ALA excretion in patients with acute porphyria [78;79] and to inhibit 5-ALA uptake into amelanotic melanoma cells [80]. This observation points to a further transport system for 5-ALA. Two research groups recently proposed the amino acid transporter SLC36A1 (PAT1) as carrier for 5-ALA [81;82]. SLC36A1 is expressed in the gastrointestinal tract and mainly in the small intestine. It is an H^+ -dependent carrier for small amino

acids, such as GABA, glycine, proline and alanine, but also for numerous drugs [83;84]. 5-ALA uptake of the physiological substrates into frog oocytes and Caco2 cells decreased upon co-incubation with 5-ALA. Inversely, 5-ALA uptake into SLC36A1 transfected COS-7 cells was inhibited by glycine, proline and GABA.

The choroid plexus represents an exceptional part of the blood-cerebrospinal fluid (CSF) barrier, lining the blood capillaries with normal (fenestrated) endothelium on one side (basolateral side) and the CSF containing brain ventricles with fenestrated ependyme on the other (apical side). It allows small molecules such as vitamins and nucleotides to penetrate into the brain, but also represents the “weak point” for the influx of drugs. PEPT2 seems to play a role in 5-ALA transport in the choroid plexus. It seems to function as an efflux pump rather than an uptake mechanism, to keep 5-ALA concentrations low in the CSF [85-87].

It is difficult to tell, whether accumulation of 5-ALA in brain tumors is a consequence of selective interaction of 5-ALA with cell transporters or the ability of the drug to diffuse passively through the blood brain barrier (BBB), or if the passage into tumor invaded areas is facilitated after disruption of the BBB. In an *in vitro* experiment, Correa Garcia et al. did not see any uptake of ¹⁴C-5-ALA into epithelial cells of isolated capillaries of the BBB [88]. Similar results were obtained by Terr et al., who analyzed the uptake of radio-labelled 5-ALA by various parts of the brain after systemic application. They found exogenous 5-ALA only in structures lacking the BBB, notably the choroid plexus, whereas other areas did not feature any 5-ALA uptake [89]. Most probably the intact BBB is impermeable for 5-ALA. In agreement with other studies [90-92] Hebeda et al. failed to detect PPIX in brains of healthy rats after systemic 5-ALA administration, but observed elevated PPIX in experimentally induced brain tumors of rats. Interestingly, the animals had higher PPIX concentrations in intact brain tissue than the control group. The decrease of fluorescence correlated with the distance from the tumor. No PPIX fluorescence was observed in the plexus region. It is likely that the brain tumors impaired the protective function of the BBB and thereby enhanced the permeation of 5-ALA into the diseased tissue [93].

Altered morphology of tumors

The vascular system of tumors exhibits alterations in the morphology of endothelial tissue, which favour the retention of large molecules in the neoplasm. This feature is referred to as

the enhanced permeability and retention (EPR) effect [94;95]. In tumors oxygen pressure is reduced and gene expression is switched to adapt to the hypoxic environment, notably through anaerobic glycolysis. The prevailing anaerobic conditions favor lactic acid formation with concomitant pH decrease in the interstitial fluid. Recent findings suggest that low extracellular pH in neoplastic tissue is also mediated by the over-expression of tumoral carboanhydrases. These enzymes catalyze the reaction of a physiologic buffering system by generating bicarbonate and protons from CO₂ and water. Formed bicarbonate is shovelled into the cell to ensure neutral pH for enzyme functioning, thus leading to elevated extracellular proton concentrations [96]. The pH in tumors is about 0.2-0.4 units lower than in normal tissue. The change of pH has been considered to have an effect on the supply of iron for FC (see Sect. 3.2), but also on the selectivity of 5-ALA uptake in cancer cells. 5-ALA-mediated PPIX production is decreased at extracellular pH below 6.0 and above 7.0 [97-101]. According to Bech et al. this may be explained by an activity decrease of enzymes of the heme cycle such as PBGD [102]. This explanation stands in contrast to the elevated PBGD levels observed in tumor cells as described under sect. 3.1.

Despite apparently lower PPIX levels at decreased pH, it was observed that the susceptibility of 5-ALA treated cells to PDT was higher. This phenomenon was mainly attributed to impairment of cellular repair enzymes and raise the cells susceptibility to PDT [98;103]. It should be mentioned at this point that the stability of 5-ALA as well as the fluorescence PPIX change with pH [101;104;105].

The requirement for nutrients and oxygenation from blood circulation prompts tumors to express angiogenic growth factors (e.g. vascular endothelial growth factor, platelet derived growth factor). However, the poor coordination of the growth leads to a network of incomplete, fenestrated vascular structures. Depending on the tumor, the gaps in neoplastic vascular endothelium may attain several hundred nanometers, making it an adequate target for large molecular 5-ALA derivatives and modern formulations such as liposomes and nanoparticles (see Sect. 4.3.2). In addition, the typically underdeveloped lymphatic system in neoplasms prevents the evacuation of same said molecules and particles. The high density of microvessels associated with inflammation responsive signals furthermore lead to elevated temperature in tumor tissue [106;107].

Moan et al. investigated the influence of temperature on the PPIX production *in vitro*. After incubation of WiDr cells with 5-ALA at 37°C for 20 minutes they monitored the PPIX accu-

mulation over several hours, PPIX induced fluorescence increased with incubation temperature up to 37°C, but did not seem to influence 5-ALA penetration into the cell [108]. The results were in accordance with observations on 5-ALA treated skin of 3 volunteers and two other studies on the temperature dependent PPIX production on mouse skin after topical 5-ALA application. In the first study, temperature was changed before and after a 10 minute application of a 5-ALA containing cream. In the second study, temperature was varied during the application period. Temperature did not seem to have any effect on the penetration of 5-ALA into the skin. However, PPIX formation from 5-ALA as well as its esters correlated with temperature increase [109;110]. The authors hypothesized that a temperature increase may have a positive influence on the activation of the bottleneck-enzyme PBGD, where the activation energy changes from 21.7 kcal/mol for temperature lower than 35°C to 12.7 for temperatures between 35-46°C [109;111]. The result of the first study should be considered with caution; since 5-ALA application times were short, it is conceivable that the diffusion process through the stratum corneum was not completed when the skin was heated or cooled after cream application. Van den Akker et al. observed that PPIX induction on the back skin of healthy volunteers depended on the skin temperature during 15 minute application of 5-ALA using a hydrogel [112].

A non-negligible aspect is the temperature-dependent release of 5-ALA from its application form. Unfortunately, none of the studies on temperature dependent PPIX induction provide data on in vitro release kinetics for direct comparison.

As already mentioned for the BBB, the invasive character of neoplastic tissue affects the architecture of surrounding tissue, notably of epithelial cell linings. Epithelia delineate organs and tissues in the organism and have a protective barrier function. Drugs of small size may diffuse passively through small gaps between epithelial cells into the underlying tissue. The limiting factor for this mode of entrance is constituted of intercellular tight junctions. Alternatively, the drug may interact with cellular receptors and transporters or feature adequate physico-chemical properties in order to penetrate the cell membrane. Disruption of the epithelial cell layers, for example by tumor invasion, facilitates the accessibility of underlying tissue. The defect is advantageous for the drug delivery via the topical route.

The epithelium of the skin represents a particular structure to maintain its protective function against influences from the environment. It consists of five layers. During their life cycle of approximately 21 days, epidermal cells progressively move from the stratum basale at the bot-

tom into the overlying stratum spinosum, stratum granulosum and stratum lucidum until reaching the stratum corneum, the outermost layer, as fully differentiated corneocytes. These cells are characterized by a cornified cell envelope consisting of proteins and lipids and the lack of a nucleus. They are embedded into a lipid layer containing approximately 41% ceramids, 39% cholesterol and cholesterol derivatives and 9% free fatty acids, which form a lipophilic film at the surface of the skin. Eventually the corneocytes scale off through the contact with the outer world.

The lipophilic nature of the stratum corneum, which – one should note – is only a few microns thick, prevents the dehydration of the body from excessive evaporation, and represents the main protective barrier from external influences. In combination with the underlying cell layers (the dermis containing lymph vessels, sebaceous glands and small blood vessels and the subcutis hosting large blood vessels, nerve endings and hair follicles), the skin represents an organ with alternating hydrophilic and lipophilic layers. This feature makes drug delivery through the skin particularly challenging. On the other hand it leaves way for the targeted delivery of drugs to parts where the penetration barrier is damaged, e.g. by skin diseases.

The trespassing of a compound through the intact epidermis is controlled by its diffusivity within the cell layers [113]. Removal of the lipophilic stratum corneum may augment the permeation capacity of the compound. Several studies recorded a higher amount of PPIX accumulation in healthy skin after topical application of 5-ALA with prior tape stripping or micro-dermabrasion than in skin without pretreatment [109;114-118]. In a permeation study on mouse skin Tsai et al. modified the permeability of the skin with acetone, and showed *ex vivo* that transdermal flux of 5-ALA corresponded to the level of transepidermal water loss (TEWL), an indicator for the degree of corneal disruption. According to an E_{\max} model, the flux correlated with the *in vivo* PPIX fluorescence at the respective TEWL levels using the same concentration of 5-ALA formulation [119]. In agreement with Tsai's findings, a group at the Radboud University Medical Center in Nijmegen stated that the extent of PPIX formation in psoriatic skin is dependent on the thickness of overlying stratum corneum rather than on patho-physiological characteristics of the epidermal cells [120;121]. In other hyperkeratotic diseases the variation of fluorescence after topical 5-ALA administration could be also ascribed to the poor penetration of 5-ALA through the overlying stratum corneum.

Means to improve PPIX formation

Various techniques have been explored to improve 5-ALA delivery to its site of action with the principal aim of increasing PPIX generation at the target. As it is beyond the scope of this chapter to review all the studies relating this topic, the reader is referred to several excellent reviews treating this matter [122-126]. The following sections shall nevertheless give some insight into the approaches that have been evaluated so far.

One can distinguish between physical, chemical and galenic means to direct a drug to its target. Physical methods describe the application of a treatment prior to or in combination with the drug that physically alters the tissue or creates a physical driving force for the molecule to reach its target. Chemical means imply the derivatization of the 5-ALA molecule, into a compound with more advantageous properties with respect to bioavailability. The term “galenics”, finally, stands for the science of preparing and optimizing the drug dosage form, i.e. the drug vehicle in order to obtain the required delivery profile. This involves the right choice of the drug carrier and possible adjuvants.

Physical Means

Surface ablation

In certain skin diseases, such as actinic keratosis, psoriasis, basal- and squamous cell carcinoma, the presence of a hyper-keratotic layer impedes the penetration of the photosensitizer and also the penetration of light. Curettage or debulking of the tissue may overcome this constraint.

In other situations, debulking and curettage defines the removal of solid parts of the tumor in an invasive manner as in the case of thick, solid tumors. In many clinical protocols for topical PDT gentle curettage or debulking prior to photosensitizer administration is applied as standard procedure [127;128]. Unfortunately, many trials lack control groups that did not undergo mechanical tissue removal, so that the true impact of this method is difficult to evaluate.

Moseley et al. examined the effect of the removal of the outermost layer of the lesions by gentle abrasion prior to exposure to 5-ALA on 16 lesions in 15 patients with superficial non-melanoma skin cancer. Comparing the fluorescence of curetted parts with untreated parts of

the same lesion, they could not find any difference between treatment and control group. They concluded that pre-treating lesions by gentle curettage does not influence 5-ALA penetration into the tissue [129]. On the other hand, Soler et al. treated patients with basal cell carcinoma (BCC) of at least 2 mm thickness with 5-ALA in combination with dimethyl sulfoxide (DMSO). In the test group, BCCs were debulked using a curette; the control group did not get any pre-treatment. After an average follow-up of 17 months 95% of curetted lesions showed complete response versus 50% in the control group [130]. A follow-up study with a similar treatment modality reported complete response for 81% of the treated lesions after 6 years [131]. The study, however, does not mention the response of the control group. Itoh et al. used an electro-curettage technique to remove melanin in 16 patients with pigmented BCC prior to 5-ALA administration. This form of BCC is usually not prone to standard PDT due to light absorption by melanin in the lesion. In this study, however, 14 out of 16 patients showed complete response to the treatment [132].

Shen et al. chose an erbium:yttrium-aluminum-garnet (Er:YAG) laser for tissue ablation on mice bearing skin cancer lesions [133]. In this technique, the instant evaporation of water through absorption of the laser beam leads to a micro-explosion ejecting desiccated skin from the surface until a depth of 10-15 μm [134]. Laser-treated BCCs prior to topical 5-ALA application, accumulated PPIX faster and in significantly higher amount than non-pre-treated lesions [133]. In agreement with this finding, although less pronounced, a clinical study on patients with recurrent and nodular BCC had a better outcome in the case of PDT using the combination of Er:YAG laser and 5-ALA methyl ester on human skin than when using Er:YAG laser or PDT alone (final efficacy of 98.97%, 91.75% and 94.85%, respectively) [135]. Other lasers, for example a CO₂ laser, have been used for the same purpose [136].

Pretreatment of the target surface with penetration enhancers (see Sect. 4.3.1) and/or keratolytics, such as salicylic acid and urea, may facilitate the ablation of the stratum corneum [120;137;138]. In an attempt to remove plantar warts by 5-ALA PDT, Fabbrocini et al. combined the keratolytic treatment with 5-ALA PDT. They applied an ointment containing 10% urea and 10% salicylic acid onto plantar warts for 7 days before removing the surface by gentle curettage. Three weeks after PDT surface of plantar warts was reduced by 70% in patients treated with 5-ALA versus 30% in patients with placebo PDT [137].

Skin perforation

Recently, micro-needle perforation techniques [139] and needle-free jet injection [140] have been explored to optimize 5-ALA delivery through the skin. Micro-needle arrays consist of a multitude of small perforators of defined form and size attached to a small platform. The platform functions as support for the perforators; it also controls their penetration depth into the skin and prevents the stimulation of nociceptive nerve endings in deeper lying tissue. After gentle pressure to the skin, the micro-needles leave small pores, which facilitate the permeation for water-soluble compounds, such as 5-ALA.

In jet injection, the drug is delivered subcutaneously, intradermally or intramuscularly by a high velocity liquid jet. Penetration depth depends on pressure and speed of the jet and the mechanical resistance of the skin. *Ex vivo* studies on porcine skin revealed a positive effect on the penetration capacity of 5-ALA. For micro-perforated murine skin *in vivo*, a faster induction of PPIX accumulation was visible. Higher PPIX amounts were detected when low concentrations of 5-ALA were applied. Delivery of 5-ALA methyl ester (MAL) to nodular BCCs by means of oxygen pressure injection showed better results in PPIX induction than application of MAL alone [141].

Ultrasound and Iontophoresis

Iontophoresis takes advantage of the ability of molecules to migrate in an electric field. In the context of drug delivery, the procedure involves the application of two electrode compartments on the surface of the skin connected to a power source. Charged compounds are loaded into the electrode compartment bearing the same charge. Application of a low electric potential between the two electrodes establishes a current flow and consequently sways the ions to migrate through the skin. The two driving forces dictating this phenomenon are electromigration and electro-osmosis. In the former, the movement of ions is driven by the electric field force. The delivered drug dose usually correlates directly with the charge of the drug and the magnitude of the applied current. Electro-osmosis, in contrast, implies the passive transport of molecules with the liquid flow caused by electric current [142].

Several *in vivo* and *ex vivo* studies have shown that 5-ALA penetration through healthy skin in combination with iontophoresis reduces the application time to observe a fluorescence signal [143]. PPIX fluorescence correlated with the applied iontophoretic charge [144-146]. Mi-

zutani et al. performed PDT supported by direct-current pulsed iontophoresis in 5 patients with thin to moderate actinic keratosis. Differing from the usual lag time of 4-5 hours, they detected PPIX within 1 hour [147]. Lopez et al. and Merclin et al. reported that the efficacy of 5-ALA iontophoresis is dependent on the ionic strength and type of 5-ALA formulation [143;148]. Decrease from pH 7.4 to pH 4 does not affect 5-ALA electromobility. This is surprising, since one would expect that the driving force of electrophoretic transport at neutral pH is electro-osmosis. Below pH 4.5 electro-migration should synergistically augment the transport with decreasing pH. However, low pH also impedes the electro-osmotic flow. The authors, therefore, concluded that electro-migration compensates the effect of the electro-osmotic flow rather than enhancing it [145].

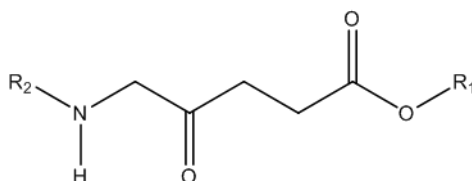
In parallel to the beginnings of 5-ALA iontophoresis, Ma et al. examined the influence of ultrasound (1 MHz) on PPIX induction in subcutaneous tumors in BALB/c nude mice. Fluorescence intensity was the same after one hour with 5-ALA and ultrasound compared to 3 hours incubation with 5-ALA alone [149]. Charoenbanpachon et al. used ultrasound in combination with 5-ALA formulated in Eucerin[®] on dysplastic and healthy oral mucosa of hamsters. 5-ALA induced PPIX fluorescence increased significantly after 20 minutes when ultrasound was applied. The same PPIX fluorescence intensity appeared after 180 minutes when applying a 5-ALA in Eucerin[®] and a penetration enhancer containing formulation (Pluronic[®] Lecithin Organogel) without ultrasound, respectively. PPIX fluorescence was higher in dysplastic tissue than in normal tissue. It also increased when ultrasound of higher frequency was applied, suggesting that higher amounts of 5-ALA levels reached the target tissue with this method [150].

Chemical means

5-ALA esters

The likeliness of a molecule to diffuse through the cell membrane is dictated by certain physical-chemical characteristics, which have been resumed by Lipinski's "rule of five". According to this rule the cell permeation of a molecule is promoted, when its octanol-water partition coefficient (expressed as logP) is smaller than 5, the molecular weight is under 500 and the molecule contains less than 5 hydrogen bond donors and no more than 10 hydrogen bond acceptors [151].

Tab. 2. Approaches for chemical modification of 5-ALA . a: mouse, b: mouse skin, c: human skin



Class	R ₁	R ₂	Data	Reference
Ester	Alkyl	H	in vitro, in vivo ^a in vivo ^a ex vivo ^b in vitro in vitro ex vivo ^{b,c} in vitro in vitro	Kloek et al.[153] Peng et al.[154] De Rosa et al.[160;161] Uehlinger et al.[152] Rud et al.[70] Casas et al.[157] Moan et al.[156;158] Chen et al.[162]
	Acyloxyalkyl	H	in vitro	Berkovitch et al. [163]
Peptide	H	Amino acid	in vitro	Bourré et al.[164]
	Alkyl ethylene oxide	di-, tripeptide	in vitro	Berger et al.[165]
	H	oligopeptide	in vitro	Dixon et al.[166]
Den-drimer	Dendrimer	H	in vitro in vitro in vitro in vitro	Battah et al.[167-169] Brunner et al.[170] Di Venosa et al.[171] Casas et al.[172]
Vitamine	Tocopherol, Cholecalciferol, Biotin	H	in vitro (only synthesis)	Vallinayagam et al. [173]
Glucoside	Monosacharide	H	in vitro	Vallinayagam et al. [174]
Nucleo-side	Adenosine	H	in vitro	Gurba et al. [175]

The partition coefficient is crucial for the ability of a drug to passively penetrate biological barriers. A molecule with a negative logP, hence with good solubility in water, is not likely to trespass the lipophilic cell membrane. This may be improved by raising the lipophilicity of the molecule. However, if the logP is too high, partition into the intracellular aqueous environment is low, i.e. the molecule remains “trapped” in the membrane.

With a negative logP (- 1.5) [152] and a zwitterionic structure at physiological pH, 5-ALA represents a highly water-soluble molecule. The only possible way into the cytosol is therefore restricted to active transport systems, such as amino acid and peptide transporters (see Sect.3.3). For the topical application this brings the drawback of inhomogeneous distribution in the target tissue. Instability in aqueous media and its susceptibility to the first pass effect make 5-ALA less suitable for oral and intravenous application. High doses are necessary to obtain a pharmacologically satisfying response thereby increasing the risk of neurological side effects.

Knowing that lipophilicity of a drug may have a positive impact on the bioavailability, Kloek et al. [153] and Peng et al. [154] were the first to substitute 5-ALA with lipophilic residues. When applied topically, ester-induced fluorescence remained confined to the area of application. In contrast, the fluorescence induced by free 5-ALA was detected in collateral sites of the application site and persisted for a longer time [115;155-158]. Uehlinger et al. esterified 5-ALA at the carboxyl end with a homologous series of aliphatic alcohols to investigate a controlled change of lipophilicity in a simple manner [152;153]. The esterification of the carboxyl group turns the previously zwitterionic amino acid into a cation, which facilitates the interaction with the negatively charged cell surface [159]. All 5-ALA esters induced PPIX formation in J82 and T24 bladder carcinoma cells, an A459 human lung carcinoma cell line, and in BEAS-2B immortalized normal human bronchial epithelial cells. The extent depended on the type and the concentration of the ester. 5-ALA hexyl ester induced the highest amount of PPIX at a concentration about 10 times lower than free 5-ALA [152]. De Rosa et al. observed that short alkyl esters with a chain length of up to 6 carbons induce PPIX fluorescence at low concentrations. Longer esters failed to do so [160]. According to the influence of the logP on the penetration capacity of a small molecule, one may conclude, that contrarily to free 5-ALA, 5-ALA alkyl esters diffuse through skin or the cell membrane [161].

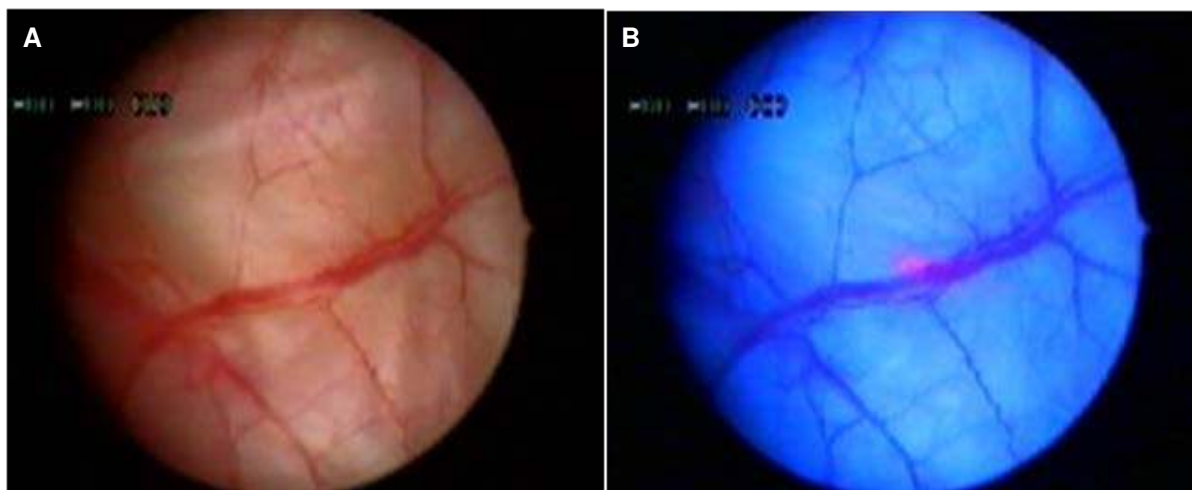


Fig. 4. Endoscopic image of human bladder carcinoma in situ visualized under white (A) and blue (B) light after instillation with 5-ALA hexyl ester. Under blue light the carcinoma appears with a red fluorescence due to preferential accumulation of PPIX mediated by 5-ALA hexyl ester (B). The same carcinoma is not distinguishable under white light (A)

Chen et al. found that esterification of 5-ALA also has positive influence on the chemical stability. He observed that in aqueous solution 5-ALA hexyl ester forms less dimers than free 5-ALA [162].

The vast possibilities derivatizing the 5-ALA molecule have been extensively explored and the reader is referred to a review written by Fotinos et al. [125] for a more detailed description of the methodology. Table 2 provides an overview of some chemical strategies to improve 5-ALA mediated PPIX accumulation in the target tissue.

So far the most promising derivatives have proven to be 5-ALA alkyl esters. In fact, the new findings on 5-ALA derivatives represented a breakthrough for their introduction into the market. Today, the 5-ALA products Levulan[®] Kerastick[®] (for treatment of actinic keratosis) and Gliolan[®] (detection of malignant glioma during surgery), as well as two 5-ALA esters, 5-ALA methyl ester (Metvix[®]) and 5-ALA hexyl ester (Hexvix[®]), have obtained marketing authorization (see table 1). Metvix is approved for the treatment of precancerous and cancerous skin lesions in Europe, Australia and USA. Hexvix[®] is commercialized in Europe for the detection of recurrent bladder cancer and recently gained marketing authorization in the USA under the name Cysview[®] (see fig 4).

A novel approach was tempted by Berkovitch et al., who attached an acyl oxy alkyl component to 5-ALA. Metabolization of the prodrug leads to the release of formaldehyde and butyric acid [163]. They favor the formation of ROS and apoptosis and thus may increase the effect of PDT.

5-ALA peptides

The possible translocation of 5-ALA by the dipeptide transporter on one hand, and the targeting of tumoral aminopeptidases on the other, led to the synthesis of 5-ALA derivatives with peptidic structure. Casas et al. [157] and Berger et al. [176] found that some, but not all amino acid- and short peptide derivatives induce PPIX formation *in vitro* and *in vivo*. An advantage of amino acid derivatives is their increased stability in aqueous solutions at physiological pH, provided that the amino terminal group is protected or longer peptides are used for the conjugation [165;176;177]. Berger et al. discussed that the occupation of the amino functional group prevents the cyclization of the molecule by Schiff base reaction between the amine and the γ -carbonyl moiety of 5-ALA [165].

However, activation of these compounds necessitates the presence of peptidases. In this context, the conjugated amino acid as well as the N-terminal group determines the compounds' susceptibility to the respective amino peptidase. As an example, 5-ALA methyl ester conjugated with neutral amino acids such as L- phenyl-alanine induces porphyrin formation in A549 human lung carcinoma cells. This cell lines expresses the aminopeptidase N/M, which has a high affinity to neutral amino acids. 5-ALA methyl ester conjugated N-acetylated L-phenyl alanine failed to induce PPIX formation [165;178] in A549 cells. Incubation of the spontaneously transformed murine keratinocyte cell line PAM212 with the same conjugate resulted in 3 times higher PPIX accumulation than with free 5-ALA [177;178]. PPIX accumulation was drastically decreased when silencing the acylpeptide hydrolase gene, a peptidase detaching acylated amino acid residues from oligopeptides [164].

Dixon et al. synthesized the first 5-ALA conjugated oligopeptide, comprising 8 amino acids. Unlike short amino-acid compounds, which are taken up by the cell transporters or via diffusion, oligo peptides self-trigger their internalization by endocytosis. They can carry multiple payloads, which makes them an interesting alternative for the intracellular drug delivery. The 5-ALA oligopeptide was successfully internalized by endocytosis. However, PPIX induction

was only half compared to porphyrin induction with equimolar amounts of free 5-ALA. Therefore, further improvement of this approach is required [166].

5-ALA conjugates with macromolecules

Lately, several groups conjugated 5-ALA and its esters with macromolecules. Such structures may be loaded with multiple 5-ALA units and improve tumor penetration by enhanced permeability and retention (see Sect 3.4) due to their large size. Attachment of residues interacting with tumor receptors may favor tumor uptake.

A high payload may especially be achieved with dendrimers. These highly branched polymers (dendron = greek: tree) consist of a core molecule, from which arise linker chains in a star shape. A functional group at the end of the linker allows the attachment of active moieties or functional groups, such as hydrophilic moieties to improve solubility.

During screening assays of various 5-ALA esters to improve porphyrin induction, Battah et al. [167] and Brunner et al. [170] found that certain 5-ALA dendrimers were able to induce PPIX formation in tumor cells. Further research revealed that the type and length of the linker influenced the bioavailability of 5-ALA. Functional groups that make the ester bonds more sensitive to cleavage, increased 5-ALA discharge, while dendrimers with sterically hindered ester bonds delivered 5-ALA less efficiently [169]. Logically, the susceptibility of ester bonds to cleavage together with the number of 5-ALA molecules bound to the dendrimer determines the kinetics of PPIX generation. A second generation dendrimer conjugated with 18 5-ALA molecules induced sustained PPIX formation over a period of 48 hours *in vitro* [169] and *in vivo* [172], while PPIX levels were significantly lower already after 24 hours when free 5-ALA was applied. While small dendrimers seem to follow an internalisation mechanism similar to that of free 5-ALA or its derivatives [168;171], large dendrimers reach the cytosol by endocytosis [169].

The synthesis of 5-ALA conjugates with vitamins, monosaccharides and nucleosides has also been reported [173-175].

Galenic approaches

To achieve the wanted effect with a treatment it is not sufficient to use a drug with satisfying pharmacodynamics. It is equally important to deliver the drug to the targeted sight of action, at the right time and in concentrations that correspond to the therapeutic window.

An alternative way to physical penetration enhancement methods and chemical derivatization of the active compound is to optimize the vehicle from which the drug is delivered. The release of 5-ALA and its derivatives from topical formulations such as creams, gels and solutions has been extensively studied [156;179-184]. However, the expansion of possible target sites for 5-ALA PDT, e.g. its use for topically inaccessible tumors, demands more adequate vehicles.

During the development of a drug formulation several factors must be taken into consideration: First, the formulation may considerably influence the chemical stability of the contained drug. Under alkaline conditions, for example, 5-ALA forms biologically inactive dimers of pyrazine and pyrrol structure [185-187]. Following an Arrhenius plot, Elffson et al. predicted a shelf life (time after which 10% of the product are degraded) of only 10 minutes for a 10% aqueous solution of 5-ALA at pH 7.5. Stability can be improved by decreasing pH, concentration and temperature of the aqueous solution [188].

In a further aspect, the excipients of the formulation have a strong impact on the pharmacokinetics of the drug. On one hand, the affinity of a drug with high logP to its carrier increases with the lipophilicity of the vehicle. As a consequence, release of the drug from the vehicle may be slower than from a more hydrophilic formulation. Collaud et al. reported that release of 5-ALA hexyl ester was more complete from thermosetting hydrogels than from a cold cream and a lipophilic base (Unguentum M[®]) [180]. The findings are in agreement with studies, in which 5-ALA hexyl ester formulations in lipophilic ointments did not efficiently induce PPIX production [189;190].

On the other hand, a pronounced hydrophilicity of the vehicle can be disadvantageous for the solubilization of a lipophilic compound and thus be inadequate for its delivery.

Topical formulations

Casas et al. performed extensive research on the release of 5-ALA and its esters from topical formulations. 5-ALA hexyl ester induced twice as much PPIX when applied in an oil in water (O/W) cream than when applied from an aqueous solution [191]. For 5-ALA the best results were observed for hydrophilic saline solution (preferably containing additional penetration enhancers) and hydrophilic lotions [155;181].

In a clinical trial, Hürlimann et al. applied a nanocolloid gel containing 10% 5-ALA to patients with BCC prior to irradiation with white light. They reported complete response in 84% during a follow-up of at least 6 months. Unfortunately the exact formulation parameters have not been reported [192].

Aiming at stabilizing 5-ALA and derivatives by liposomal encapsulation, Batlle et al. recently showed, that the loading capacity of liposomes drastically increases for more lipophilic 5-ALA esters [193;193-197]. The use of negatively charged lipids further improved the loading. Thus, 5-ALA loading of conventional phosphatidyl choline liposomes increased from 5% to 87% when using 5-ALA undecanoyl ester and 20% phosphatidyl glycerol, which is anionic at pH of the skin. Encapsulated 5-ALA esters remained stable up to one week [196]. However, compared to the free compound, undecanoyl ester liposomes failed to induce the formation of higher intracellular amounts of porphyrins [198]. Similar results were obtained when using free versus liposomal 5-ALA or 5-ALA hexyl ester [193]. Han et al. prepared DMPC-DMPG-CH-DOTAP (Dimyristol phosphatidyl choline- dimyristol phosphatidyl glycerol – cholesterol – dioleoyl trimethyl ammonium propane; 7/1/2/1) liposomes and observed elevated PPIX production in pilosebaceous glands on dorsal rat skin [199]. The selective targeting of pilosebaceous gland may be of interest for PDT aided hair removal.

A new approach is the incorporation of 5-ALA into solid lipid microparticles. Al-Kassas et al. proposed Witepsol H 15 as topical drug vehicle. Witepsol H15 is an established suppository base consisting of saturated mono-, di- and triglycerides with a melting point close to body temperature. The rationale behind the use of such a base is to physically impede 5-ALA dimerisation at room temperature by entrapment into a solid. Melting of the base at contact with the body surface allows instant drug release. Indeed, microparticle entrapped 5-ALA remained stable for at least 9 months. The microparticles further improved transdermal 5-ALA flux in an *ex vivo* skin permeation model [200]. Their application in practice, however, is more complicated, since bulk particles only adhere poorly to the skin. Therefore, incorpora-

tion into bio-adhesive systems is required. As solution, the formulation into bioadhesive semi-solid carriers was investigated, with the outcome that semi-solids influence release- and penetration profiles of the drug. The most appropriate vehicle was a propylene glycol based gel. PPIX production with this formulation was comparable to a cream containing the same amount of 5-ALA [201].

The topical delivery of a drug is especially challenging for mucosa and moist undulated parts of the skin. These areas are often exposed to frictional stress (e.g. digestive contractions in gastro intestinal tract (GIT) or movement of the patient), which complicates the exposure of the targeted area to 5-ALA or 5-ALA derivatives during the incubation period.

Thermosetting gels have been shown to be advantageous for the drug delivery to surfaces such as mucosa of oesophagus, stomach or cervix. The liquid state below room temperature facilitates the incorporation of water-soluble drugs. It also allows the application of the formulation in a liquid state, which is particularly advantageous for targeting the inner cavities. With increasing temperature (i.e. in contact with the body) the gel then reaches the visco-elastic state. When targeting the oesophageal mucosa, for example, the patient may drink the formulation. The gel solidifies on the oesophageal mucosa, thus securing the contact of 5-ALA with its target site. Removal of the gel is possible by washing it away with a cold liquid, which puts it back into the sol state. One challenge in the formulation of drug delivery systems with changing physical properties is the coordination of formulation parameters. The type and concentration of the gelling agent, as well as of the incorporated drug influence the thermosetting temperature of the gel. Thus, 5-ALA increased the thermosetting temperature of a simple poloxamer gel containing the polymer and water [202]. The effect was the opposite in a gel using the same gelling agent, this time in combination with isopropanol, dimethyl isosorbide, medium chain triglycerides and water [203]. 5-ALA concentration had no effect on the setting temperature of a gel containing the same polymer with additional sorbic acid (0.15%) in citrate phosphate buffer pH 4.0 [180].

Sites exposed to high frictional stress, such as rectum or vulva or crease areas of the skin, require even more stable and rigid dosage forms than semi solids. Donnelly et al. developed of a bioadhesive patch in order to address this problem. The patch consists of a bioadhesive water soluble poly (methylvinylether/maleic anhydride (PVME/MA) layer, which contains 5-ALA, and a backing poly vinyl chloride (PVC) layer [204-208]. In 2009, the patch was tested on 23 patients with vulval intraepithelial neoplasia. It showed adequate adhesion; however, photo-

dynamic treatment of the lesions after patch application did not improve response with respect to conventional treatment [207].

Another dermatological patch was invented by Lee et al. [209] and recently gained marketing authorisation in Europe under the name Alacare[®] and Effala[®] for the treatment of mild actinic keratosis on hairless areas of skin and scalp (see table1) [210]. The drug is incorporated in its crystalline state into a poly acrylate methacrylate (Eudragit[®]) matrix, which is backed by a poly ethylene aluminium poly ester film. The system can be advantageously applied to the lesion without previous curettage or occlusion. In two randomized controlled trials including 449 patients with mild to moderate actinic keratosis, single dose PDT in combination with the patch showed a statistically significant better result than cryosurgery and placebo PDT. After a 12 week follow-up complete response was observed in 82% (patch PDT) versus 19% (placebo PDT) in the first trial and 89% versus 29% second trial, respectively. The response rate was favorable in comparison to treatment with the commercially available alcoholic 5-ALA solution (Levulan[®] Kerastick[®], 66% complete response after single treatment) and 5-ALA methyl ester containing cream (Metvix[®], 86.9% after single treatment) [211]. 74% of the patch-treated patients still showed complete response after 12 months [212].

As mentioned above, the access of 5-ALA from the skin to underlying tissues is limited by poor permeation. Penetration enhancers have therefore been considered for a pre-treatment or as additives for dermatologic 5-ALA formulations.

Typically, penetration enhancers alter the highly organized structure of the stratum corneum by interacting with intracellular proteins and lipid structures through lysis and/or hydration of keratinocytes. They may also function as solubilizers for the drug in the stratum corneum.

The best established penetration enhancer is DMSO. In fact, it is the sole chemical penetration enhancer mentioned in the Guidelines of the British Photodermatology Group [213]. Many studies reported the positive effect of DMSO as adjuvant or in combination with other targeting strategies for enhanced 5-ALA delivery [130;131;143]. The mechanism, by which this substance acts as penetration enhancer in the skin is not completely elucidated. However, it is assumed to denaturate intracellular proteins and to enhance the fluidity of the lipid bilayer by dissolving lipid structures [214]. DMSO is further known to trigger cell differentiation in neoplastic cells. An explanation for this may be the induction of certain enzymes of the heme cycle [215].

Synergistically to their effect on alteration of heme biosynthesis, chelating agents have been considered as modulators of tumor cell proliferation and immune response following PDT. This argument is well conceivable since iron acts also as regulator in transcriptional processes in the nucleus [216].

The relevance of iron disposability for the accumulation of PPIX becomes most obvious through the use of chelating agents.

Chelators intervene in the heme cycle by depriving FC from its substrate ferrous iron. This leads to an accumulation of PPIX in normal tissue [217]. Since exogenous 5-ALA induces PPIX formation, it may be assumed that the combined application of the PPIX precursor with an iron chelator has a synergistic effect [216;218]. Taking further into account that 5-ALA has preferential affinity for dysplastic tissue, the synergistic effect is even more pronounced in tumors [219;220]. An iron chelator may therefore allow to down-size 5-ALA concentrations and hence reduce cytotoxic side effects, while maintaining a high free porphyrin concentration in the cells.

Ethylenediaminetetra-acetate (EDTA) is a well-established metal ion chelator. Experiments with EDTA support the concept of enhanced porphyrin accumulation through the chelation of iron [221;222]. Low specificity and poor penetration of EDTA through the cell membrane reduce its potential for clinical use. Deferoxamine (DFO) permeation of the cell membrane exceeds that of EDTA. The chelator was originally discovered as bacterial siderophore [223]. Today, it is used for the therapy of iron overload diseases such as thalassemia. However, the response to topically applied DFO varies greatly and is not well reproducible. It should be used together with other penetration enhancers. Another molecule that gained growing interest during the last decade is CP94, a benzopyrrolidinone. It was originally developed to improve iron binding in the treatment of hemochromatosis. CP94 permeates the skin and reaches the intracellular cell pool faster than EDTA and DFO. These properties can be attributed to its low molecular weight and higher lipophilicity, which also render it suitable for oral application.

In a study on subcutaneously implanted C26 colon carcinoma in mice, Malik et al. compared the PPIX induction capacity of a formulation containing 20% 5-ALA alone, 5-ALA + 2% DMSO and 5-ALA + 2% DMSO + 2% EDTA, respectively. In agreement with a similar study conducted by Casas et al. [155] the DMSO containing formulation induced faster and overall higher PPIX accumulation in tumors than the plain 5-ALA cream. The effect was even

more pronounced in the skin overlying the tumor [224]. Addition of the iron chelator increased PPIX fluorescence. In a clinical trial on patients with nodular BCC (nBCC), Peng et al. applied a cream with 20% ALA alone, 20% ALA+ 20% DMSO + 4% EDTA, respectively, onto the lesions and monitored the PPIX fluorescence. Part of the nBCCs was also pre-treated with 99% DMSO for 15min. They observed four times higher fluorescence in lesions treated with DMSO prior to 5-ALA application than in lesions that were treated with topical 5-ALA alone. DMSO containing cream also induced higher PPIX fluorescence than the control. The best penetration into the lesions was achieved upon DMSO pre-treatment. nBCCs treated with DMSO containing cream showed a twofold higher fluorescence and an improved penetration depth [225]. In another study DMSO enhanced 5-ALA penetration and PPIX accumulation on healthy murine skin *in vivo* and *ex vivo*. The increase of PPIX fluorescence was significant when using formulations containing 1.5% 5-ALA + 20% DMSO and 5% 5-ALA + 10% DMSO, respectively. DMSO neither had an effect on the partition coefficient neither in isopropylmyristate/water, nor in stratum corneum/phosphate buffer saline pH 5.0. One may therefore speculate that the action of DMSO on 5-ALA diffusion into the skin occurs through restructuring the skin rather than solubility mediation. The addition of 3% EDTA to the formulation did not have a significant effect on the PPIX accumulation in skin [226]. Based on the positive effect of the combination 5-ALA/DMSO/EDTA, Ziolkowski et al. made an attempt to improve PPIX accumulation in dysplastic skin diseases by adding glycolic acid. This α -hydroxy acid increases the penetration of hydrophilic drugs [227] possibly due to hydration of the stratum corneum [228]. In the squamous cell carcinoma cell line A431 and skin fibroblasts glycolic acid led to a twofold increase of PPIX concentration. In adenocarcinoma bearing BALBc mice PPIX accumulated faster when glycolic acid was added to the formulation (4 hours versus 6 hours without glycolic acid). In patients with squamous cell carcinoma (SCC) complete response was obtained for all lesions (size 2 to 9 millimeters) after PDT using glycolic acid formulation. When using the formulation without glycolic acid the same result could only be obtained for SCCs smaller than 3 millimeters [229].

Other penetration enhancers have been assessed as alternative for DMSO. Oleic acid impedes the barrier function of the skin by interacting with lipid structures in the stratum corneum and propylene glycol typically increases the drug solubility in the stratum corneum [230]. It was observed that PPIX amounts in murine skin were significantly higher when 5-ALA was formulated with a combination of propylene glycol and oleic acid than with propylene glycol alone (approximately twice as much) [231]. The replacement of oleic acid by glycerol mono

oleate showed similar results [232]. Glycerol mono oleate is a well established biodegradable penetration promoter. In the GIT it is generated endogenously during fat digestion. Next to its surfactant properties it functions as gelling agent in aqueous dispersion. At adequate concentrations it will form a so-called cubic phase. A cubic phase is characterized by a continuous, three dimensional lipid bilayer network of gel like texture. The amphiphilic nature of the formulation allows the dissolution of hydrophilic, as well as hydrophobic compounds. In 2003, Turchiello et al. investigated the stability of 5-ALA and its esters in such a system and concluded that it is an adequate vehicle for the delivery of the PPIX precursor [233]. In murine skin, 5-ALA methyl ester-induced fluorescence from cubic phase gels was up to two times higher compared to an ethanolic solution and up to 5 times higher than after application of 5-ALA methyl ester in Unguentum M and an aqueous solution, respectively [234].

Similar to oleic acid, azone modifies the lipid structure of the stratum corneum [235]. Pre-treatment with this pyrrolidone derivative enhances the response of plantar warts to 5-ALA PDT. In patients bearing two types of plantar warts, myrmecia and mosaic warts, pre-treatment with a 3% azone formulation achieved 100% and 66.7% response, whereas the response was 37.5% and 70%, for warts without pre-treatment, respectively [236].

The commercially available 5-ALA formulation Levulan[®] Kerastick[®] is a hydrophilic alcohol mixture. PPIX fluorescence induction in porcine skin from this formulation was faster and more effective than from a hydrophilic gel containing 40% DMSO and the same 5-ALA concentration [237].

Formulations for systemic application

Since its introduction on the market, 5-ALA is becoming an established pro-drug for fluorescence guided resection and PDT of topical tumors. Current research is trying to exploit this treatment/detection modality for other neoplastic (solid tumors, interstitial cancers: mammary carcinoma, cervical cancer, prostate cancer, ocular application) and non-neoplastic diseases (mycosis, oral leukoplakia, anti-bacterial therapy) as well as cosmetic purposes (skin rejuvenation, hair removal).

In some of these cases the target site is not or only difficult to access for topical administration. Therefore, parenteral formulations are needed to deliver appropriate amounts of 5-ALA or its derivatives to the site of interest. Nevertheless, intravenous formulations are rare. This

can be attributed to drawbacks such as instability of free 5-ALA at physiological pH. Intravenous application necessitates high drug doses, which cause neurovisceral side effects. Free 5-ALA esters, in turn, have shown high acute toxicity in mice [238]. A way to overcome such problems is by encapsulation of the drug into nanoparticles [239]. The size of these midget delivery devices is below 1 μ m [240]. They are small enough to freely circulate in the blood. They may be extravasated through the typically fenestrated neoplastic blood vessel into tumors, where they are trapped due to the enhanced permeability and retention. However, they are too big to trespass the intact epithelia, which prevent their accumulation in healthy tissue. Many organic and inorganic materials can be converted into nanosize particles. 5-ALA has previously been adsorbed onto inorganic nanoparticles made of superparamagnetic iron oxide [241] and gold [242]. However, these materials are inconvenient for intravenous application, because they are not biodegradable. In fact, only three biocompatible polymers (poly lactic acid, poly (lactic co-glycolid acid) and poly ϵ -caprolactone), are approved by the American Food and Drug Administration (FDA) for systemic drug delivery. Their formulation into nanoparticles involves the use of an organic solvent and an aqueous dispersion phase. The hydrophilic to amphiphilic nature of 5-ALA and its esters make it a challenging candidate for the nano-encapsulation, since the molecule has the tendency to stay in the aqueous phase or only adsorb to the surface of the particle.

Conclusion

Literature research reveals that 5-ALA mediated PDT and PD have gained considerable interest over the past 20 years, especially in the therapy of neoplastic diseases. For PDT, this may be attributed to the advantage of the drug to induce less severe side effects than traditional chemotherapeutic agents. Furthermore, the different mechanism of action, low interference with other chemotherapeutics and the possibility of repeated application in a short time, make it suitable for the combination with other therapeutic agents and therapies. PD serves as a powerful tool to visualize neoplasms. It may be carried out by the surgeon *in situ* during tumorresection. As alternative to long lasting procedures of tumor margin determination by biopsy, it may considerably speed up the surgical process.

The use of 5-ALA for PDT and PD is particularly interesting: being an endogenous molecule itself, exogenous 5-ALA serves as prodrug for PPIX, the direct precursor of heme. PPIX, in turn, takes up the function of a photosensitizer.

Approaches to optimize 5-ALA mediated PDT and PD involve physical and chemical methods as well as the modification of the drug carrier.

The chemical derivatization into more lipophilic esters has proven to be of great value, as it could drastically increase bioavailability of the compound. Nevertheless, the use of 5-ALA and its derivatives is still limited to topical application. Therefore, the recent trend goes towards the development of modern systems, which can be administered systemically. These systems include the synthesis of 5-ALA conjugates with macromolecules, such as dendrimers, or the formulation of lipophilic 5-ALA derivatives into injectable polymeric nanoparticles.

Looking at the biosynthesis of heme, the generation of PPIX is theoretically possible through another way than the conversion 5-ALA. 5-ALA transformation follows the heme pathway in its physiological way. The second way, in contrary, implies the generation of PPIX from heme and thus goes against the direction of the heme cycle. The retrieval of iron from heme was until now known to occur via cleavage of the tetrapyrrol skeleton into biliverdin by heme oxygenases or homologues. Recently, Letoffé et al. proposed two proteins in *Escherichia coli*, YfeX and EfeB, to retrieve iron from heme without breaking the tetrapyrrol structure. Since this mechanism rewinds the action of the enzyme FC, they referred to this newly found activity as *deferrochelatase activity* [243]. Taking into consideration that YfeX and EfeB are highly spread in Gram-negative and Gram-positive bacteria, alternative ways of PPIX formation, e.g. by using heme as precursor, may become of interest in future research.

Reference List

1. Rimington C. Was Hippocrates the 1st to Describe A Case of Acute Porphyrin. *Int J Biochem* 1993; **25**: 1351-1352
2. Battle AMD. Porphyrins, Porphyrins, Cancer and Photodynamic Therapy - A Model for Carcinogenesis. *Photochem Photobiol B* 1993; **20**: 5-22
3. Gazzaniga V. Uroporphyrin: Some notes on its ancient historical background. *Am J Nephrol* 1999; **19**: 159-162
4. Norman RA. Past and Future: Porphyrin and Porphyrins. *Skinmed* 2005; **4**: 287-292
5. Brooke J. Historical Implications of Porphyrin. *Br Med J* 1968; **1**: 109-111
6. Macalpine I, Hunter R, Rimington C. Porphyrin in Royal Houses of Stuart Hanover and Prussia - A Follow-Up Study of George 3Rd Illness. *Br Med J* 1968; **1**: 7-18

7. Cox AM. Porphyria and Vampirism - Another Myth in the Making. *Postgrad Med J* 1995; **71**: 643-644
8. Illis L: On Porphyria and the Aetiology of Werwolves. *P Roy Soc Med - London* 1964; **57**: 23-26
9. Scherer J. Untersuchungen Liebigs. *Ann Chem Pharm* 1841; **40**: 1-64
10. Hoppe-Seyler F. Das Hämatin. *Tübinger Med Chem Untersuchungen* 1971; **4**: 441-460
11. Meyer-Betz F. Wirkung des Hämatoporphyrins und anderer Derivate des Blut- und Gallenfarbstoffs. *Dtsch Arch Klin Med* 1913; **112**: 476-503
12. Policard A. Etudes sur les aspects offerts par des tumeurs experimentales examine à la lumière de Wood. *Comp Rend Soc Biol* 1924; **91**: 1423-1428
13. Auler H, Banzer G. Untersuchung über die Rolle der Porphyrine bei geschwulstkranken Menschen und Tieren. *Z Krebsforsch* 1942; **53**: 65-68
14. Peck GC, Mack HP, Holbrook WA, Abels C. Use of hematoporphyrin fluorescence in biliary and cancer surgery. *Ann Surg* 1955; **21**: 181-188
15. Figge FH, Weiland GS. The affinity of neoplastic embryonic and traumatized tissue for porphyrins and metalloporphyrins. *Anat Rec* 1948; **100**: 659
16. Figge FH, Weiland GS, Manganiello LO. Cancer detection and therapy. Affinity of neoplastic, embryonic and traumatized regenerating tissues for porphyrins and metalloporphyrins. *Proc Soc Exp Biol Med* 1948; **68**: 640-641
17. Schwartz SK, Absolon K, Vermund H. Some relationships of porphyrins X-rays and tumours. *Univ Minn Med Bull* 1955; **27**: 7-8
18. Lipson RL, Baldes EJ. The Photodynamic Properties of A Particular Hematoporphyrin Derivative. *Arch Dermatol* 1960; **82**: 508-516
19. Lipson RL, Baldes EJ, Olsen AM. Use of A Derivative of Hematoporphyrin in Tumor Detection. *J Natl Cancer I* 1961; **26**: 1-12
20. Diamond I, Jaenicke R, Wilson CB, Mcdonagh AF, Nielsen S, Granelli SG. Photodynamic Therapy of Malignant Tumors. *Lancet* 1972; **2**: 1175-7
21. Dougherty TJ, Grindey GB, Fiel R, Weishaupt KR, Boyle DG. Photoradiation therapy. II. Cure of animal tumors with hematoporphyrin and light. *J Natl Cancer Inst* 1975; **55**: 115-121
22. Kennedy JC, Pottier RH, Pross DC. Photodynamic therapy with endogenous protoporphyrin IX: basic principles and present clinical experience. *Photochem Photobiol B* 1990; **6**: 143-148
23. Ajioka RS, Phillips JD, Kushner JP. Biosynthesis of heme in mammals. *BBA Mol Cell Res* 2006; **1763**: 723-736

24. Battersby AR, McDonald E. Biosynthesis of Porphyrins and Corrins. *Philos T Roy Soc B* 1976; **273**: 161-180
25. Moore MR. The biochemistry of heme synthesis in porphyria and in the porphyrias. *Clin Dermatol* 1998; **16**: 203-223
26. Heinemann IU, Jahn M, Jahn D. The biochemistry of heme biosynthesis. *Arch Biochem and Biophys* 2008; **474**: 238-251
27. Ferreira GC, Zhang JS. Mechanism of 5-aminolevulinate synthase and the role of the protein environment in controlling the cofactor chemistry. *Cell Mol Biol* 2002; **48**: 827-833
28. Emanuelli T, Pagel FW, Alves LB, Regner A, Souza DO. 5-Aminolevulinic acid inhibits [³H]muscimol binding to human and rat brain synaptic membranes. *Neurochem Res* 2001; **26**: 101-105
29. Bogorad L. Enzymatic Synthesis of Porphyrins from Porphobilinogen .2. Uroporphyrin-III. *J Biol Chem* 1958; **233**: 510-515
30. Battersby AR. Tetrapyrroles: the pigments of life. *Nat Prod Rep* 2000; **17**: 507-526
31. Sassa S. Diagnosis and therapy of acute intermittent porphyria. *Blood Rev* 1996; **10**: 53-58
32. Freeseemann AG, Gross U, Bensidhoum M, de Verneuil H, Doss MO. Immunological, enzymatic and biochemical studies of uroporphyrinogen III synthase deficiency in 20 patients with congenital erythropoietic porphyria. *Eur J Biochem* 1998; **257**: 149-153
33. Mesenhöller M, Matthews EK. A key role for the mitochondrial benzodiazepine receptor in cellular photosensitisation with d-aminolaevulinic acid. *Eur J Pharmacol* 2000; **406**: 171-180
34. Ratcliffe SL, Matthews EK. Modification of the Photodynamic-Action of Delta-Aminolevulinic-Acid (Ala) on Rat Pancreatoma Cells by Mitochondrial Benzodiazepine Receptor Ligands. *Br J Cancer* 1995; **71**: 300-305
35. Taketani S, Kohno H, Furukawa T, Tokunaga R. Involvement of Peripheral-Type Benzodiazepine Receptors in the Intracellular-Transport of Heme and Porphyrins. *J Biochem* 1995; **117**: 875-880
36. Rebeiz N, Arkins S, Kelley KW, Rebeiz CA. Enhancement of coproporphyrinogen III transport into isolated transformed leukocyte mitochondria by ATP. *Arch Biochem Biophys* 1996; **333**: 475-481
37. Hardwick M, Fertikh D, Culty M, Li H, Vidic B, Papadopoulos V. Peripheral-type benzodiazepine receptor (PBR) in human breast cancer: correlation of breast cancer cell aggressive phenotype with PBR expression, nuclear localization, and PBR-mediated cell proliferation and nuclear transport of cholesterol. *Cancer Res* 1999; **59**: 831-842

38. Batra S, Iosif CS. Peripheral benzodiazepine receptor in human endometrium and endometrial carcinomas. *Anticancer Res* 2000; **20**: 463-466
39. Batra S, Iosif CS. Elevated concentrations of mitochondrial peripheral benzodiazepine receptors in ovarian tumors. *Int J Oncol* 1998; **12**: 1295-1298
40. Venturini I, Zeneroli ML, Corsi L, Avallone R, Farina F, Alho H, Baraldi C, Ferrarese C, Pecora N, Frigo M, Ardizzone G, Arrigo A, Pellicci R, Baraldi M. Up-regulation of peripheral benzodiazepine receptor system in hepatocellular carcinoma. *Life Sciences* 1998; **63**: 1269-1280
41. Black KL, Ikezaki K, Toga AW. Imaging of Brain-Tumors Using Peripheral Benzodiazepine Receptor Ligands. 1989; *J Neurosurg* 71: 113-118
42. Katz Y, Eitan A, Amiri Z, Gavish M. Dramatic Increase in Peripheral Benzodiazepine Binding-Sites in Human Colonic Adenocarcinoma As Compared to Normal Colon. *Eur J Pharmacol* 1988; **148**: 483-484
43. Grandchamp B, Phung N, Nordmann Y. Mitochondrial Localization of Coproporphyrinogen-III Oxidase. *Biochem J* 1978; **176**: 97-102
44. Deybach JC, DaSilva V, Grandchamp B, Nordmann Y. The Mitochondrial Location of Protoporphyrinogen Oxidase. *Eur J Biochem* 1985; **149**: 431-435
45. Dean G. Porphyria Variegata. *Acta Dermat-Vener* 1982; 81-85
46. McKay R, Druyan R, Getz GS, Rabinowi M. Intramitochondrial Localization of Delta-Aminolaevulate Synthetase and Ferrochelatase in Rat Liver. *Biochem J* 1969; **114**: 455-6
47. Gardner LC, Cox TM. Biosynthesis of Heme in Immature Erythroid-Cells - the Regulatory Step for Heme Formation in the Human Erythron. *J Biol Chem* 1988; **263**: 6676-6682
48. Kondo M, Hirota N, Takaoka T, Kajiwara M. Heme-Biosynthetic Enzyme-Activities and Porphyrin Accumulation in Normal Liver and Hepatoma-Cell Lines of Rat. *Cell Biol Toxicol* 1993; **9**: 95-105
49. Navone NM, Polo CF, Frisardi AL, Andrade NE, Battle AMD. Heme-Biosynthesis in Human Breast-Cancer Mimetic Invitro Studies and Some Heme Enzymatic-Activity Levels. *Int J Biochem* 1990; **22**: 1407-1411
50. Gibson SL, Cupriks DJ, Havens JJ, Nguyen ML, Hilf R. A regulatory role for porphobilinogen deaminase (PBGD) in delta-aminolaevulinic acid (delta-ALA)-induced photosensitization? *Br J Cancer* 1998; **77**: 235-242
51. Gibson SL, Nguyen ML, Havens JJ, Barbarin A, Hilf R. Relationship of delta-aminolevulinic acid-induced protoporphyrin IX levels to mitochondrial content in neoplastic cells in vitro. *Biochem Biophys Res Com* 1999; **265**: 315-321

52. Hilf R, Havens JJ, Gibson SL. Effect of delta-aminolevulinic acid on protoporphyrin IX accumulation in tumor cells transfected with plasmids containing porphobilinogen deaminase DNA. *Photochem Photobiol* 1999; **70**: 334-340
53. Gibson SL, Havens JJ, Metz L, Hilf R. Is delta-aminolevulinic acid dehydratase rate limiting in heme biosynthesis following exposure of cells to delta-aminolevulinic acid? *Photochem Photobiol* 2001; **73**: 312-317
54. Li G, Szewczuk MR, Pottier RH, Kennedy JC. Effect of mammalian cell differentiation on response to exogenous 5-aminolevulinic acid. *Photochem Photobiol* 1999; **69**: 231-235
55. Schwartz DI, Gozlan Y, Greenbaum L, Babushkina T, Katcoff DJ, Malik Z. Differentiation-dependent photodynamic therapy regulated by porphobilinogen deaminase in B16 melanoma. *Br J Cancer* 2004; **90**: 1833-1841
56. Krieg RC, Messmann H, Rauch J, Seeger S, Knuechel R. Metabolic characterization of tumor cell-specific protoporphyrin IX accumulation after exposure to 5-aminolevulinic acid in human colonic cells. *Photochem Photobiol* 2002; **76**: 518-525
57. Krieg RC, Fickweiler S, Wolfbeis OS, Knuechel R. Cell-type specific protoporphyrin IX metabolism in human bladder cancer in vitro. *Photochem Photobiol* 2000; **72**: 226-233
58. Bartosova J, Hrkal Z. Accumulation of protoporphyrin-IX (PpIX) in leukemic cell lines following induction by 5-aminolevulinic acid (ALA). *Comp Biochem Phys C* 2000; **126**: 245-252
59. Hinnen P, de Rooij FWM, Terlouw EM, Edixhoven A, van Dekken H, van Hillegersberg R, Tilanus HW, Wilson JHP, Siersema PD. Porphyrin biosynthesis in human Barrett's oesophagus and adenocarcinoma after ingestion of 5-aminolaevulinic acid. *Br J Cancer* 2000; **83**: 539-43
60. Morgan EH. Effect of Ph and Iron Content of Transferrin on Its Binding to Reticulocyte Receptors. *Biochim Biophys Acta* 1983; **762**: 498-502
61. Morgan EH. Studies on the Mechanism of Iron Release from Transferrin. *Biochim Biophys Acta* 1979; **580**: 312-326
62. Richardson DR, Ponka P. The molecular mechanisms of the metabolism and transport of iron in normal and neoplastic cells. *BBA - Rev Biomembranes* 1997; **1331**: 1-40
63. Kearsley JH, Furlong KL, Cooke RA, Waters MJ. An Immunohistochemical Assessment of Cellular Proliferation Markers in Head and Neck Squamous-Cell Cancers. *Br J Cancer* 1990; **61**: 821-827
64. Parodi MT, Tonini GP, Bologna R, Franchini E, Cornaglia-Ferraris P. Cisplatin-induced erythroid differentiation in K562 cells: modulation of transferrin receptor. *B I Sieroter Milan* 1988; **67**: 142-148

65. Prutki M, Poljak-Blazi M, Jakopovic M, Tomas D, Stipancic I, Zarkovic N. Altered iron metabolism, transferrin receptor 1 and ferritin in patients with colon cancer. *Cancer Lett* 2006; **238**: 188-196
66. Page MA, Baker E, Morgan EH. Transferrin and Iron Uptake by Rat Hepatocytes in Culture. *Am J Physiol* 1984; **246**: G26-G33
67. Vandewalle B, Hornez L, Revillion F, Lefebvre J. Secretion of Transferrin by Human-Breast Cancer-Cells. *Biochem Biophys Res Com* 1989; **163**: 149-154
68. Kwok JC, Richardson DR. The iron metabolism of neoplastic cells: alterations that facilitate proliferation? *Crit Rev Oncol Hemat* 2002; **42**: 65-78
69. Hibbs JB, Taintor RR, Vavrin Z. Iron Depletion - Possible Cause of Tumor-Cell Cytotoxicity Induced by Activated Macrophages. *Biochem Biophys Res Com* 1984; **123**: 716-723
70. Rud E, Gederaas O, Hogset A, Berg K. 5-aminolevulinic acid, but not 5-aminolevulinic acid esters, is transported into adenocarcinoma cells by system BETA transporters. *Photochem Photobiol* 2000; **71**: 640-647
71. McGivan JD, Pastoranglada M. Regulatory and Molecular Aspects of Mammalian Amino-Acid-Transport. *Biochem J* 1994; **299**: 321-334
72. Bermudez MM, Correa GS, Perotti C, Batlle AM, Casas A. Delta-Aminolevulinic acid transport in murine mammary adenocarcinoma cells is mediated by beta transporters. *Br J Cancer* 2002; **87**: 471-474
73. Brennan MJW, Cantrill RC. Delta-Aminolevulinic-Acid Is A Potent Agonist for Gaba Autoreceptors. *Nature* 1979; **280**: 514-515
74. Kasche A, Luderschmidt S, Ring J, Hein R. PDT induces less pain in patients treated with MAL compared to ALA. *JDD* 2006; **5**: 353-356
75. Wiegell SR, Stender IM, Na R, Wulf HC. Pain associated with photodynamic therapy using 5-aminolevulinic acid or 5-aminolevulinic acid methylester on tape-stripped normal skin. *Arch dermatol* 2003; **139**: 1173-1177
76. Wiegell SR, Wulf HC. Photodynamic therapy of acne vulgaris using 5-aminolevulinic acid versus methyl aminolevulinate. *J Am Acad Dermatol* 2006; **54**: 647-651
77. Doring F, Walter J, Will J, Focking M, Boll M, Amasheh S, Clauss W, Daniel H (1998) Delta-aminolevulinic acid transport by intestinal and renal peptide transporters and its physiological and clinical implications. *J Clin Invest* **101**: 2761-2767
78. Richards FF, Scott JJ. Glycine Metabolism in Acute Porphyrria. *Clin Sci* 1961; **20**: 387-400
79. Prato V, Massaro AL, Mazza U, Bianco G, Accatino G. Modificazioni del Metabolismo Porfirinico Dopo Doppio Carico di Glicina .I. in Uomini Apparentemente Sani. *B Soc Ital Biol Speriment* 1965; **41**: 1074

80. Langer S, Abels C, Botzlar A, Pahernik SA, Rick K, Szeimies RM, Goetz AE Active and higher intracellular uptake of 5-aminolevulinic acid in tumors may be inhibited by glycine. *J Invest Dermatol* 1999; **112**: 723-728
81. Frolund S, Marquez OC, Larsen M, Brodin B, Nielsen CU. delta-Aminolevulinic acid is a substrate for the amino acid transporter SLC36A1 (hPAT1). *Br J Pharmacol* 2010; **159**: 1339-1353
82. Anderson CMH, Jevons M, Thangaraju M, Edwards N, Conlon NJ, Woods S, Ganapathy V, Thwaites DT. Transport of the Photodynamic Therapy Agent 5-Aminolevulinic Acid by Distinct H⁺-Coupled Nutrient Carriers Coexpressed in the Small Intestine. *J Pharmacol Exp Ther* 2010; **332**: 220-228
83. Thwaites DT, Mcewan GTA, Hirst BH, Simmons NL H⁺-Coupled Alpha-Methylaminoisobutyric Acid Transport in Human Intestinal Caco-2 Cells. *BBA Biomembranes* 1995; **1234**: 111-118
84. Chen Z, Fei YJ, Anderson CMH, Wake KA, Miyauchi S, Huang W, Thwaites DT, Ganapathy V. Structure, function and immunolocalization of a proton-coupled amino acid transporter (hPAT1) in the human intestinal cell line Caco-2. *J Physiol* 2003; **546**: 349-361
85. Ennis SR, Novotny A, Xiang J, Shakui P, Masada T, Stummer W, Smith DE, Keep RF. Transport of 5-aminolevulinic acid between blood and brain. *Brain Res* 2003; **959**: 226-234
86. Novotny A, Xiang J, Stummer W, Teuscher NS, Smith DE, Keep RF. Mechanisms of 5-aminolevulinic acid uptake at the choroid plexus. *J Neurochem* 2000; **75**: 321-328
87. Hu YJ, Shen H, Keep RF, Smith DE. Peptide transporter 2 (PEPT2) expression in brain protects against 5-aminolevulinic acid neurotoxicity. *J Neurochem* 2007; **103**: 2058-2065
88. Garcia SC, Moretti MB, Garay MV, Batlle AM. Delta-aminolevulinic acid transport through blood-brain barrier. *Gen Pharmacol* 1998; **31**: 579-582
89. Terr L, Weiner LP. An Autoradiographic Study of Delta-Aminolevulinic-Acid Uptake by Mouse-Brain. *Exp Neurol* 1983; **79**: 564-568
90. Di Venosa G, Batlle AM, Fukuda H, MacRobert AJ, Casas A. Distribution of 5-aminolevulinic acid derivatives and induced porphyrin kinetics in mice tissues. *Cancer Chemother Pharmacol* 2006; **58**:478-86
91. Stummer W, Stocker S, Novotny A, Heimann A, Sauer O, Kempfski O, Plesnila N, Wietzorrek J, Reulen HJ. In vitro and in vivo porphyrin accumulation by C6 glioma cells after exposure to 5-aminolevulinic acid. *Photochem Photobiol B* 1998; **45**: 160-169
92. Lilge L, Olivo MC, Schatz SW, MaGuire JA, Patterson MS, Wilson BC. The sensitivity of normal brain and intracranially implanted VX2 tumor to interstitial photodynamic therapy. *Br J Cancer* 1996; **73**: 332-343

93. Hebeda KM, Saarnak AE, Olivo MC, Sterenborg HJ, Wolbers JG. 5-Aminolevulinic acid induced endogenous porphyrin fluorescence in 9L and C6 brain tumours and in the normal rat brain. *Acta Neurochir* 1998; **140**: 503-512
94. Maeda H, Wu J, Sawa T, Matsumura Y, Hori K. Tumor vascular permeability and the EPR effect in macromolecular therapeutics: a review. *J Control Release* 2000; **65**: 271-284
95. Maeda H, Bharate GY, Daruwalla J. Polymeric drugs for efficient tumor-targeted drug delivery based on EPR-effect. *Eur J Pharm Biopharm* 2009; **71**: 409-419
96. Svastova E, Hulikova A, Rafajova M, Zat'ovicova M, Gibadulinova A, Casini A, Cecchi A, Scozzafava A, Supuran CT, Pastorek J, Pastorekova S. Hypoxia activates the capacity of tumor-associated carbonic anhydrase IX to acidify extracellular pH. *Febs Letters* 2004; **577**: 439-445
97. Piot B, Rousset N, Lenz P, Eleouet S, Carre J, Vonarx V, Bourre L, Patrice T. Enhancement of delta aminolevulinic acid-photodynamic therapy in vivo by decreasing tumor pH with glucose and amiloride. *Laryngoscope* 2001; **111**: 2205-2213
98. Wyld L, Reed MW, Brown NJ. The influence of hypoxia and pH on aminolaevulinic acid-induced photodynamic therapy in bladder cancer cells in vitro. *Br J Cancer* 1998; **77**: 1621-1627
99. Fuchs C, Riesenberger R, Siegert J, Baumgartner R. pH-dependent formation of 5-aminolaevulinic acid-induced protoporphyrin IX in fibrosarcoma cells. *Photochem Photobiol B* 1997; **40**: 49-54
100. Bech O, Berg K, Moan J. The pH dependency of protoporphyrin IX formation in cells incubated with 5-aminolevulinic acid. *Cancer Lett* 1997; **113**: 25-29
101. Krammer B, Uberriegler K. In-vitro investigation of ALA-induced protoporphyrin IX. *Photochem Photobiol B* 1996; **36**: 121-126
102. Bech O, Berg K, Moan J. The pH dependency of protoporphyrin IX formation in cells incubated with 5-aminolevulinic acid. *Cancer Lett* 1997; **113**: 25-29
103. Bech O, Berg K, Moan J. The pH dependency of protoporphyrin IX formation in cells incubated with 5-aminolevulinic acid. *Cancer Lett* 1997; **113**: 25-29
104. Kaliszewski M, Kwasny M, Juzeniene A, Juzenas P, Graczyk A, Ma LW, Iani V, Mikolajewska P, Moan J. Biological activity of 5-aminolevulinic acid and its methyl ester after storage under different conditions. *Photochem Photobiol B* 2007; **87**: 67-72
105. Bech Gadmar O, Moan J, Scheie E, Ma LW, Peng Q. The stability of 5-aminolevulinic acid in solution. *Photochem Photobiol B* 2002; **67**: 187-193
106. Stefanadis C, Chrysochoou C, Markou D, Petraki K, Panagiotakos DB, Fasoulakis C, Kyriakidis A, Papadimitriou C, Toutouzas PK. Increased temperature of malignant urinary bladder tumors in vivo: the application of a new method based on a catheter technique. *J Clin Oncol* 2001; **19**: 676-681

107. Yahara T, Koga T, Yoshida S, Nakagawa S, Deguchi H, Shirouzu K. Relationship between microvessel density and thermographic hot areas in breast cancer. *Surg Today* 2003; **33**: 243-248
108. Moan J, Berg K, Gadmar OB, Iani V, Ma LW, Juzenas P. The temperature dependence of protoporphyrin IX production in cells and tissues. *Photochem Photobiol* 1999; **70**: 669-673
109. Juzenas P, Sorensen R, Iani V, Moan J. Uptake of topically applied 5-aminolevulinic acid and production of protoporphyrin IX in normal mouse skin: dependence on skin temperature. *Photochem Photobiol* 1999; **69**: 478-481
110. Juzeniene A, Juzenas P, kaalhus O, Iani V, Moan J. Temperature effect on accumulation of protoporphyrin IX after topical application of 5-aminolevulinic acid and its methylester and hexylester derivatives in normal mouse skin. *Photochem Photobiol* 2002; **76**: 452-456
111. Shioi Y, Nagamine M, Kuroki M, Sasa T. Purification by Affinity-Chromatography and Properties of Uroporphyrinogen-I Synthetase from *Chlorella-Regularis*. *Biochim Biophys Acta* 1980; **616**: 300-309
112. van den Akker JT, Boot K, Vernon DI, Brown SB, Groenendijk L, van Rhoon GC, Sterenborg HJ. Effect of elevating the skin temperature during topical ALA application on in vitro ALA penetration through mouse skin and in vivo PpIX production in human skin. *Photochem Photobiol Sci* 2004; **3**: 263-267
113. Walters KA. Drug Delivery - Topical and Transdermal Routes. In: Swarbrick J, Boylan J.C. (eds) *Encyclopedia of Pharmaceutical Technology*. Marcel Dekker, New York, Basel, 2002; pp 945-960
114. van den Akker JT, Holroyd JA, Vernon DI, Sterenborg HJ, Brown SB. Comparative in vitro percutaneous penetration of 5-aminolevulinic acid and two of its esters through excised hairless mouse skin. *Lasers Surg Med* 2003; **33**: 173-181
115. van den Akker JT, Iani V, Star WM, Sterenborg HJ, Moan J. Systemic component of protoporphyrin IX production in nude mouse skin upon topical application of aminolevulinic acid depends on the application conditions. *Photochem Photobiol* 2002; **75**: 172-177
116. Ibbotson SH, Jong C, Lesar A, Ferguson JS, Padgett M, O'Dwyer M, Barnetson R, Ferguson J. Characteristics of 5-aminolaevulinic acid-induced protoporphyrin IX fluorescence in human skin in vivo. *Photodermatol Photo* 2006; **22**: 105-110
117. Goff BA, Bachor R, Kollias N, Hasan T. Effects of Photodynamic Therapy with Topical Application of 5-Aminolevulinic Acid on Normal Skin of Hairless Guinea-Pigs. *Photochem Photobiol B* 1992; **15**: 239-251
118. Katz BK, Truong S, Maiwald DC, Frew KE, George D. Efficacy of Microdermabrasion Preceding ALA application in reducing the incubation time of ALA in Laser PDT. *JDD* 2007; **6**: 140-142

119. Tsai JC, Chen IH, Wong TW, Lo YL. In vitro/in vivo correlations between transdermal delivery of 5-aminolaevulinic acid and cutaneous protoporphyrin IX accumulation and effect of formulation. *Br J Dermatol* 2002; **146**: 853-862
120. Kleinpenning MM, Smits T, Ewalds E, van Erp PEJ, van de Kerkhof PCM, Gerritsen MJP. Heterogeneity of fluorescence in psoriasis after application of 5-aminolaevulinic acid: an immunohistochemical study. *Br J Dermatol* 2006; **155**: 539-545
121. Smits T, van Laarhoven AIM, Staassen A, van de Kerkhof PCM, van Erp PEJ, Gerritsen MJP. Induction of protoporphyrin IX by aminolaevulinic acid in actinic keratosis, psoriasis and normal skin: preferential porphyrin enrichment in differentiated cells. *Br J Dermatol* 2009; **160**: 849-857
122. Gerritsen MJP, Smits T, Kleinpenning MM, van de Kerkhof PCM, van Erp PEJ. Pre-treatment to Enhance Protoporphyrin IX Accumulation in Photodynamic Therapy. *Dermatology* 2009; **218**: 193-202
123. Lopez RF, Lange N, Guy R, Bentley MV. Photodynamic therapy of skin cancer: controlled drug delivery of 5-ALA and its esters. *Adv Drug Deliv Rev* 2004; **56**: 77-94
124. Fritsch C, Goerz G, Ruzicka T. Photodynamic therapy in dermatology. *Arch dermatol* 1998; **134**: 207-214
125. Fotinos N, Campo MA, Popowycz F, Gurny R, Lange N. 5-Aminolevulinic acid derivatives in photomedicine: Characteristics, application and perspectives. *Photochem Photobiol* 2006; **82**: 994-1015
126. Fritsch C, Lang K, Neuse W, Ruzicka T, Lehmann P. Photodynamic diagnosis and therapy in dermatology. *Skin Pharmacol Appl Skin Physiol* 1998; **11**: 358-373
127. Soler AM, Warloe T, Berner A, Giercksky KE. A follow-up study of recurrence and cosmesis in completely responding superficial and nodular basal cell carcinomas treated with methyl 5-aminolaevulinate-based photodynamic therapy alone and with prior curettage. *Br J Dermatol* 2001; **145**: 467-471
128. Wennberg AM, Larko O, Lonroth P, Larson G, Krogstad AL. Delta-aminolevulinic acid in superficial basal cell carcinomas and normal skin-a microdialysis and perfusion study. *Clin Exp Dermatol* 2000; **25**: 317-322
129. Moseley H, Brancalion L, Lesar AE, Ferguson J, Ibbotson SH. Does surface preparation alter ALA uptake in superficial non-melanoma skin cancer in vivo? *Photodermatol Photo* 2008; **24**: 72-75
130. Soler AM, Warloe T, Tausjo J, Berner A. Photodynamic therapy by topical aminolevulinic acid, dimethylsulphoxide and curettage in nodular basal cell carcinoma: a one-year follow-up study. *Acta Dermato-Venereologica* 1999; **79**: 204-206
131. Christensen E, Skogvoll E, Viset T, Warloe T, Sundstrom S. Photodynamic therapy with 5-aminolaevulinic acid, dimethylsulfoxide and curettage in basal cell carcinoma: a 6-year clinical and histological follow-up. *J Eur Acad Dermatol* 2009; **23**: 58-66

132. Itoh Y, Henta T, Ninomiya Y, Tajima S, Ishibashi A. Repeated 5-aminolevulinic acid-based photodynamic therapy following electro-curettage for pigmented basal cell carcinoma. *J Dermatol* 2000; **27**: 10-15
133. Shen S, Lee W, Fang Y, Hu C, Fang J. In vitro percutaneous absorption and in vivo protoporphyrin IX accumulation in skin and tumours after topical 5-aminolevulinic acid application with enhancement using erbium:YAG Laser. *J Pharm Sci* 2006; **95**: 929-938
134. Kalia YN, Bachhav YG, Bragagna T, Boehler C. Intraepidermal Delivery - P.L.E.A.S.E. a new laser microporation technology. *Drug Deliv Tech* 2008; **8**:
135. Smucler R, Vlk M. Combination of Er : YAG laser and photodynamic therapy in the treatment of nodular basal cell carcinoma. *Lasers Surg Med* 2008; **40**: 153-158
136. Fukui T, Watanabe D, Tamada Y, Matsumoto Y. Photodynamic Therapy Following Carbon Dioxide Laser Enhances Efficacy in the Treatment of Extramammary Paget's Disease. *Acta Dermato-Venereologica* 2009; **89**: 150-154
137. Fabbrocini G, Di Costanzo MP, Riccardo AM, Quarto M, Colasanti A, Roberti G, Monfrecola G. Photodynamic therapy with topical delta-aminolaevulinic acid for the treatment of plantar warts. *Photochem Photobiol B* 2001; **61**: 30-34
138. Radakovic-Fijan S, Blecha-Thathammer U, Schleyer V, Szeimies RM, Zwingers T, Honigsmann H, Tanew A. Topical aminolaevulinic acid-based photodynamic therapy as a treatment option for psoriasis? Results of a randomized, observer-blinded study. *Br J Dermatol* 2005; **152**: 279-283
139. Donnelly RF, Morrow DIJ, McCarron PA, Woolfson AD, Morrissey A, Juzenas P, Juzeniene A, Iani V, McCarthy HO, Moan J. Microneedle-mediated intradermal delivery of 5-aminolevulinic acid: Potential for enhanced topical photodynamic therapy. *J Control Release* 2008; **129**: 154-162
140. Donnelly RF, Morrow DIJ, McCarron PA, Garland MJ, Woolfson AD. Influence of solution viscosity and injection protocol on distribution patterns of jet injectors: Application to photodynamic tumortargeting. *Photochem Photobiol B* 2007; **89**: 98-109
141. Campbell SM, Pye A, Horton S, Matthew J, Helliwell P, Curnow A. A clinical investigation to determine the effect of pressure injection on the penetration of topical methyl aminolevulinate into nodular basal cell carcinoma of the skin. *J Environ Pathol Tox* 2007; **26**: 295-303
142. Kalia YN, Naik A, Garrison J, Guy RH. Iontophoretic drug delivery. *Adv Drug Deliv Rev* 2004; **56**: 619-658
143. Lopez RF, Bentley MV, Delgado-Charro BM, Guy RH. Optimization of aminolevulinic acid delivery by iontophoresis. *J Control Release* 2003; **88**: 65-70
144. Rhodes LE, Tsoukas MM, Anderson RR, Kollias N. Iontophoretic delivery of ALA provides a quantitative model for ALA pharmacokinetics and PpIX phototoxicity in human skin. *J Invest Dermatol* 1997; **108**: 87-91

145. Lopez RFV, Vitoria M, Bentley LB, Delgado-Charro MB, Guy RH. Iontophoretic delivery of 5-aminolevulinic acid (ALA): Effect of pH. *Pharm Res* 2001; **18**: 311-315
146. Gerscher S, Connelly JP, Beijersbergen van Henegouwen MJ, MacRobert AJ, Watt P, Rhodes LE. A quantitative assessment of protoporphyrin IX metabolism and phototoxicity in human skin following dose-controlled delivery of the prodrugs 5-aminolaevulinic acid and 5-aminolaevulinic acid-n-pentylester. *Br J Dermatol* 2001; **144**: 983-990
147. Mizutani K, Watanabe D, Akita Y, Akimoto M, Tamada Y, Matsumoto Y. Photodynamic therapy using direct-current pulsed iontophoresis for 5-aminolevulinic acid application. *Photodermatol Photo* 2009; **25**: 280-282
148. Merclin N, Bender J, Sparr E, Guy RH, Ehrsson H, Engstrom S. Transdermal delivery from a lipid sponge phase--iontophoretic and passive transport in vitro of 5-aminolevulinic acid and its methyl ester. *J Control Release* 2004; **100**: 191-198
149. Ma LW, Moan J, Peng Q, Iani V. Production of protoporphyrin IX induced by 5-aminolevulinic acid in transplanted human colon adenocarcinoma of nude mice can be increased by ultrasound. *Int J Cancer* 1998; **78**: 464-469
150. Charoenbanpachon S, Krasieva T, Ebihara A, Osann K, Wilder-Smith P. Acceleration of ALA-induced PpIX fluorescence development in the oral mucosa. *Lasers Surg Med* 2003; **32**: 185-188
151. Lipinski CA, Lombardo F, Dominy BW, Feeney PJ. Experimental and computational approaches to estimate solubility and permeability in drug discovery and development settings. *Adv Drug Deliv Rev* 2001; **46**: 3-26
152. Uehlinger P, Zellweger M, Wagnieres G, Juillerat-Jeanneret L, van den BH, Lange N. 5-Aminolevulinic acid and its derivatives: physical chemical properties and protoporphyrin IX formation in cultured cells. *Photochem Photobiol B* 2000; **54**: 72-80
153. Kloek J, Beijersbergen van Henegouwen MJ. Prodrugs of 5-aminolevulinic acid for photodynamic therapy. *Photochem Photobiol* 1996; **64**: 994-1000
154. Peng Q, Moan J, Warloe T, Iani V, Steen HB, Bjorseth A, Nesland JM. Build-up of esterified aminolevulinic-acid-derivative-induced porphyrin fluorescence in normal mouse skin. *Photochem Photobiol B* 1996; **34**: 95-96
155. Casas A, Fukuda H, Di Venosa G, Batlle AM. The influence of the vehicle on the synthesis of porphyrins after topical application of 5-aminolaevulinic acid. Implication in cutaneous photodynamic sensitization. *Br J Dermatol* 2000; **143**: 564-572
156. Moan J, Ma LW, Iani V. On the pharmacokinetics of topically applied 5-aminolevulinic acid and two of its esters. *Int J Cancer* 2001; **92**: 139-143
157. Casas A, Batlle AM, Butler AR, Robertson D, Brown EH, MacRoberts A, Riley PA. Comparative effect of ALA derivatives on protoporphyrin IX production in human and rat skin organ cultures. *Br J Cancer* 1999; **80**: 1525-1532

158. Moan J, Ma LW, Juzeniene A, Iani V, Juzenas P, Apricena F, Peng Q. Pharmacology of protoporphyrin IX in nude mice after application of ALA and ALA esters. *Int J Cancer* 2003; **103**: 132-135
159. Gederaas O, Holroyd A, Brown SB, Vernon DI, Moan J, Berg K. 5-Aminolaevulinic acid methyl ester transport on amino acid carriers in a human colon adenocarcinoma cell line. *Photochem Photobiol* 2001; **73**: 164-169
160. De Rosa FS, Lopez RF, Thomazini JA, Tedesco AC, Lange N, Bentley MV. In vitro metabolism of 5-ALA esters derivatives in hairless mice skin homogenate and in vivo PpIX accumulation studies. *Pharm Res* 2004; **21**: 2247-2252
161. De Rosa FS, Tedesco AC, Lopez RF, Riemma Pierre MB, Lange N, Marchetti JM, Gomes Rotta JC, Bentley MV. In vitro skin permeation and retention of 5-aminolevulinic acid ester derivatives for photodynamic therapy. *J Control Release* 2003; **89**: 261-269
162. Chen JY, Peng Q, Jodl HJ. Infrared spectral comparison of 5-aminolevulinic acid and its hexyl ester. *Spectrochim Acta A* 2003; **59**: 2571-2576
163. Berkovitch G, Doron D, Nudelman A, Malik Z, Rephaeli A. Novel Multifunctional Acyloxyalkyl Ester Prodrugs of 5-Aminolevulinic Acid Display Improved Anticancer Activity Independent and Dependent on Photoactivation. *J Med Chem* 2008; **51**: 7356-7369
164. Bourre L, Giuntini F, Eggleston IM, Wilson M, MacRobert AJ. Protoporphyrin IX enhancement by 5-aminolaevulinic acid peptide derivatives and the effect of RNA silencing on intracellular metabolism. *Br J Cancer* 2009; **100**: 723-731
165. Berger Y, Ingrassia L, Neier R, Juillerat-Jeanneret L. Evaluation of dipeptide-derivatives of 5-aminolevulinic acid as precursors for photosensitizers in photodynamic therapy. *Bioorg Med Chem* 2003; **11**: 1343-1351
166. Dixon MJ, Bourre L, MacRobert AJ, Eggleston IM. Novel prodrug approach to photodynamic therapy: Fmoc solid-phase synthesis of a cell permeable peptide incorporating 5-aminolaevulinic acid. *Bioorg Med Chem Lett* 2007; **17**: 4518-4522
167. Battah SH, Chee CE, Nakanishi H, Gerscher S, MacRobert AJ, Edwards C. Synthesis and biological studies of 5-aminolevulinic acid-containing dendrimers for photodynamic therapy. *Bioconjug Chem* 2001; **12**: 980-988
168. Battah SH, O'Neill S, Edwards C, Balaratnam S, Dobbin P, MacRobert AJ. Enhanced porphyrin accumulation using dendritic derivatives of 5-aminolaevulinic acid for photodynamic therapy: an in vitro study. *Int J Biochem Cell Biol* 2006; **38**: 1382-1392
169. Battah SH, Balaratnam S, Casas A, O'Neill S, Edwards C, Battle AM, Dobbin P, MacRobert AJ. Macromolecular delivery of 5-aminolaevulinic acid for photodynamic therapy using dendrimer conjugates. *Mol Cancer Ther* 2007; **6**: 876-885
170. Brunner H, Hausmann F, Knuechel R. New 5-aminolevulinic acid esters - efficient protoporphyrin precursors for photodetection and photodynamic therapy. *Photochem Photobiol* 2003; **78**: 481-486

171. Di Venosa G, Casas A, Battah SH, Dobbin P, Fukuda H, MacRobert AJ, Batlle AM. Investigation of a novel dendritic derivative of 5-aminolaevulinic acid for photodynamic therapy. *Int J Biochem Cell Biol* 2006; **38**: 82-91
172. Casas A, Battah S, Di Venosa G, Dobbin P, Rodriguez L, Fukuda H, Batlle A, MacRobert AJ. Sustained and efficient porphyrin generation in vivo using dendrimer conjugates of 5-ALA for photodynamic therapy. *J Control Release* 2009; **135**: 136-143
173. Vallinayagam R, Weber J, Neier R. Novel Bioconjugates of Aminolevulinic Acid with Vitamins. *Org Lett* 2008; **10**: 4453-4455
174. Vallinayagam R, Schmitt F, Barge J, Wagnieres G, Wenger V, Neier R, Juillerat-Jeanneret L. Glycoside esters of 5-aminolevulinic acid for photodynamic therapy of cancer. *Bioconjugate Chem* 2008; **19**: 821-839
175. Gurba P, Vallinayagam R, Schmitt F, Furrer J, Juillerat-Jeanneret L, Neier R. Novel Bioconjugates of Aminolevulinic Acid with Nucleosides. *Synthesis* 2008; 3957-3962
176. Berger Y, Greppi A, Siri O, Neier R, Juillerat-Jeanneret L. Ethylene glycol and amino acid derivatives of 5-aminolevulinic acid as new photosensitizing precursors of protoporphyrin IX in cells. *J Med Chem* 2000; **43**: 4738-4746
177. Bourre L, Giuntini F, Eggleston IM, Wilson M, MacRobert AJ. 5-aminolaevulinic acid peptide prodrugs enhance photosensitization for photodynamic therapy. *Mol Cancer Ther* 2008; **7**: 1720-1729
178. Giuntini F, Bourre L, MacRobert AJ, Wilson M, Eggleston IM. Improved Peptide Prodrugs of 5-ALA for PDT: Rationalization of Cellular Accumulation and Protoporphyrin IX Production by Direct Determination of Cellular Prodrug Uptake and Prodrug Metabolization. *J Med Chem* 2009; **52**: 4026-4037
179. Tsai JC, Chen IH, Wong TW, Lo YL. In vitro/in vivo correlations between transdermal delivery of 5-aminolaevulinic acid and cutaneous protoporphyrin IX accumulation and effect of formulation. *Br J Dermatol* 2002; **146**: 853-862
180. Collaud S, Peng QA, Gurny R, Lange N. Thermosetting gel for the delivery of 5-aminolevulinic acid esters to the cervix. *J Pharm Sci* 2008; **97**: 2680-2690
181. Casas A, Fukuda H, Batlle AMD. Tissue distribution and kinetics of endogenous porphyrins synthesized after topical application of ALA in different vehicles. *Br J Cancer* 1999; **81**: 13-18
182. van den Akker JT, de Bruijn HS, Beijersbergen van Henegouwen MJ, Star WM, Sterenborg HJ. Protoporphyrin IX fluorescence kinetics and localization after topical application of ALA pentyl ester and ALA on hairless mouse skin with UVB-induced early skin cancer. *Photochem Photobiol* 2000; **72**: 399-406
183. Morrow DIJ, McCarron PA, Woolfson AD, Donnelly RF. Practical Considerations in the Pharmaceutical Analysis of Methyl and Hexyl Ester Derivatives of 5-Aminolevulinic Acid. *Open Anal Chem J* 2009; **3**: 6-15

184. Ackermann G, Abels C, Baumler W, Langer S, Landthaler M, Lang EW, Szeimies RM. Simulations on the selectivity of 5-aminolaevulinic acid-induced fluorescence in vivo. *Photochem Photobiol B* 1998; **47**: 121-128
185. Novo M, Hüttmann G, Diddens H. Chemical instability of 5-aminolevulinic acid used in fluorescence diagnosis of bladder tumours. *Photochem Photobiol B* 1996; **34**: 143-148
186. Butler AR, George S. The Non-enzymatic Cyclic Dimerization of 5-Aminolevulinic Acid. *Tetrahedron* 1992; **48**: 7879-7886
187. Bunke A, Zerbe O, Burmeister G, Merkle HP, Gander B. Degradation mechanism and stability of 5-aminolevulinic acid. *J Pharm Sci* 2000; **89**: 1335-1341
188. Elfsson I, Wallin I, Eksborg S, Rudaeus K, Ros AM, Ehrsson H. Stability of 5-aminolevulinic acid in aqueous solution. *Eur J Pharm Sci* 1998; **7**: 87-91
189. Juzeniene A, Ma LW, Juzenas P, Iani V, Lange N, Moan J. Production of protoporphyrin IX from 5-aminolevulinic acid and two of its esters in cells in vitro and tissues in vivo. *Cell Mol Biol* 2002; **48**: 911-916
190. Tunstall RG, Barnett AA, Schofield J, Griffiths J, Vernon DI, Brown SB, Roberts DJH. Porphyrin accumulation induced by 5-aminolaevulinic acid esters in tumorcells growing in vitro and in vivo. *Br J Cancer* 2002; **87**: 246-250
191. Casas A, Perotti C, Fukuda H, Rogers L, Butler AR, Batlle AM. ALA and ALA hexyl ester-induced porphyrin synthesis in chemically induced skin tumours: the role of different vehicles on improving photosensitization. *Br J Cancer* 2001; **85**: 1794-1800
192. Hurlimann AF, Hanggi G, Panizzon RG. Photodynamic therapy of superficial basal cell carcinomas using topical 5-aminolevulinic acid in a nanocolloid lotion. *Dermatology* 1998; **197**: 248-254
193. Casas A, Perotti C, Saccoliti M, Sacca P, Fukuda H, Batlle AM. ALA and ALA hexyl ester in free and liposomal formulations for the photosensitisation of tumororgan cultures. *Br J Cancer* 2002; **86**: 837-842
194. Fukuda H, Paredes S, Batlle AM. Tumor-localizing properties of porphyrins. In vitro studies using the porphyrin precursor, aminolevulinic acid, in free and liposome encapsulated forms. *Drug Des Deliv* 1989; **5**: 133-139
195. Fukuda H, Paredes S, Batlle AM. Tumour-localizing properties of porphyrins. In vivo studies using free and liposome encapsulated aminolevulinic acid. *Comp Biochem Physiol B* 1992; **102**: 433-436
196. Di Venosa G, Hermida L, Batlle A, Fukuda H, Defain MV, Mamone L, Rodriguez L, MacRobert A, Casas A. Characterisation of liposomes containing aminolevulinic acid and derived esters. *Photochem Photobiol B* 2008; **92**: 1-9
197. Casas A, Batlle A. Aminolevulinic acid derivatives and liposome delivery as strategies for improving 5-aminolevulinic acid-mediated photodynamic therapy. *Curr Med Chem* 2006; **13**: 1157-1168

198. Di Venosa G, Hermida L, Fukuda H, Defain MV, Rodriguez L, Mamone L, MacRobert A, Casas A, Batlle A. Comparison of liposomal formulations of ALA Undecanoyl ester for its use in photodynamic therapy. *Photochem Photobiol B* 2009; **96**: 152-158
199. Han I, Jun MS, Kim SK, Kim M, Kim JC. Expression pattern and intensity of protoporphyrin IX induced by liposomal 5-aminolevulinic acid in rat pilosebaceous unit throughout hair cycle. *Arch Dermatol Res* 2005; **297**: 210-217
200. Al Kassas R, Donnelly RF, McCarron PA (2009) Aminolevulinic acid-loaded Witepsol microparticles manufactured using a spray congealing procedure: implications for topical photodynamic therapy. *J Pharm Pharmacol* **61**: 1125-1135
201. Donnelly RF, McCarron PA, Al Kassas R, Juzeniene A, Juzenas P, Iani V, Woolfson AD, Moan J. Influence of Formulation Factors on PpIX Production and Photodynamic Action of Novel ALA-loaded Microparticles. *Biopharm Drug Dispos* 2009; **30**: 55-70
202. Bourre L, Thibaut S, Briffaud A, Lajat Y, Patrice T. Potential efficacy of a delta 5-aminolevulinic acid thermosetting gel formulation for use in photodynamic therapy of lesions of the gastrointestinal tract. *Pharmacol Res* 2002; **45**: 159-165
203. Gruning N, Muller-Goymann CC. Physicochemical characterisation of a novel thermogelling formulation for percutaneous penetration of 5-aminolevulinic acid. *J Pharm Sci* 2008; **97**: 2311-2323
204. McCarron PA, Donnelly RF, Zawislak A, Woolfson AD, Price JH, McClelland R. Evaluation of a water-soluble bioadhesive patch for photodynamic therapy of vulval lesions. *Int J Pharm* 2005; **293**: 11-23
205. McCarron PA, Donnelly RF, Andrews GP, Woolfson AD. Stability of 5-aminolevulinic acid in novel non-aqueous gel and patch-type systems intended for topical application. *J Pharm Sci* 2005; **94**: 1756-1771
206. McCarron PA, Donnelly RF, Zawislak A, Woolfson AD. Design and evaluation of a water-soluble bioadhesive patch formulation for cutaneous delivery of 5-aminolevulinic acid to superficial neoplastic lesions. *Eur J Pharm Sci* 2006; **27**: 268-279
207. Zawislak A, Donnelly RF, McCluggage WG, Price JH, McClelland HR, Woolfson AD, Dobbs S, Maxwell P, McCarron PA. Clinical and immunohistochemical assessment of vulval intraepithelial neoplasia following photodynamic therapy using a novel bioadhesive patch-type system loaded with 5-aminolevulinic acid. *Photodiagnos Photodyn Ther* 2009; **6**: 28-40
208. Donnelly RF, Ma LW, Juzenas P, Iani V, McCarron PA, Woolfson AD, Moan J. Topical bioadhesive patch systems enhance selectivity of protoporphyrin IX accumulation. *Photochem Photobiol* 2006; **82**: 670-675
209. Lee G, Szeimies RM. Dermal for aminolaevulinic acid. **10/332547[PCT/EP01/08131]**. 2005. United states. 13-7-2001.

210. Public Assessment Report, Decentralised Procedure, Alacare 8 mg Medicated Plaster. **UK/H/1533/001/DC**. 2009. Medicines and Healthcare Products Regulatory Agency.
211. Hauschild A, Stockfleth E, Popp G, Borrosch F, Bruning H, Dominicus R, Mensing H, Reinhold U, Reich K, Moor ACE, Stocker M, Ortlund C, Brunnert M, Szeimies RM. Optimization of photodynamic therapy with a novel self-adhesive 5-aminolaevulinic acid patch: results of two randomized controlled phase III studies. *Br J Dermatol* 2009; **160**: 1066-1074
212. Szeimies RM, Stockfleth E, Popp G, Borrosch F, Bruning H, Dominicus R, Mensing H, Reinhold U, Reich K, Moor ACE, Stocker M, Ortlund C, Brunnert M, Hauschild A. Long-term follow-up of photodynamic therapy with a self-adhesive 5-aminolaevulinic acid patch: 12 months data. *Br J Dermatol* 2010; **162**: 410-414
213. Morton CA, Brown SB, Collins S, Ibbotson S, Jenkinson H, Kurwa H, Langmack K, McKenna K, Moseley H, Pearse AD, Stringer M, Taylor DK, Wong G, Rhodes LE. Guidelines for topical photodynamic therapy: report of a workshop of the British Photodermatology Group. *Br J Dermatol* 2002; **146**: 552-567
214. Walker RB, Smith EW. The role of percutaneous penetration enhancers. *Adv Drug Deliv Rev* 1996; **18**: 295-301
215. Conder LH, Woodard SI, Dailey HA. Multiple Mechanisms for the Regulation of Heme-Synthesis During Erythroid Cell-Differentiation - Possible Role for Coproporphyrinogen Oxidase. *Biochem J* 1991; **275**: 321-326
216. Chang SC, McRobert AJ, Porter JB, Bown SG. The efficacy of an iron chelator (CP94) in increasing cellular protoporphyrin IX following intravesical 5-aminolaevulinic acid administration: an in vivo study. *J Photochem Photobiol B* 1997; **38**: 114-122
217. Juzeniene A, Juzenas P, Iani V, Moan J. Topical applications of iron chelators in photosensitization. *Photochem Photobiol Sci* 2007; **6**: 1268-1274
218. Curnow A, McIlroy BW, Postle-Hacon MJ, Porter JB, MacRobert AJ, Bown SG. Enhancement of 5-aminolaevulinic acid-induced photodynamic therapy in normal rat colon using hydroxypyridinone iron-chelating agents. *Br J Cancer* 1998; **78**: 1278-1282
219. Bech O, Phillips D, Moan J, McRobert AJ. A hydroxypyridinone (CP94) enhances protoporphyrin IX formation in 5-aminolaevulinic acid treated cells. *J Photochem Photobiol B* 1997; **41**: 136-144
220. Pye A, Campbell S, Curnow A. Enhancement of methyl-aminolevulinate photodynamic therapy by iron chelation with CP94: an in vitro investigation and clinical dose-escalating safety study for the treatment of nodular basal cell carcinoma. *J Cancer Res Clin* 2008; **134**: 841-849
221. Hanania J, Malik Z. The Effect of Edta and Serum on Endogenous Porphyrin Accumulation and Photodynamic Sensitization of Human K562 Leukemic-Cells. *Cancer Lett* 1992; **65**: 127-131

222. Harth Y, Hirshowitz B, Kaplan B. Modified topical photodynamic therapy of superficial skin tumors, utilizing aminolevulinic acid, penetration enhancers, red light, and hyperthermia. *Dermatol Surg* 1998; **24**: 723-726
223. Miller MJ. Syntheses and therapeutic potential of hydroxamic acid based siderophores and analogues. *Chem Rev* 1989; **89**: 1563-1579
224. Malik Z, Kostenich G, Roitman L, Ehrenberg B, Orenstein A. Topical application of 5-aminolevulinic acid, DMSO and EDTA: protoporphyrin IX accumulation in skin and tumours of mice. *Photochem Photobiol B* 1995; **28**: 213-218
225. Peng Q, Warloe T, Moan J, Heyerdahl H, Steen HB, Nesland JM, Giercksky KE. Distribution of 5-aminolevulinic acid-induced porphyrins in noduloulcerative basal cell carcinoma. *Photochem Photobiol* 1995; **62**: 906-913
226. De Rosa FS, Marchetti JM, Thomazini JA, Tedesco AC, Bentley MV. A vehicle for photodynamic therapy of skin cancer: influence of dimethylsulphoxide on 5-aminolevulinic acid in vitro cutaneous permeation and in vivo protoporphyrin IX accumulation determined by confocal microscopy. *J Control Release* 2000; **65**: 359-366
227. Copovi A, Diez-Sales O, Herraiez-Dominguez JV, Herraiez-Dominguez M. Enhancing effect of alpha-hydroxyacids on "in vitro" permeation across the human skin of compounds with different lipophilicity. *Int J Pharm* 2006; **314**: 31-36
228. Kraeling MEK, Bronaugh RL. In vitro percutaneous absorption of alpha hydroxy acids in human skin. *J Soc Cosmet Chem* 1997; **48**: 187-197
229. Ziolkowski P, Osiecka BJ, Oremeck G, Siewinski M, Symonowicz K, Saleh Y, Bronowicz A. Enhancement of photodynamic therapy by use of aminolevulinic acid/glycolic acid drug mixture. *J Exp Ther Oncol* 2004; **4**: 121-129
230. Moser K, Kriwet K, Naik A, Kalia YN, Guy RH. Passive skin penetration enhancement and its quantification in vitro. *Eur J Pharm Biopharm* 2001; **52**: 103-112
231. Pierre MBR, Ricci E, Tedesco AC, Bentley MVLB. Oleic acid as optimizer of the skin delivery of 5-aminolevulinic acid in photodynamic therapy. *Pharm Res* 2006; **23**: 360-366
232. Steluti R, De Rosa FS, Collett J, Tedesco AC, Bentley MVLB. Topical glycerol monooleate/propylene glycol formulations enhance 5-aminolevulinic acid in vitro skin delivery and in vivo protoporphyrin IX accumulation in hairless mouse skin. *Eur J Pharm Biopharm* 2005; **60**: 439-444
233. Turchiello RF, Vena FC, Maillard P, Souza CS, Bentley MV, Tedesco AC. Cubic phase gel as a drug delivery system for topical application of 5-ALA, its ester derivatives and m-THPC in photodynamic therapy (PDT). *J Photochem Photobiol B* 2003; **70**: 1-6
234. Bender J, Ericson MB, Merclin N, Iani V, Rosen A, Engstrom S, Moan J. Lipid cubic phases for improved topical drug delivery in photodynamic therapy. *J Control Release* 2005; **106**: 350-360

235. Hadgraft J, Peck J, Williams DG, Pugh WJ, Allan G. Mechanisms of action of skin penetration enhancers retarders: Azone and analogues. *Int J Pharm* 1996; **141**: 17-25
236. Ziolkowski P, Osiecka BJ, Siewinski M, Bronowicz A, Ziolkowska J, Gerber-Leszczyn H. Pretreatment of plantar warts with azone enhances the effect of 5-aminolevulinic acid photodynamic therapy *J Environ Pathol Tox* 2006; **25**: 403-409
237. Maisch T, Worlicek C, Babilas P, Landthaler M, Szeimies RM. A HCl/alcohol formulation increased 5-aminolevulinic acid skin distribution using an ex vivo full thickness porcine skin model *Exp Dermatol* 2008; **17**: 813-820
238. Perotti C, Casas A, Fukuda H, Sacca P, Batlle AM. ALA and ALA hexyl ester induction of porphyrins after their systemic administration to tumorbearing mice. *Br J Cancer* 2002; **87**: 790-795
239. Konan YN, Gurny R, Allemann E. State of the art in the delivery of photosensitizers for photodynamic therapy 2002; *J Photochem Photobiol B* **66**: 89-106
240. Allemann E, Gurny R, Doelker E. Drug-loaded nanoparticles - Preparation methods and drug targeting issues 1993; *Eur J Pharm Biopharm* **39**: 173-191
241. Park SI, Lim JH, Kim JH, Yun HI, Kim CO. In vivo and in vitro investigation of photosensitizer-adsorbed superparamagnetic nanoparticles for photodynamic therapy. *Ieee T Magn* 2005; **41**: 4111-4113
242. Oo MKK, Yang X, Du H, Wang H. 5-aminolevulinic acid-conjugated gold nanoparticles for photodynamic therapy of cancer. *Nanomedicine* 2008; **3**: 777-786
243. Letoffe S, Heuck G, Delepelaire P, Lange N, Wandersman C. Bacteria capture iron from heme by keeping tetrapyrrol skeleton intact. *Proc Natl Acad Sci USA* 2009; **106**: 11719-11724

Part A: Formulation of Hexaminolevulinic Acid into Polymeric Nanoparticles

Chapter 2. Matrix mediated Fluorescence Enhancement - Why Nanoparticles and PPIX make a friendly Couple

Gesine Heuck and Norbert Lange

Department of Pharmaceutical Technology, School of Pharmaceutical Sciences, University of Geneva, University of Lausanne, University of Geneva, 30, Quai Ernest Ansermet, CH – 1211 Geneva 4, Switzerland

Journal of Porphyrins and Phthalocyanines, in press

ABSTRACT. The hexyl ester of 5-aminolevulinic acid (HAL) is an efficient inducer of the endogenous photosensitizer protoporphyrin IX (PPIX) in neoplastic tissue and approved for the fluorescence photodetection of bladder cancer. It is, however, limited to topical application due to unsuitable pharmacokinetic and pharmacodynamic properties following systemic administration. In this study we sought to prepare HAL laden polymeric nanoparticles made from polylactic acid (PLA) as possible means to improve the systemic bioavailability of HAL. Nanoparticles were prepared by nanoprecipitation. Particle size and morphology of freshly prepared and dehydrated nanoparticles were assessed and the ability to generate PPIX fluorescence was tested on a T24 human bladder carcinoma cell line. Fluorescence intensities of cells incubated with nanoencapsulated HAL were significantly higher than in presence of free HAL. Interestingly, the effect was - at least partly - provoked by the direct interaction of exogenously induced PPIX with the nanoparticles.

Keywords: fluorescence photodetection, hexaminolevulinic acid, protoporphyrin IX, polylactic acid, nanoparticles, bladder carcinoma

Introduction

Among intra – operative imaging techniques in clinical oncology, fluorescence photodetection (PD) of neoplasms represents a simple, high resolution, cost effective and easily applicable alternative to non-optical techniques such as magnetic resonance imaging (MRI), computerized tomography (CT) or ultrasound. These techniques are often associated with high costs, low resolution, limited accessibility to the patient due to bulky instrumentation, and safety issues such as radiation exposure of patient and medical staff [1, 2]. In PD, a fluorescence marker accumulates selectively in the target tissue. Irradiation with light of an appropriate wavelength allows detection of early lesions and the delineation of tumor margins *in situ* or on a screen.

One marker shown to be effective in numerous *in vitro* and *in vivo* studies as well as in clinical practice is hexaminolevulinic acid (HAL) [3-12]. HAL is the n-hexyl ester of the early heme precursor 5-aminolevulinic acid (5-ALA) currently approved for the PD of bladder cancer (Hexvix[®], Cysview[®]). Owing to its lipophilicity and the high metabolic turnover in neoplastic tissue, HAL accumulates selectively in neoplastic tissue, where it is converted by the enzymes of the heme biosynthetic pathway into the fluorescent heme precursor protoporphyrin IX (PPIX).

At present, the use of HAL is limited to topical administration due to insufficient bioavailability when applied systemically [13, 14]. This impairs the exploitation of HAL for PD of pathologies that are difficult to access including lung, breast, prostate, and brain cancer.

In recent years polymeric nanoparticles have gained much interest as possible means to improve the systemic bioavailability of drugs. The prolonged circulation time of nanoparticles in the blood in combination with their typical tumor targeting properties entail the possibility of administering low drug doses and decrease the risk of adverse effects [15, 16]. Furthermore, a labile drug may be protected from a potentially hostile environment.

The study presented in this article aimed at assessing biocompatible and biodegradable HAL laden polylactic acid (PLA) nanoparticles with respect to the generation of porphyrin fluorescence in a T24 human bladder carcinoma cell line. The particles were characterized according to their size and morphology. Some surprising observations lead us to further investigate the interaction of PPIX with unladen PLA nanoparticles.

Materials and methods

Solvents and salts for buffers, protoporphyrin IX, iodine and potassium iodide were purchased from Sigma-Aldrich (Buchs, Switzerland). Polylactic acid (Resomer[®]) R205 was purchased from Evonic (Ingelheim am Rhein, Germany). Polyvinyl alcohol (PVAL, Mowiol[®] 8-44, Mw 31000) was provided from Clariant GmbH (Frankfurt am Main, Germany). HAL was obtained from Biosynth AG (Staad, Switzerland). GFP transfected T24 human bladder carcinoma cells were a gift of Med Discovery SA (Geneva, Switzerland). Cell media and supplements as well as trypsin (0.05%)-EDTA were obtained from Invitrogen (Lucerne, Switzerland).

Preparation and characterization of nanoparticles

Nanoparticles were prepared by nanoprecipitation with a modified technique previously described by Zeisser-Labouèbe et al. [17]. In brief, 500 mg of PLA were dissolved in 50 mL acetone. The solution was injected into 100 mL of a 0.4% aqueous PVAL solution at room temperature under continuous magnetic stirring. Acetone was evaporated under continuous stirring of the suspension for 12 hours at room temperature. For encapsulation of HAL, 125 mg HAL were dissolved in 5 mL ethanol and added to 45 mL PLA solution in acetone.

Particles were purified by centrifugation at 55 000 x g for 25 minutes. The supernatant was discarded. The particles were re-suspended in supplemented DMEM media (see below) and used for cell incubation. For the preparation of dehydrated samples the particle pellet was re-suspended in distilled water with a final nanoparticle concentration of 10 mg particles per milliliter. The suspension was flash frozen in liquid nitrogen and the water was removed by lyophilization for 24 hours. The dehydrated nanoparticles were resuspended in aqueous media prior to further investigations (see below).

Size and ζ -potential of the nanoparticles was determined in 1 mM NaCl aqueous solution by photon correlation spectroscopy (Zetasizer[®] 3000HS, Malvern instruments, Worcestershire, UK).

Residual PVAL on nanoparticles was measured with a colorimetric assay using Lugol's iodine. Nanoparticles were dissolved in 2 N NaOH solution and neutralized with HCl. To 80 μ L sample were added 300 μ l of 4% boric acid in water and 60 μ l Lugol's iodine solution (12.5 g/L iodine and 25.0 g/L potassium iodide in water). The mixture was completed to 1 mL

with distilled water and measured by UV spectrophotometry at 644 nm using a multiwell plate reader (Tecan Safire, Männerdorf, Austria).

The nanoparticle morphology was examined by scanning electron microscopy (SEM) (JEOL JSM-7001FA, Tokyo, Japan). Samples were prepared by depositing 10 μ L of the particle suspension on the sample holder. Water was evaporated under vacuum for 24 hours and the particles were electrochemically coated with gold at 0.05 mbar for 90 seconds. The applied current was 15 mA. The sample distance to the cathode was 5 cm. Images were taken using SMILE view software.

The HAL loading of particles was determined after dissolving the nanoparticles in 1 mL dichloromethane and extracting HAL into 1 mL of 20 mM HCl solution. Forty microliters of the extract were diluted in 1 mL borate buffer pH 8.5. The dilution was combined with 120 μ L of a 1 mg/mL fluorescamine solution in acetone. The amine-fluorescamine complex was excited at 390 nm and fluorescence was measured at 470 nm using a fluorescence multi-well plate reader (Tecan Safire, Männerdorf, Austria). The assay was done in triplicate.

PPIX interaction with unladen nanoparticles

PPIX interaction with blank nanoparticles was assessed in 96-well microplates. A 100 μ M stock solution of PPIX in ethanol/dimethyl sulfoxide (DMSO)/acetic acid (20/80/1 v/v/v) was prepared and diluted to 100 nM with plain or fetal bovine serum albumin (FBS) supplemented Dulbecco's Modified Eagle Medium (DMEM) containing 10 μ g/mL streptomycin and 100 IE/mL penicillin.

The PPIX containing mixture was used to suspend freshly prepared or lyophilized nanoparticles at indicated concentrations. PPIX fluorescence was measured at 37°C with a fluorescence multi-well plate reader (Tecan Safire, Männerdorf, Austria) and fitted to spectra of media containing no PPIX. The excitation wavelength was 405 nm.

Cell culture and PPIX fluorescence induction

T24 human bladder carcinoma cells were grown as monolayers in Dulbecco's Modified Eagle Medium (DMEM) supplemented with 10% fetal bovine serum albumin (FBS), 10 μ g/mL

streptomycin and 100 IE/mL penicillin under a 5% CO₂/95% air atmosphere at 37°C. Monolayers of 10 000 cells/well were seeded into 96-well plates and grown for 24 hours. For fluorescence induction assays, the cells were incubated with 150 µL complete medium containing 0.3 mM and 1 mM HAL as free hydrochloric acid salt, in the nanoencapsulated form or in presence of unladen nanoparticles, respectively. Porphyrin fluorescence was monitored at 37°C with a fluorescence multiplate reader (Saphire, Tecan, Männerdorf, Austria) as described above. Spectra of HAL mediated cell fluorescence were fitted to a control of cells grown in medium only, to extract genuine PPIX fluorescence. Each series included 3 incubation experiments. For statistical analysis the two-way ANOVA was used.

For PPIX extraction, 1 000 000 cells were seeded into a T24 flask and grown as monolayers for 24 hours as indicated above. The cells were then incubated with 13 mL cell medium containing 1 mM HAL in the presence or absence of 20 mg/mL nanoparticles. After 12 hours the incubation medium was removed for further analysis of potentially contained PPIX. The cells were washed thrice with 5 mL phosphate buffered saline (PBS) and the buffer was added to the incubation medium. Thereafter, the cells were detached with 2 mL trypsin-EDTA for 5 minutes and collected by centrifugation (5 minutes, 1200 x g). The supernatant was removed and 1 mL of ethanol/DMSO/acetic acid (80/20/1) was added to the cell pellet. PPIX was extracted by sonicating the cells with a sonicator probe (5 times for 5 seconds, amplitude 10%). Cell debris was removed by centrifugation (10 minutes, 14 000 x g) and the extract was analyzed by high performance liquid chromatography (HPLC) using a solvent gradient as described by Létouffé et al. [18]. The HPLC system (LaChrom, Merck, Darmstadt, Germany) was equipped with a fluorescence detector for recording. The quantification included total amounts PPIX found in incubation medium and in cells. The experiment was done in duplicate.

Results

We prepared HAL laden nanoparticles by nanoprecipitation in an aqueous 0.4% PVAL solution with the objective to produce a safe HAL formulation for intravenous administration. SEM micrographs (Fig.1) revealed that blank as well as HAL laden nanoparticles were spherical with a smooth surface. The main particle characteristics are summarized in Table. 1. Residual PVAL on particles was between 1 and 2 per cent. Particle loading with HAL was

0.5% (w/w). After dehydration, mean size and polydispersity index (P.I.) were larger presumably due to particle aggregation.

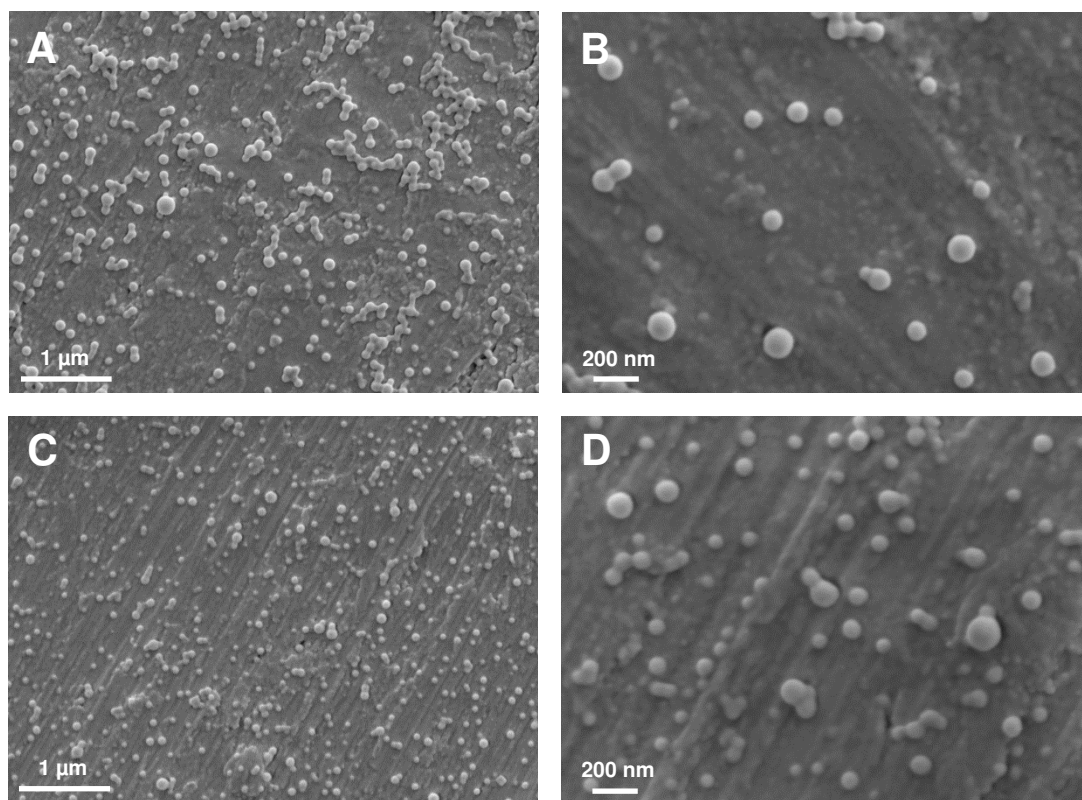


Fig. 1. Scanning electron micrographs of HAL laden (A, B) and blank (C, D) nanoparticles. Images were taken at x20 000 (A, C) and x50 000 (B, D) magnification.

Optimal fluorescence for free HAL was achieved when cells were incubated with a concentration of 1 mM (Fig. 2). At concentrations above 3 mM no fluorescence was observed presumably due to cell toxicity. At concentrations below 1 mM cell fluorescence occurred during shorter time periods, which may be due to decreased substrate availability. This tendency was similar in cells incubated with HAL laden nanoparticles. However, fluorescence intensities were significantly higher. Fluorescence in cells incubated with freshly prepared nanoencapsulated HAL at 1 mM concentration was 3 times higher than in cell incubations with free HAL (Fig. 3A) ($p < 0.05$).

Tab. 1. Mean size, ζ -potential and polydispersity index of freshly prepared and dehydrated HAL laden and blank nanoparticles prepared by nanoprecipitation.

	Fresh nanoparticles			Dehydrated nanoparticles		
	size [nm]	ζ -potential	P.I.	size [nm]	ζ -potential	P.I.
HAL laden	155.5	1.4	0.068	>1000	n.a.	> 1.0
blank	169.4	2.0	0.013	383.7	2.1	0.607

When using dehydrated nanoparticles, fluorescence intensities were increased 7 fold ($p < 0.001$) (Fig. 3A). An increase was also observed for cells incubated with dehydrated nanoparticles at 0.3 mM HAL concentration ($p < 0.001$). The difference between the fluorescence intensities induced by fresh and dehydrated HAL laden nanoparticles was significant with $p < 0.001$ for both HAL concentrations. T24 cells incubated with HAL featured porphyrin emission maxima at 625 nm. The peak was shifted to 632 nm in the presence of nanoparticles (data not shown).

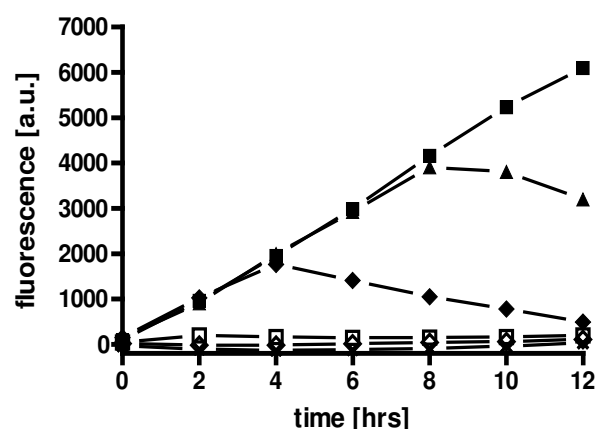


Fig. 2. Fluorescence-time profile of T24 cells incubated with HAL HCl 0.1 (\blacklozenge), 0.3 (\blacktriangle), 1 (\blacksquare), 3 (\square), 10 (\blacklozenge) and 30 (\times) mM concentrations.

Surprisingly, PPIX fluorescence was also doubled ($p < 0.001$) in cells incubated with 1 mM free HAL in presence of unladen nanoparticles (Fig. 4). However, it was still significantly

lower compared to nanoencapsulated HAL ($p < 0.01$). The fluorescence intensities correlated with the nanoparticle concentration in the medium (Fig. 5).

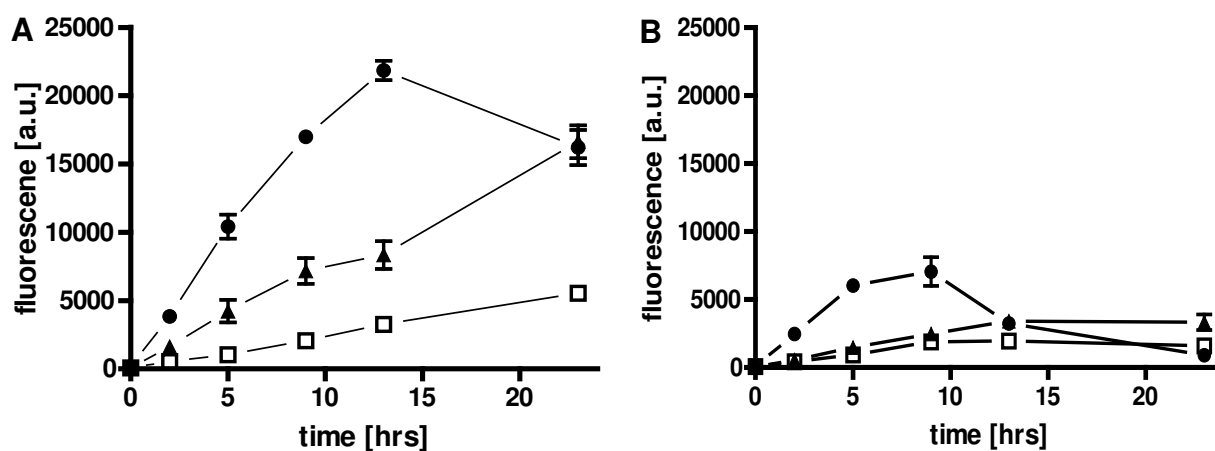


Fig. 3. Fluorescence-time profiles of T24 cells incubated with freshly prepared (▲) and dehydrated (●) HAL laden nanoparticles, and free HAL (□). The HAL concentrations were 1mM (A), 0.3mM (B).

To investigate a possibly improved transport of HAL into the cell by adsorption to nanoparticles, we sought to quantify cellular PPIX produced by cells incubated with 1 mM HAL in presence or absence of 20 mg/mL nanoparticles. PPIX was extracted from cells into an ethanol/DMSO/acetic acid solvent mixture for fluorescence HPLC analysis (Fig. 6A). The same was done for the incubation media, to include potentially secreted PPIX (Fig. 6B).

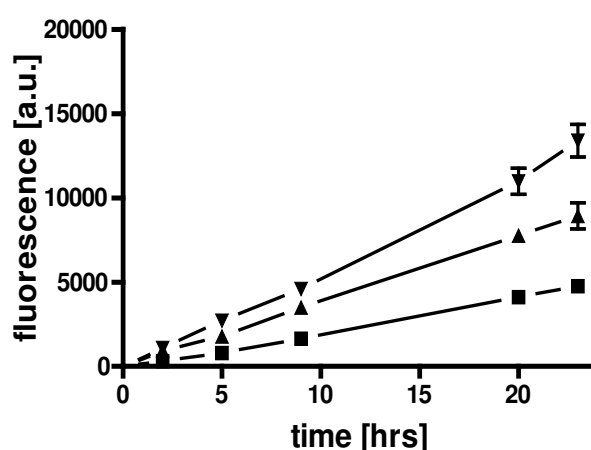


Fig. 4. Fluorescence-time profile of T24 cells incubated with 1 mM HAL as free compound (■), in presence of 50 mg/mL freshly prepared blank nanoparticles (▲) and nanoencapsulated in 50 mg/mL (▼).

Interestingly, the quantification revealed even lower amounts of PPIX produced by the cells in the presence of nanoparticles (Fig. 6D). Therefore, we assumed that at least part of the fluorescence increase in presence of HAL laden nanoparticles must result from an optical signal enhancement provided by the nanoparticulate microenvironment.

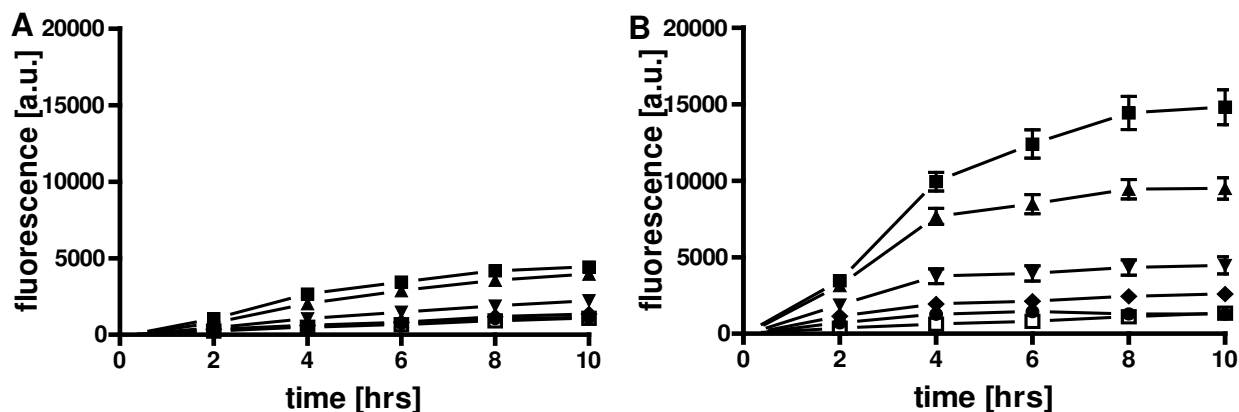


Fig. 5. Fluorescence time profile of T24 cells incubated with free 1mM HAL in presence of freshly prepared (A) and dehydrated (B) blank PLA nanoparticles with 0 (\square), 2.5 (\bullet), 5 (\blacklozenge), 10 (\blacktriangledown), 20 (\blacktriangle) and 40 (\blacksquare) mg/mL nanoparticle concentrations.

To test this hypothesis we assessed the interaction of PPIX with nanoparticles in absence of cells. Since albumin and other proteins associate with both, PPIX and nanoparticles [19, 20], we performed the assay in serum free DMEM as well as in DMEM supplemented with 10% foetal bovine serum albumin (DMEM+FBS) (Fig. 7A). In the absence of nanoparticles, the fluorescence of free PPIX was completely quenched in plain DMEM; contrastingly, an emission peak was measurable in presence of FBS at 624 nm. In serum free DMEM a fluorescence peak appeared at 628nm after the addition of nanoparticles. The intensity increased proportionally with the nanoparticle concentration (Fig. 7A, white dotted columns). When adding freshly prepared nanoparticles to DMEM+FBS, the fluorescence signal first decreased and re-increased after addition of higher amounts of nanoparticles (Fig. 7A, white striped columns and Fig. 7B). The initial fluorescence was re-established above a nanoparticle concentration of 16.7 mg/mL (Fig. 7B). After addition of dehydrated nanoparticles (Fig. 7A dark columns) fluorescence intensities in PPIX-containing DMEM and DMEM+FBS, were 4 times stronger than with fresh nanoparticles, respectively.

The addition of nanoparticles to DMEM supplemented with FBS lead to a bathochromic shift of the emission peaks from 624 nm to 631 nm in both freshly prepared and dehydrated nanoparticles.

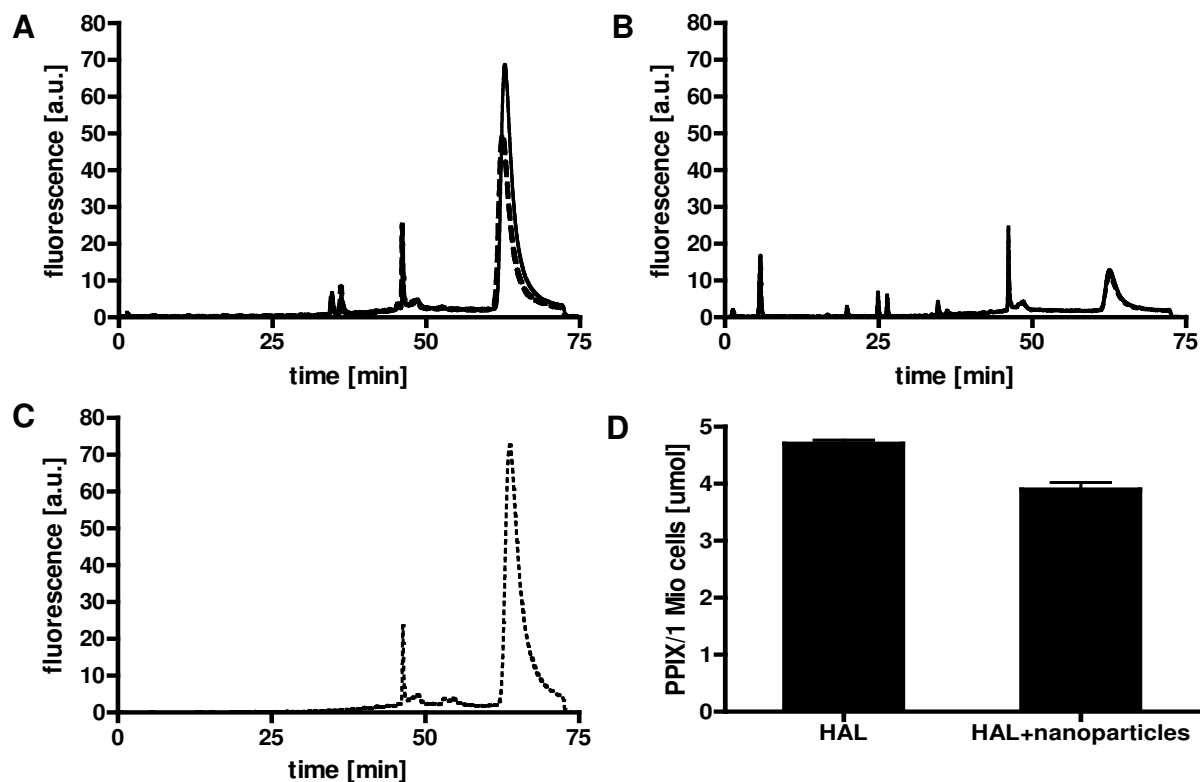


Fig. 6. Fluorescence chromatograms of cellular (A) and incubation medium extracts (B) of T24 cells incubated with 1 mM free HAL (—) and 1 mM HAL in the presence of 20 mg/mL freshly prepared blank nanoparticles (---) and of a PPIX standard solution (C) in ethanol/DMSO/acetic acid, (80/20/1, v/v/v). D shows the PPIX concentration per 1 Mio cells extracted for cells incubated with 1 mM free HAL or in presence of 20 mg/mL nanoparticles.

Discussion

Our *in vitro* experiments showed that fresh and dehydrated polymeric nanoparticles enhance PPIX fluorescence intensities in T24 cells. Surprisingly, we could not find higher amounts of PPIX produced by cells when incubated in presence of nanoparticles. Therefore, we assume that the apolar surface of the particles may function as matrix for PPIX adsorption and influence the spectral properties of the fluorophore. Our assumption is supported by the observation of a bathochromic shift of the emission peak in presence of nanoparticles and fluorescence development during co-incubation of PPIX with nanoparticles in cell medium [21, 22]. Association of porphyrins with surfaces and macromolecules, notably proteins [23-

25], leads to a shift of absorption and emission maxima, fluorescence yield and life time [26-31]. Brancalion et al. reported that bovine serum albumin (BSA) and human serum albumin (HSA) cause a red shift of the PPIX emission maximum, which is accompanied by a fluorescence increase [23, 24].

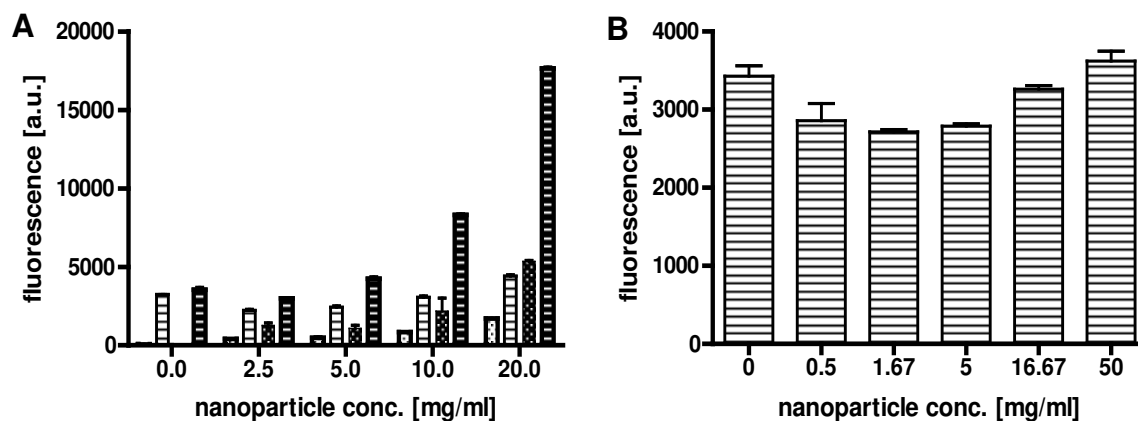


Fig. 7. A: *In vitro* fluorescence intensity of PPIX in presence of freshly prepared (white columns) and dehydrated (black columns) blank nanoparticles. The PPIX fluorescence was measured in unsupplemented DMEM (dotted columns) and DMEM supplemented with 10% FBS (striped columns). B: PPIX fluorescence in presence of freshly prepared blank nanoparticles in DMEM supplemented with 10% FBS. Dilutions were done in half log steps.

We equally observed PPIX fluorescence in DMEM in presence of nanoparticles. Interestingly, in DMEM+FBS the fluorescence was quenched in presence of low nanoparticle concentrations. Since albumin is known to adsorb to nanoparticles, we are tempted to conclude that the decrease of PPIX fluorescence may be caused by a competitive adsorption of serum proteins to nanoparticles, which becomes less pronounced when raising the nanoparticle concentration. The fact that the fluorescence emission was enhanced in cells but not during direct incubation of PPIX when using fresh particles in supplemented medium, suggests that PPIX association with the nanoparticle surface cannot be the only factor for this physicochemical phenomenon. Other processes, e.g. nanoparticle accumulation in the cell, association with the cell membrane and cellular proteins may also play a role. Moreover, since HAL laden nanoparticles still induced higher fluorescence in cells than blank nanoparticles in combination with free HAL, we speculate that HAL transport into the cell may further contribute to the augmented fluorescence. However, this remains subject to further investigation.

Cellular and *in vitro* PPIX fluorescence was considerably higher when using dehydrated rather than fresh nanoparticles. Using the same amount of dehydrated nanoparticles for incubation, the number of actual particles in the suspension is less due to partial aggregation. Moreover, the provided surface area for potential adsorption of proteins and PPIX is reduced. Therefore, if a change of PPIX fluorescence intensities was to be observed, we expected it to be lower. Although it is difficult to attribute the effect to one single cause, we hypothesize that apolar sites in dehydrated nanoparticles more easily adsorb proteins and PPIX.

Our observations confirm that nanoparticles may not only serve as carriers to deliver photosensitizers to the target but also influence their optical properties. For the development of drug formulations and PD/PDT protocols we conclude that possible surface interactions with polymeric matrices such as nanoparticles must be considered and a possible impact on fluorescence and singlet oxygen yield carefully assessed. The fluorescence enhancing effect caused by the application of nanoparticles may allow a reduction of the photosensitizer dose and/or shorter incubation times to obtain the same fluorescence as with higher free PS concentrations. However, these findings need further investigations *in vivo*. It should be also noted that the increase in fluorescence intensity was merely observed at high nanoparticle concentrations.

Reference List

1. Peters TM. Image-guidance for surgical procedures. *Phys Med Biol* 2006; **51**: R505-R40.
2. Keereweer S, Kerrebijn JDF, van DPBAA et al. Optical image-guided surgery--where do we stand? *Mol Imaging Biol* 2011; **13**: 199-207.
3. Endlicher E, Rummele P, Hausmann F et al. Protoporphyrin IX distribution following local application of 5-aminolevulinic acid and its esterified derivatives in the tissue layers of the normal rat colon. *Br J Cancer* 2001; **85**: 1572-6.
4. Endlicher E, Rummele P, Hausmann F et al. Detection of dysplastic lesions by fluorescence in a model of chronic colitis in rats after local application of 5-aminolevulinic acid and its esterified derivatives. *Photochem Photobiol* 2004; **79**: 189-92.
5. Juzeniene A, Juzenas P, Ma LW et al. Topical application of 5-aminolaevulinic acid, methyl 5-aminolaevulinate and hexyl 5-aminolaevulinate on normal human skin. *Br J Dermatol* 2006; **155**: 791-9.

6. Lange N, Jichlinski P, Zellweger M et al. Photodetection of early human bladder cancer based on the fluorescence of 5-aminolaevulinic acid hexylester-induced protoporphyrin IX: a pilot study. *Br J Cancer* 1999; **80**: 185-93.
7. Geavlete B, Jecu M, Multescu R et al. HAL blue-light cystoscopy in high-risk nonmuscle-invasive bladder cancer--re-TURBT recurrence rates in a prospective, randomized study. *Urology* 2010; **76**: 664-9.
8. Marti A, Jichlinski P, Lange N et al. Comparison of aminolevulinic acid and hexylester aminolevulinate induced protoporphyrin IX distribution in human bladder cancer. *J Urol* 2003; **170**: 428-32.
9. Soergel P, Loehr-Schulz R, Hillemanns M et al. Effects of photodynamic therapy using topical applied hexylaminolevulinate and methylaminolevulinate upon the integrity of cervical epithelium. *Lasers Surg Med* 2010; **42**: 624-30.
10. Soergel P, Wang X, Stepp H et al. Photodynamic therapy of cervical intraepithelial neoplasia with hexaminolevulinate. *Lasers Surg Med* 2008; **40**: 611-5.
11. Stenzl A, Burger M, Fradet Y et al. Hexaminolevulinate guided fluorescence cystoscopy reduces recurrence in patients with nonmuscle invasive bladder cancer. *J Urol* 2010; **184**: 1907-13.
12. Yung A, Stables GI, Fernandez C et al. Microbiological effect of photodynamic therapy (PDT) in healthy volunteers: a comparative study using methyl aminolaevulinate and hexyl aminolaevulinate cream. *Clin Exp Dermatol* 2007; **32**: 716-21.
13. Fotinos N, Campo MA, Popowycz F. The chick embryo model for the evaluation of 5-aminolevulinic acid derivatives. Atelier de reproduction de la Section de Physique, Geneva: University of Geneva; 2007.
14. Perotti C, Casas A, Fukuda H et al. ALA and ALA hexyl ester induction of porphyrins after their systemic administration to tumour bearing mice. *Br J Cancer* 2002; **87**: 790-5.
15. Soppimath KS, Aminabhavi TM, Kulkarni AR, Rudzinski WE. Biodegradable polymeric nanoparticles as drug delivery devices. *J Control Release* 2001; **70**: 1-20.
16. Van Butsele K, Jerome R, Jerome C. Functional amphiphilic and biodegradable copolymers for intravenous vectorisation. *Polymer* 2007; **48**: 7431-43.
17. Zeisser-Labouebe M, Lange N, Gurny R, Delie F. Hypericin-loaded nanoparticles for the photodynamic treatment of ovarian cancer. *Int J Pharm* 2006; **326**: 174-81.
18. Letoffe S, Heuck G, Delepelaire P et al. Bacteria capture iron from heme by keeping tetrapyrrol skeleton intact. *Proc Natl Acad Sci U S A* 2009; **106**: 11719-24.
19. Allemann E, Gravel P, Leroux J-C et al. Kinetics of blood component adsorption on poly(DL-lactic acid) nanoparticles: evidence of complement C3 component involvement. *J Biomed Mater Res* 1997; **37**: 229-34.

20. Verrecchia T, Huve P, Bazile D et al. Adsorption/desorption of human serum albumin at the surface of poly(lactic acid) nanoparticles prepared by a solvent evaporation process. *J Biomed Mater Res* 1993; **27**: 1019-28.
21. Ricchelli F. Photophysical properties of porphyrins in biological membranes. *Photochem Photobiol B* 1995; **29**: 109-18.
22. Siggel U, Bindig U, Endisch C et al. Photophysical and photochemical properties of porphyrin aggregates. *Ber Bunsen-Ges* 1996; **100**: 2070-5.
23. Brancaleon L, Magennis SW, Samuel IDW et al. Characterization of the photoproducts of protoporphyrin IX bound to human serum albumin and immunoglobulin G. *Biophys Chem* 2004; **109**: 351-60.
24. Brancaleon L, Moseley H. Effects of photoproducts on the binding properties of protoporphyrin IX to proteins. *Biophys Chem* 2002; **96**: 77-87.
25. Moseley H, Ibbotson S, Woods J et al. Clinical and research applications of photodynamic therapy in dermatology: experience of the Scottish PDT Centre. *Lasers Surg Med* 2006; **38**: 403-16.
26. De Napoli M, Nardis S, Paolesse R et al. Hierarchical porphyrin self-assembly in aqueous solution. *J Am Chem Soc* 2004; **126**: 5934-5.
27. Paolesse R, Tortora L, Monti D et al. Dip and wait: a facile route to nanostructured porphyrin films for QCM functionalization. *Procedia Chem* 2009; **1**: 180-3.
28. Monti D, De Rossi M, Sorrenti A et al. Supramolecular Chirality in Solvent-Promoted Aggregation of Amphiphilic Porphyrin Derivatives: Kinetic Studies and Comparison between Solution Behavior and Solid-State Morphology by AFM Topography. *Chem-Eur J* 2010; **16**: 860-70.
29. Dolci LS, Marzocchi E, Montalti M et al. Amphiphilic porphyrin film on glass as a simple and selective solid-state chemosensor for aqueous Hg^{2+} . *Biosens Bioelectron* 2006; **22**: 399-404.
30. Di Natale C, Monti D, Paolesse R. Chemical sensitivity of porphyrin assemblies. *Mater Today* 2010; **13**: 37-43.
31. Jhonsi MA, Kathiravan A, Renganathan R. Interaction between certain porphyrins and CdS colloids: A steady state and time resolved fluorescence quenching study. *Spectrochim Acta A* 2008; **71**: 1507-11.

Annotation

The use of HAL laden nanoparticles showed to be favourable for the induction of PPIX fluorescence in cells. However, the poor loading and hence the necessity to apply large amounts of particles is a limiting factor for *in vivo* application. In an attempt to improve the encapsulation of HAL in polymeric PLA and/or PLGA nanoparticles we screened several parameters as summarized in Tab. 4.

Drug loading remained below 1% under the tested condition. We attributed this outcome to an increased affinity of HAL to the aqueous phase in the presence of surfactants. In fact, with a logP of 1.8 HAL is poorly soluble in pure water. However, the presence of surfactants, ions and even blank nanoparticles raises the solubility of HAL assumingly due to the free ammonium group, which gives the molecule an amphiphilic character. In some methods using water miscible solvents, e.g. in nanoprecipitation, particle formation was reported to be also successful in pure water. This was not the case for our formulation, where HAL seems to destabilize the particle forming process.

Beside a low solubility in the aqueous medium, a drug should have sufficient affinity to the polymer and organic solvent. Variation of polymer type (PLA or PLGA, endcapped or non-endcapped) and molecular weight did not improve the encapsulation rate. Therefore, we sought to raise HAL affinity to the polymer by replacing the small chloride counter ion of the ammonium group by a lipophilic alkylbenzene sulfonate. This so-called ion-pairing concept is widely used in the chemical, biological and pharmaceutical field. Ion pairing may change the physicochemical properties of a molecule, while preserving its pharmacological profile.

Against our expectations, lipophilization of HAL had a minimal effect on the encapsulation efficiency into the compound: during solvent evaporation the HAL salt precipitated or HAL escaped into the aqueous phase. The results lead us to apply a nanoparticle forming method that abides the use of an outer aqueous phase. We chose an advanced spray drying procedure known as the aerosol flow reactor method developed at Aalto University, Helsinki, Finland. The following article presents our findings for HAL encapsulation into PLA nanoparticles with the aforementioned

technique resulting from the collaboration with Professor Kauppinen's group of Aalto University.

Tab. 4. Parameter variation to improve HAL loading of polymeric nanoparticles.

Variable factor	Rationale	Parameter details
Polymer	The hydrophobicity of the polymer changes with the polymer chain length, the presence of free carboxyl groups and the glycolic to lactic acid ratio. A free carboxylic group may favour the association with the ammonium group of HAL	PLA: R202H, R202S, R205S, R206, R207, PLGA: RG503, RG502H
Solvent for organic phase	The organic solvent should be chosen according to the solubility of the active principle and the polymer. Both compounds should have similar solubility in the solvent/solvent mixture	acetone, ethanol, THF, dichloromethane, chloroform, ethylacetate, DMSO
Aqueous phase:		
pH	At high pH the ammonium group of the polymer is uncharged which should raise the affinity towards the aqueous phase.	pH 5 , pH 7.4, pH 8, pH 9
Surfactant	HAL shows low solubility in water, it is however increased in presence of surfactants. Adaptation of the surfactant type and concentration may decrease the solubility of HAL in the organic phase while ensuring adequate nanoparticle formation.	no surfactant polyvinyl alcohol poloxamer bovine serum albumin Tween®
Temperature	The temperature influences the evaporation system enthalpy during particle formation. It may also influence drug diffusion into the aqueous phase.	4°C 20°C
Preparation method	The preparation method was adapted according to the used polymer and organic solvent.	Nanoprecipitation Emulsion evaporation Salting out Double emulsion evaporation
HAL counter ion	Exchange of the chloride ion in HAL HCl vs a counter ion with higher lipophilicity should increase the affinity to organic phase.	mesylate, tosylate, AOT, salicylate, ETBS, BUTBS, HEXBS, OCTBS, DBS

Chapter 3. Nanoencapsulation of lipophilic Salts of 5-Aminolevulinic Acid Hexyl Ester by an Aerosol Flow Reactor Method

Gesine Heuck¹; Antti Rahikkala²; David Scanu¹; Janne Raula²; Esko I. Kauppinen²;
Norbert Lange¹

¹Department of Pharmaceutical Technology, School of Pharmaceutical Sciences, University of Geneva, University of Lausanne, 30, Quai Ernest Ansermet, CH – 1211 Geneva 4, Switzerland

²Department of Applied Physics, Aalto University School of Science, P.O. Box 15100, FI-00076, Finland

Submitted to the European Journal of Pharmaceutics and Biopharmaceutics

ABSTRACT. Hexaminolevulinic acid (HAL) is an efficient inducer of the endogenous photosensitizer protoporphyrin IX (PPIX). Until now it is limited to topical application sites that are easy to access. Encapsulation into polymeric nanoparticles may represent a suitable drug formulation to make HAL available for interstitial sites via the inhalative or intravenous route. However, conventional nanoparticle preparation methods have so far been less successful. With the scope to develop nanoparticulate HAL formulation with sustained drug release for the detection of lung cancer, we employed the aerosol flow reactor method to obtain polylactic acid nanoparticles with high HAL loading and encapsulation efficiency. We further investigated the effect of ion pairing the HAL cation with lipophilic anions on the *in vitro* drug release fluorescence induction kinetics of the formulation. The particles were characterized with respect to size and morphology. Their ability to induce PPIX fluorescence was assayed on a GFP transfected T24 cell line derived from squamous cell bladder carcinoma. The most promising formulation was further tested on A549 lung carcinoma tumor nodules implanted into the chorionallantoic membrane of the chicken embryo.

Keywords: aerosol flow reactor, 5-aminolevulinic acid, fluorescence photodetection, hexyl ester, ion pair, nanoparticles, polylactic acid

Introduction

Fluorescence photodetection (PD) is an established technique for the *in situ* detection of early stage neoplastic lesions. It requires the administration of a photoactive compound able to accumulate preferentially in the tissue of interest and to fluoresce upon excitation with light. Several clinical studies have reported a positive therapeutic outcome for the detection and photodynamic treatment of pre- and early malignant bronchial neoplastic diseases [1-5]. The majority of the studies were performed with intravenously injected Photofrin[®], a mixture of polymer oligomers, endorsing the inconvenience of skin photosensitization for several weeks post administration.

5-ALA has been previously exploited for the fluorescence detection of early lung cancer. Due to its zwitterionic nature, however, high substrate concentrations are required to induce sufficient amounts of PPIX in the target tissue [5-8]. Owing to a facilitated diffusion through the cell membrane, the hexyl ester of 5-ALA (HAL) was reported to be highly selective for neoplastic tissue [9]. Similarly to the parent compound, it enters the cell where it is converted by enzymes involved in the heme biosynthesis and converges in the accumulation of PPIX [10-13].

HAL HCl is approved as a precursor of the endogenous photosensitizer protoporphyrin IX (PPIX) for the PD of bladder cancer. Nevertheless, because of the low systemic bioavailability and a toxic systemic effect [14, 15], the preferential route remains the topical application. As for the improvement of HAL over 5-ALA in the context of bladder cancer, we hypothesize that similar achievements can be obtained for early stage lung cancer. Inhalation is a convenient way for the localized drug delivery to the lung, provided the challenges of fast lung clearance, macrophageal phagocytosis and penetration of the thick pulmonary mucus layer are overcome. This may be achieved by using nanoparticles. The submicron sized carriers penetrate the pulmonary mucus readily and are recognized to lower extent by alveolar macrophages than micron-sized particle. Therefore they show prolonged retention in the lung [16, 17]. Furthermore, polymeric nanoparticles may be engineered to yield a sustained drug release, by tuning the drug-to-polymer affinity.

In the most common preparation techniques, the formation of nanoparticles takes place in aqueous media [18-20]. This represents a challenge for the encapsulation of amphiphilic drugs, such as HAL, into the hydrophobic particle core. In recent years, modified aerosol-

based techniques have been successfully implemented for the production of nano-sized particles. For example, in the aerosol flow reactor method, nano-sized solute droplets are produced by atomizing a solution with a highly pressurized nitrogen carrier gas jet [21-23]. Subsequent evaporation of the solvent results in nanoparticulate precipitates of the substance(s) contained in the solution.

The sustained release of a drug can be promoted by raising its affinity to the hydrophobic polymeric matrix. For an ionic active ingredient, this can be achieved by pairing it with an adequate lipophilic counter ion. An advantage of this approach over covalent attachment is the preservation of the pharmacodynamic characteristics of the active pharmaceutical ingredient, while physicochemical characteristics such as the drug solubility change [24, 25]. Effectively, a hydrophilic ionic compound may be made soluble in hydrophobic organic solvents by pairing it with a lipophilic counter ion. Upon immersion into an aqueous salt solution, exchange of the lipophilic counter ion with small ions contained in the solution triggers the dissolution of the active ingredient [26].

The aim of the present study was to develop biodegradable and biocompatible HAL laden solid nanoparticles with a high HAL content and prolonged release profile for drug delivery to the lung. To this end we prepared lipophilic HAL salts with different counterions and incorporated them into a biocompatible and biodegradable polymer, polylactic acid (PLA), by means of the aerosol flow reactor method [22, 27]. Nanoparticles were characterized with respect to particle size, morphology, HAL loading and *in vitro* drug release. Their ability to induce PPIX fluorescence was screened on GFP transfected T24 cancer cell line derived from squamous cell carcinoma of the bladder. The most promising formulation was further assessed on 3-dimensional tumor spheroids prepared from A549 lung cancer cells *in vitro* and on A549 tumor xenografts on the chorioallantoic membrane of chicken embryos.

Materials and Methods

Polylactic acid, PLA (Resomer[®] R205), was purchased from Evonik (Ingelheim am Rhein, Germany) and 5-aminolevulinic acid hexyl ester hydrochloride, HAL HCl, from Biosynth AG (Staad, Switzerland). 1-Butylbenzene, 1-hexylbenzene, oleum and sodium octylbenzene sulfonate (Na-OCTBS) for the synthesis of HAL salts, poly(hydroxyl ethyl methacrylate), HEMA, for the coating of round bottom well plates and polyethylene glycol, PEG400, for

chorioallantoic membrane (CAM) assays were from Sigma Aldrich (Buchs, Switzerland). Dichloromethane and ethylacetate (99.9% purity) were obtained from Sigma Aldrich (Helsinki, Finland). Cell media, phosphate buffer saline (PBS), antibiotics for cell media and Hoechst 33342 trihydrochloride trihydrate for staining of cell nuclei were provided by Invitrogen (Lucerne, Switzerland). Fetal bovine serum albumin, FBS, for cell media was ordered from Sigma Aldrich (Taufkirchen, Germany). Basement membrane extract, BME, for the culture of cellular tumor spheroids was purchased from CULTREX[®] (R&D systems[®], Oxon, United Kingdom). Extracellular matrix (Matrigel[™]) for CAM implantation of tumor spheroids was from BD Biosciences (Bedford, USA).

Synthesis of HAL salts

Sodium butylbenzene sulfonate and sodium hexylbenzene sulfonate were synthesized by sulfonation of the n-alkylbenzenes with oleum according to a modified method developed by Gray et al. [28]. The alkylbenzene (4.0 g) was slowly added to 2.1 g oleum under stirring at room temperature. The mixture was kept at 55°C for 2 hours under reflux and vigorous stirring. After the reaction, the mixture was neutralized with 1M sodium hydroxide solution and salted out with a saturated NaCl solution. The resulting precipitate was washed with acetone to remove free butylbenzene. The remaining alkylbenzene sulfonate salt was dissolved in water and re-crystallized in a water-acetone mixture.

HAL salts with lipophilic counter ions were prepared from 400 mg HAL HCl and the equimolar amount of the alkylbenzene sulfonate sodium salt. The compounds were added to a biphasic system of 10 mL water and 15 mL ethyl acetate. The mixture was vigorously shaken to allow salt dissolution and partition of the lipophilic associates into the organic phase. After phase separation the organic phase was removed and the aqueous phase was washed twice with 15 mL ethyl acetate. The combined organic phases were washed with 5 mL distilled water to remove hydrophilic residuals. Ethylacetate was removed by rotary evaporation.

Salt formation was verified by ¹H-NMR (Gemini 300, 300MHz) in deuterated D₆-DMSO. NMR signals were monitored as follows: (J=coupling constant; s=singlet; d=doublet; t=triplet; q=quadruplet; m= multiplet).

HAL butyl benzene sulfonate: $^1\text{H NMR } \delta$ (D_6 -DMSO) 0.80-0.95 (m, 6H), 1.20-1.3 (m, 10H), 1.45-1.65 (m, 4H), 2.56 (t, J= 6Hz, 2H), 2.79 (t, J= 6Hz, 2H), 3.99 (s, 2H), 4.00 (t, J=7Hz, 2H), 7.11 (d, J=8Hz, 2H), 7.48 (d, J= 8Hz, 2H), 7.92 (s, 3H) ppm.

HAL hexylbenzene sulfonate: $^1\text{H NMR } \delta$ (D_6 -DMSO) 0.80-0.95 (m, 6H), 1.20-1.3 (m, 14H), 1.50-1.60 (m, 4H), 2.56 (t, J= 6Hz, 2H), 2.79 (t, J=6Hz, 2H), 3.97 (s, 2H), 7.11 (d, J=8Hz, 2H), 7.48 (d, J=8Hz, 2H), 8.01 (s, 3H) ppm.

HAL octylbenzene sulfonate: $^1\text{H NMR } \delta$ (D_6 -DMSO) 0.80-0.95 (m, 6H), 1.20-1.4 (m, 18H), 1.45-1.60 (m, 4H), 2.56 (t, J= 6Hz, 2H), 2.56 (t, J= 6Hz, 2H), 2.79 (t, J= 6Hz, 2H), 3.98 (s, 2H), 4.00 (t, J= 7Hz, 2H), 7.11 (d, J= (Hz, 2H), 7.49 (d, J=8Hz, 2H), 7.93 (s, 3H) ppm.

Spectra are displayed in Fig. S1.

Nanoparticle preparation

Solid nanoparticles were prepared by the aerosol flow reactor method [27, 29]. Briefly, 1 mg/mL PLA and 0.1, 0.2 or 0.4 mg/mL HAL salt were dissolved in dichloromethane. The solution was dispersed to nanosized droplets by atomizing with a Collison-type air jet atomizer with a constant output in a liquid re-circulation mode (TSI instruments, model 3076, St Paul, Minnesota, USA). The generated aerosol was carried with nitrogen gas (flow rate 3.3 L/min) to a tubular laminar flow reactor, where solid nanoparticles were formed at 30°C. At the reactor downstream, the aerosol was diluted with nitrogen gas (25 L/min) to avoid wall deposition prior to the collection. For scanning electron microscopic imaging, the nanoparticles were sampled onto a carbon coated copper grid (Agar Scientific LTD, Essex, UK) using an electrostatic precipitator (InTox Products, Albuquerque, USA). The collection of the particles, was conducted with a Berner-type low pressure impactor [30].

Nanoparticle size and morphology

The size of nanoparticles was analyzed from the reactor downstream with a differential mobility analyzer, DMA (model 3081, TSI Inc. Particle Instruments, St. Paul, USA) connected to a condensation particle counter (CPC, model 3027, TSI Inc. Particle Instruments, St. Paul, USA). Examples of the obtained particle size distribution plots are shown in Fig. S2.

The morphology of the nanoparticles was imaged with field-emission scanning electron microscopy, SEM (JSM-7500FA, JEOL, Japan) at an acceleration voltage of 1-5 kV. The

particles were coated with gold-palladium using a sputtering unit (K110X, Emitech Ltd., UK) to reduce charging and damage of the sample by the beam.

Nanoparticle drug loading

For drug loading assays approximately 1 mg of nanoparticles was dissolved in 1 mL dichloromethane. Ten microlitres of the solution were reacted with 30 μ L fluorescamine solution (1 mg/mL) in 200 μ L ethanol. The fluorescence spectrum (excitation wavelength 390 nm) of the amine-fluorescamine product was recorded with a microplate reader (Safire, TECAN) and the fluorescence emission was measured at 490 nm. The fluorescence intensity was correlated with a standard curve from an HAL HCl dilution series in dichloromethane, prepared with fluorescamine under the same conditions as above. The drug loading of nanoparticles and the loading efficiency were calculated using the following equations:

Theoretical drug mass loading:

$$L_{\text{mass theor}} [\%] = m_{\text{drug}} / (m_{\text{polymer}} + m_{\text{drug}}) * 100 \quad (1)$$

Experimental drug mass loading:

$$L_{\text{mass exp}} [\%] = m_{\text{drug}} / m_{\text{nanoparticles}} * 100 \quad (2)$$

Experimental drug molar loading:

$$L_{\text{mol}} [\text{mol}/100\text{mg}] = n_{\text{drug}} / m_{\text{nanoparticles}} * 100 \quad (3)$$

Drug loading efficiency:

$$E [\%] = L_{\text{mass exp}} / L_{\text{mass theor}} * 100 \quad (4)$$

where m is mass and n is mole. Drug loading tests were performed in duplicates.

In vitro drug release

Drug release assays were performed in a custom-made small scale release cell (supplementary Fig. S2). Five milligram of nanoparticles were suspended in 200 μ L PBS and placed in the

donor compartment. The receptor compartment containing 2 mL PBS was separated from the donor compartment by a regenerated cellulose dialysis membrane (5 000 Da cut-off, Diachema, Munich, Germany) permeable for HAL.

For measurement of the released amount, 10 μ L samples were taken from the receptor compartment at indicated time intervals for up to 120 min. and replaced with 10 μ L PBS. The dilution was taken into account for calculation of the released drug amount as well as the residual HAL amount in the donor compartment. Each sample was reacted with 30 μ L fluorescamine solution (1 mg/mL in acetone) in 200 μ L borate buffer pH 8.5. The fluorescence was recorded as described above. The molar drug release was related to the amount of encapsulated drug according to the experimentally determined drug loading.

Cell culture

T24 human bladder carcinoma cells expressing green fluorescent protein (GFP) were kindly provided by Med Discovery SA. The carcinoma cells were cultured in Dulbecco's Modified Eagle Medium. A549 lung carcinoma cells were taken from the laboratory's cell library and cultured in F-12K medium. All media were supplemented with 10% fetal bovine serum albumin, 10 μ g streptomycin and 100 IE penicillin per mL. Cells were grown in monolayers under a controlled 5% CO₂ and 95% air atmosphere at 37°C.

Three-dimensional tumor spheroids were prepared as described by Ivascu et al. [31]. Briefly, A549 cells of monolayer cultures were harvested using trypsin-EDTA and resuspended in culture medium containing 2.5% BME to give a final concentration of 25 000 cells per mL. Aliquot 200 μ L suspensions per well were dispensed into HEMA coated round bottom 96-well plates. The plate was centrifuged at 20°C for 10 minutes at 1000 x g to induce cell clustering. The cell medium was changed twice a week by replacing 100 μ l of the medium in each well.

Fluorescence induction in cell monolayers and tumor spheroids

For fluorescence induction assays on T24 cell monolayers, 10 000 cells per well were seeded into 96-well plates 24 hours before incubation with nanoparticles. The medium was removed and the cells were incubated with free or nano-encapsulated HAL salts dispersed in 150 μ L supplemented medium. PPIX fluorescence was monitored using a multiplate reader (Safire, Tecan). The excitation wavelength was 405 nm; fluorescence emission was recorded between 500 nm and 750 nm. To evaluate genuine cellular PPIX fluorescence (values without background noise) spectra were fitted to a negative control (cells in medium only) with the Excel solver function. PPIX fluorescence intensity was extracted at 620 nm.

The A549 tumor spheroids were grown for 4 days prior to incubation with 1 mM free or nano-encapsulated HAL HCl in 200 μ L F-12K medium. The spheroids were washed once with medium and cellular nuclei were stained by incubating the spheroids with 200 μ L Hoechst 33342 (2 μ g/mL) for 20 min. The spheroids were washed again with medium. Thereafter, they were deposited on a glass slide and covered with a glass cover slip placed on two cover slips as space holders. The spheroids were viewed with a LSM 700 Confocal Laser Scanning Microscope (Carl Zeiss, Germany) under a 10x objective. PPIX and Hoechst 33342 were excited with a 405 nm single photon laser. Hoechst 33342 was detected with a 555 nm low pass filter, PPIX was detected in simultaneous acquisition mode with a 610 nm long pass filter.

Fluorescence induction in A549 tumor nodules in the chicken chorioallantoic membrane (CAM)

For *in vivo* CAM assays, fertilized hen eggs were incubated at 37°C and 65% relative humidity. They were rotated twice a day for 4 days. Thereafter, a small hole was drilled at the narrow apex of the egg to allow detachment of the CAM. The hole was sealed with adhesive tape and the eggs were incubated in the upright position. At embryo development day (EDD) 8 the hole was enlarged to allow access to the CAM for tumor implantation. Tumor spheroids were grown to 0.5 mm size. For implantation the CAM was perforated with a 26 gauge needle and a single tumor spheroid suspended in a 1:1 mixture of cell medium and extracellular matrix (MatrigelTM) was deposited on the perforation. Eggs were sealed with parafilm and incubated in the upright position to allow tumor growth.

Tumor fluorescence generation was assayed at EDD12 as follows: HAL laden nanoparticles and free HAL were dispersed in an aqueous PEG400 solution (20%), respectively. 20 μl of the mixture were deposited with a micropipette on the tumor implant. Fluorescence was observed with a charge coupled device (CDD) camera connected to a modified fluorescence microscope (Eclipse 600 FN, Nikon, Tokyo, Japan) equipped with a CFI achromat objective of 4x magnification and 0.1 numerical aperture. Tumors were illuminated with a 100 W mercury arc lamp (filter 405 nm) and fluorescence was acquired through a 650/50 nm filter [32].

Results and Discussion

In vitro particle characterization

HAL is an esterified δ -amino acid with a logP of 1.8 [12]. Although this indicates a lipophilic character, HAL conserves amphiphilic characteristics due to the presence of a positively charged amino group under physiological conditions. These features render HAL a challenging candidate for the encapsulation into polymeric nanoparticles with methods using aqueous media as dispersion phase. Precisely, HAL particle loading and encapsulation efficiency remain below 1% when applying conventional techniques such as nanoprecipitation, emulsion evaporation and emulsion diffusion (unpublished results). This may be attributed to the fact that surfactants needed for the particle formation in aqueous medium increase the solubility of HAL in water, causing it to leach into the aqueous phase.

The drug diffusion from a polymeric matrix into an aqueous medium is also influenced by the affinity of the compound to the polymer. Thus, the release from a lipophilic vehicle should be slower for a lipophilic than a hydrophilic compound. We tested this approach with regard to HAL by preparing lipophilic HAL alkyl benzene sulfonates. The ion pairing concept was first reported by Arrhenius, who evidenced a relative decrease of conductance of a salt containing solution with increasing concentration [33]. This led to the conclusion, that depending on the conditions (temperature, dielectric constant, ion concentration) ions of opposite charge associate to neutral entities. Our NMR data confirmed a one to one cation-anion ratio for all formed HAL aryl sulfonate salts (Fig. S1).

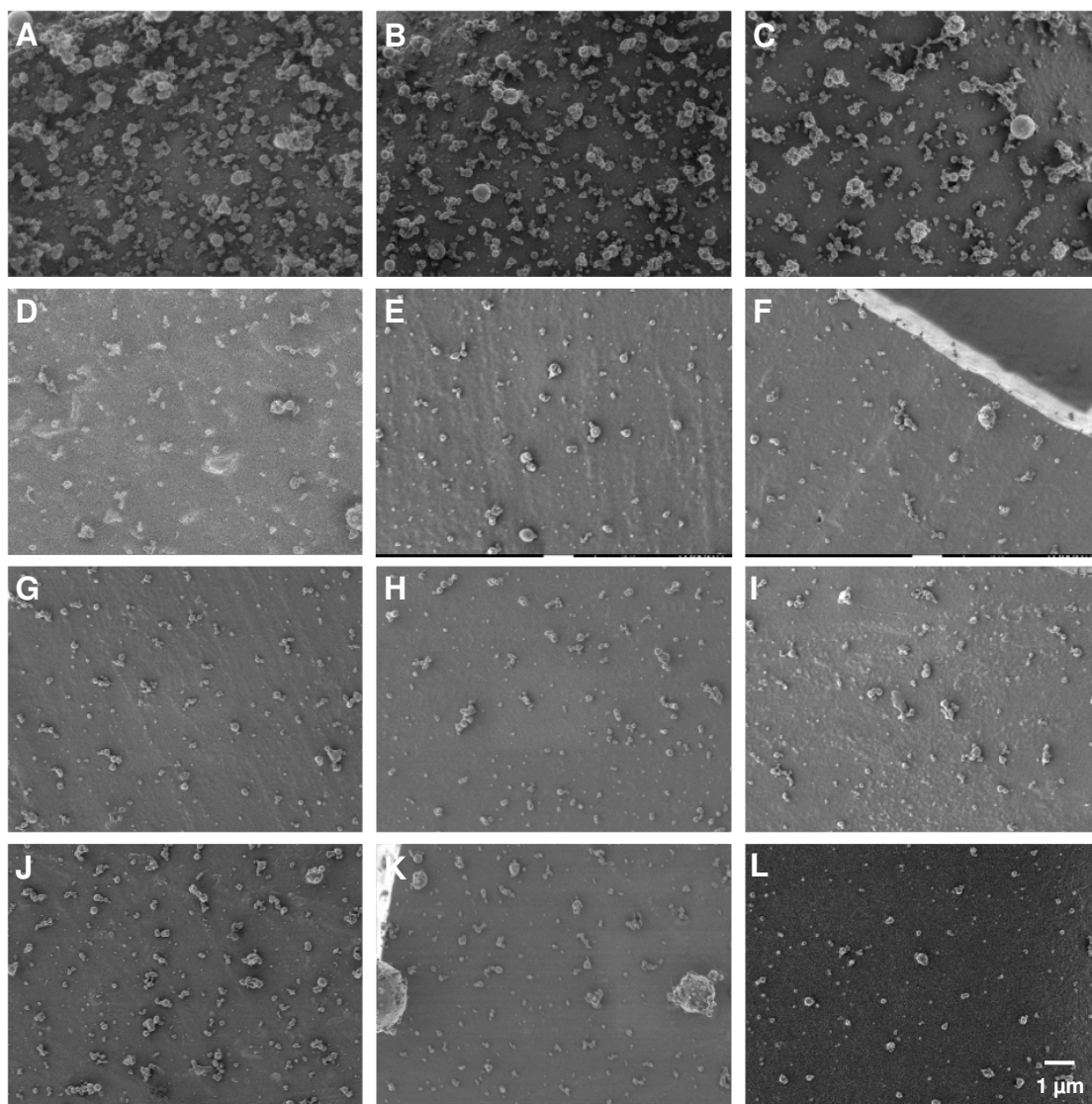


Fig. 1. SEM micrographs of nanoparticle loaded with HAL HCL (A-C,) HAL BUTBS, (D-F), HAL HEXBS (G-I) and HAL OCTBS (I-L). Particles were prepared with HAL salt:polymer ratios of 1:10 (1st column), 2:10 (2nd column) and 4:10 (3rd column).

Aiming at the development of PLA nanoparticles with improved HAL loading we applied the aerosol flow reactor method as an alternative to liquid phase techniques. The particle composition is governed by the dissolved compounds in the aerosol droplets. Consequently, the polymer/drug ratio within the nanoparticles is well controllable. Moreover, the particle morphology can be tuned according to the evaporation rate of the solvent, as well as the drug-polymer affinity.

Tab. 1. Geometrical number mean diameter (GNMD) and geometrical standard deviation of PLA nanoparticles laden with varying amounts of HAL HCl, HAL butylbenzene sulfonate (HAL BUTBS), HAL hexylbenzene sulfonate (HAL HEXBS), and octylbenzene sulfonate (HAL OCTBS). For each salt three batches were prepared with drug to polymer ratios of 1:10, 2:10, 4:10 (w/w), respectively. The particle loadings calculated are represented with the standard deviation. The molar loading was calculated according to equation (3) to compare the amount of encapsulated active substance between the different sample batches. The drug release maximum, Y_{max} , and release constants, k , including the standard errors were obtained from fitted curves corresponding to one phase exponential function $Y = Y_{max} (1 - e^{-k \cdot t})$ where Y is the amount of drug released at time, t .

Sample	size [nm]		HAL loading				HAL release	
	GNMD [nm]	GSD	drug:polym. ratio	exp. [%]	molar [$\mu\text{mol}/100\text{mg}$]	efficiency [%]	Y_{max} [%]	k
Control	127.2	1.57	0	0	0	0	110 \pm 1.8	0.043 \pm 0.002
HCL 1	158.8	1.58	1:10	5.1	20.1	55.7	70.16 \pm 2.4	0.037 \pm 0.005
HCL 2	139.6	1.52	2:10	9.7 \pm 0.6	38.4 \pm 3.7	58.0 \pm 2.4	63.39 \pm 1.3	0.038 \pm 0.003
HCL 4	145.6	1.52	4:10	22.5 \pm 4.4	89.4 \pm 15.5	78.7 \pm 17.6	51.29 \pm 1.1	0.038 \pm 0.003
BUTBS 1	135.0	1.50	1:10	6.2 \pm 0.2	14.4 \pm 2.4	67.9 \pm 0.5	88.8 \pm 2.5	0.053 \pm 0.006
BUTBS 2	147.4	1.51	2:10	11.2 \pm 0.3	26.0 \pm 1.6	66.9 \pm 0.6	67.02 \pm 1.9	0.067 \pm 0.009
BUTBS 4	158.4	1.52	4:10	21.7 \pm 2.0	50.6 \pm 6.9	75.9 \pm 4.6	60.32 \pm 0.8	0.042 \pm 0.002
HEXBS 1	152.2	1.53	1:10	5.6 \pm 0.1	12.2 \pm 0.8	61.6 \pm 0.2	n.a.	n.a.
HEXBS 2	152.2	1.51	2:10	8.4 \pm 0.9	18.3 \pm 5.5	50.2 \pm 2.0	108.9 \pm 3.2	0.036 \pm 0.004
HEXBS 4	145.6	1.53	4:10	15.6 \pm 0.2	34.1 \pm 0.8	54.5 \pm 0.5	76.34 \pm 1.8	0.057 \pm 0.006
OCTBS 1	152.9	1.52	1:10	7.0 \pm 0.2	14.3 \pm 2.1	76.5 \pm 0.4	68.28 \pm 1.1	0.026 \pm 0.001
OCTBS 2	140.6	1.53	2:10	10.2 \pm 0.8	21.1 \pm 4.6	61.4 \pm 1.6	42.92 \pm 0.7	0.029 \pm 0.002
OCTBS 4	144.3	1.55	4:10	15.9 \pm 1.5	32.7 \pm 5.1	55.6 \pm 3.0	58.51 \pm 1.8	0.016 \pm 0.001

Particles prepared by the flow reactor method were spherical and in some cases wrinkled (Fig. 1). The HAL salt type and amount influenced the particle morphology to minor extent. Particle size distributions were unimodal (Fig. S2) with a geometrical standard deviation (GSD) below 1.6 in all nanoparticle batches (Tab. 1). The geometrical number mean diameter (GNMD) was 127 nm in unladen nanoparticles; the mean diameters of HAL salt laden nanoparticles varied between 135 nm and 159 nm. The bigger size is in accordance with the higher amount of solidifiable material in the droplets. However, since the drug amount did not clearly correlate with the particle size we also suspect the implication of other parameters, such as a modification of the surface tension of the organic solution to have an effect on the

particle size. The loading efficiency was above 50% in all tested formulations (Tab. 1) confirming that the aerosol method promotes HAL partitioning into the PLA nanoparticles.

In vitro drug release

The *in vitro* molar drug release was determined using a small scale release cell composed of a donor and receptor compartment separated by a dialysis membrane (Fig. S3).

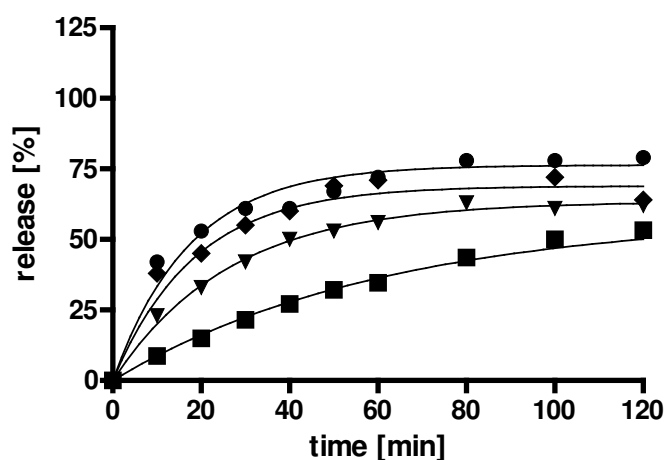


Fig. 2. Drug release profiles of nanoparticles laden with HAL HCl (▼, 38 $\mu\text{mol}/100\text{ mg}$), HAL BUTBS (◆, 26 $\mu\text{mol}/100\text{ mg}$), HAL HEXBS (●, 34 $\mu\text{mol}/100\text{ mg}$), HAL OCTBS (■, 32 $\mu\text{mol}/100\text{ mg}$).

Free HAL HCl diffused into the donor compartment within 40 minutes. The drug release profile of nanoparticles followed first order kinetics, with a maximum release that did not reach 100% (Fig. 2). The rate constants, k , of the initial drug release and the percentage, Y_{max} , of released drug are reported in Tab. 1. Particles with lower loading showed a significantly higher release maximum. This suggests that the release of HAL salts is closely related to the drug-polymer ratio. On this basis, it can be assumed that the HAL salt partitioning into the particle core is promoted by an increase of the salt concentration. We compared the drug release from particles featuring a molar drug loading close to 30 $\mu\text{mol}/100\text{ mg}$ polymer (Fig. 2). We assumed that the lipophilic compounds would be more efficiently incorporated into the particle core and thus show a sustained release. However, with the

exception of HAL OCTBS, release of HAL HCl from nanoparticles was slower than for lipophilic HAL salts.

Due to the chemical instability of free HAL in aqueous solution we were not able to assess the long term *in vitro* release of HAL from the nanoparticles. However, we presume that the higher molar concentration of HAL HCl per particle and thus higher amount of drug in the particle core may be at the origin of this result, while low water solubility of HAL OCTBS may prevent the drug from flushing into the release medium.

PPIX generation in T24 cell monolayers

The efficacy of 5-ALA and its derivatives has been extensively studied in our group on GFP transfected T24 cells [34]. GFP fluorescence intensity correlates inversally with cell viability [35, 36]. This is of special interest when assessing new compounds, where pharmacological activity must be distinguished from a cytotoxic effect. In our study we used GFP transfected T24 cells to screen the ability of four different HAL salt types, namely HAL HCl, HAL BUTBS, HAL HEXBS and HAL OCTBS, in free salt and nanoencapsulated form to generate PPIX fluorescence. We were further interested in the fluorescence generation as a function of nanoparticle loading. As it is beyond the scope of this article to present the results collected for each nanoencapsulated salt amount and type, only experiments implying nanoparticles with large amounts of HAL salt (i.e. drug:polymer ratio of 4:10) are presented (Fig. 3). It should nevertheless be noted that nanoparticles with lower loading provided similar fluorescence-time profiles to nanoparticles with high loading of the same HAL salt at the same concentrations.

Porphyrin fluorescence intensities correlated inversely with the lipophilicity of the HAL salt. Free HAL HEXBS and HAL OCTBS had a toxic effect above 0.5 and 0.125 mM concentrations, respectively, as indicated by the decrease in cellular GFP (Fig. S4 1st column). Considering the lipophilic character of HAL HEXBS and HAL OCTBS, we assume that the counter ion interferes with the lipid bilayer, which ultimately causes a metabolic shutdown. The toxic effect was less pronounced when using nanoencapsulated HAL salts (Fig. S4 2nd column).

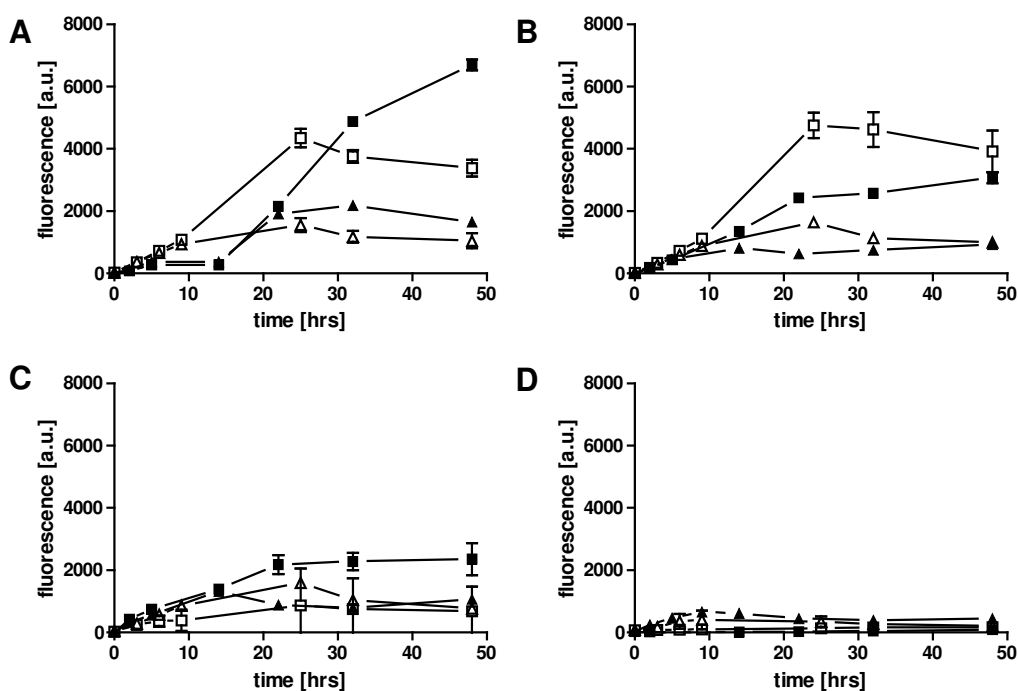


Fig. 3. Fluorescence time profiles of T24 cells incubated with free (open symbols) and nanoencapsulated (solid symbols) HAL salts at concentrations of 1 mM (square) and 0.5 mM (triangle) HAL. A: HAL HCl, B: HAL BUTBS, C: HAL HEXBS, D: HAL OCTBS.

The fluorescence-time profiles of cells incubated with HAL salt laden nanoparticles indicate sustained fluorescence over 48 hours. The strongest fluorescence was observed in cells incubated with HAL HCl laden nanoparticles. It was 1.5 times higher than the fluorescence maximum observed with 1 mM free HAL HCl, which is considered the optimal concentration for HAL-mediated porphyrin generation *in vitro*. When using free salts of HAL HCL, HAL BUTBS and HAL HEXBS, the fluorescence decreased gradually after 25 hours even at optimal concentrations. Since GFP fluorescence only diminished to minor extent, we hypothesized that substrate availability was reduced after this time, shifting the equilibrium between porphyrin production and degradation. Only minimal fluorescence was observed using either free or nanoencapsulated HAL OCTBS, which is in accordance with the toxicity data. Drug laden nanoparticles seemed to provide HAL over a longer time period as indicated by a sustained fluorescence intensity. It is not clear why fluorescence steadily increased with HAL HCl, while it remained constant with HAL HEXBS and HAL BUTBS. An interplay between delayed release and or interference of the compound with cellular metabolism of the more lipophilic compounds could be at the origin of this phenomenon not yet causing cell death.

Fluorescence generation on tumor spheroids and in CAM

HAL laden nanoparticles were evaluated *in vitro* on A549 tumor spheroids and on a tumor model on the chorioallantoic membrane of chicken embryos. Tumor spheroids represent cell aggregates of one or more different cell types. With a 3-dimensional cell arrangement they feature a similar physiology to solid tumors, where proliferation kinetics, oxygen partial pressure and nutrient availability are inconsistent [37]. 5-ALA or HAL have previously been shown to induce porphyrin fluorescence in tumor spheroids cultured from several glioma cell lines, EMT 6 mammary carcinoma and bladder carcinoma cells, respectively [38-41]. The confocal micrographs in Fig. 4 show that these findings can be extended to the use of free and nanoencapsulated HAL HCl on tumor spheroids from an A549 lung carcinoma cell line. No differences in fluorescence pattern or fluorescence intensities between HAL laden nanoparticles and the corresponding free salt has been observed at a concentration of 1mM.

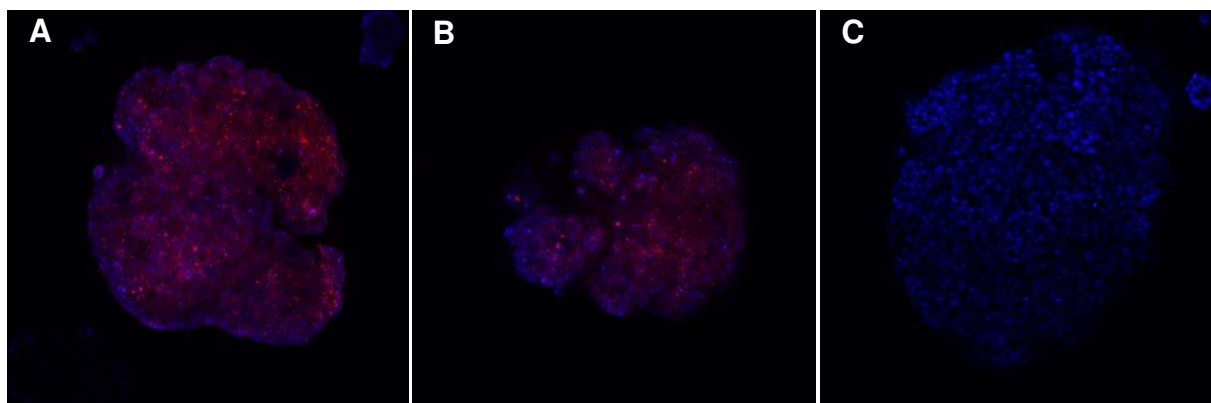


Fig. 4. Confocal images of A549 tumor spheroids incubated with 1mM free HAL HCl (A), HAL HCl laden nanoparticles (B), and F-K12 medium only (C) for 12 hours. Cell nuclei were stained with Hoechst 33342 (blue fluorescence). The control showed no red fluorescence.

Upon reaching a certain size *in vivo* tumors develop a necrotic center and trigger neovascularization. Necrotic structures appear in tumor spheroids larger than 0.2 mm. Therefore, such *in vitro* models are only suitable to mimic the early developmental stages of the neoplasm. However, spheroids can generate vessel growth *in vivo* as neoplastic implants [42]. The CAM of the immunodeficient chick embryo represents an adequate host for such xenografts. Thus, implantation of tumor spheroids into the CAM at EDD7 leads to the growth of vascularized tumor nodules by EDD12. With the perspective of using nanoparticles as drug

carriers for delivery of HAL to the lung, we monitored the tumor fluorescence on the CAM after deposition of HAL laden nanoparticles and compared the fluorescence induced by free HAL HCl. HAL laden nanoparticles successfully generated PPIX fluorescence (Fig. 5). However, it was comparable to the fluorescence induced with free HAL HCl. To improve nanoparticle redispersion we suspended the nanoparticles in a 20% PEG400 solution in water. The presence of the surfactant may have triggered a faster release of HAL.

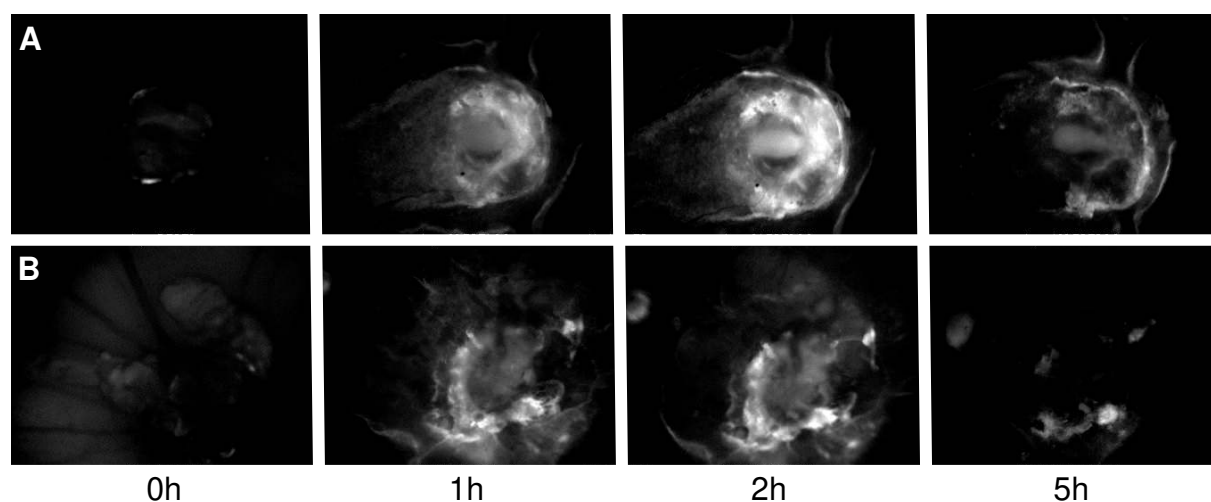


Fig. 5. Fluorescence of A549 tumors implanted on the CAM of the chick embryo after topical application of HAL HCl laden nanoparticles (A) corresponding to 1 mM HAL and 1 mM free HAL (B). Fluorescence was monitored at time points 0, 1, 2, 4 and 20 hours.

Conclusion

From the results of our study we conclude that the aerosol flow reactor method is a suitable technique for the efficient nanoencapsulation HAL HCl and its lipophilic salts into polymeric nanoparticles. Nanoencapsulation decreased the cytotoxicity of HAL salts and allowed a sustained fluorescence induction in a T24 bladder carcinoma cell line. Lipophilization of HAL altered the *in vitro* drug release profile of nanoparticles; however, it had no influence on the sustained fluorescence generation on a T24 cell line. HAL HCl laden nanoparticles were at least as efficient as free HAL HCl when administered topically onto CAM-implanted A549 tumor nodules. Therefore, they may serve as a potential tool to deliver photosensitizers to pulmonary neoplasms, while diminishing the fast lung clearance. Future emphasis should also be put on the development of appropriate protocols for the re-suspension in aqueous media to explore the formulation for the intravenous application.

Acknowledgements

We would like to acknowledge Jonas Iivanainen for his help in SEM imaging of the nanoparticles and Jérôme Bosset for his valuable advice for confocal microscopy of the tumor spheroids. We further thank Dr. Karine Mondon and Dr. Andrej Babic for their help with the acquiry of NMR spectra.

Reference List

1. Cortese DA, Edell ES, Kinsey JH. Photodynamic therapy for early stage squamous cell carcinoma of the lung. *Mayo Clin Proc* 1997; **72**: 595-602.
2. Kato H, Furukawa K, Sato M et al. Phase II clinical study of photodynamic therapy using mono-L-aspartyl chlorin e6 and diode laser for early superficial squamous cell carcinoma of the lung. *Lung Cancer* 2003; **42**: 103-11.
3. Moghissi K, Dixon K, Stringer M et al. The place of bronchoscopic photodynamic therapy in advanced unresectable lung cancer: experience of 100 cases. *Eur J Cardiothorac Surg* 1999; **15**: 1-6.
4. Vonk-Noordegraaf A, Postmus PE, Suttedja TG. Bronchoscopic treatment of patients with intraluminal microinvasive radiographically occult lung cancer not eligible for surgical resection: a follow-up study. *Lung Cancer* 2003; **39**: 49-53.
5. Hautmann H, Pichler JP, Stepp H et al. In-vivo kinetics of inhaled 5-aminolevulinic acid-induced protoporphyrin IX fluorescence in bronchial tissue. *Resp Res* 2007; **8**: 33.
6. Baumgartner R, Huber RM, Schulz H et al. Inhalation of 5-aminolevulinic acid: a new technique for fluorescence detection of early stage lung cancer. *Photochem Photobiol B* 1996; **36**: 169-74.
7. Gamarra F, Lingk P, Marmarova A et al. 5-Aminolevulinic acid-induced fluorescence in bronchial tumours: dependency on the patterns of tumour invasion. *Photochem Photobiol B* 2004; **73**: 35-42.
8. Gamarra F, Wagner S, Al-Batran S et al. Kinetics of 5-aminolevulinic acid-induced fluorescence in organ cultures of bronchial epithelium and tumor. *Respiration* 2002; **69**: 445-50.

9. Lange N, Jichlinski P, Zellweger M et al. Photodetection of early human bladder cancer based on the fluorescence of 5-aminolaevulinic acid hexylester-induced protoporphyrin IX: a pilot study. *Br J Cancer* 1999; **80**: 185-93.
10. Gerscher S, Connelly JP, Griffiths J et al. Comparison of the pharmacokinetics and phototoxicity of protoporphyrin IX metabolized from 5-aminolevulinic acid and two derivatives in human skin in vivo. *Photochem Photobiol* 2000; **72**: 569-74.
11. Marti A, Lange N, van den Bergh H et al. Optimisation of the formation and distribution of protoporphyrin IX in the urothelium: an in vitro approach. *J Urology* 1999; **162**: 546-52.
12. Uehlinger P, Zellweger M, Wagnieres G et al. 5-Aminolevulinic acid and its derivatives: physical chemical properties and protoporphyrin IX formation in cultured cells. *Photochem Photobiol B* 2000; **54**: 72-80.
13. Xiang W, Weingandt H, Liessmann F et al. Photodynamic effects induced by aminolevulinic acid esters on human cervical carcinoma cells in culture. *Photochem Photobiol* 2001; **74**: 617-23.
14. Perotti C, Casas A, Fukuda H et al. ALA and ALA hexyl ester induction of porphyrins after their systemic administration to tumour bearing mice. *Br J Cancer* 2002; **87**: 790-5.
15. Fotinos N, Campo MA, Popowycz F. The chick embryo model for the evaluation of 5-aminolevulinic acid derivatives. Geneva: University of Geneva; 2007.
16. Lehardt T, Roesler S, Beck-Broichsitter M, Kissel T. Polymeric nanocarriers for drug delivery to the lung. *J Drug Deliv Sci Technol* 2010; **20**: 171-80.
17. Rytting E, Nguyen J, Wang X, Kissel T. Biodegradable polymeric nanocarriers for pulmonary drug delivery. *Expert Opin Drug Deliv* 2008; **5**: 629-39.
18. Alonso MJ. Nanoparticulate Drug Carrier Technology. *Drugs Pharmaceut Sci* 1996; **77**: 203-25.
19. Quintanar-Guerrero D, Allemann E, Fessi H, Doelker E. Preparation techniques and mechanisms of formation of biodegradable nanoparticles from preformed polymers. *Drug Dev Ind Pharm* 1998; **24**: 1113-28.
20. Vauthier C, Bouchemal K. Methods for the Preparation and Manufacture of Polymeric Nanoparticles. *Pharm Res* 2009; **26**: 1025-58.
21. Chan H-K, Kwok PCL. Production methods for nanodrug particles using the bottom-up approach. *Adv Drug Deliv Rev* 2011; **63**: 406-16.
22. Eerikäinen H, Watanabe W, Kauppinen EI, Ahonen PP. Aerosol flow reactor method for synthesis of drug nanoparticles. *Eur J Pharm Biopharm* 2003; **55**: 357-60.

23. Beck-Broichsitter M, Schweiger C, Schmehl T et al. Characterization of novel spray-dried polymeric particles for controlled pulmonary drug delivery. *J Control Release* 2011; doi:10.1016/j.jconrel.2011.10.030.
24. Apte SP. Excipient counterion dependent mechanisms in Pharmaceutical Development: a review. *J Excipients Food Chem* 2011; **2**: 28-40.
25. Abu T.M S. Salt formation to improve drug solubility. *Adv Drug Deliv Rev* 2007; **59**: 603-16.
26. Yoo HS, Choi H-K, Park TG. Protein-fatty acid complex for enhanced loading and stability within biodegradable nanoparticles. *J Pharm Sci* 2001; **90**: 194-201.
27. Eerikainen H, Peltonen L, Raula J et al. Nanoparticles containing ketoprofen and acrylic polymers prepared by an aerosol flow reactor method. *Aaps Pharmscitech* 2004; **5**.
28. Gray FW, Gerecht JF, Krems IJ. The preparation of model long-chain alkylbenzenes and a study of their isomeric sulfonation products. *J Org Chem* 1955; **20**: 511-24.
29. Raula J, Eerikainen H, Kauppinen EI. Influence of the solvent composition on the aerosol synthesis of pharmaceutical polymer nanoparticles. *Int J Pharmaceut* 2004; **284**: 13-21.
30. Hillamo RE, Kauppinen EI. On the performance of the Berner low pressure impactor. *Aerosol Sci Technol* 1991; **14**: 33-47.
31. Ivascu A, Kubbies M. Rapid generation of single-tumor spheroids for high-throughput cell function and toxicity analysis. *J Biomol Screening* 2006; **11**: 922-32.
32. Lange N, Ballini JP, Wagnieres G, van dBH. A new drug-screening procedure for photosensitizing agents used in photodynamic therapy for CNV. *Invest Ophthalmol Vis Sci* 2001; **42**: 38-46.
33. Kraus CA. The ion-pair concept: its evolution and some applications. *J Phys Chem* 1956; **60**: 129-41.
34. Fotinos N, Campo MA, Gurny R, Lange N. Optimization of 5-aminolevulinic acid derivative-mediated photomedicine: new strategies, models and applications [PhD]. Aterlier de reproduction de la Section de Physique, Geneva: University of Geneva; 2007.
35. Steff AM, Fortin M, Arguin C, Hugo P. Detection of a decrease in green fluorescent protein fluorescence for the monitoring of cell death: An assay amenable to high-throughput screening technologies. *Cytometry* 2001; **45**: 237-43.
36. Aguilera RJ, Montoya J, Primm TP, Varela-Ramirez A. Green fluorescent protein as a biosensor for toxic compounds. *Rev Fluoresc* 2006; **3**: 463-72.

37. Santini MT, Rainaldi G. Three-dimensional spheroid model in tumor biology. *Pathobiology* 1999; **67**: 148-57.
38. Bigelow CE, Mitra S, Knuechel R, Foster TH. ALA- and ALA-hexylester-induced protoporphyrin IX fluorescence and distribution in multicell tumour spheroids. *Br J Cancer* 2001; **85**: 727-34.
39. Etminan N, Peters C, Lakbir D et al. Heat-shock protein 70-dependent dendritic cell activation by 5-aminolevulinic acid-mediated photodynamic treatment of human glioblastoma spheroids in vitro. *Br J Cancer* 2011; **105**: 961-9.
40. Hirschberg H, Baek S-K, Kwon YJ et al. Bypassing the blood-brain barrier: delivery of therapeutic agents by macrophages. *Proc SPIE* 2010; **7548**: 75483Z/1-Z/5.
41. Steinbach P, Kriegmair M, Baumgartner R et al. Intravesical instillation of 5-aminolevulinic acid: the fluorescent metabolite is limited to urothelial cells. *Urology* 1994; **44**: 676-81.
42. De MN, Liaw L-HL, Berns M et al. Applications of a new in vivo tumor spheroid based shell-less chorioallantoic membrane 3-D model in bioengineering research. *J Biomed Sci Eng* 2010; **3**: 20-6.

Supplementary Figures

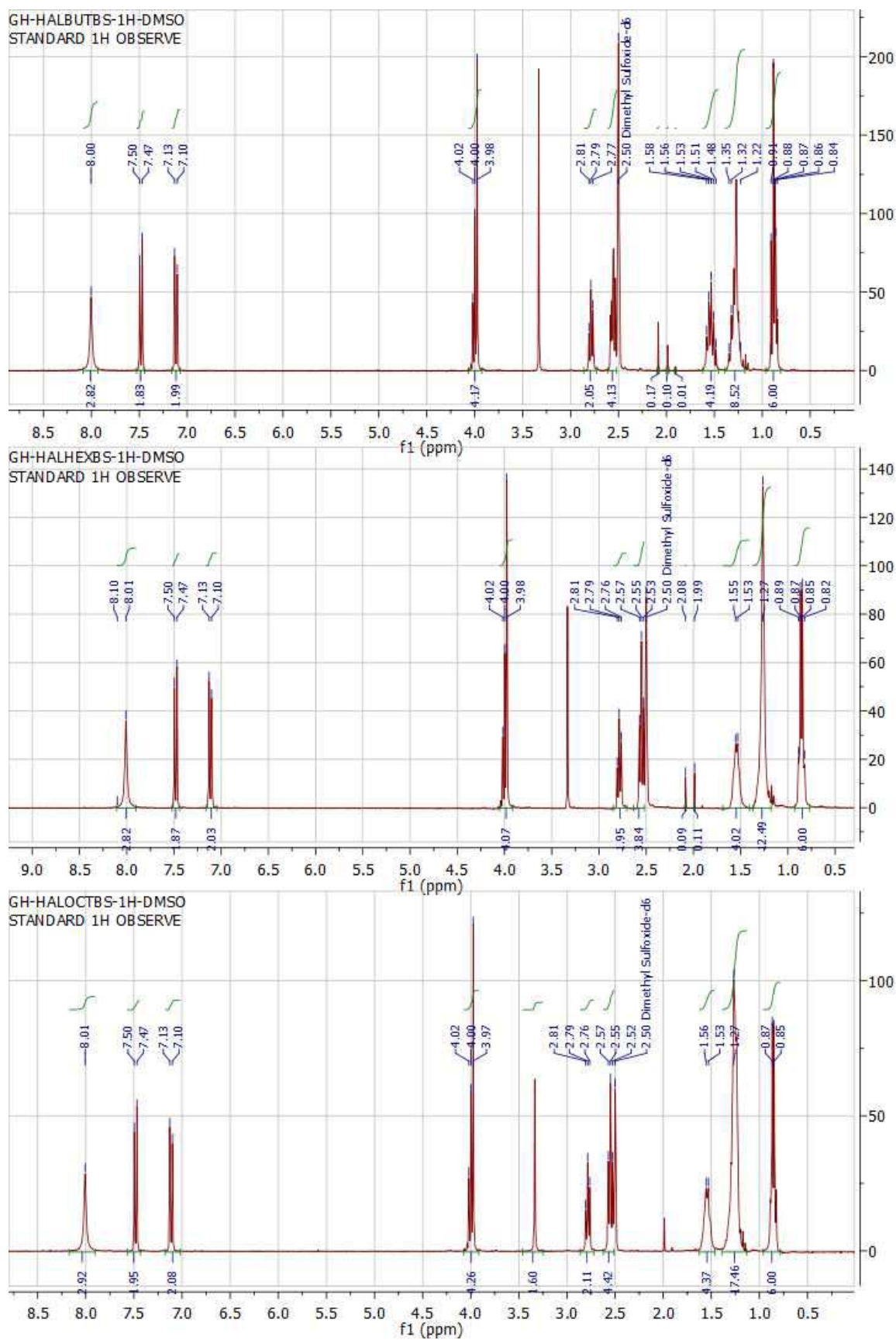


Fig. S1. ^1H NMR spectra of HAL BUTBS, HAL HEXBS and HAL OCTBS.

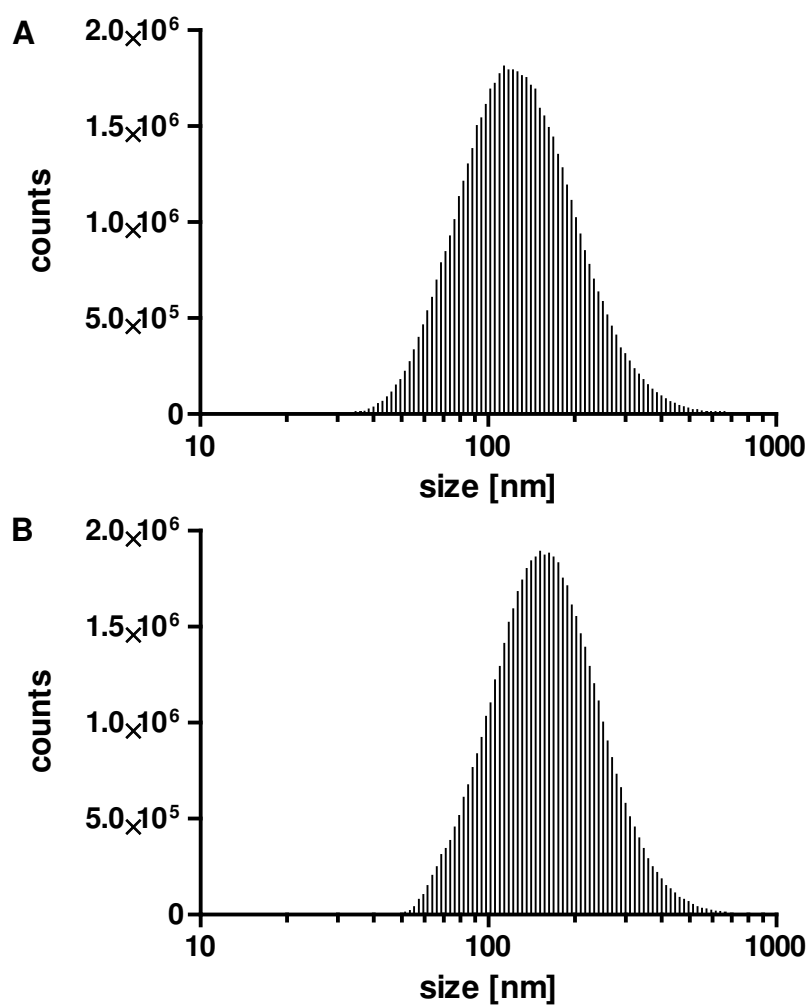


Fig. S2. Examples of nanoparticle size distributions determined by differential mobility analysis (DMA) combined with a condensation particle counter (CPC) of A: unladen PLA nanoparticles and HAL BUTBS laden nanoparticles (mass loading 21.0%).

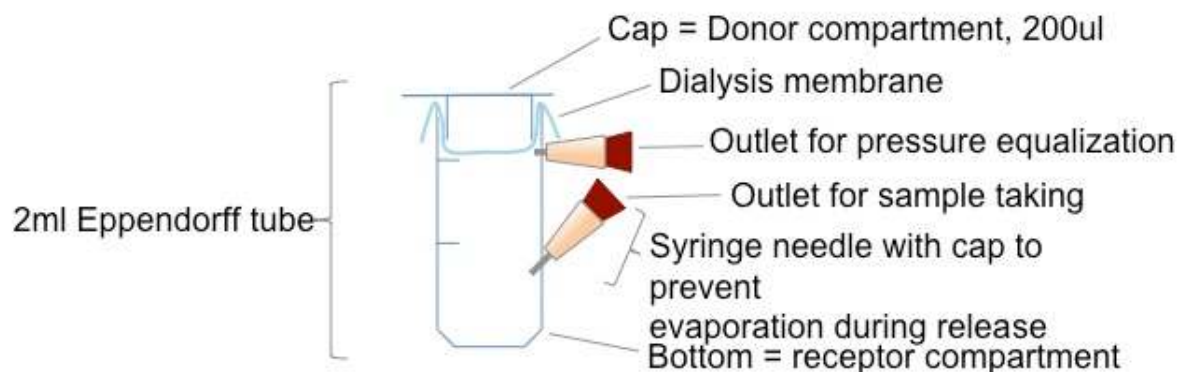


Fig. S3. Small scale release cell for in vitro drug release from polymeric nanoparticles. The cell is placed on a shaker during the drug release assay at 37°C. 200µL donor solution is placed in the Eppendorff cap and covered with a dialysis membrane before fitting the body of the Eppendorff vial on the cap. The body of the Eppendorff vial is provided with two outlets made from cut-off syringe needles to allow filling of the vial body with the receptor medium (2 mL PBS buffer) and sampling (lower outlet). The upper outlet ensures pressure equalization in the cell during sampling. The outlets are capped during incubation to prevent leakage of the release medium.

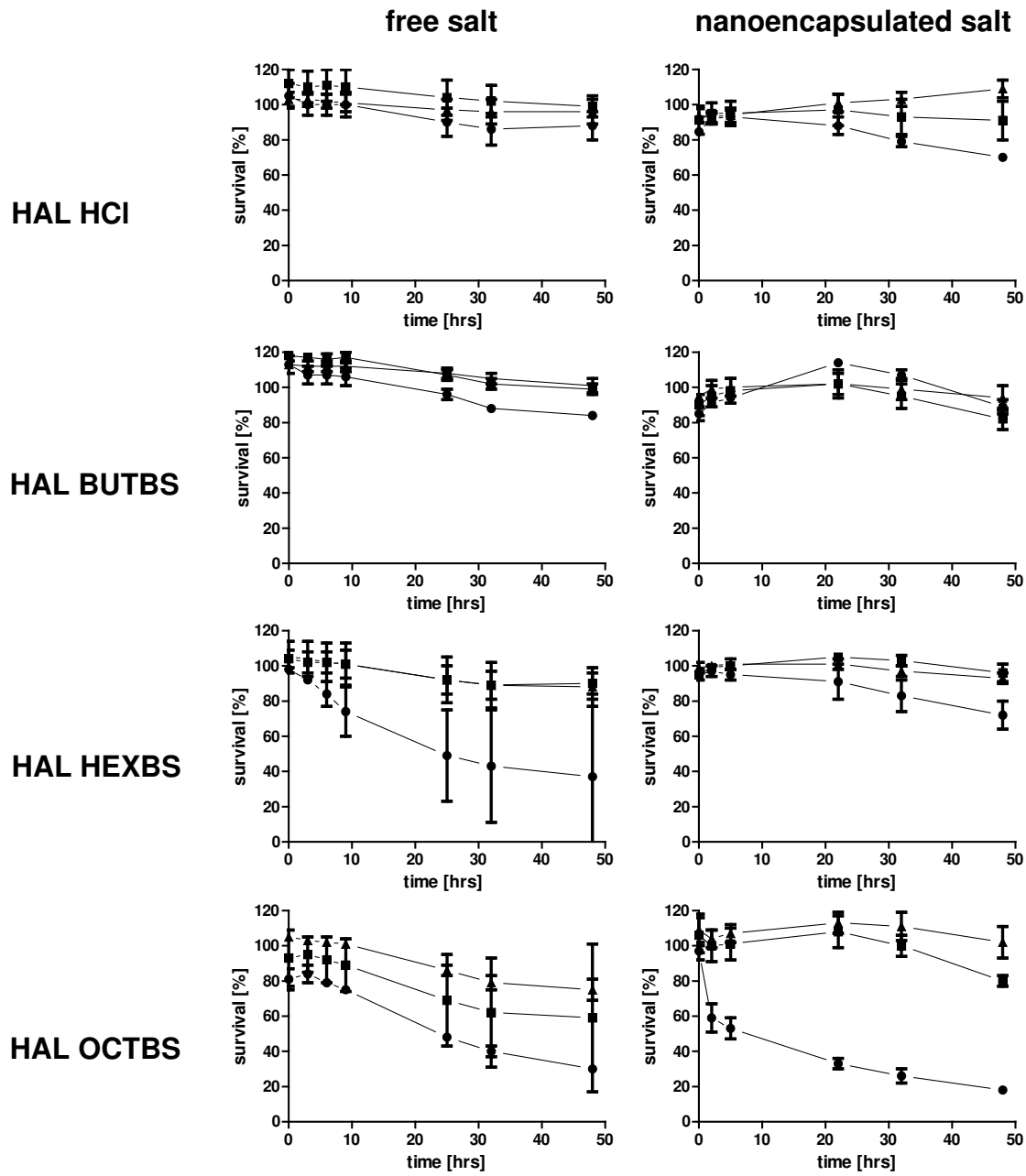


Fig. S4. GFP fluorescence over time of T24 cells incubated with 1(●), 0.5(■) and 0.25(▲)mM free and nanoencapsulated HAL salt, respectively.

PART B: Photodynamic Inactivation of *Escherichia coli* with a new Protoporphyrin IX generating Mechanism

Annotation

The discovery of penicillin by Alexander Fleming likely represents the greatest success story in the treatment of bacterial infections. It triggered the research on antibiotics into certain directions, while other antibacterial approaches fell into oblivion. Yet, the uncontrolled use of antibiotics resulted in a global situation, where the appearance of multiresistant clinical strains poses an increasing burden on antimicrobial strategies. Today, a number of formerly “last choice” antibiotics are no more effective. This is why research is urged to explore new concepts in antimicrobial therapy. It was already known in the pre-penicillin era that bacteria can be sensitized to obliteration by light. The modest development of resistance after repeated exposure to light turns out to be a major advantage in photodynamic inactivation (PDI) of bacteria. Consequently, PDI regained attention during the past two decades.

Bacteria require iron for maintenance of their cellular metabolism. They developed various mechanisms to scavenge iron from their host, where heme represents an abundant source for the element. The group of Professor Cécile Wandersman at the Institut Pasteur, Paris, France, studies bacterial iron uptake mechanisms with regard to heme in particular. The group notably observed that certain Gram-negative bacteria internalize exogenous heme and subsequently extract iron from heme into the cytosol.

The following two chapters describe the results of experiments that were conducted in collaboration with Professor Wandersman’s group. The first part presents the identification of a new mechanism for iron extraction from the tetrapyrrol backbone of heme resulting in the generation of PPIX in bacteria. The second part describes experiments challenging the system to photosensitization and the role of the TolC multidrug efflux pump in the export of PPIX from the cytosol.

Chapter 4. Bacteria capture Iron from Heme by keeping the Tetrapyrrol Skeleton intact

Sylvie Létoffé¹, Gesine Heuck², Philippe Delepelaire¹, Norbert Lange², Cécile Wandersman¹

¹ Unité des Membranes Bactériennes, Département de Microbiologie, Institut Pasteur, 75724 Paris Cedex 15 France. CNRS URA 2172.

² Laboratory of Pharmaceutics and Biopharmaceutics, School of Pharmaceutical Sciences, University of Geneva, University of Lausanne, Quai Ernest Ansermet 30 1211 Genève 4, Switzerland.

Published in: Proceedings of the National Academy of Sciences of the United States of America, 106 (28), 11719-11724, 2009

ABSTRACT. Because heme is a major iron-containing molecule in vertebrates, the ability to use heme bound iron is a determining factor in successful infection by bacterial pathogens. Until today, all known enzymes performing iron extraction from heme did so through the rupture of the tetrapyrrol skeleton. Here, we identified 2 *Escherichia coli* paralogs, YfeX and EfeB, without any previously known physiological functions. YfeX and EfeB promote iron extraction from heme preserving the tetrapyrrol ring intact. This novel enzymatic reaction corresponds to the deferrochelation of the heme. YfeX and EfeB are the sole proteins able to provide iron from exogenous heme to *E. coli*. YfeX is located in the cytoplasm. EfeB is periplasmic and enables iron extraction from heme in the periplasm and iron uptake in the absence of any heme permease. YfeX and EfeB are widespread and highly conserved in bacteria. We propose that their physiological function is to retrieve iron from heme.

Keywords: deferrochelation activity, Dyp peroxidase, heme iron extraction, new bacterial function, heme permease

Introduction

Heme is ubiquitous, abundant and vitally necessary as a cofactor in oxidoreduction, and gas transport. Most microorganisms display a complete heme biosynthetic pathway, but are able to acquire the essential ferrous iron from exogenous heme [1]. Free heme or heme arising from hemoproteins is internalized intact and subsequently degraded in the cytosol.

Various mechanisms for heme uptake have been identified in bacteria. They involve extracellular hemoproteins (hemophores) that capture heme and deliver it to bacteria [2] and cell surface receptors that bind heme, hemoproteins and/or hemophores. Surface receptors of Gram-positive bacteria are cell-wall-anchored proteins that scavenge heme from host hemoproteins and relay it to specific ABC transporters involved in heme internalization [3].

Gram-negative bacterial surface receptors are outer membrane proteins that actively transport heme through this membrane. Although the *Escherichia coli* K12 laboratory strain is missing its own heme outer membrane receptor, it acquires the ability to use heme as an iron source owing to the expression of a foreign heme receptor such as the *Serratia marcescens* HasR receptor. Once in the periplasm, heme is caught by heme permease which consist of a periplasmic heme binding protein and an ABC transporter sharing similarities with Gram-positive heme ABC transporters [1]. An alternative heme permease has been identified in *E. coli* K12. It comprises the dipeptide ABC transporter DppBCDF functioning with 2 interchangeable periplasmic peptide/heme binding proteins, either DppA or MppA [4].

In the cytoplasm, iron is extracted through the action of heme-degrading enzymes that cleave the tetrapyrrol ring. For this purpose, some bacteria use orthologs of the mammalian heme oxygenases (HO). This class of enzymes degrades heme into biliverdin, carbon monoxide (CO) and iron [5]. Furthermore, non-HO homolog heme degrading enzymes have been reported for some Gram-positive and Gram-negative bacteria [6-8]. Although heme degradation by this class of weakly similar enzymes has been confirmed by CO production, the precise nature of the resulting products remains controversial [9].

However, genome BLAST searches fail to identify orthologs of any heme-degrading enzymes in many species including *Shigella dysenteriae*, *Salmonella typhi*, *E. coli* pathogenic strains, despite their ability to use heme as an iron source. This is also the case of the *E. coli* K12 laboratory strain expressing a foreign heme receptor.

In this study, we identified two *E.coli* paralogs, YfeX and EfeB without previously known cellular functions that surprisingly release iron from heme without tetrapyrrol degradation, a novel enzymatic reaction corresponding to the deferrochelation of the heme.

We demonstrate here the role of YfeX and EfeB in the recovery of exogenous heme iron.

Methods

Bacterial strains and plasmids

E. coli K12 strains FB8 (wild type, F⁻) and FB827 (*entF::Tn10*), MG1655, JP313 and C600 are from laboratory collections. Strains JW2424 (*yfeX::Km*) and JW1004 (*efeB::Km*) were obtained from the National BioResource Project (*E. coli* Hub) by means of the *E. coli* database “GenoBase” (<http://ecoli.aist-nara.ac.jp/>). *E. coli* O157:H7 EDL 933 was a gift of Dr. Le Bouguenec. pAM238 and pBAD24 are from the laboratory collection.

Media and growth conditions

Hemin (> 90%, pure), bovine hemoglobin (Hb) and 2,2'-dipyridyl (Dip) were obtained from Sigma. Protoporphyrin IX (PPIX), meso-heme and meso-protoporphyrin (MPPIX) were purchased from Frontier Scientific.

Bacteria were grown aerobically at 37°C in LB medium, in M63 or in M63 without added iron salt (M63*). All minimal media were supplemented with 0.4% glucose (glu) or glycerol (gly). For arabinose induction, 0.2% L-arabinose (ara) was added to induce the pBAD24 promoter. When required, Dip was added to a final concentration of 80 µM to M63*. Antibiotics were added at the usual concentrations for *E. coli*. Dip and ara inducer concentrations are not indicated in the text.

Growth promotion assays were done as described in ref [29].

Genetic and molecular biology techniques were done by standard methods

The double $\Delta yfeX\ efeB ::Km$ mutant was constructed by P1 transduction after $yfeX ::Km$ excision by specific recombination mediated by FLP recombinase encoded by the pCP20 plasmid. Verification of the Km cassette excision was done by PCR.

MG1655 chromosomal DNA fragments partially digested with *Sau3A* were ligated into pBAD24 plasmid and introduced into strain C600. The transformed cells were plated on LB Amp, Ara agar to induce the pBAD promoter. The plasmid DNA inserts conferring the screened phenotype were sequenced to identify the cloned gene.

Plasmid constructions

Plasmids carrying *efeB* from *E. coli* K12 and *efeUOB* from *E. coli* O157:H7 were constructed by amplification of MG1655 genomic DNA and *E. coli* O157:H7, respectively, using complementary oligonucleotides (sequences available on demand). Amplified fragments were inserted into pBAD24. In-phase *efeO* deletion was performed using the quick-change site-directed mutagenesis kit Stratagene with complementary oligonucleotides (sequences available on demand). Amplified mutant and wild type genes were checked by DNA sequencing.

The NdeI-XhoI 700 bp DNA fragment carrying the *P. aeruginosa pigA* gene in PET21 plasmid was purified and cloned into pBAD 24 digested with XbaI-SalI.

Membrane and soluble fraction preparations

Cultures of JP313 (pBAD24-*yfeX*) and JP313 (pBAD24-*efeB*) were grown overnight at 30°C in M63 Gly Ara medium. Cells were harvested by centrifugation for 15 minutes at 8 000 x g at 4°C. Each cell pellet was resuspended in Bug Buster buffer (Novagen) for a concentration of 1 g of bacterial dry weight in 5mL of buffer (100 OD₆₀₀/ml). The mixtures were incubated 30 minutes at room temperature to lyse the cells and centrifuged again for 10 min at 10 000 x g at 4°C. Supernatants contained the soluble fractions (cytoplasm + periplasm), and the pellet

contained all membranes. The soluble fractions were dialyzed overnight against 50 mM Tris·HCl, pH8, at 4°C.

Porphyrin extraction procedure, HPLC separation and mass determination by mass spectrometry

Quantitative extraction of porphyrins from soluble fractions, membrane pellets and whole cell pellets was achieved by adding 300 µl of extraction solvent (ethanol/DMSO/acetic acid; 80/20/1; v/v/v) to 200 µl of soluble fraction and 1 ml of extraction solvent to the membrane, respectively. Samples were subjected to 5 sonication cycles of 5 seconds at 0°C, amplitude 10% using a sonicator probe (Branson Digital Sonifier). The samples were subsequently centrifuged at 12 500 x g for 5 minutes and the porphyrin containing supernatant was used for subsequent HPLC analysis. Re-extraction of the samples was performed until no further fluorescence of the extract could be observed under UV light (excitation wavelength: 405 nm, lamp: Karl Storz endoscope).

Porphyrin separation was achieved as described before [10] and detailed procedures are given in the legend of Fig. S2.

YfeX and EfeB activities in soluble fractions

Time course studies of PPIX formation were performed with 200 µL samples of soluble fractions of JP313 (pBAD24-yfeX), JP313 (pBAD24-efeB) JP313 (pBAD24) cell cultures resuspended for an OD₆₀₀ of 20. Reactions were initiated by the addition of either 50 µM hemin or meso-heme, or buffer alone to the samples and incubation at room temperature. At times t = 0, t = 5 min, t = 10 min, t = 20 min, t = 30 min, t = 60 min, total porphyrins in the samples were extracted by the addition of 300 µl of extraction solvent (ethanol/DMSO/acetic acid; 80/20/1; v/v/v) and analyzed by HPLC.

YfeX purification

A 1 ml sample of C600 (pBAD24-yfeX) soluble fraction was incubated with hemin 50 μM or without hemin at room temperature for 30 min. After centrifugation for 5 min at 10 000 $\times g$ to discard aggregates, the mixtures were loaded on anion exchange chromatography (mono Q) pre-equilibrated with 50 mM Tris-HCl pH 8. Elution was performed with a 0 to 1 M NaCl gradient in the same buffer. Fractions were collected and their YfeX content and purity evaluated by SDS-PAGE. Purified YfeX with an apparent molecular weight of 33 kDa was eluted into 2 fractions with different UV/visible absorption spectra. One fraction had only a 280 nm protein absorption peak which corresponded to apo-YfeX. The N-terminal amino acid sequence was determined by the « Plateforme d'Analyse et de Microséquence des Protéines » of the Institut Pasteur. It corresponded to the N-terminus of YfeX: SQVQSG. Apo-YfeX was used in the binding experiments. YfeX_{H215A} was purified following the same protocol.

YfeX binding studies

PPIX and hemin binding studies were carried out at room temperature. ApoYfeX was in Tris-HCl 50 mM pH 8. Concentration was evaluated from absorbance at 277 nm with a calculated $\epsilon = 32,500 \text{ M}^{-1} \text{ cm}^{-1}$. Apo-YfeX was diluted to 1 μM , a concentration which gives a measurable signal. Hemin and PPIX solutions were diluted in Tris-HCl 50 mM pH 8 for a 20 μM final. Aliquots of 1 to 5 μl of either hemin or PPIX were successively added to cell containing 1 ml of the apoprotein. This corresponds to PPIX or hemin range of final concentrations from 100 nM up to 1.5 μM for hemin and 100 nM up to 2.5 μM for PPIX. Absorption spectra were recorded 5 minutes after each hemin or PPIX addition in a 0.2-1 cm path length cells on a Beckman DU 800 spectrophotometer and were followed by measuring the absorbance from 250 nm to 700 nm. Absorbances at the Soret bands (404 nm for hemin and 407 nm for PPIX) were reported as a function of hemin and protoporphyrin IX concentration, corrected for the absorbance of free heme and PPIX.

To determine the K_d for hemin and PPIX, titration curves could be fitted according to a one-site binding model using FitP software. Heme and PPIX binding to apo-YfeX were done following the same protocol.

Results

Isolation of E. coli genes potentially involved in heme degradation

E. coli features no orthologs of known heme-degrading enzymes. Yet *E. coli* K12 expressing a heterologous heme outer membrane receptor such as the *S. marcescens* HasR receptor, in combination with its native heme/ dipeptide inner membrane permease DppABCDF, is able to use exogenous heme as an iron source. We therefore hypothesized that it might be equipped with enzyme(s) displaying iron capturing activity. We developed a screening method based on the fluorescence properties of heme metabolites in order to find such enzymes [11, 12]. A strain expressing *P. aeruginosa* heme oxygenase (PigA) was used as a positive control. C600 (pBAD24-PigA) colonies could be easily distinguished from colonies carrying the empty vector pBAD24 on LB ara plates by their color and by their fluorescence under near-UV light irradiation (405 nm). A genomic library of *E. coli* K12 MG1655 in pBAD24 was screened for its ability to confer such a phenotype upon strain C600 on LB Ara plates. Out of the 100,000 clones screened, one recombinant plasmid, carrying the *yfeX* gene was responsible for a bright red fluorescent colony phenotype. YfeX is a protein of unknown function belonging to the family of dye-decolorizing peroxidases (Dyp-peroxidase) identified in fungi [13]. *E. coli* has another protein belonging to the Dyp family, EfeB [14]. Both proteins, YfeX and EfeB share only a low level of sequence similarity and are thus distantly related paralogs. The *E. coli* K12 MG1655 *efeB* gene was cloned into pBAD24. Strain C600 (pBAD24-efeB) also gave rise to fluorescent colonies upon arabinose induction. Additionally, bacterial cell cultures expressing either PigA, YfeX or EfeB showed differing colours under visible light. The strain expressing PigA was dark green, whereas strains expressing either YfeX or EfeB were coloured red (supporting information (SI) Fig. S1). The fluorescence as well as the red color is characteristic of strains accumulating porphyrins.

The major fluorescent compound produced by strains overexpressing YfeX or EfeB is protoporphyrin IX (PPIX)

To determine the chemical nature of compounds accumulated by strains overexpressing either YfeX or EfeB, intracellular porphyrins of cell soluble fractions of these strains incubated without addition of exogenous hemin were extracted and separated by fluorescence-based HPLC. Using naturally occurring porphyrins as standards, the main peak of the cell extracts

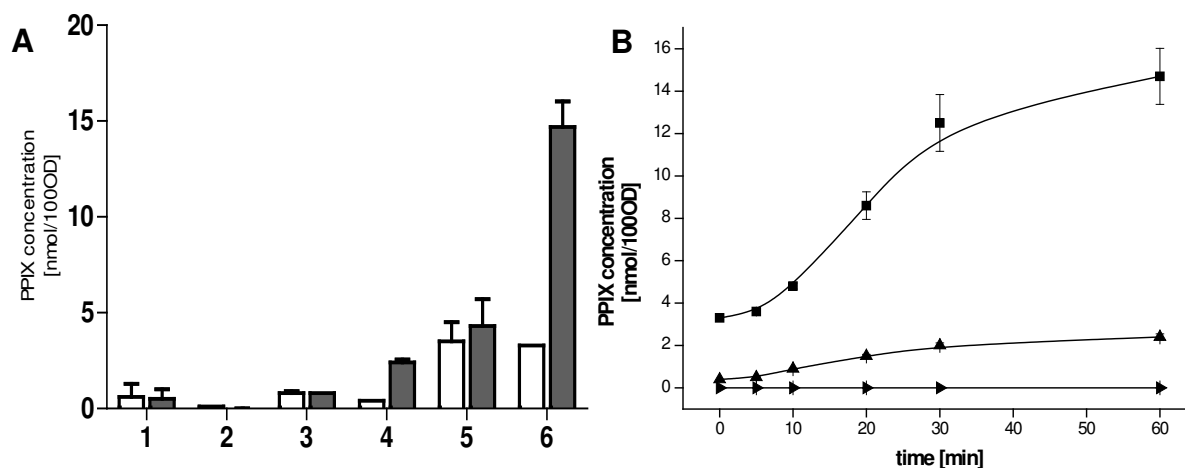


Fig. 1. PPIX concentrations in cell soluble fractions incubated with and without hemin. Soluble fractions of JP313 carrying pBAD24 (empty vector), pBAD24-yfeX, pBAD24-efeB cultures were prepared as described in Methods. Porphyrin concentrations were normalized to represent the porphyrin amount in cell lysates corresponding to a bacterial suspension with an optical density of 100 at 600 nm (OD₆₀₀ 100). A: PPIX concentrations in cell lysates incubated at room temperature for 0 min (white bars) and 60 min (grey bars) without or with addition of hemin at a final concentration of 50 μ M. (1) JP313 (pBAD24) incubation without added hemin, (2) JP313 (pBAD24) incubation with added hemin; (3) JP313 (pBAD24-efeB) incubation without added hemin; (4) JP313 (pBAD24-efeB) incubation with added hemin; (5) JP313 (pBAD24-yfeX) incubation without added hemin; (6) JP313 (pBAD24-yfeX) incubation with added hemin. B: Time dependent PPIX formation in the same cell lysates as in A, after incubation with added hemin (50 μ M). PPIX concentration was measured over time with the starting point at hemin addition to cell soluble fraction of the following strains: JP313 (pBAD24) (►), JP313 (pBAD24-efeB) (▲) and JP313 (pBAD24-yfeX) (■). The data points represent the means of duplicate experiments and the error bars represent the standard deviation.

eluted at the same time as PPIX. Mass spectrometry confirmed that the chemical nature of this compound was PPIX (Fig. S2 A and B). Both strains contained large amounts of PPIX (3 and 10 times higher than the control strain, respectively) (Fig. 1A, lanes 1, 3, 5). Besides a very low level of coproporphyrin (COP) III, no other pigments including biliverdin were found neither in pellets nor soluble fractions of cells overexpressing YfeX or EfeB. Thus, strains

overproducing either YfeX or EfeB accumulated PPIX, which was presumably formed from intracellular heme.

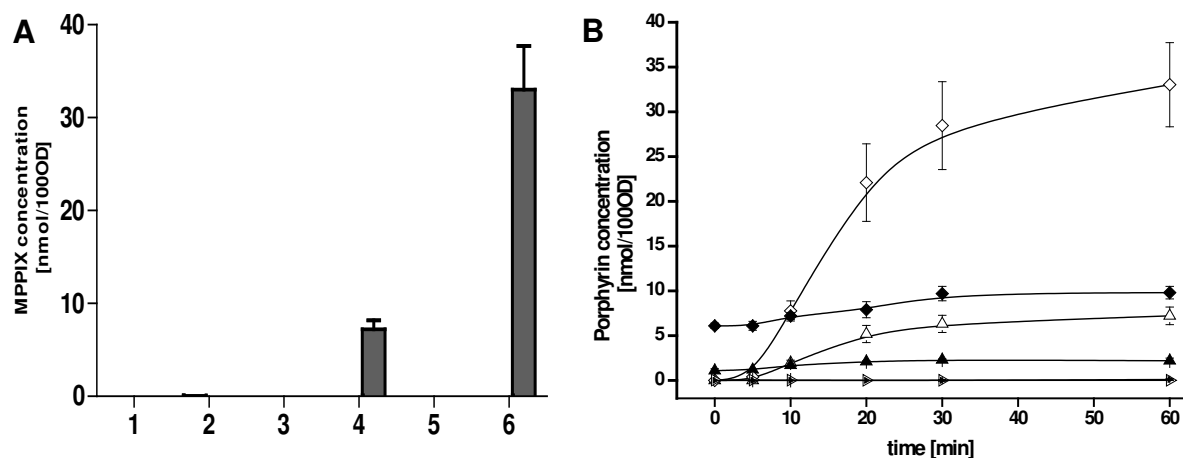


Fig. 2. PPIX and MPPIX concentration in cell soluble fractions incubated with and without meso-heme. The procedures are the same as in Fig. 1. A: MPPIX concentrations in cell lysates incubated at room temperature for 0 min (white bars) and 60 min (grey bars) without or with meso-heme addition at a final concentration of 50 μ M. (1) JP313 (pBAD24) incubation without meso-heme; (2) JP313 (pBAD24) incubation with meso-heme; (3) JP313 (pBAD24-efeB) incubation without meso-heme; (4) JP313 (pBAD24-efeB) incubation with meso-heme; (5) JP313 (pBAD24-yfeX) incubation without meso-heme; (6) JP313 (pBAD24-yfeX) incubation with meso-heme. No MPPIX was detected at $t=0$ in either of the samples. B: MPPIX and PPIX production as a function of time in the same cell lysates as in A, after meso-heme (50 μ M) addition. PPIX (solid symbols) and MPPIX (open symbols). Concentrations were measured over time with the starting point at meso-heme addition to cell soluble fractions of the following strains: JP313 (pBAD24) (\blacktriangleright), JP313 (pBAD24-efeB) (\blacktriangle) and JP313 (pBAD24-yfeX) (\blacksquare). The data points represent the mean and the error bars represent the standard deviation.

Exogenous heme and meso-heme are converted to PPIX and meso-PPIX (MPPIX) by cell lysates producing YfeX or EfeB

We hypothesized that PPIX could also be formed from exogenous heme upon the action of either YfeX or EfeB. To test this, exogenous hemin (50 μ M) was added to soluble cell

fractions and incubated for 60 minutes. PPIX concentration increased over the incubation time only in extracts from YfeX or EfeB overproducing cells (Fig. 1A lane 2, 4, 6). The respective PPIX accumulation time profiles show a steady increase of PPIX during the first 30 minutes of incubation and a plateau (Fig. 1B) for longer incubation times. This strongly suggests that exogenous heme was transformed into PPIX under the action of these 2 proteins.

To further demonstrate that YfeX and EfeB have an effect on PPIX formation from exogenous sources, we used a nonnaturally occurring heme, meso-heme, as substrate that is not produced by bacterial heme biosynthesis [15]. Standard PPIX and meso-PPIX (MPPIX) could be separated by fluorescence-based HPLC (Fig. S3 A-C). Meso-heme (50 μ M) or buffer was added at room temperature to soluble cell fractions of the control strain or strains overproducing YfeX and EfeB, respectively, and accumulation of MPPIX and PPIX was monitored as a function of time after extraction from cell lysates and separation by fluorescence based HPLC (Fig. S3D). No detectable amount of MPPIX was found in the absence of meso-heme as substrate, confirming that MPPIX is not a natural byproduct of the heme biosynthesis (Fig. 2A, lane 1, 3, 5). However, in the presence of meso-heme, in soluble cell fractions of strains expressing either YfeX or EfeB but not of the control strain (Fig. 2A, lanes 2, 4, 6), a steadily increasing accumulation of MPPIX over 30 minutes of incubation passing into a plateau was observed thereafter (Fig. 2B). At the plateau, 8 to 30 times more MPPIX accumulated in strains overexpressing EfeB and YfeX, respectively, than in the control strain (Fig. 2B). We also measured PPIX accumulation in the cell lysates incubated with meso-heme (Fig. 2B). PPIX as well as COPIII levels remained unchanged upon addition of meso-heme, indicating that meso-heme does not impair the natural heme biosynthetic pathway. Thus YfeX and EfeB are involved in the conversion of exogenous heme into PPIX and are expected to bind heme and PPIX. We tested this hypothesis on purified YfeX.

YfeX binds heme and PPIX in vitro

Addition of PPIX or hemin to purified apo-YfeX (Fig. S4) led to different Soret band at 407 nm for PPIX and 404 nm for hemin and very distinctive features in the 450-800 nm part of the spectra. (Fig. S5 A and B). Hemin and PPIX affinities to apo-YfeX (1 μ M) were measured by monitoring the Soret bands with absorption spectroscopy. Titration curves shown in Fig. SA and B indicate that YfeX interacts with both, hemin and PPIX at a molar ratio of 1 and

with a K_d of 3.9 ± 1.6 nM for hemin and of 4.8 ± 2.8 nM for PPIX. Unexpectedly, the saturation curve presents a slightly sigmoidal shape for PPIX titration that might indicate a cooperative effect that was not further investigated.

PPIX loaded YfeX was incubated with an excess of heme for 2 h. After elimination of unbound tetrapyrroles, UV-visible spectra showed a hemin loaded profile, demonstrating that hemin displaced PPIX from YfeX (Fig. S5C).

Dyp peroxidase structural and sequence comparisons have revealed the conservation of the residues surrounding heme, including the histidine axial iron ligand [13]. Structure modeling of YfeX identified H215 as the corresponding iron binding histidine residue in YfeX (Fig. S7). After mutation to alanine, intracellular porphyrins of the cell soluble fraction of the strain overexpressing YfeX_{H215} were extracted and analyzed as described above. The observed basal porphyrin level was similar to that of the control strain carrying the empty vector (Fig. S2C). Subsequently, the YfeX_{H215A} mutant protein was produced in amounts similar to the wild type protein. It was stable and purified according to the protocol for wild type YfeX (Fig. S4). As expected, the affinity for hemin was strongly reduced and more surprisingly, PPIX binding as well with a K_d higher than 10^{-5} M (data not shown), suggesting that heme and PPIX at least partially share a common ligand pocket.

YfeX is loaded with PPIX in vivo

In addition to the apo-YfeX fraction used in the experiments described above, we were able to collect a second YfeX containing fraction during YfeX purification that exhibited an absorption peak at 407 nm. YfeX containing fractions were purified from cell lysates incubated with or without hemin for 30 minutes at room temperature. After incubation with hemin, the apoprotein fraction decreased with a concomitant increase of the fluorescent fraction. HPLC separation of the pigments bound to the YfeX fluorescent fraction showed that YfeX was loaded with PPIX (Fig. 3). These results indicate that PPIX produced from hemin through the action of YfeX partly remains bound to YfeX.

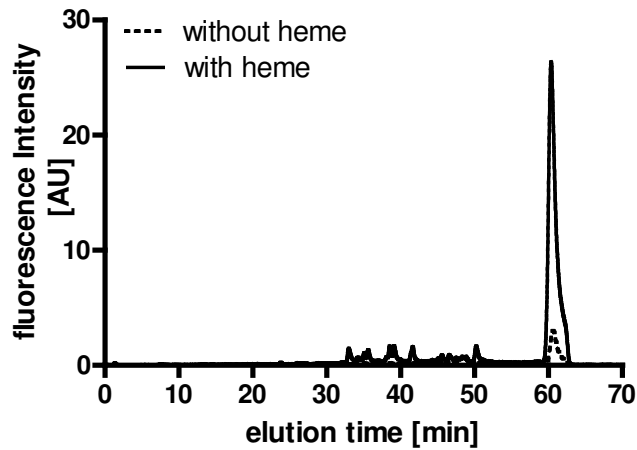


Fig. 3. PPIX binding to YfeX *in vivo*. The fluorescent YfeX fraction was purified from C600 (pBAD 24-yfeX) cell lysates incubated with and without hemin (50 μ M) for 30 minutes at room temperature by anion exchange chromatography and exhibited an absorption peak at 406 nm. Pigments bound to the pure protein were extracted, separated by HPLC and identified as described in the legend of Fig. S2. The peak at 60.3 minutes corresponds to PPIX. The dotted line corresponds to purification cell lysate without added hemin. The solid line corresponds to purification of cell lysate with added hemin.

YfeX and EfeB are required for exogenous heme iron acquisition

Taken together, our *in vitro* results indicate that YfeX and EfeB are PPIX and heme binding proteins and that they are involved in the heme transformation into PPIX. To test whether the activity is related to the use of exogenous heme as an iron source, the *yfeX* and *efeB* genes replaced by a Km cassette were transduced into strain FB827 (pAM238-hasR). This strain lacks enterobactin, the major *E. coli* siderophore, and owing to HasR is able to acquire exogenous heme. The strains were tested for growth on minimal iron chelated plates (M63* Gly Ara Dip) around wells containing various hemoglobin concentrations. Both FB827 *yfeX*::Km (pAM238-hasR) and FB827 *efeB*::Km (pAM238-hasR) grew less efficiently than the wild type strain around the hemoglobin-containing wells: significant growth was only observed around wells containing 50 μ M hemoglobin, whereas the wild type FB827 (pAM238-hasR) strain still formed a significant growth halo around wells containing a fifty-times-lower hemoglobin concentration of 1 μ M (Table 1 and Fig. S8). The double mutant FB827 Δ *yfeX efeB*::Km (pAM238-hasR) was unable to grow around the hemoglobin-containing wells at any tested concentration (Table 1). This demonstrates that the 2 proteins

are the sole proteins able to retrieve iron from heme. It also suggests that the 2 YfeX and EfeB paralogs fulfill similar functions in heme iron utilization.

YfeX and EfeB can complement each other and both are complemented by the P. aeruginosa heme oxygenase PigA

To test whether *yfeX* and *efeB* can complement each other, FB827 (pAM238-hasR) carrying either *yfeX* or *efeB* mutations was transformed with either pBAD24-*yfeX* or pBAD24-*efeB*. Each mutant having a defect in heme iron acquisition, this was fully complemented by overexpressing the corresponding wild type allele or the wild type paralog (Table 1). This intergenic complementation demonstrated that the 2 genes *yfeX* and *efeB* have at least partially redundant functions. The pBAD24-*yfeX*_{H215A} expressing the mutated YfeX protein affected in heme and PPIX binding did not complement the *yfeX* mutation (Table 1). Addition of iron instead of hemoglobin (FeCl₃ or FeSO₄ 0.1 mM) to the wells restored growth of all 3 mutants (the 2 single and the double *yfeX efeB* ::Km) (data not shown).

Expression of (pBAD24-PigA) in FB827 *yfeX* ::Km (pAM238-hasR) and FB827 *efeB* ::Km (pAM238-hasR) mutants fully restored the ability of the strain to grow around hemoglobin-containing wells (Table 1). The complementation for heme-iron use by a gene encoding heme oxygenase strongly suggests that YfeX and EfeB are involved in intracellular iron release from heme.

Inactivation of Dpp permease abolishes heme iron acquisition in the E. coli K12 strain overexpressing either YfeX or EfeB

EfeB is exported to the periplasm via the twin arginine translocation system (TAT) [14]. The periplasmic localization of EfeB suggests that it could retrieve iron from heme in that cellular compartment. Periplasmic iron released from heme would be picked up by inner membrane iron transporters such as Feo or Fec [16]. However, we have shown previously that Dpp permease is essential for heme iron transport, suggesting that only cytoplasmic heme can provide iron [4]. Nevertheless, this was not done in conditions of overexpression of YfeX or EfeB. To address this question, FB827 *dppF*::Km (pAM238-hasR) was transformed with either pBAD24-*yfeX* or pBAD24-*efeB*. Overproduction of these proteins failed to restore

wild type growth on M63* Gly Ara Dip plates around wells containing hemoglobin (Table 1). Thus, in *E. coli* K12, despite a periplasmic localization of EfeB, only cytoplasmic heme was able to provide iron, suggesting that EfeB is at least partly active in the cytoplasm.

Tab. 1. yfeX and efeB role in heme-iron acquisition. The relevant chromosomal mutations carried by strain FB827 (pAM-hasR) and the plasmid-borne complementing genes carried on pBAD 24 are indicated in the first column. Cultures of strain FB827 (pAM 238-hasR) carrying the various mutations and plasmids were grown in M63 Gly media at 37°C to an OD₆₀₀ of 1, and 100 µl aliquots were mixed with 3.5 ml of M63 soft agar 0.7% and poured onto M63* Dip plates containing 100 µM Dip to chelate any residual iron and 0.02% L-arabinose to induce the pBAD24-encoded genes. Aliquots of 50 µl of bovine hemoglobin at various concentrations were provided in wells punched in the solidified agar. Plates were incubated for 48h at 37°C and the growth halo radius around the wells was measured. All experiments were reproduced 3 times. The second column indicates the various strain growth around wells containing various Hb concentrations. The plates were incubated 48 h at 37°C, and the radius of the growth around wells was measured. +++, radius of 10 mm; ++, radius of 6 mm; +, radius of 2 mm; -, no growth around the wells. All experiments were repeated 3 times.*

Strain FB827 (pAM-hasR) carrying the relevant mutation and/ or plasmids	Growth on M63* Dip around wells containing Hb (mM):			
	50	10	5	1
none	+++	++	+	+
<i>yfeX</i> ::Km	+	+/-	-	-
<i>efeB</i> ::Km	+	+/-	-	-
<i>D yfeX efeB</i> ::Km	-	-	-	-
<i>yfeX</i> ::Km pBAD 24- <i>yfeX</i>	+++	++	+	+
<i>yfeX</i> ::Km pBAD 24- <i>efeB</i>	+++	++	+	+
<i>yfeX</i> ::Km pBAD 24- <i>pigA</i>	+++	++	+	+
<i>efeB</i> ::Km pBAD 24- <i>efeB</i>	+++	++	+	+
<i>efeB</i> ::Km pBAD 24- <i>yfeX</i>	+++	++	+	+
<i>efeB</i> ::Km pBAD 24- <i>pigA</i>	+++	++	+	+
<i>dppF</i> ::Km pBAD 24	-	-	-	-
<i>dppF</i> ::Km pBAD 24- <i>efeB</i>	-	-	-	-
<i>dppF</i> ::Km pBAD 24- <i>yfeX</i>	-	-	-	-
<i>dppF</i> ::Km pBAD24- <i>efeUOB</i> _{O157:H7}	+++	++	+	+
<i>dppF</i> ::Km pBAD24- <i>efeUB</i> _{O157:H7}	-	-	-	-

The efeUOB operon of E. coli O157:H7 allows heme iron acquisition in the dppF mutant

efeB belongs to the iron-regulated *efeUOB* operon involved in Fe²⁺ uptake under acidic conditions [17]. EfeU is homologous to the yeast high affinity iron permease Frtp1 [17, 18]. This iron uptake system is defective in *E. coli* K12 due to a frameshift mutation interrupting the *efeU* reading frame after amino acid 37 [18]. Unlike *E. coli* K12, many other *E. coli* strains, such as enterohemorrhagic O157:H7, have an intact *efeU* sequence and their *efeUOB* genes expressed in *E. coli* K12 stimulate iron uptake. All 3 genes were also shown to be necessary for Fe²⁺ uptake [17]. We tested whether expression of a non-mutated *efeUOB* operon would allow heme-iron acquisition from the periplasm, i.e. in the absence of the Dpp permease. *efeUOB* genes of *E. coli* O157:H7 were amplified and cloned into pBAD24. While FB827 *dppF::Km* (pAM238-hasR) (pBAD24) could not grow around the hemoglobin-containing wells (Table 1), FB827 *dppF::Km* (pAM238-hasR) (pBAD24-*efeUOB*_{O157:H7}) was able to use heme iron as well as the wild type strain. Thus, O157:H7 *efeUOB* genes were epistatic over the *dppF* mutation for heme-iron utilization. The in-frame deletion of *efeO* was constructed and the corresponding plasmid was tested for heme-iron acquisition. FB827 *dppF::Km* (pAM238-hasR) (pBAD24-*efeUB*_{O157:H7}) could not grow around the hemoglobin-containing wells (Table 1). These results indicate that iron can be extracted from heme in the periplasm by EfeB and that EfeU and EfeO proteins are required for iron internalization.

Discussion

To identify new bacterial proteins involved in iron extraction from heme, we developed a screening method based on the fluorescent properties of tetrapyrrol molecules lacking their iron. We succeeded in finding 2 such *E. coli* paralogs, YfeX and EfeB. Either protein, when overexpressed, promotes the accumulation of PPIX, an intermediate in the heme biosynthetic pathway. This could be the result of a higher heme biosynthetic activity due to a reduced intracellular heme pool [19, 20]. To challenge this hypothesis, YfeX and EfeB activities were tested with meso-heme, a non-natural porphyrin. Exogenously added meso-heme is converted into meso-PPIX by YfeX or EfeB producing cell extracts. Thus, unambiguously, the increased PPIX pool is issued from the YfeX and EfeB activities on the exogenous heme. YfeX binds both heme and PPIX with a stoichiometry of one for each and with comparable affinities for heme and for PPIX. We found a displacement of PPIX by heme, suggesting that

they bind to the same or overlapping sites. Moreover, the effect of the YfeX H215A mutation on both heme and PPIX affinities for YfeX also indicates that PPIX and heme share a common binding site. Spectroscopic analysis of pigments which are *in vivo* bound to YfeX before purification showed that part of the protein is loaded with PPIX and that incubation with heme strongly increases the PPIX loaded protein.

Although YfeX is involved in heme conversion into PPIX in cell lysates, the conversion of heme into PPIX was not observed with purified YfeX protein. It is likely that the reaction requires a cofactor which is not present on the purified protein.

Our genetic data on the *E. coli* K12 strain, which has been made competent for heme uptake by the expression of the heme outer membrane HasR, show experimental evidence that the *yfeX*, *efeB* double mutant is unable to use heme as an external iron source and thus unquestionably establish that YfeX and EfeB are the sole proteins that can provide heme-iron to *E. coli* K12. Each single *yfeX* or *efeB* gene deletion mutant has a partial defect in using heme as an exogenous iron source, indicating that the corresponding proteins have limiting activities when chromosomally encoded and that they might have complementary functions. In addition, when plasmid encoded, YfeX and EfeB fully complement the deletion of the other gene. Thus, YfeX and EfeB have at least partially redundant functions and can function independently from each other.

YfeX is cytoplasmic, whereas EfeB which has a double arginine signal peptide is exported to the periplasm [14]. How can proteins that belong to different cellular compartments complement each other? One reason for such complementation could be that iron produced in the periplasm by EfeB is transported to the cytoplasm by an inner membrane iron transporter. This is not the case in *E. coli* K12, because inactivation of the DppABCDF heme permease prevents heme iron acquisition showing that only cytoplasmic heme is an iron source. As a matter of fact, the aerobic iron permease EfeU, encoded by the *efeUOB* operon is nonfunctional in *E. coli* K12 owing to a frame shift mutation. Unlike *E. coli* K12, many other *E. coli* strains, such as the enterohemorrhagic O157:H7, have an intact *efeU* sequence [17]. When the complete *efeUOB* operon of *E. coli* O157:H7 is provided to *E. coli* K12, it allows heme iron acquisition from the periplasm, i.e. in the absence of the DppABCDF heme permease. All 3 genes are necessary for heme iron acquisition in the absence of the heme permease. Consistent with its role in providing iron from heme, the *efeUOB* operon is induced in iron restricted conditions and is not cryptic in *E. coli* strains having heme receptor genes.

To explain the EfeB activity in *E. coli* K12 in the absence of iron transport, it is more likely that some EfeB is active in the cytoplasm. EfeB is translocated by the TAT system, a pathway dedicated to prefolded proteins, some of which carrying a cofactor. EfeB binds heme in the cytoplasm and the mature heme loaded protein is detected in the cytoplasm [14]. This cytoplasmic form is likely to be active in heme-iron extraction.

Taken together, our data indicate that YfeX and EfeB are capable of extracting iron from heme while preserving the protoporphyrin ring intact, an enzymatic reaction which has not been previously described and which corresponds to a demetallation of heme. In some cases, ferrochelatases from meat [21] and from *Haemophilus influenzae* [22] have been shown to catalyze the reverse reaction *in vitro* in the presence of reductants. However, YfeX and EfeB do not have significant sequence similarities to any known ferrochelatase and thus most likely have evolved separately to achieve the reaction by a mechanism distinct from ferrochelatases. The new enzymatic activity described here is referred to as deferrochelation activity.

YfeX and EfeB belong to the Dyp peroxidase family which differ from other peroxidases in their fold and their heme ligands. Many hemoproteins including hemoglobin have been shown to have peroxidase activity in the presence of peroxide [23]. This *in vitro* peroxidase activity of the Dyp proteins may not correspond to their physiological activity. The molecular mechanism allowing iron extraction from heme is presently unknown. Spontaneously, iron is removed from heme by treatment with HCl [24]. The enzymatic reaction could involve a distortion of the tetrapyrrol ring, as it is achieved by ferrochelatase during metal insertion [25]. However, in the heme-TyrA structure (a YfeX ortholog), the protoporphyrin ring is plane [26].

YfeX and EfeB proteins are widespread and highly conserved in Gram-positive and Gram-negative bacteria. We propose that deferrochelation activity represents their physiological function, enabling heme-iron acquisition without heme internalization in the case of EfeB orthologs and without production of CO, an antibacterial gas.

On the other hand, the 2 proteins are absent in higher eukaryotic organisms, making them potential targets for new antibacterial drugs, especially since there is growing evidence that heme utilization systems are required for bacterial virulence.

Acknowledgements

We thank Dr Daniel Béal IBPC for precious advices in fluorescence colony screening under near-UV light, Dr Chantal Le Bouguennec and Dr Alain Chaffotte for strains and helpful discussions and Dr Simon Andrews for constructive advice. Furthermore, we thank Dr Karine Ndjoko Ioset and Dr Jean Luc Wolfender for their valuable help with the HPLC-MS analysis. We are grateful to Dr Elie Dassa for careful reading of the manuscript.

Reference List

1. Wandersman C, Delepelaire P. Bacterial iron sources: from siderophores to hemophores. *Annu Rev Microbiol* 2004; **58**: 611–47.
2. Cescau S, Cwerman H, Létoffé S et al. Heme acquisition by hemophores. *Biometals* 2007; **20**: 603-13.
3. Reniere M, Torres V, Skaar E. Intracellular metalloporphyrin metabolism in *Staphylococcus aureus*. *Biometals* 2007; **3-4**: 333-45.
4. Létoffé S, Delepelaire P, Wandersman C. The housekeeping dipeptide permease is the *Escherichia coli* heme transporter and functions with two optional peptide binding proteins. *Proc Natl Acad Sci U S A* 2006; **103**: 12891-6.
5. Frankenberg-Dinkel N. Bacterial heme oxygenases. *Antioxid Redox Signal* 2004; **5**: 825-34.
6. Skaar E, Gaspar A, Schneewind O. *Bacillus anthracis* IsdG, a heme-degrading monooxygenase. *J Bacteriol* 2006; **188**: 1071-80.
7. Puri S, O'Brian M. The hmuQ and hmuD genes from *Bradyrhizobium japonicum* encode heme-degrading enzymes. *J Bacteriol* 2006; **188**: 6476-82. .
8. Wu R, Skaar E, Zhang R et al. *Staphylococcus aureus* IsdG and IsdI, heme-degrading enzymes with structural similarity to monooxygenases. *J Biol Chem* 2005; **280**: 2840-6.
9. Lee W, Reniere M, Skaar E, Murphy M. Ruffling of metalloporphyrins bound to IsdG and IsdI, two heme degrading enzymes in *Staphylococcus aureus*. *J Biol Chem* 2008; **283**: 30957-63.
10. Fotinos N, Convert M, Piffaretti J et al. Effects on gram-negative and gram-positive bacteria mediated by 5-aminolevulinic acid and 5-aminolevulinic acid derivatives. *Antimicrob Agents Chemother* 2008; **52**: 1366-673.
11. Wilks A, Ortiz de Montellano P, Rabsch W. Rat liver heme oxygenase. High level expression of a truncated soluble form and nature of the meso-hydroxylating species. *J Biol Chem* 1993; **268**: 22357-62.

12. Frustaci J, O'Brian M. Characterization of a Bradyrhizobium japonicum ferrochelatase mutant and isolation of the hemH gene. *J Bacteriol* 1992; **174**: 4223-9.
13. Sugano Y. DyP-type peroxidases comprise a novel heme peroxidase family. *Cell Mol Life Sci* 2008; **PMID: 19099183** 1-13.
14. Sturm A, Schierhorn A, Lindenstrauss U et al. YcdB from Escherichia coli reveals a novel class of Tat-dependently translocated hemoproteins. *J Biol Chem* 2006; **281**: 13972-13978.
15. Perttila U, G. S. The heme environment of leghemoglobin. Absorption and circular dichroism spectra of artificial leghemoglobins and myoglobins. *BBA* 1980; **624**: 316-28.
16. Koster W. Cytoplasmic membrane iron permease systems in the bacterial cell envelope. *Front Biosci* 2005 **10**: 462-77.
17. Cao J, Woodhall M, Alvarez J et al. EfeUOB (YcdNOB) is a tripartite, acid-induced and CpxAR-regulated, low-pH Fe²⁺ transporter that is cryptic in Escherichia coli K-12 but functional in E. coli O157:H7. *Mol Microbiol* 2007; **65**: 857-75.
18. Grosse C, Scherer J, Koch D et al. A new ferrous iron-uptake transporter, EfeU (YcdN), from Escherichia coli. *Mol Microbiol* 2006; **62**: 120-31.
19. Woodard S, Dailey H. Regulation of heme biosynthesis in Escherichia coli. *Arch Biochem Biophys* 1995 **316**: 110-5.
20. Verderber E, Lucast LJ, Van Dehy JA et al. Role of the hemA gene product and delta-aminolevulinic acid in regulation of Escherichia coli heme synthesis. *J Bacteriol* 1997; **179**: 4583-90.
21. Taketani S, Ishigaki M, Mizutani A et al. Heme Synthase (Ferrochelatase) Catalyzes the Removal of Iron from Heme and Demetalation of Metalloporphyrins. *Biochemistry*, 2007; **46** 15054 -61.
22. Loeb M. Ferrochelatase activity and protoporphyrin IX utilization in Haemophilus influenzae. *J Bacteriol* 1995; **177**: 3613-5.
23. Cooper C, Silaghi-Dumitrescu R, Rukengwa M et al. Peroxidase activity of hemoglobin towards ascorbate and urate: A synergistic protective strategy against toxicity of Hemoglobin-Based Oxygen Carriers (HBOC). *Biochim Biophys Acta* 2008; **1784**: 1415-20.
24. Dawson RMC, DC. E, Elliott W, Jones K. Data for Biochemical Research. 1986; **Oxford: Clarendon Press**
25. Karlberg T, Hansson M, Yengo R et al. Porphyrin binding and distortion and substrate specificity in the ferrochelatase reaction: the role of active site residues. *J Mol Biol* 2008; **378**: 1074-83.

26. Zubieta C, Joseph R, Krishna S et al. Identification and structural characterization of heme binding in a novel dye-decolorizing peroxidase, TyrA. *Proteins* 2007; **69**: 234-43.

Supplementary Figures

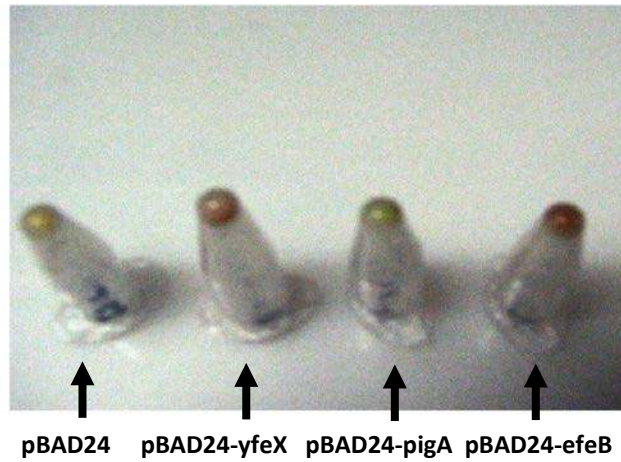


Fig. S1. Cell pellet coloration of strains JP313 carrying the indicated plasmids. JP313 cells carrying the indicated plasmids were grown overnight at 37°C in LB Ara and were harvested by centrifugation. Cells were photographed under visible light.

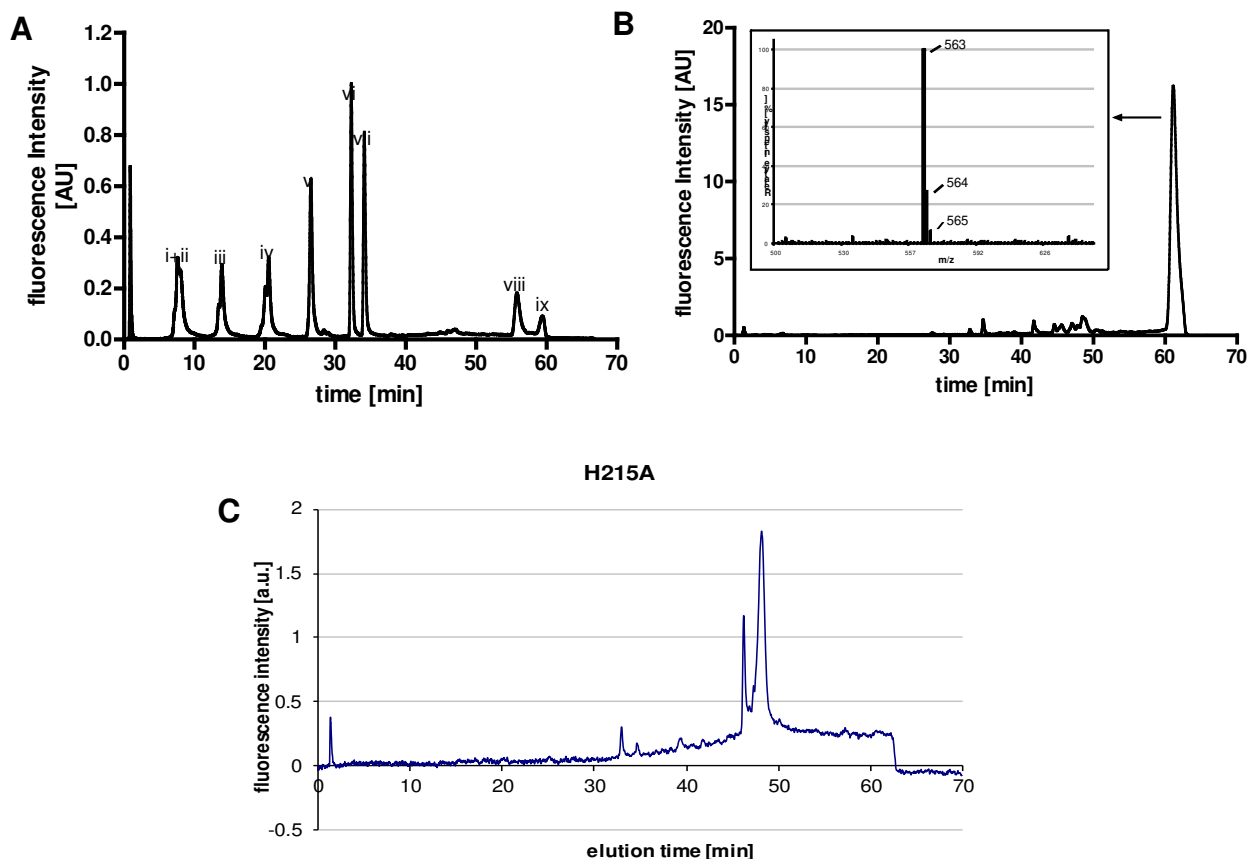


Fig. S2. Fluorescence spectroscopy chromatograms of porphyrins and PPIX chemical nature confirmed by mass spectrometry. Porphyrin separation was achieved with a 125/4 Nucleodur C18 gravity 3 μm column (Macherey-Nagel) and a corresponding pre-column using a LaChrom chromatographic system (Merck). An elution gradient was run over 70 min with solvent A (acetate buffer pH5.1, 0.5 M/acetonitrile; 90:10; v/v) and solvent B (methanol/acetonitrile; 90:10; v/v). The flow rate was 1 ml/min. Porphyrins were detected at an excitation wavelength of 405 nm and emission wavelength of 620 nm by means of a LaChrom L-7480 fluorescence detector (Merck). Peak identification was accomplished with help of a porphyrin standard solution purchased from Frontier Scientific. Retention times of the respective porphyrins were as follows: Uroporphyrin I (7.6 min) and III (8.2 min; linear range (LR) = 0-2 μM), 7-carboxyporphyrin (7-CP; 13.5 min; LR= 0-2 μM), 6-carboxyporphyrin (6-CP, 20.2 min; LR= 0-2 μM), 5-carboxyporphyrin (26.7 min; LR= 0-2 μM), COPI (32.1 min; LR= 0-2 μM), COPIII (34.2 min; LR= 0-2 μM), PPIX (59.5 min; LR= 0-1.5 μM).

For mass spectrometry the flow was split in a 1:9 ratio. Data was obtained in positive ion mode over a mass range of m/z 400-650, using a Finnigan LCQ ion trap spectrometer (San

Jose, CA, USA) equipped with a Finnigan ESI source. The system was controlled by X-Calibur version 1.3 software. Capillary temperature and voltage were 300°C and 3.7 V, respectively. In source collision-induced dissociation of 10 eV was used. Nitrogen as nebulisation gas was maintained at a pressure of 50 psi. A: Fluorescence chromatogram of porphyrin standards with uroporphyrin I and III (i+ii), 7-CP (iii) 6-CP (iv), 5-CP (v), COPI (vi), COPIII (vii), 3-CP (viii) and PPIX (ix). B: Analysis of pigments present in the cell lysate of JP313 (pBAD24-yfeX) with a peak at 59,5 minute corresponding to PPIX;. inset: mass spectrum of PPIX extracted from cell lysate of C600 (pBAD24-yfeX). C: Analysis of pigments present in the cell lysate of JP313 (pBAD24-yfeX H215A).

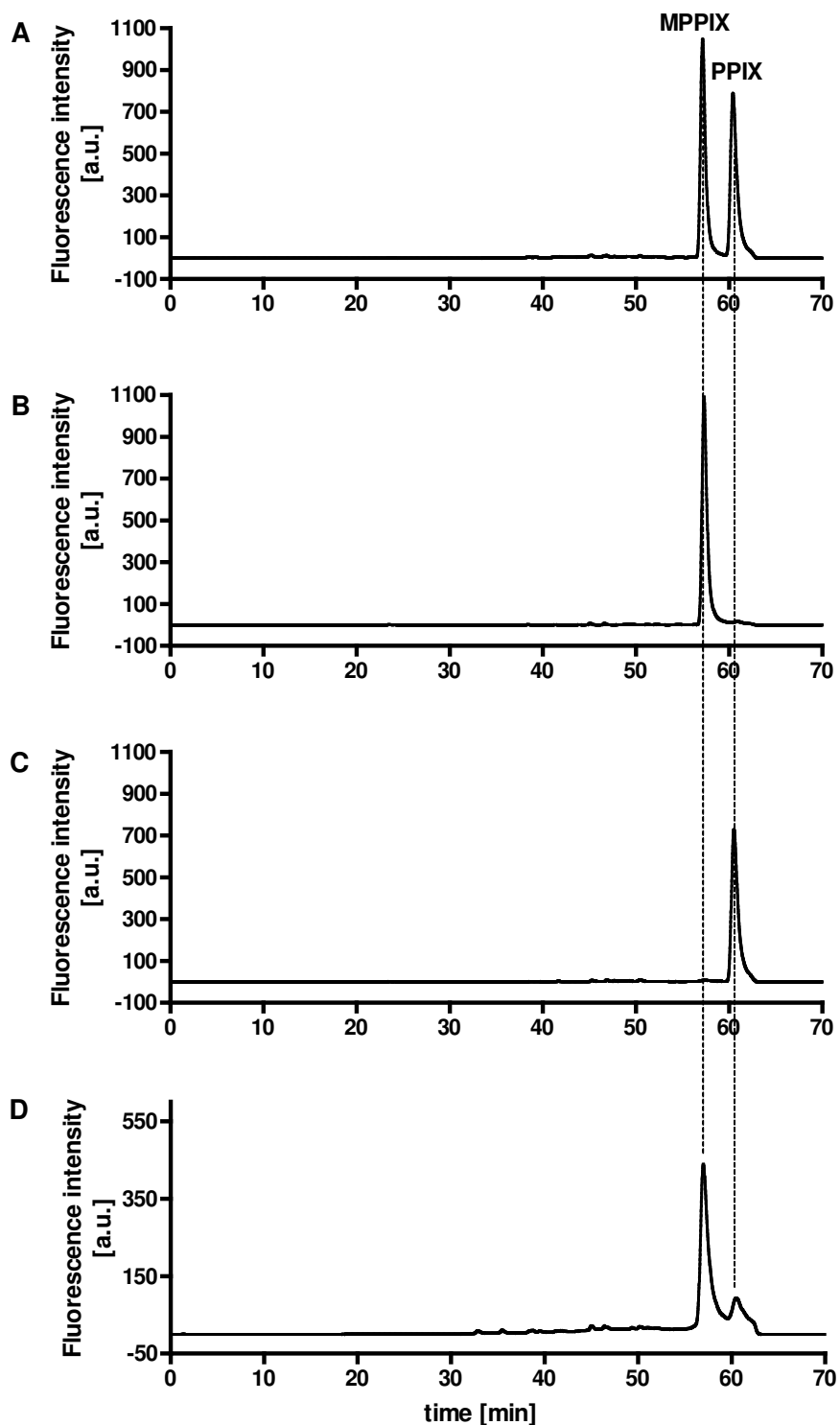


Fig. S3. HPLC fluorescence spectroscopy chromatograms of MPPiX and PPIx. A: mixture of MPPiX and PPIx standards; B: MPPiX standard; C: PPIx standard; D: soluble fraction extract from JP313 (*pBAD-yfeX*) cell lysate incubated with meso-heme for 60 minutes. Porphyrins were eluted with a gradient resulting in retention times of 56.5 (± 0.5) and 60.3 (± 0.5) minutes for MPPiX and PPIx, respectively.

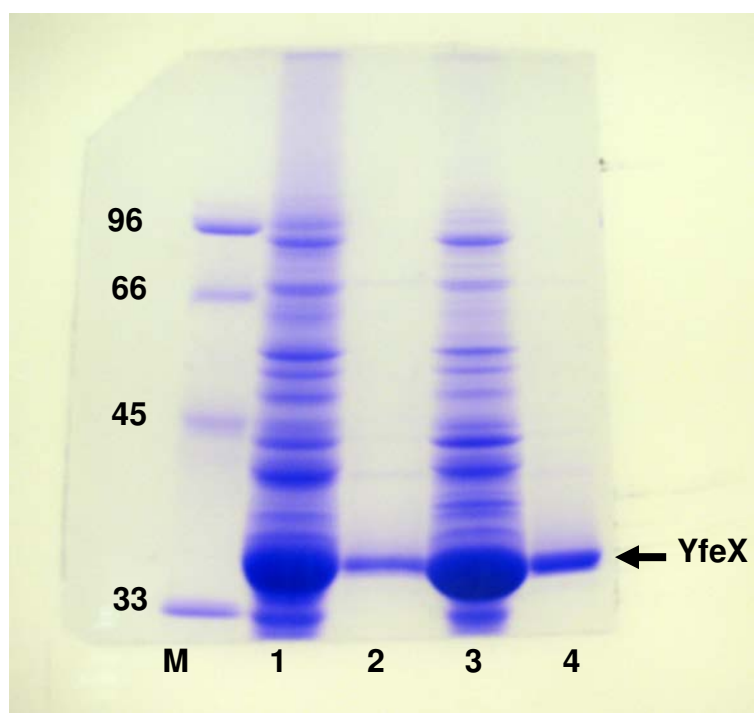


Fig. S4. Purification of YfeX and YfeX_{H215A} proteins. SDS /PAGE analysis of whole cell extract of C600 (pBAD24-yfeX) and C600 (pBAD24-yfeX_{H215A}) and of purified YfeX wild type and mutant proteins. (M) molecular weight markers in kDa ; (1) concentrated soluble fraction of C600 (pBAD24-yfeX); (2) purified YfeX protein. (The N-terminal sequence was determined as SQVQSG corresponding to the YfeX ORF); (3) concentrated soluble fraction of C600 (pBAD24-yfeX_{H215A}); (4) purified YfeX_{H215A} protein.

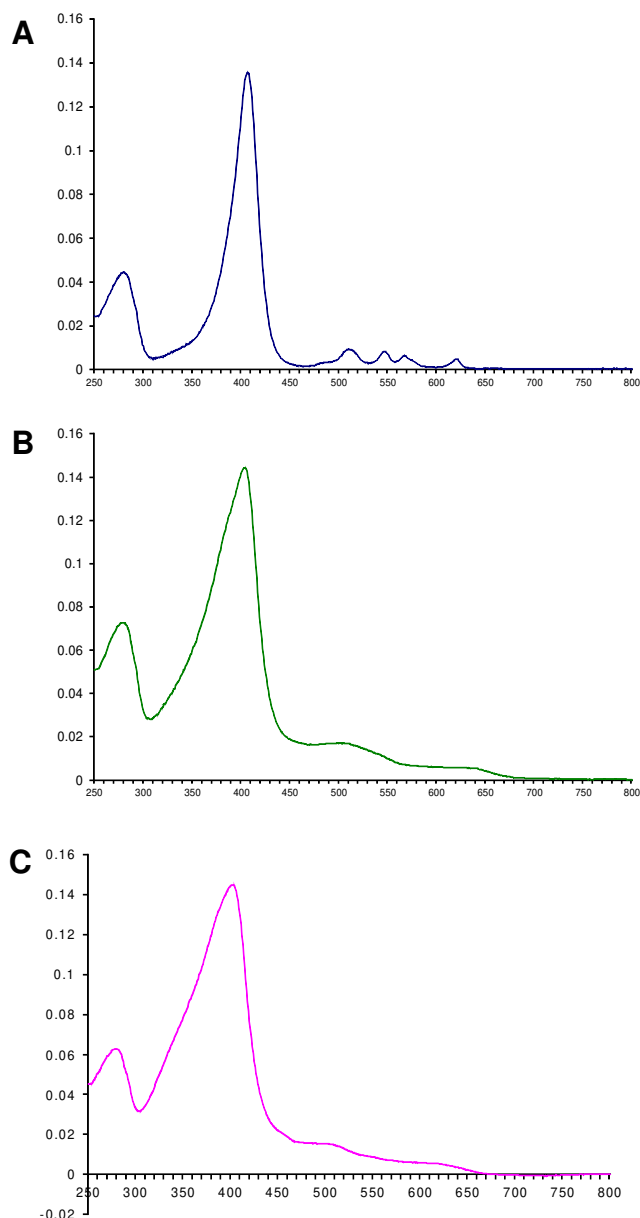


Fig. S5. UV- visible spectra of hemin or PPIX bound to YfeX and displacement of PPIX by hemin. Hemin was dissolved in 0.1 M NaOH. PPIX was dissolved in DMSO. Heme and PPIX solutions were added at a final concentration of 20 μM to apo-YfeX (in Tris-HCl 50 mM pH 8) at 1 μM concentration. Unbound hemin or PPIX were eliminated by gel filtration after 20 min incubation at room temperature. Absorption spectra were recorded on a Beckman DU 800 spectrophotometer and were followed by measuring the absorbance from 250 nm to 700 nm. For PPIX displacement by hemin, pure apo-YfeX (1 μM) was first incubated with PPIX (20 μM) for 20 min and then with hemin (50 μM). After 2 more hours of incubation, the unbound tetrapyrroles were eliminated by gel filtration. A: PPIX absorption spectroscopy; B: hemin absorption spectroscopy; C: PPIX displacement by hemin.

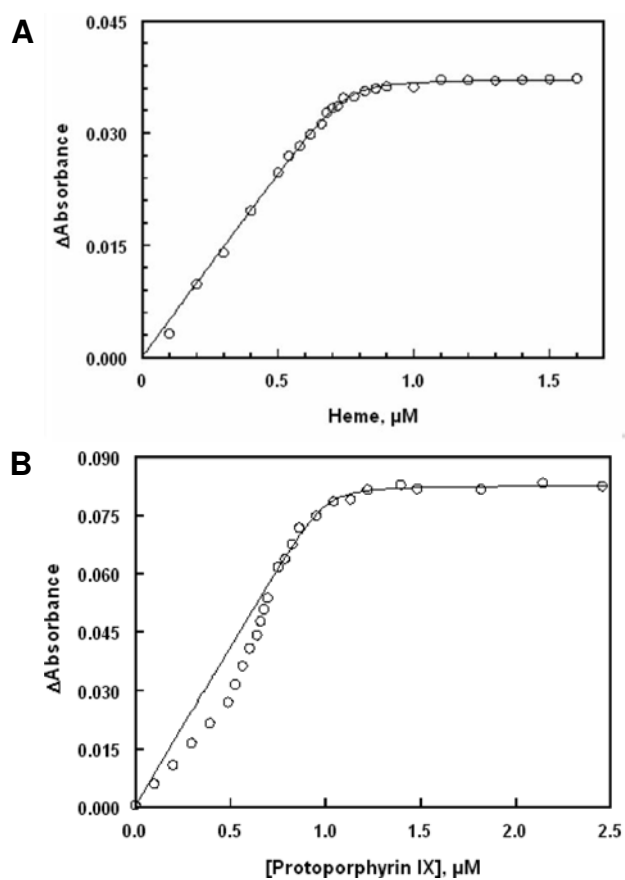


Fig. S6. Spectroscopic measure of PPIX and hemin binding to apo-YfeX. A: 1 to 5 μl aliquots of hemin (20 μM) were successively added to 1 ml of apo-YfeX. Absorbance at the Soret band (404 nm) was reported versus hemin concentration. B: 1 to 5 μl aliquots of PPIX solution (20 μM) were successively added to 1 ml of apo-YfeX (1 μM). Absorbance at the Soret band (407 nm) was reported versus PPIX concentration, corrected for absorbance of free PPIX at the same concentration.

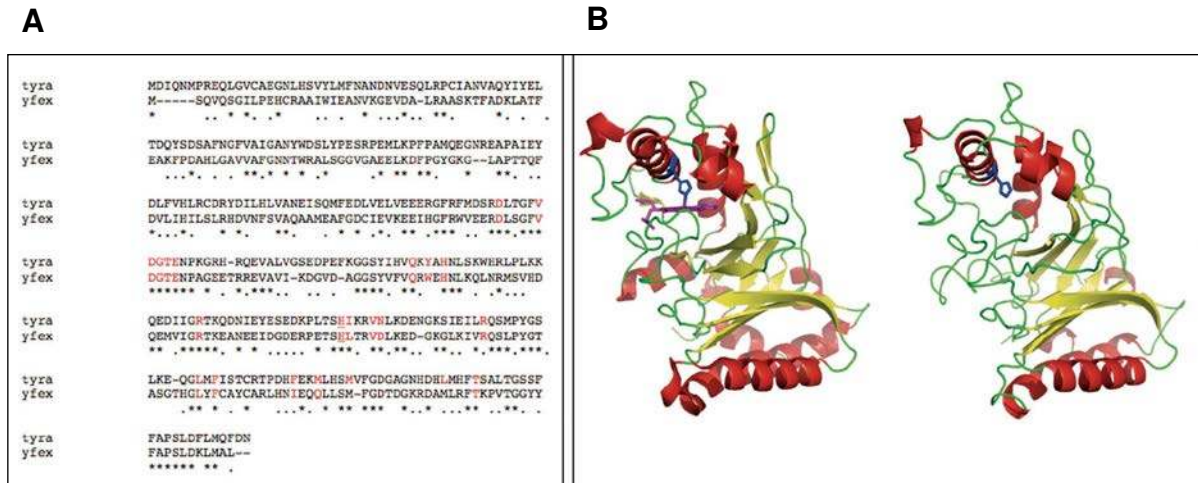


Fig. S7. TyrA and YfeX sequence alignment and structural comparison. A: ClustalW TyrA and YfeX sequence alignment. The heme pocket residues are in red. The conserved histidine iron axial ligand is underlined. B: (Left) crystal structure of TyrA/heme complex from *Shewanella oneidensis*; (Right) Swiss-modeling of YfeX using x-ray TyrA 3D structure as a template.

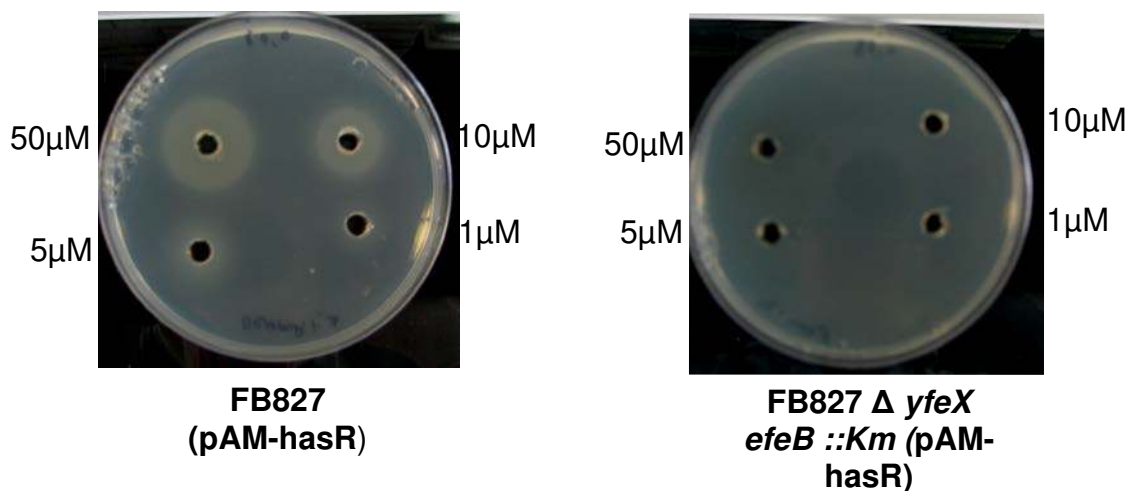


Fig. S8. Example of the heme iron acquisition plates. Petri dishes containing the indicated strains were photographed after 48h incubation at 37°C.

Chapter 5. Counterclockwise – Photodynamic Inactivation of *Escherichia coli* with Protoporphyrin IX generated from Heme

Gesine Heuck¹, Jeffrey R. Mellin², Norbert Lange¹

¹Université de Genève, Laboratoire de Technologie Pharmaceutique, Université de Genève, Université de Lausanne, 30 Quai Ernest Anserment, CH-1211 Genève 4, Switzerland

²Institut Pasteur, Paris, 25-28 rue du docteur Roux, 75015, Paris France

Submitted to Journal of Photochemistry and Photobiology

ABSTRACT. Drug resistance of bacteria is an emerging problem in medical care. Therefore, effective strategies are crucial to ensure the success of antibacterial therapies. One promising approach is to increase the susceptibility of bacteria to eradication by light in combination with a photosensitizer. Interestingly the activity of certain bacterial enzymes is known to produce endogenous photosensitizers. One such enzyme is YfeX, a dye decolorizing peroxidase that generates the endogenous photosensitizer protoporphyrin IX (PPIX) from heme by a reverse ferrochelatase mechanism. We examined the suitability of exploiting YfeX activity for bacterial photodynamic inactivation (PDI) by overexpressing YfeX in *E. coli* K12 FB8-27 and exposing bacteria to light doses of 5, 10, 15 and 20 J/cm². We further tested whether exogenous heme could function as a prodrug leading to increased PPIX generation. In the course of these studies we also investigated and demonstrated a role for the multidrug efflux pump TolC for the export of PPIX from *E.coli*. We observed that YfeX overexpressing *tolC* mutants accumulated high levels of PPIX and were highly sensitive to light. Surprisingly, however, exogenous heme did not act as a prodrug leading to greater intracellular accumulation of PPIX but rather provided a photoprotective effect.

Keywords: photodynamic therapy, efflux pump, *E. coli*, TolC, deferrochelatase, protoporphyrin IX.

Introduction

In the search for new antibacterial strategies, photodynamic therapy is an attractive alternative to conventional therapies. Numerous photosensitizers have shown to be effective antimicrobial compounds in the treatment of dermatological [1-5], dental [6, 7] and gastric infectious diseases [8]. They are also used in the sterilization of blood, water and surfaces [9-15]. While most photosensitizers are exogenously applied compounds, investigations have shown that the photosensitizing properties of certain endogenous molecules can be exploited to enhance microbial killing [3, 16-23]. As part of the heme biosynthetic pathway, protoporphyrin IX (PPIX) is one such photosensitizer of bacterial origin that has the potential to be used for novel antimicrobial therapies. In the physiological context, however, the tight regulation of the enzymes involved in the biosynthesis of heme, prevents PPIX accumulation and hence prevents its phototoxic effects under normal conditions. The regulation of heme biosynthesis involves a negative feedback loop, whereby high concentrations of heme enhance proteolytic degradation of the glutamyl-tRNA reductase HemA [24, 25]. HemA catalyzes the formation of glutamate- δ -aminolevulinic acid, which serves as the first building block of heme biosynthesis in proteobacteria (Fig. 1). This intermediate compound is then converted to 5-aminolevulinic acid (5-ALA) [26-30]. Exogenous addition of 5-ALA, or derivatives thereof, to a bacterial population bypasses the negative feedback control on HemA and effectuates the temporary accumulation of high levels of heme intermediate [3, 31-34]. In particular, the accumulation of PPIX leads to subsequent susceptibility to destruction by photodynamic inactivation (PDI). Such approaches have been exploited for the treatment of several microbial infections such as methicillin resistant *Staphylococcus aureus* (MRS) [35].

We recently demonstrated a new mechanism for the generation of excess PPIX in iron scavenging *E. coli* through the overexpression of a protein, YfeX, with previously unknown function [36]. YfeX is a dye decolorizing peroxidase whose catalytic activity results in the removal of the central iron ion from the tetrapyrrole skeleton of heme. In contrast to heme oxygenases that cleave the porphyrin structure during extraction of iron from heme [37, 38], YfeX leaves the tetrapyrrole ring intact. This results in the production of PPIX. As this activity corresponds to the inverse reaction catalyzed by the ferrochelatase enzyme during heme biosynthesis, YfeX was termed as deferrochelatase.

With the aim of potentially exploiting the newly discovered mechanism of PPIX formation to photosensitize microorganisms, our study sought to assess the susceptibility of *E. coli* K12

overexpressing YfeX to UV light exposure. Furthermore, we tested the practicality of using exogenous heme as a prodrug for PPIX generation by YfeX. A recent study reported that another intermediate of the heme biosynthesis pathway, coproporphyrinogen III (COPgenIII), is a substrate for the TolC efflux pump [1]. Therefore, we also investigated the photosensitizing effects of YfeX driven PPIX accumulation in a *tolC* mutant.

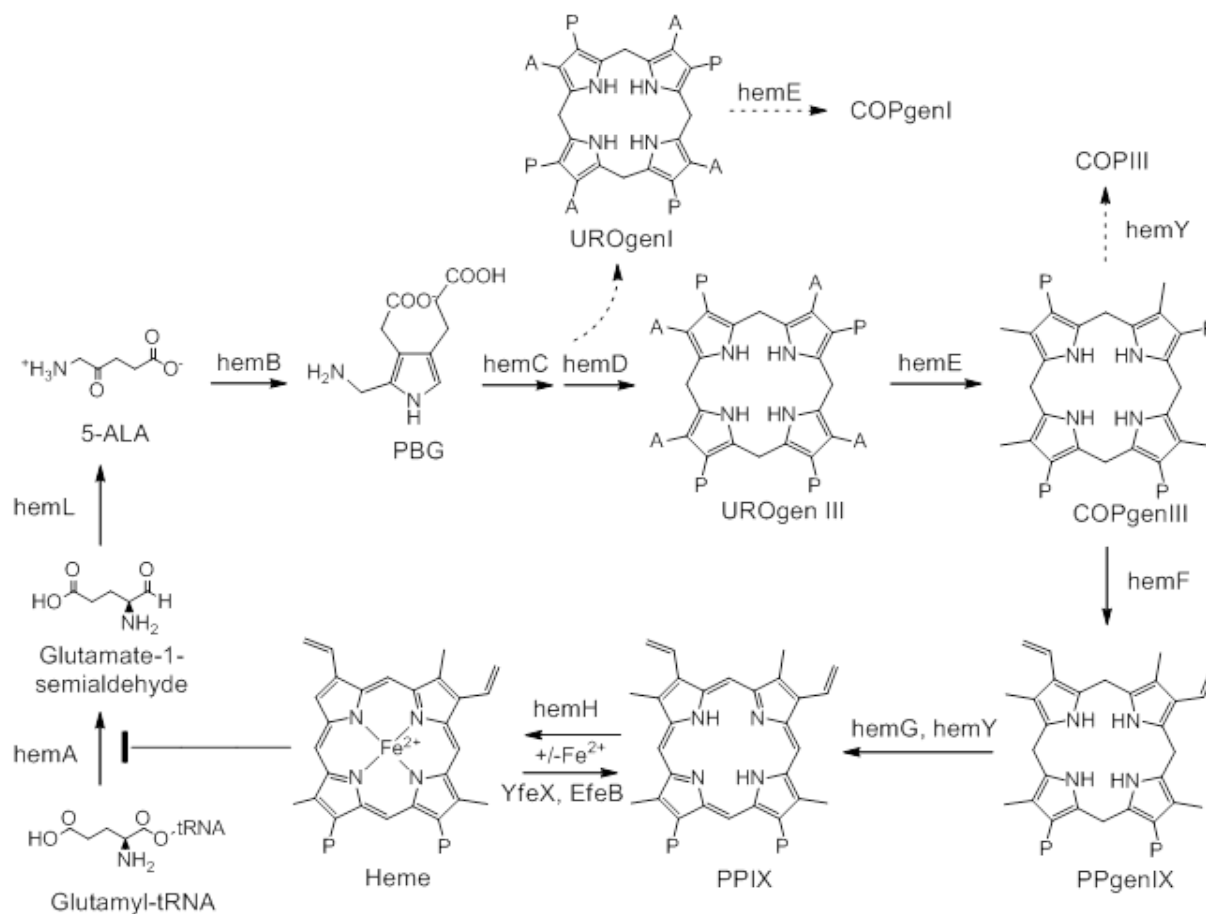


Fig. 1. Bacterial heme biosynthesis. A = acetic acid, P = propionic acid

Materials and Methods

Bacterial strains and plasmids

The wild-type *E. coli* K12 FB8-27 (Δ lac entF:: TnphoA'5) and an *isogenic tolC* mutant from the laboratory collection were described previously [36]. Both strains carry plasmid pam238 constitutively expressing the HasR receptor. *yfeX* was expressed from the pBAD24 plasmid under the control of an arabinose inducible promoter described in [39].

Media and growth conditions

Bacteria were grown aerobically in suspension at 37°C in LB medium supplemented with 50 µg/mL spectinomycin and 100 µg/mL ampicillin for maintenance of the pam238 and pBAD24 plasmids. YfeX expression was induced by addition of 0.2% L-arabinose to the medium. For growth on solid media cells were grown on LB agar plates supplemented with antibiotics and/or arabinose as described above. Experiments involving the addition of heme were carried out in minimal medium M63B1 supplemented with 0.4% glycerol, 50 µl arabinose solution (10% in water), 50 µg/mL spectinomycin and 100 µg/mL ampicillin, as well as 1 µM heme.

Porphyrin extraction and HPLC analysis

For quantitation of porphyrin contents in cells, bacteria were grown overnight in LB broth supplemented with 50 µg/mL spectinomycin and 100 µg/mL ampicillin. In the morning, cultures were diluted 1:100 into fresh media supplemented with the appropriate antibiotics in either the presence or absence of arabinose to induce YfeX overexpression. Cultures were grown to mid-log phase, pelleted and then resuspended in 1 mL of BugBuster[®] extraction reagent (Merck, Darmstadt, Germany) to an OD₆₀₀ of 100/mL. Lysates were left at room temperature for 1 hour and then centrifuged at 15 700 x g for 10 min to remove cellular debris. To extract porphyrins from soluble fractions, 800 µL of extraction solvent (ethanol/DMSO/acetic acid; 80/20/1; v/v/v) were added to 200 µL of the supernatant. The mixture was sonicated in 5 cycles of 5 seconds at 0°C, amplitude 10% using a sonicator probe (Branson Digital Sonifier, Danbury, USA). The sample was centrifuged at 12 500 x g for 5 minutes and the porphyrin containing supernatant was used for analysis. Exhaustive extraction of porphyrins from the sample was verified by the absence of porphyrin fluorescence in the pellet.

Porphyrins were separated by HPLC (LaChrom, Merck, Darmstadt, Germany) as described before using a 125/4 Nucleodur C18 gravity 3 µm column (Macherey-Nagel, Oensingen, Switzerland) with the corresponding pre-column [36]. An elution gradient was run over 80 minutes with solvent A (acetate buffer pH5.1, 0.5 M/ acetonitrile; 90:10; v/v) and solvent B

(methanol/acetonitrile; 90:10; v/v). The flow rate was 1 mL/min. Porphyrins were excited at 405 nm and measured at 620 nm using a LaChrom L-7480 fluorescence detector (Merck, Darmstadt, Germany). Porphyrin peaks were identified by comparison with a chromatogram of porphyrin standard solutions (Frontier Scientific, Carnforth, United Kingdom). The HPLC solvent gradient was adjusted so that the retention time increased with the lipophilicity of the analyte.

Irradiation experiments

Irradiation experiments were carried out with *E. coli* K12 FB8-27 or an isogenic *tolC* mutant carrying the pAM238-hasR plasmid and either the pBAD24 empty plasmid or pBAD24*yfeX*. Bacteria were cultured overnight and diluted 100-fold in the morning. When cultures reached mid-log level growth, they were diluted again into PBS buffer to obtain a final OD₆₀₀ of 0.0001. Aliquot volumes of each suspension (2.5 mL) were dispensed into 6-well polystyrene plates (diameter 35mm) and placed on a light table equipped with Narwa, LT 18W/O18 light tubes (PCI Biotech, Oslo, Norway). The radiation intensity was 1.375 mW/cm². Cells were irradiated for up to 4 hours. Aliquots were taken at the corresponding time points, serially diluted and cell survival was assessed by counting the number of colony forming units (CFU's) in irradiated and mock irradiated samples.

Results

TolC mutants of E. coli accumulate PPIX

The TolC protein is a beta barrel channel protein, which spans the outer membrane of Gram-negative bacteria. It extends approximately half-way into the periplasmic space and pairs with inner membrane heterodimeric complexes such as AcrAB located in the inner membrane and periplasm to form an efflux pump of wide substrate specificity [40-42]. It was recently demonstrated that *tolC* mutants treated with exogenous 5-ALA accumulate the heme precursor (COPIII) to a significantly higher level than their wild-type counterparts [1]. Thus, TolC is involved in alleviating the accumulation of toxic intermediates formed during heme biosynthesis. In order to assess the influence of TolC on the efflux of another toxic heme intermediate, PPIX, we overexpressed *Yfex* from an arabinose inducible promoter. As shown

previously, overexpression of YfeX leads to the accumulation of PPIX in *E. coli* [36]. As PPIX is a fluorescent compound, we subsequently examined the fluorescence of either the wild-type or a *tolC* mutant under UV light as a proxy for PPIX accumulation (Fig. 2). Both, the wild-type (Fig. 2A) and *tolC* mutant (Fig. 2B) showed the characteristic red porphyrin fluorescence under UV light. However, the fluorescence intensity of the *tolC* mutant was considerably higher.

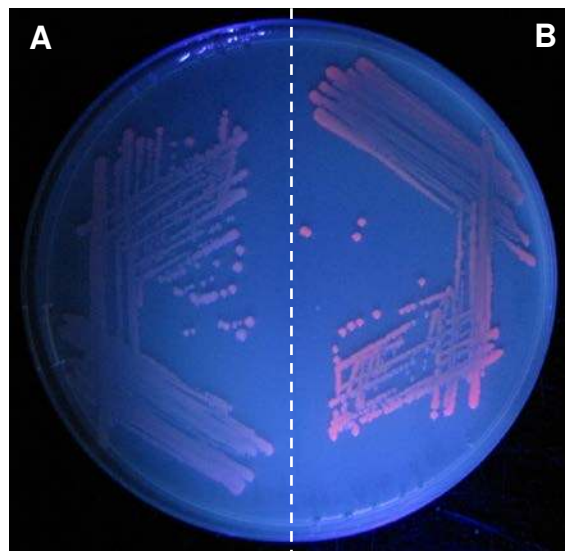


Fig. 2. TolC “wild type” (A) and mutated (B). E.coli K12 FB 8-27 strains transformed with pBADyfeX and viewed under UV light. The tolC mutated strain (B) features a typical red fluorescence of porphyrins.

To examine if the observed fluorescence corresponded to an increased accumulation of PPIX and not other intermediates of the heme biosynthesis we examined soluble cell extracts by fluorescence HPLC. Cells were grown in LB broth to mid-log phase in presence or absence of arabinose to induce YfeX overexpression. Cells were pelleted by centrifugation, and porphyrins were extracted from soluble fractions by solvent treatment. Using a solvent gradient it is possible to separate the respective porphyrin intermediates of the heme biosynthetic pathway enabling us to differentiate and quantify the levels of each porphyrin compound present in the samples. In wild-type cells not induced for YfeX expression, negligible levels of porphyrins were identified (Fig. 3). In contrast, in wild-type cells grown in the presence of arabinose (overexpressing YfeX), coproporphyrin I (COP I), COP III and PPIX

were elevated (3, 5 and 6 fold higher in comparison to the wild type strain without YfeX overexpression, respectively), indicating that the overexpression of YfeX leads to the accumulation of a number of heme pathway intermediates.

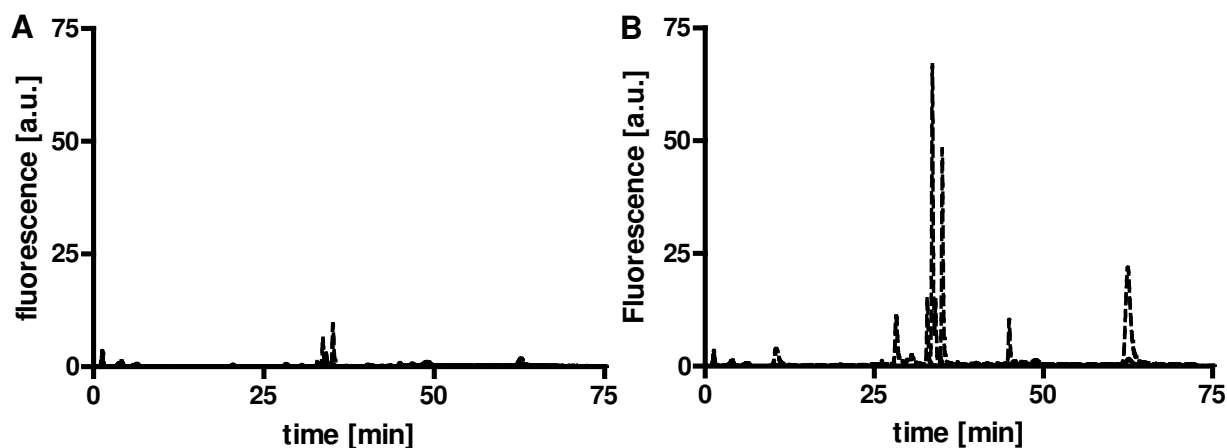


Fig. 3. Chromatograms of cellular extracts from either *tolC* wildtype (solid line) and *tolC* mutated (dashed line) *E. coli* K12 FB 8-27 strains transfected with the *pBAD* empty vector (A) or *pBAD yfeX* (B). *COPI*, *COPIII* and *PPIX* elution times were 35.5, 37.0 and 62.0 minutes, respectively.

In the *tolC* mutant grown in the absence of inducer, *PPIX* and especially *COPI* and *COPIII*, levels were also increased (6, 30 and 30 fold, respectively). Thus, even in the absence of YfeX overexpression the *tolC* mutant shows a higher accumulation of intermediates of the heme biosynthesis (Fig. 3).

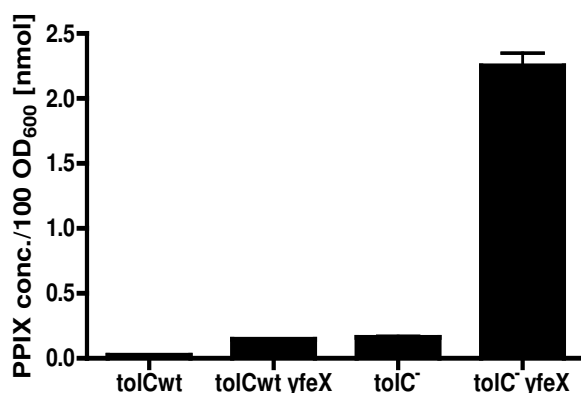


Fig. 4. *PPIX* concentrations in extracts from *tolC* mutated and *tolC* wildtype *E. coli* K12 FB 8-27 strains without and with (*yfeX*) induced *YfeX* expression, respectively.

In the *tolC* mutant grown in the presence of arabinose (overexpressing YfeX), levels of COPI, COPIII and PPIX were all significantly increased with the most prominent component being PPIX (Fig. 4). This indicates that the fluorescence of cells overexpressing YfeX grown on solid media is due to an accumulation of various porphyrin compounds in the cell, primarily PPIX. This extends the role of the TolC pump to the efflux not only of the COPIII heme intermediate but also of COPI and PPIX. It also suggests that TolC is important for maintaining low levels of these compounds during heme synthesis.

PPIX accumulation in tolC mutants leads to increased photosensitivity

The augmentation of photosensitivity by forced overproduction of porphyrin heme intermediates and the subsequent clearance of microbes by photodynamic therapy is an established antimicrobial treatment. We wished to assess whether bacteria overexpressing YfeX with an increased accumulation of PPIX were more sensitive to light irradiation. To examine this, we grew cells in the presence of arabinose to induce expression of the YfeX protein. We subsequently exposed cells to light doses of up to 20 J/cm² and examined cell survival by plating and counting colony forming units (CFU) (Fig. 5).

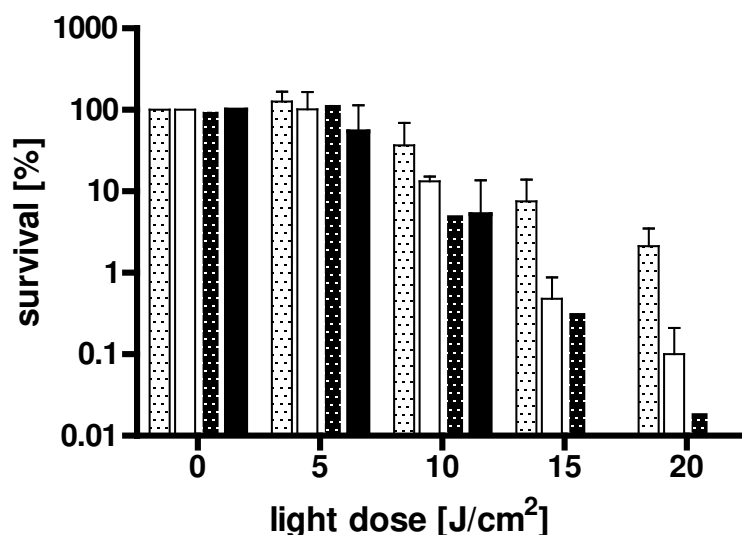


Fig. 5. Cell survival of *tolC* wt (light columns) and *tolC* mutated (dark columns) *E.coli* K12 FB8-27 strains). Cells were grown either in absence (dotted columns) or presence (solid columns) of the YfeX inducer arabinose.

All cells showed at least a 1.5 log decline in survival after exposure to 20 J/cm² light as compared to the samples kept in the dark, which was not unexpected. The decline in survival of cells overexpressing YfeX, was reduced a further 1.5 logs. Notably, the *tolC* mutant cells showed a significant reduction in survival of nearly 4 logs. No cell survival was observed in *tolC* mutants grown in arabinose after exposure to a light dose of 20 J/cm². Thus, *E. coli* cells overproducing YfeX show increased photosensitivity. This effect is likely due to the accumulation of PPIX and other heme pathway intermediates. Furthermore, the effect is significantly enhanced in a *tolC* mutant, which is unable to efflux excess porphyrins.

Exogenous heme does not increase PPIX accumulation or photosensitivity in YfeX overexpressing cells

To examine the effect of heme as a prodrug for YfeX mediated PPIX generation and subsequent PDI, we grew YfeX overexpressing cells in presence of 1 μM heme prior to exposure to a 10 J/cm² light dose. We reasoned that provision of heme to *E. coli* cells able to scavenge exogenous heme could result in increased porphyrin production and increased photosensitivity in cells overexpressing YfeX.

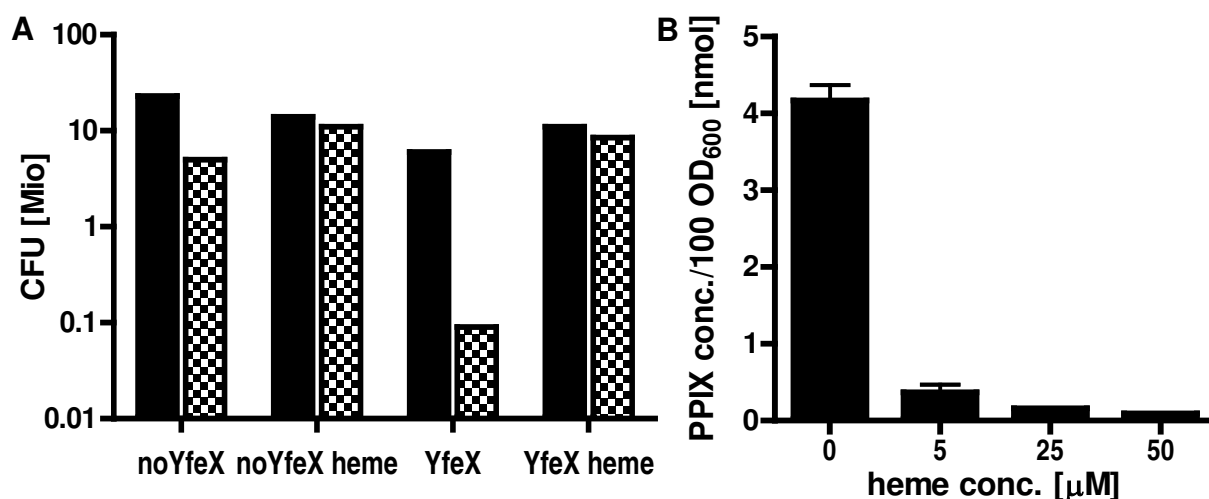


Fig. 6. (A) Cell survival of *E. coli* K12 FB 8-27 strains prior to (solid columns) and after light exposure (10 J/cm²) (checkered columns). Slight killing occurred in absence of heme in cells without induced YfeX. It was enhanced in cells where YfeX was induced. No killing was achieved when cells were grown in presence of 1 μM heme. (B) PPIX concentration in K12 FB8-27 grown in M63 medium supplemented with 0, 5, 25 and 50 μM heme, respectively.

Interestingly, addition of exogenous heme negated the photosensitizing effect and in fact protected cells from the sensitivity to irradiation (Fig. 6A). Examination of PPIX levels in cells incubated with varying heme concentrations revealed that the cellular PPIX content was significantly reduced upon incubation with heme, indicating a possible interference of exogenous heme with YfeX activity (Fig. 6B). However, the mechanism through which exogenous heme prevents endogenous PPIX accumulation and photosensitization by YfeX overexpression remains unclear.

Discussion

The rise of bacterial resistance to existing antibiotics necessitates the development of novel antimicrobial compounds and therapies. One promising approach has focused on the use of photodynamic therapy to sensitize bacteria to eradication by exposure to light. In our study we showed that bacteria accumulating the photosensitizer PPIX upon overexpression of the protein YfeX after exposure to irradiation are more readily killed. Interestingly, we found that PPIX accumulation, along with two other porphyrin intermediates of the heme biosynthesis, COPI and COPIII, was also significantly increased in mutants lacking the efflux pump TolC. This implies an important role for TolC in the efflux of numerous toxic intermediates of the heme biosynthesis pathway. Finally, we showed that cells, which accumulated porphyrins are sensitized to UV light and this was particularly acute in the *tolC* mutant cells.

The exploitation of endogenous porphyrin intermediates for bacterial PDI has been demonstrated in several reports. Commonly, the production of endogenous porphyrins such as PPIX is induced by the administration of exogenous 5-ALA and its derivatives [3, 17, 20-23, 32, 43-45]. These heme precursors by-pass the negative feedback controlling heme biosynthesis through the regulation of HemA (glutamyl-tRNA reductase) activity and provoke the accumulation of PPIX and other heme intermediates. In our study, we instead generated excess endogenous PPIX through the overexpression of the YfeX deferrochelatase. YfeX belongs to the family of dye-decolorizing peroxidases (Dyp-family). These enzymes use heme as co-factor to catalyze the reduction of peroxides. YfeX and its paralog EfeB remove iron from heme, generating PPIX as a by-product and cells overexpressing YfeX accumulate high levels of PPIX. Notably, extracts of *E. coli* cells overexpressing YfeX also contained elevated levels of coproporphyrin I and III, which are earlier intermediates in the heme biosynthesis pathway. This raised the question how YfeX overexpression was affecting COPI and COPIII formation in addition to PPIX. It is possible that due to the deferrochelation activity of YfeX,

high concentrations of PPIX drive the reactions of the heme pathway in reverse, leading to the formation of the earlier heme intermediates; however we view this mechanism as unlikely. Another possibility is that the sequestration of heme by YfeX disrupts the normal negative feedback regulation, controlling HemA activity at the first step of heme biosynthesis [25, 46]. This would lead to increased 5-ALA formation and increased flux through the heme biosynthesis pathway. In combination with bottlenecks at the level of uroporphyrinogen III formation and coproporphyrinogen conversion to protoporphyrinogen IX this could result in the accumulation of COPI and COPIII along with PPIX as observed [43, 47-52].

Recent data, however, suggest another explanation. It was stated that EfeB mutated in the Asp²³⁵, Arg³⁴⁷ and His³²⁹ residues lost the ability to produce PPIX but was still able to bind heme [53]. Thus, while maintaining the ability to sequester heme, no PPIX accumulation was noted, indicating that heme sequestration does not lead to the deregulation of heme biosynthesis. The findings suggest for our experiments that YfeX sequestration of heme likely does not account for the observed porphyrin accumulation. A more plausible explanation has recently been hinted at by the observation that YfeX is able to oxidize protoporphyrinogen and coproporphyrinogen III to PPIX and COPIII [54]. We therefore favour the hypothesis that the accumulation of multiple heme intermediates in our experiments is a result of the dual catalytic activity of YfeX. This includes the oxidation of porphyrinogens to the corresponding porphyrins and the production PPIX through the deferrochelation of heme.

A major challenge for antibacterial therapy of Gram-negative bacteria is the trespassing of the double-layered bacterial cell wall. Since YfeX generates PPIX through an intracellular deferrochelation mechanism and functions in combination with bacterial heme transporters, the potential exploitation of an endogenous physiological system for antibacterial purposes is appealing. In this vein we wished to test if exogenous heme could act as a prodrug for the PPIX generation by YfeX. To our surprise, the addition of exogenous heme to cultures negated the photosensitizing effect of YfeX overexpression rather than augmenting it. How heme provides a photoprotective effect against irradiation is not clear. It is possible that heme in the media partially acts as an optical shield preventing light to reach bacteria during irradiation. However, considering PPIX levels were significantly decreased in strains incubated with heme, we presume that exogenous heme interferes with the ability of YfeX to generate PPIX from endogenous heme. It is tempting to speculate that during its uptake, exogenous heme represses the flux of the heme biosynthesis pathway thus eliminating endogenous heme substrate for YfeX and preventing PPIX accumulation. This would also

suggest that YfeX may not be able to access exogenous heme in the same manner as endogenous heme. Clearly, further research, is required to elucidate this phenomenon; however, it suggests that the use of exogenous heme is unlikely to drive PDI through the exploitation of a deferrochelation mechanism.

The observation of significant PPIX accumulation in a *tolC* mutant indicates that PPIX is a substrate of TolC-mediated efflux. A recent report showed that another heme pathway intermediate, coproporphyrin (COPIII), is also a substrate for TolC dependent efflux from *E.coli* [1]. Thus TolC appears able to efflux both the hydrophilic porphyrin COPIII and the lipophilic porphyrin PPIX, suggesting a broad specificity for TolC to potentially toxic intermediates generated in the heme biosynthesis. TolC acts as part of a tripartite efflux pump involved in the export of a large variety of molecules. TolC is responsible for the resistance of numerous clinical bacterial strains, such as *E. aerogenes*, the *K. oxytoca* and *H. influenza* [55-57] to various drugs and dyes, such as aminoglycosides, chloramphenicol and crystal violet. Our study and others indicate that inhibition of multidrug efflux pumps may improve the photosensitizing effect [1, 58-60]. In this regard it will be interesting to identify the partners of TolC in PPIX efflux. TolC is known to frequently function in combination with the AcrAB proteins. In this tripartite complex, the inner membrane protein AcrB, a trimeric proton antiporter of the resistance-nodulation-cell division (RND) family, recruits the substrate from either the cytoplasm or periplasm. It connects to AcrA, a dimeric membrane fusion protein in the periplasm that acts as linker between AcrB and TolC by bringing the inner and outer membrane into close vicinity of each other [42, 61]. Nevertheless, there are up to 31 additional inner membrane protein pairs that TolC is thought to be able to pair with to efflux compounds from the cell. Which particular partners are required for the efflux of PPIX or other porphyrins remains to be determined. It is possible that there is significant redundancy with TolC and multiple possible partner pumps.

Conclusion

In this study we showed that PPIX accumulates in cells overexpressing YfeX and leads to photosensitization. The photosensitizing effect is significantly augmented in a TolC mutant. TolC appears to be an important mediator of toxicity associated with multiple heme pathway intermediates. Importantly, YfeX, together with its Gram-positive paralog EfeB, are the only

enzymes in *E.coli* reported to carry out deferrochelation of heme resulting in the production of PPIX. Since they are widespread and highly conserved in Gram-positive and Gram-negative bacteria they may represent promising starting points for new antibacterial strategies.

Acknowledgments

The authors wish to acknowledge Dr. Cécile Wandersman for her help and valuable advice during this project.

Reference List

1. Tatsumi R, Wachi M. TolC-dependent exclusion of porphyrins in Escherichia coli. *J Bacteriol* 2008; **190**: 6228-33.
2. Bryld LE, Jemec GBE. Photodynamic therapy in a series of rosacea patients. *J Eur Acad Dermatol Venereol* 2007; **21**: 1199-202.
3. Fotinos N, Mikulic J, Convert M et al. 5-ALA derivative-mediated photoinactivation of Propionibacterium acnes. *J Dermatol Sci* 2009; **56**: 212-4.
4. Hamblin MR, O'Donnell DA, Zahra T et al. Targeted photodynamic therapy for infected wounds in mice. *Proc SPIE-Int Soc Opt Eng* 2002; **4612**: 48-58.
5. Koenig K, Meyer H. Photodynamically induced inactivation of Propionibacterium acnes using the photosensitizer methylene blue and red light. *Dermatol Monatsschr* 1992; **178**: 297-300.
6. Dortbudak O, Haas R, Bernhart T, Mailath-Pokorny G. Lethal photosensitization for decontamination of implant surfaces in the treatment of peri-implantitis. *Clin Oral Implants Res* 2001; **12**: 104-8.
7. Haas R, Baron M, Dortbudak O, Watzek G. Lethal photosensitization, autogenous bone, and e-PTFE membrane for the treatment of peri-implantitis: preliminary results. *Int J Oral Maxillofac Implants* 2000; **15**: 374-82.
8. Hamblin MR, Viveiros J, Yang C et al. Helicobacter pylori accumulates photoactive porphyrins and is killed by visible light. *Antimicrob Agents Chemother* 2005; **49**: 2822-7.
9. Brovko L, Romanova NA, Leslie C et al. Photodynamic treatment for surface sanitation. *Proc SPIE-Int Soc Opt Eng* 2005; **5969**: 596914/1-6.

10. Carvalho CMB, Gomes ATPC, Fernandes SCD et al. Photoinactivation of bacteria in wastewater by porphyrins: Bacterial β -galactosidase activity and leucine-uptake as methods to monitor the process. *Photochem Photobiol B* 2007; **88**: 112-8.
11. Jemli M, Alouini Z, Sabbahi S, Gueddari M. Destruction of fecal bacteria in waste water by three photosensitizers. *J Environ Monit* 2002; **4**: 511-6.
12. Kuznetsova NA, Makarov DA, Kaliya OL, Vorozhtsov GN. Photosensitized oxidation by dioxygen as the base for drinking water disinfection. *J Hazard Mater* 2007; **146**: 487-91.
13. Luksiene Z, Buchovec I, Paskeviciute E. Inactivation of several strains of *Listeria monocytogenes* attached to the surface of packaging material by Na-Chlorophyllin-based photosensitization. *Photochem Photobiol B* 2010; **101**: 326-31.
14. Magaraggia M, Faccenda F, Gandolfi A, Jori G. Treatment of microbiologically polluted aquaculture waters by a novel photochemical technique of potentially low environmental impact. *J Environ Monit* 2006; **8**: 923-31.
15. Ruane PH, Edrich R, Gampp D et al. Photochemical inactivation of selected viruses and bacteria in platelet concentrates using riboflavin and light. *Transfusion* 2004; **44**: 877-85.
16. Ramstad S, Anh-Vu N, Johnsson A. The temperature dependence of porphyrin production in *Propionibacterium acnes* after incubation with 5-aminolevulinic acid (ALA) and its methyl ester (m-ALA). *Photochem Photobiol Sci* 2006; **5**: 66-72.
17. Dietel W, Pottier R, Pfister W et al. 5-Aminolaevulinic acid (ALA) induced formation of different fluorescent porphyrins: a study of the biosynthesis of porphyrins by bacteria of the human digestive tract. *Photochem Photobiol B* 2007; **86**: 77-86.
18. Ashkenazi H, Malik Z, Harth Y, Nitzan Y. Eradication of *Propionibacterium acnes* by its endogenous porphyrins after illumination with high intensity blue light. *FEMS Immunol Med Microbiol* 2003; **35**: 17-24.
19. Bisland SK, Chien C, Wilson BC, Burch S. Pre-clinical in vitro and in vivo studies to examine the potential use of photodynamic therapy in the treatment of osteomyelitis. *Photochem Photobiol Sci* 2006; **5**: 31-8.
20. Hongcharu W, Taylor CR, Chang Y et al. Topical ALA-photodynamic therapy for the treatment of acne vulgaris. *J Invest Dermatol* 2000; **115**: 183-92.
21. Karrer S, Szeimies RM, Ernst S et al. Photodynamic Inactivation of Staphylococci with 5-Aminolaevulinic Acid or Photofrin. *Lasers Med Sci* 1999; **14**: 54-61.
22. Nitzan Y, Kauffman M. Endogenous Porphyrin Production in Bacteria by d-Aminolaevulinic Acid and Subsequent Bacterial Photoeradication. *Lasers Med Sci* 1999; **14**: 269-77.
23. Nitzan Y, Salmon-Divon M, Shporen E, Malik Z. ALA induced photodynamic effects on gram positive and negative bacteria. *Photochem Photobiol Sci* 2004; **3**: 430-5.

24. Schobert M, Jahn D. Regulation of heme biosynthesis in non-phototrophic bacteria. *J Mol Microbiol Biotechnol* 2002; **4**: 287-94.
25. Wang L, Elliott M, Elliott T. Conditional stability of the HemaA protein (glutamyl-tRNA reductase) regulates heme biosynthesis in *Salmonella typhimurium*. *J Bacteriol* 1999; **181**: 1211-9.
26. Avissar YJ, Ormerod JG, Beale SI. Distribution of δ -aminolevulinic acid biosynthetic pathways among phototrophic bacterial groups. *Arch Microbiol* 1989; **151**: 513-19.
27. Chen W, Wright L, Lee S et al. Expression of glutamyl-tRNA reductase in *Escherichia coli*. *BBA - Gene Struct Expr* 1996; **1309**: 109-21.
28. Ferreira GC, Zhang JS. Mechanism of 5-aminolevulinic acid synthase and the role of the protein environment in controlling the cofactor chemistry. *Cell Mol Biol* 2002; **48**: 827-33.
29. Jahn D, Chen MW, Soll D. Purification and functional characterization of glutamate-1-semialdehyde aminotransferase from *Chlamydomonas reinhardtii*. *J Biol Chem* 1991; **266**: 161-7.
30. Jahn D, O'Neill GP, Verkamp E, Soll D. Glutamate tRNA: involvement in protein synthesis and aminolevulinic acid formation in *Chlamydomonas reinhardtii*. *Plant Physiol Biochem* 1992; **30**: 245-53.
31. Doss M, Philipp-Dormston WK. Porphyrin and heme biosynthesis from endogenous and exogenous δ -aminolevulinic acid in *Escherichia coli*, *Pseudomonas aeruginosa*, and *Achromobacter metalcaligenes*. *Hoppe-Seyler's Z Physiol Chem* 1971; **352**: 725-33.
32. Fotinos N, Convert M, Piffaretti J-C et al. Effects on Gram-negative and Gram-positive bacteria mediated by 5-aminolevulinic acid and 5-aminolevulinic acid derivatives. *Antimicrob Agents Chemother* 2008; **52**: 1366-73.
33. Kloek J, Beijersbergen van Henegouwen MJ. Prodrugs of 5-aminolevulinic acid for photodynamic therapy. *Photochem Photobiol* 1996; **64**: 994-1000.
34. Philipp-Dormston WK, Doss M. Comparison of porphyrin and heme biosynthesis in various heterotrophic bacteria. *Enzyme* 1973; **16**: 57-64.
35. Maisch T, Bosl C, Szeimies RM et al. Determination of the antibacterial efficacy of a new porphyrin-based photosensitizer against MRSA ex vivo. *Photochem Photobiol Sci* 2007; **6**: 545-51.
36. Letoffe S, Heuck G, Delepelaire P et al. Bacteria capture iron from heme by keeping tetrapyrrole skeleton intact. *Proc Natl Acad Sci U S A* 2009; **106**: 11719-24.
37. Yoshida T, Migita CT. Mechanism of heme degradation by heme oxygenase. *J Inorg Biochem* 2000; **82**: 33-41.
38. Frankenberg-Dinkel N. Bacterial heme oxygenases. *Antioxid Redox Sign* 2004; **6**: 825-34.

39. Guzman L-M, Belin D, Carson MJ, Beckwith J. Tight regulation, modulation, and high-level expression by vectors containing the arabinose pBAD promoter. *J Bacteriol* 1995; **177**: 4121-30.
40. Li XZ, Nikaido H. Efflux-mediated drug resistance in bacteria. *Drugs* 2004; **64**: 159-204.
41. Nikaido H, Zgurskaya HI. AcrAB and related multidrug efflux pumps of *Escherichia coli*. *J Mol Microb Biotech* 2001; **3**: 215-8.
42. Pos KM. Drug transport mechanism of the AcrB efflux pump. *BBA - Prot Proteom* 2009; **1794**: 782-93.
43. Jacobs NJ, Jacobs JM, Morgan HE, Jr. Comparative effect of oxygen and nitrate on protoporphyrin and heme synthesis from Δ -aminolevulinic acid in bacterial cultures. *J Bacteriol* 1972; **112**: 1444-5.
44. Szocs K, Csik G, Kaposi AD, Fidy J. In situ detection of ALA-stimulated porphyrin metabolic products in *Escherichia coli* B by fluorescence line narrowing spectroscopy. *BBA - Mol Cell Res* 2001; **1541**: 170-8.
45. Szocs K, Gabor F, Csik G, Fidy J. δ -Aminolaevulinic acid-induced porphyrin synthesis and photodynamic inactivation of *Escherichia coli* B. *Photochem Photobiol B* 1999; **50**: 8-17.
46. Verderber E, Lucast LJ, VanDehy JA et al. Role of the hemA gene product and delta-aminolevulinic acid in regulation of *Escherichia coli* heme synthesis. *J Bacteriol* 1997; **179**: 4583-90.
47. Olsson U, Billberg A, Sjovald S et al. In vivo and in vitro studies of *Bacillus subtilis* ferrochelatase mutants suggest substrate channeling in the heme biosynthesis pathway. *J Bacteriol* 2002; **184**: 4018-24.
48. Jacobs NJ, Jacobs JM, Brent P. Characterization of Late Steps of Microbial Heme Synthesis - Conversion of Coproporphyrinogen to Protoporphyrin. *J Bacteriol* 1971; **107**: 203-9.
49. Philipp-Dormston WK, Doss M. Comparison of porphyrin and heme biosynthesis in various heterotrophic bacteria. *Enzyme* 1973; **16**: 57-64.
50. Woodard SI, Dailey HA. Regulation of Heme-Biosynthesis in *Escherichia-Coli*. *Arch Biochem Biophys* 1995; **316**: 110-5.
51. Breckau D, Mahlitz E, Sauerwald A et al. Oxygen-dependent coproporphyrinogen III oxidase (HemF) from *Escherichia coli* is stimulated by manganese. *J Biol Chem* 2003; **278**: 46625-31.
52. Freeseemann AG, Gross U, Bensidhoum M et al. Immunological, enzymatic and biochemical studies of uroporphyrinogen III synthase deficiency in 20 patients with congenital erythropoietic porphyria. *Eur J Biochem* 1998; **257**: 149-53.

53. Liu X, Du Q, Wang Z et al. Crystal structure and biochemical features of EfeB/YcdB from Escherichia coli O157: Asp235 plays divergent roles in different enzyme-catalyzed processes. *J Biol Chem* 2011; **286**: 14922-31.
54. Dailey HA, Septer AN, Daugherty L et al. The Escherichia coli protein YfeX functions as a porphyrinogen oxidase, not a heme dechelataase. *mBio* 2011; **2**: e00248-11.
55. Li XZ, Nikaido H. Efflux-Mediated Drug Resistance in Bacteria An Update. *Drugs* 2009; **69**: 1555-623.
56. Fenosa A, Fuste E, Ruiz L et al. Role of TolC in Klebsiella oxytoca resistance to antibiotics. *J Antimicrob Chemoth* 2009; **63**: 668-74.
57. Dean CR, Narayan S, Daigle DM et al. Role of the AcrAB-TolC efflux pump in determining susceptibility of Haemophilus influenzae to the novel peptide deformylase inhibitor LBM415. *Antimicrob Agents Chemother* 2005; **49**: 3129-35.
58. Tegos GP, Masago K, Aziz F et al. Inhibitors of bacterial multidrug efflux pumps potentiate antimicrobial photoinactivation. *Antimicrob Agents Chemother* 2008; **52**: 3202-9.
59. Tegos GP, Hamblin MR. Phenothiazinium antimicrobial photosensitizers are substrates of bacterial multidrug resistance pumps. *Antimicrob Agents Chemother* 2006; **50**: 196-203.
60. George S, Hamblin MR, Kishen A. Uptake pathways of anionic and cationic photosensitizers into bacteria. *Photochem Photobiol Sci* 2009; **8**: 788-95.
61. Elkins CA, Nikaido H. 3D structure of AcrB: the archetypal multidrug efflux transporter of Escherichia coli likely captures substrates from periplasm. *Drug Resist Update* 2003; **6**: 9-13.

Summary and Conclusion

Photodynamic therapy (PDT) and fluorescence photodetection (PD) gain increasing relevance for the treatment and *in situ* detection of pre-malignant and early stage neoplastic lesions. A breakthrough was achieved with the exploitation of endogenous photosensitizers that emanate from the heme biosynthesis pathway by exogenous topical application of 5-aminolevulinic acid (5-ALA). A literature review (Chapter 1) shows that numerous approaches have been undertaken to increase the selective generation of the endogenous photosensitizer protoporphyrin IX (PPIX) in tumors. However, appropriate systemic formulations of 5-ALA are still not available.

PDT is also an attractive alternative to conventional treatment of bacterial infections, where the development of resistant clinical strains is on the rise. One problem faced in the destruction of Gram-negative bacteria with light is the efficient accumulation of the photosensitizer in the cell. This underlines the need of new strategies to improve photodynamic inactivation of Gram-negative bacteria.

PART A. Polymeric nanoparticles loaded with hexaminolevulinic acid

Chapter 2. Matrix assisted fluorescence enhancement - why PPIX and nanoparticles make a friendly couple.

With the aim to develop a formulation for hexaminolevulinic acid (HAL) that facilitates drug delivery to tumors with difficult access, Part A of the thesis was dedicated to the encapsulation of HAL into polylactic acid (PLA) nanoparticles. We screened 4 commonly

used techniques, nanoprecipitation, emulsion evaporation, double emulsion evaporation and salting out, to obtain the highest possible loading and loading efficiency. The screening included the variation of factors such as solvent composition, pH of the aqueous phase, surfactant type and concentration, temperature during particle formation, polymer type and molecular weight, as well as the pairing of the HAL cation with lipophilic alkylbenzene sulfonate counter ions. Particle loading remained below 1% in all formulations. The low loading efficiency must be considered insufficient for parenteral or inhalative application. Experiments on the fluorescence generation in cells mediated by HAL laden nanoparticles produced by nanoprecipitation, however, revealed the following results:

- i. HAL laden nanoparticles generated 3 times higher fluorescence in T24 cells than free HAL. The fluorescence was increased 7 fold when using nanoparticles that were dehydrated prior to application on the cells.
- ii. PPIX fluorescence enhancement also occurred upon incubation with free HAL in the presence of unladen PLA particles. HPLC analysis of cell extracts and incubation media revealed similar HAL induced PPIX concentrations in the presence or absence of unladen nanoparticles.

From the observations we concluded that nanoparticles must modulate the optical properties of PPIX. For verification we incubated PPIX with nanoparticles in complete cell medium. Since proteins adsorb to PPIX and to nanoparticles, we also investigated PPIX-nanoparticle interaction in the absence of fetal bovine serum albumin (FBS). Dried nanoparticles significantly increased PPIX fluorescence in presence and absence of FBS. Freshly prepared nanoparticles also enhanced PPIX fluorescence in FBS free medium although to a smaller extent. Low nanoparticle concentrations had a suppressing effect on PPIX fluorescence in FBS supplemented medium. The exact mechanism of this phenomenon remains unclear; however, we presume that competitive factors between PPIX, albumin and nanoparticles to each other at its origin.

Chapter 3. Nanoencapsulation of lipophilic salts of 5-aminolevulinic acid hexyl ester by an aerosol flow reactor method

Ascribing the low rate of HAL nanoencapsulation with conventional methods to persisting drug affinity to the surfactant containing dispersion medium, we decided to replace the

aqueous phase by a gas. We applied the aerosol-flow-reactor method that generates particles from an organic drug-polymer solution down to a size of 100 nm. The process involves the atomization of the organic solution containing the drug and the polymer into a carrier gas at controlled temperature, and subsequent evaporation of the solvent.

We pursued the paradigm that higher lipophilicity of the HAL salt may influence the release rate and drug distribution in the particles. Accordingly, we paired the HAL cation with a butylbenzene sulfonate, hexylbenzene sulfonate and octylbenzene sulfonate anion, respectively.

The aerosol-flow-reactor method proved suitable for the production of HAL-laden spherical PLA nanoparticles of 100-200 nm size. Loadings of up to 30% (w/w) were achieved with loading efficiencies of up to 78%. Next, we assayed the ability of nanoencapsulated and free HAL salts to generate PPIX fluorescence in a GFP transfected T24 bladder carcinoma cell line and monitored GFP fluorescence to follow a potential toxic effect. The cytotoxicity of HAL salts increased with increasing chain length of the benzene sulfonate counter ion, while their ability to generate fluorescence was diminished. Nanoencapsulation of the compounds decreased the cytotoxic effect. Moreover, fluorescence could be maintained over a longer time period (at least 24 hours longer than with free HAL salts). The best results in molar drug loading and encapsulation efficiency were obtained with HAL laden nanoparticles (89 $\mu\text{mol}/100\text{ mg}$ particles and 78%, respectively). Therefore, we chose this formulation for experiments on A549 lung carcinoma tumor nodules implanted in the chorionallantoic membrane (CAM) of the chick embryo. The nanoparticle formulation successfully induced fluorescence on CAM implanted tumors. However, the fluorescence remained similar to that induced by an aqueous PEG solution containing free HAL (1 mM).

Part B. Photodynamic inactivation of *E. coli* with a new porphyrin generating mechanism

Chapter 4. Bacteria capture iron from heme by keeping the tetrapyrrol skeleton intact

In the majority of bacteria the pathway for heme biosynthesis is the same or similar to that in eukaryotic cells. It is therefore not surprising that exogenous 5-ALA and 5-ALA derivatives result in the intracellular accumulation of porphyrins, which renders the bacteria susceptible to destruction by light.

Bacteria require exogenous iron for the heme biosynthesis as well as other intracellular processes. To this end, they have developed mechanisms to internalize exogenous heme and withdraw the iron for the innate metabolism. Commonly, the reaction involves heme oxygenases or orthologs that degrade the iron complexing tetrapyrrol structure to biliverdin. However, in chapter 4 we describe the finding of two *E.coli* proteins, YfeX and EfeB fostering iron extraction from heme without cleavage of the tetrapyrrol ring:

Up to date, genome BLAST identification of heme oxygenase orthologs in *E.coli* has been unsuccessful. The laboratory strain *E.coli* K12 is able to withdraw iron from exogenous heme in the presence of the foreign *Serratia marescens* heme receptor HasR. Searching for the pathway that catalyses iron retrieval from heme in *E.coli* the group of Cécile Wandersman at the Institut Pasteur in Paris screened the genomic library of the bacterial strain, based on the evidence that tetrapyrrolic heme degradation products fluoresce under UV light. Fluorescence was distinguished in cells overexpressing the proteins YfeX and EfeB, respectively.

Interestingly, we identified the main fluorescing compound in these strains to be PPIX, which suggested that differently to cleavage of the tetrapyrrol, these enzymes withdraw the iron ion by leaving the PPIX skeleton intact. We confirmed the hypothesis by adding the non-natural heme analog, meso-heme to extracts of cells overexpressing YfeX and EfeB, respectively. YfeX and EfeB effectively generated meso-PPIX from meso-heme. A *yfeX, efeB* double mutant of HasR expressing *E.coli* K12 showed that the strain was not competent to use exogenous heme as iron source. Further protein binding studies revealed a common binding site for PPIX and heme on YfeX. The activity of YfeX and EfeB reverses the ferrochelatase catalyzed insertion of iron into the PPIX skeleton. Therefore, it was termed as deferrochelatase activity.

Chapter 5. Counterclockwise: PDI with PPIX generated from heme

The discovery of YfeX as a new PPIX generating path inclined us to challenge the system for the photodynamic inactivation of bacteria. A recent publication (Tatsumi, R. and M. Wachi (2008). J. Bacteriol. 190, 6228-6233) described the involvement of the bacterial multi-drug efflux pump TolC in the export of hydrophilic heme cycle intermediates, such as coproporphyrin (COP). We were interested, whether this also holds true for the lipophilic heme precursor PPIX.

First we examined the porphyrin profile of *E.coli* K12 transfected with a *yfeX* carrying pBAD24 vector with an arabinose inducible promoter. The cells were optionally mutated at the level of *tolC*. We then exposed bacteria to light doses of up to 20 J/cm². We showed that YfeX overexpression promotes the accumulation of PPIX, but also COPIII in bacteria. We presume the accumulation to be the result of the dual oxidase-deferriochelatase activity of YfeX. PPIX levels were further increased in the *tolC* mutated strain. Intracellular porphyrin concentrations were reflected in the susceptibility of bacteria to destruction by blue light: Survival of strains overexpressing either YfeX or carrying the *tolC* mutant was decreased by over 3 logs after exposure to light doses of 20 J/cm². YfeX overexpressing *tolC* mutants showed no survival after exposure to 15 J/cm² light.

We were curious whether exogenous heme could act as prodrug for PPIX in the YfeX overexpressing bacterial strain. Therefore, we provided cells with 1 μM heme during growth. Against our expectations, virtually no destruction was perceived in cells grown in presence of heme, indicating that heme abolishes the photosensitizing effect of PPIX. Another experiment investigating bacterial growth in presence of varying heme concentrations revealed that the intracellular PPIX concentration correlated inversely with the applied heme concentration. We were not able to clarify at this stage, why PPIX levels and the photosensitizing effect were decreased. However we assume that heme interferes with the YfeX mechanism.

Conclusion

From Part A of the thesis we conclude that efficient HAL loading of PLA nanoparticles can be achieved by means of an aerosol flow reactor method. The particles induce sustained fluorescence *in vitro* for at least 48 hours in monolayered cultures of the T24 bladder carcinoma cell line. They were also effective on xenografted A549 lung carcinoma tumor nodules implanted in the chorioallantoic membrane of the chick embryo. However, compared to free HAL the fluorescence was not improved. We were unable to test the intravenous administration of our formulation due to partial aggregation of the particles during the re-suspension process in aqueous media. Therefore, we recommend the inclusion of a step in the production process to prevent particle agglomeration. This may imply the addition of a surfactant in the organic phase, or the co-atomization of a surfactant containing aqueous solution with subsequent surfactant precipitation around the formed particle. Surmounting the

challenge of homogenous particle dispersion upon re-suspension in a liquid medium may bring HAL a step closer to the systemic treatment of interstitial tumors.

Finally, for experiments with high nanoparticle concentrations one should take into account possible adsorption of PPIX to the polymer matrix. Such an interaction may influence the fluorescence properties of the photosensitizer.

In part B, we demonstrated that bacteria may accumulate PPIX through an additional mechanism to that used by exogenous 5-ALA and its derivatives: the dye decolorizing peroxidase YfeX and its paralog EfeB can extract ferrous iron from heme. The process generates PPIX with subsequent sensitization of the cells to light. We further showed that PPIX is a substrate for the multidrug efflux pump TolC and that inhibition of the exporter increases the photosensitivity of bacteria effect. YfeX also extracted iron from exogenous heme, as evidenced upon addition of the non-natural heme analog, meso-heme, to cell lysates. However, heme had a photoprotective effect on bacteria. Since the uptake and metabolization of exogenous heme by Gram-negative bacteria is a highly controlled process, we are sceptical with regard to the exploitation of the deferrochelation mechanism for photodynamic inactivation of bacteria with heme.

A number of questions remain: What is the fate of PPIX after iron extraction? How does the role of TolC relate to this fate? Which, if any, are the partners of TolC in the export of PPIX? How important is the role of YfeX for the virulence of clinical bacterial strains?

YfeX and EfeB are highly conserved and widespread in Gram-positive and Gram-negative bacteria. Therefore, they may represent attractive targets for antibacterial strategies. The answers to the aforementioned questions and the clarification of the full function of the YfeX mechanism are indispensable for complete understanding.

Résumé et Conclusion

Au cours de la dernière décennie, la thérapie photodynamique (PDT, photodynamic therapy) et la détection par fluorescence (PD, fluorescence photodetection) se sont imposées comme des techniques efficaces pour le traitement et la détection de lésions cancéreuses ainsi que d'autres pathologies néoplasmiques et bactériennes. Ces techniques consistent à appliquer un agent photosensibilisant qui, en action conjointe avec une lumière de longueur d'onde adéquate conduit à l'effet désiré: l'éradication de cellules et/ou le marquage par fluorescence. Le photosensibilisateur (PS) est une petite molécule polycyclique capable d'absorber la lumière dans le domaine ultraviolet (UV), visible ou infra rouge (IR). L'absorption de photons élève la molécule dans un état d'énergie supérieur, qui est instable. Par conséquent, le PS retourne à son état initial et libère l'excès d'énergie par différents moyens. La première possibilité est que l'énergie soit libérée par émission d'un photon (fluorescence). Ce processus est exploité lors de la détection de lésions néoplasmiques malignes et pré-malignes. Une autre possibilité est que le PS transfère l'énergie à une molécule d'oxygène. Celle-ci ainsi rendue très réactive, induit la formation d'espèces d'oxygène réactives (ROS, reactive oxygen species) cytotoxiques. Ce mécanisme constitue la base de la PDT.

A ce jour, une multitude de PS a été développée et plus d'une dizaine est cliniquement approuvée, dont temoporfine (m-THPC, Foscan®), sodium de porfimer (HpD, Photofrin®), acide 5-aminolévulinique (Levulan®) et deux de ses alkyl esters (methyl, Metvix® et hexyl, Hexvix®). La possibilité de générer des photosensibilisateurs endogènes par administration exogène d'un précurseur d'hème, l'acide 5-aminolévulinique (5-ALA), fut une avancée considérable dans la recherche pour la PDT et la PD. Le 5-ALA est transformé par les

enzymes biosynthétiques de l'hème, entraînant l'accumulation de produits intermédiaires, notamment de protoporphyrine IX (PPIX).

Le succès du 5-ALA peut être attribué en grande partie à la sélectivité améliorée envers le tissu ciblé et donc l'occurrence diminuée de l'effet adverse primaire des photosensibilisateurs, la photosensibilisation de la peau. Cependant, en raison de sa nature hydrophile, le 5-ALA ne peut accéder le cytosol que par transport actif ce qui restreint sa biodisponibilité. Cette limitation a pu être améliorée par l'estérification du groupement carboxylique avec des n-alkanoles, notamment l'hexanol, qui favorisent la pénétration de la membrane cellulaire et la répartition passive du principe actif dans la cellule. Le véhicule d'administration peut aussi améliorer l'accumulation du 5-ALA dans le tissu ciblé. Toutefois, il n'existe à ce jour que des formulations topiquement applicables, ce qui restreint l'accès pour les pathologies interstitielles difficiles d'accès, comme le cancer du poumon.

Dans le but d'explorer de nouveaux mécanismes d'induction de porphyrines endogènes pour le marquage par fluorescence et la thérapie photodynamique, deux voies principales ont été étudiées. D'une part, la formulation de nanoparticules était envisagée en vue de rendre l'héxyl ester de l'acid 5-aminolévulinique (HAL) applicable par voie inhalative et/ou systémique. D'autre part un nouveau mécanisme bactérien, la déferrochélation, a été testé comme technique possible pour photosensibiliser une souche d'*Escherichia coli*.

Les nanoparticules polymériques sont des systèmes de libération adaptés à l'application par voie orale, parentérale ou par inhalation. Hormis le fait d'entraîner potentiellement une libération prolongée, la petite taille des nanoparticules permet d'éviter la perception par les macrophages et donc d'augmenter le temps de rétention dans le sang ou les poumons.

Malgré son coefficient de partage octanol-eau (logP) élevé, l'encapsulation du HAL par des méthodes conventionnelles utilisant, pour la plupart, un milieu aqueux contenant un tensio-actif (e.g. alcool polyvinylique) comme phase dispersante, s'avère difficile. La présence du tensio-actif, même à faible concentration, augmente considérablement la solubilité d'HAL dans l'eau, provoquant ainsi le passage du principe actif dans la phase aqueuse. Ce phénomène s'explique par le fait que l'HAL est appliqué sous forme de sel hydrochlorique (HAL HCL). La présence du groupement aminé chargé lui confère un caractère amphiphile.

Afin de remédier à ce problème, nous avons préparé les nanoparticules dans un réacteur à flux d'aérosol (aerosol flow reactor). De plus, suivant l'hypothèse, qu'une libération continue peut

être atteinte en augmentant l'affinité du principe actif vers le polymère, nous avons échangé le contre-ion de chlorure d'HAL contre un anion de sulfonate de benzène alkylé, plus spécifiquement le butyl, hexyl ou octyl benzene sulfonate.

Dans le système de réacteur à flux d'aérosol, une solution organique contenant le polymère et le principe actif est atomisée par un flux de gaz inerte (nitrogène) générant ainsi un aérosol hautement dispersé. L'aérosol est ensuite guidé à travers un tube métallique thermostaté (le réacteur) où le solvant est évaporé de façon contrôlée. Cette technique a permis d'encapsuler HAL avec une efficacité de 78%. La taille des particules obtenues était de 100 à 200 nm. L'examen d'induction de fluorescence sur des monocouches de cellules cancéreuses de la vessie (T24) a démontré un effet prolongé par rapport au sel d'HAL libre. Les meilleurs résultats étant obtenus avec l'HAL HCl, nous avons appliqué cette formulation sur des nodules de tumeurs de poumon (A549) implantées dans la membrane chorioallantoïque (chorioallantoic membrane, CAM) de l'embryon de poulet. L'efficacité des nanoparticules dans l'induction de fluorescence sélective dans les tumeurs du CAM était comparable à une solution contenant du HAL HCl, franchissant ainsi un premier pas pour l'application potentielle pour le cancer du poumon. Néanmoins, des tests *in vivo* avec un modèle d'inhalation sont nécessaires pour examiner une potentielle supériorité des nanoparticules envers la molécule libre, portant sur le temps de rétention pulmonaire prolongé.

Par ailleurs, il est envisageable d'appliquer ces nanoparticules par voie systémique. Pour ce faire, la resuspension des particules dans un milieu aqueux doit être mis au point par exemple en ajoutant à la solution organique un tensio-actif macromoléculaire, comme le PEG, qui s'accumulerait à la surface des particules pendant l'évaporation du solvant. Une autre possibilité serait de co-nébuliser une solution aqueuse de tensio-actif avec la solution organique, résultant dans la précipitation du tensio-actif à la surface de nanoparticules.

La deuxième partie de la thèse décrit l'accumulation de PPIX dans *E. coli* par un mécanisme différent de celui utilisé par 5-ALA: l'enzyme YfeX et son paralogue EfeB sont capables de générer de la PPIX en extrayant l'ion de fer, un élément essentiel pour la virulence des bactéries, à partir d'hème exogène. Entre les nombreux mécanismes développés par les bactéries, notamment en internalisant l'hème, l'extraction de fer du complexe tetrapyrrolique par YfeX et EfeB dans *E. coli* n'était pas connue jusqu'à présent. L'activité étant l'inversion de la réaction de ferrochélatase, on y réfère en tant que déferrochélation.

La PPIX étant un agent photosensibilisant, nous étions intéressés, si la génération de PPIX par YfeX rend *E.coli* susceptible à l'éradication par rayons UV. L'effet photosensibilisant de la PPIX était significativement augmenté dans une souche surexprimant YfeX. Suite aux résultats obtenus nous avons testé la potentielle fonction d'hème en tant que prodrogue pour la génération de PPIX par YfeX. L'incubation de bactéries avec de l'hème exogène anéantit la production de PPIX et en conséquence la photosensibilisation.

La pompe d'efflux, TolC, étant capable de transporter des porphyrines hydrophiles nous étions par ailleurs intéressés, si la PPIX, molécules hydrophobes est aussi un substrat pour ce mécanisme de multirésistance. La souche d'*E.coli* mutée au niveau de *tolC* accumulait de la PPIX, la rendant sensible à l'irradiation par UV.

YfeX et EfeB sont répandus et hautement conservés à travers les bactéries Gram-positives et négatives. Ils pourraient donc représenter des cibles intéressantes pour de nouvelles stratégies antibactériennes. Néanmoins, l'assimilation d'hème par les bactéries, ainsi que sa métabolisation sont des processus minutieusement réglés. Pour cela, il est incertain que l'hème représente une prodrogue adéquate pour l'exploitation du système YfeX pour l'inactivation de bactéries par la PDT.

Pour conclure, de nombreuses questions sur le fonctionnement exact de la déferrochélation restent ouvertes: quel est le sort de la PPIX après l'extraction du fer? Quelle importance faut-il attribuer à YfeX et EfeB dans les souches de bactéries cliniques? La pompe d'efflux, TolC, joue-t-elle un rôle physiologique dans l'exportation de produits intermédiaires du cycle de l'hème? Quelles sont les protéines impliquées dans la transmission de PPIX à TolC?

L'éclaircissement de ces points permettrait une meilleure évaluation du potentiel pharmaceutique de la déferrochélation.

Abbreviations

A549	human lung carcinoma cells
5-ALA	5-aminolevulinic acid
AIP	acute intermittent porphyria
ALAD	ALA-dehydratase
ALAS	ALA-synthase
Ara	arabinose
AOT	dioctyl sodium sulfosuccinate
ATP	adenosine triphosphate
BBB	blood brain barrier
BCC	basal cell carcinoma
BME	basement membrane extract
BSA	bovine serum albumin
BUTBS	butyl benzenesulfonate
CFU	cell forming unit
CH	cholesterol
CMC	condensation particle counter
COP I	coproporphyrin I
COPIII	coproporphyrin III
COPgenI	coproporphyrinogen I
COPgenIII	coproporphyrinogen III
COPO	coproporphyrinogen III oxidase
CSF	cerebrospinal fluid
CT	computerized tomography
DFO	deferoxamine
Dip	2,2-Dipyridyl
DMA	differential mobility analyzer
DMEM	Dulbecco's Modified Eagle's Medium
DMPC	dimyristol phosphatidyl choline
DMPG	dimyristol phosphatidyl glycerol
DMSO	dimethyl sulfoxide
DOTAP	Dioleyl trimethyl ammonium propane
Dyp peroxidase	dye-decolorizing peroxidase
<i>E. coli</i>	<i>Escherichia coli</i>
EDD	embryo development day
EDTA	ethylene diamine tetracetic acid
EPR	enhanced permeability and retention
Er:YAG	erbium:yttrium-aluminium-garnet
ETBS	ethyl benzenesulfonate
FBS	fetal bovine serum albumin
FC	ferrochelataase
FDA	United States Food and Drug Administration
GABA	gamma amino butyric acid
GFP	green fluorescent protein
GIT	gastrointestinal tract
GNMD	geometrical number mean diameters

Abbreviations

GSD	geometric standard deviation
HAL	5-aminolevulinic acid hexyl ester, hexaminolevulinic acid
HAS	human serum albumin
HasR	<i>Serratia marescens</i> heme receptor
Hb	bovine hemoglobin
HemA	glutamyl-tRNA transferase
HEMA	poly (hydroxyl ethyl methacrylate)
HEXBS	hexyl benzenesulfonate
HO	heme oxygenase
HP	haematoporphyrin
HpD	haematoporphyrin derivative
HPLC	high performance liquid chromatography
HPLC-MS	high performance liquid chromatography - mass spectrometry
LDL	low density lipoproteins
MAL	5-aminolevulinic acid methyl ester
MBR	mitochondrial benzodiazepine receptor
MO	molecular orbital
MPPIX	mesoporphyrin IX
MRI	magnetic resonance imaging
MRSA	methicillin resistant staphylococcus aureus
nBCC	nodular basal cell carcinoma
O/W	oil-in-water
OCTBS	octyl benzenesulfonate
OD	optical density
P.I.	polydispersity index
PBG	porphobilinogen
PBGD	porphobilinogen deaminase
PBGS	porphobilinogen synthase
PBS	phosphate buffer saline
PCL	polycaprolactone
PD	fluorescence photodetection
PDI	photodynamic inactivation
PDT	photodynamic therapy
PEG	polyethylene glycol
PGA	polyglycolic acid
PigA	<i>pseudomonas aeruginosa</i> heme oxygenase
PLA	polylactic acid
PLGA	poly(lactic-co-glycolic) acid
PMVE/MA	poly(methylvinylether/maleic anhydride)
PPIX	protoporphyrin IX
PPgenIX	protoporphyrinogen IX
PROTO	protoporphyrinogen IX oxidase
PS	photosensitizer
PVAL	polyvinyl alcohol
PVC	polyvinyl chloride
ROS	reactive oxygen species
SCC	squamous cell carcinoma
SDS/PAGE	sodium dodecyl sulfate/ polyacrylamide gel electrophoresis
SEM	scanning electron microscopy

Abbreviations

T24	human bladder carcinoma cells
TAT	twin arginine translocation system
TEWL	transepidermal waterloss
T _f	transferrin
THF	tetrahydrofuran
T _f R	transferrin receptor
tRNA	transfer ribonucleic acid
UROD	uroporphyrinogen III decarboxylase
UROI	uroporphyrin I
UROIII	uroporphyrin III
UROgenI	uroporphyrinogen I
UROgenIII	uroporphyrinogen III
UROS	uroporphyrinogen III synthase
W/O	water-in-oil
W/O/W	water-in-oil-in-water
RND family	resistance-nodulation-cell division family